A Thesis Submitted for the Degree of PhD at the University of Warwick

Permanent WRAP URL:

http://wrap.warwick.ac.uk/137710
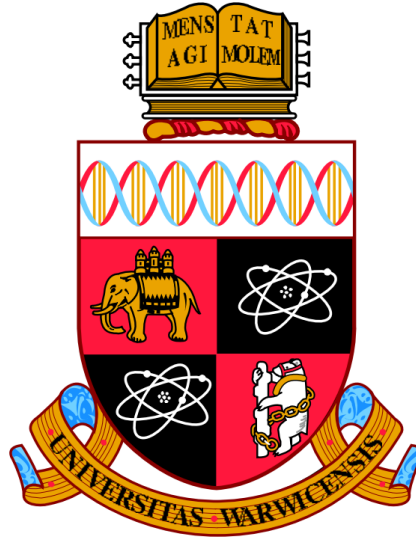
warwick.ac.uk/lib-publications

Direct Observation of Swelling Coal Particles

Using high-temperature confocal scanning laser microscopy to examine some intrinsic and extrinsic influences on the unconstrained thermal swelling of discrete coal particles

Ian A. Moore

A thesis submitted in partial fulfilment of the requirements for the degree of

Doctor of Philosophy in Engineering

University of Warwick

Warwick Manufacturing Group

August 2019

Contents

List of figures

List of tables

Acknowledgements

Declaration

This thesis is submitted to the University of Warwick in support of my application for the degree of Doctor of Philosophy. It has been composed by myself and has not been submitted in any previous application for any degree. The work presented (including data generated and data analysis) was carried out by the author except in the cases outlined below:

- Coal dilatation carried out by Shaun Elliott
- Coal ash chemistry analysis by Simon Blanchard
- Differential thermo-gravimetric analysis of coal samples (at 100 K/min only) by Chris Kooij

Parts of this thesis have been published by the author:

Spooner, S., Moore, I., Seetharaman, S., Li, Z. (2018), "Using High-Temperature Confocal Scanning Laser Microscopy to Study Transient Phenomena: Swelling and Spontaneous Emulsification", paper presented to the 147th Annual Meeting and Exhibition of The Minerals Metals and Materials Society, Phoenix, Arizona, 11th-15th March 2018.

Abstract

Steel is the most important engineering and construction material in the world, with global production predicted to continue rising to meet the needs of a growing population. The steel industry is therefore economically important, but also energy intensive and thus a significant source of carbon emissions.

The blast furnace–basic oxygen furnace (BF-BOF) integrated route to steelmaking will retain a strong contribution to steel production throughout the current century, as such its continued improvement is desirable. Pulverised coal injection (PCI) is a key part of modern blast furnace ironmaking as it reduces the dependence upon coke, which is costly and environmentally unfriendly to produce. PCI involves injecting fine coal particles into the raceway of a blast furnace via the tuyeres.

Different coal types vary in their suitability for blast furnace injection, therefore a thorough understanding of all aspects of coal behaviour during blast furnace injection is necessary for optimised PCI operation. A relevant feature of coal behaviour is the thermoplastic swelling of coal particles; however, little is known about the effects of coal thermoplasticity on blast furnace performance. The high temperature confocal scanning laser microscope (HT-CSLM) offers a potential novel technique to evaluate the thermoplastic swelling properties of coal particles.

This thesis investigates the applicability of the HT-CSLM technique to the study of the thermal swelling of discrete coal particles. Four types of coal are included. The effect of heating rate on swelling behaviour is investigated, as is the effect of particle density. A study of the influence of particle size on swelling behaviour was conducted using size and density separated samples in an attempt to mitigate against the segregation of components during comminution. A drop tube furnace (DTF) was used to 'scale-up' the experiments by providing a heating environment closer to that of the blast furnace raceway.

Results show that the HT-CSLM is a suitable technique for this type of study, although with a limitation regarding highly fluid coals. The maximum swelling ratio of coal particles is shown to increase with increasing heating rate. Lighter particles are found to be generally more highly swelling, which can be related to composition. The effect of particle size differed between coal types and suggested the possibility of a coal type-dependent optimum particle size in relation to maximum swelling ratio. The HT-CSLM and DTF swelling results were in agreement provided certain assumptions were made. Char reactivity results indicated that a greater degree of swelling led to more reactive char particles, however no evidence was found that swelling increased the rate of coal conversion at short residence times.

Abbreviations

BET	Brunauer-Emmett-Teller
BF	Blast furnace
BOF	Basic oxygen furnace
CO	Coke ovens
daf	Dry ash free basis
db	Dry basis
DD	Dial divisions
DDPM	Dial divisions per minute
diff	Calculated by difference
DTF	Drop tube furnace
DTG	Differential thermal gravimetric
HT-CSLM	High temperature confocal scanning laser microscope
MS	Mass spectrometer
PCI	Pulverised coal injection
RAFT	Raceway adiabatic flame temperature
RSD	Relative standard deviation
SEM	Scanning electron microscope
SR	Swelling ratio
TGA	Thermogravimetric analysis
VM	Volatile matter
Vol. %	Percentage by volume
Wt. %	Percentage by mass
XRF	X-ray fluorescence

1 Introduction, problem formulation and thesis structure

1.1 Introduction

Steel is the most important engineering and construction material in the world, in 2012 the global steel industry had an estimated turnover of 800 billion US dollars and, in 2014, employed eight million people (World Steel Association, 2014). In 2017 1.7 million tonnes of crude steel were produced (World Steel Association, 2018) and this figure is predicted to continue rising to meet the needs of a growing world population (Pauliuk *et al.*, 2013) (Figure 1.1).

The steel industry is therefore economically important, but it is also energy intensive and thus a significant source of carbon emissions globally. Energy requirements constitute up to 40 % of the total cost of steelmaking in certain circumstances (World Steel Association, 2018), whilst steel production accounts for 25 % of industrial carbon emissions (Pauliuk *et al.*, 2013).
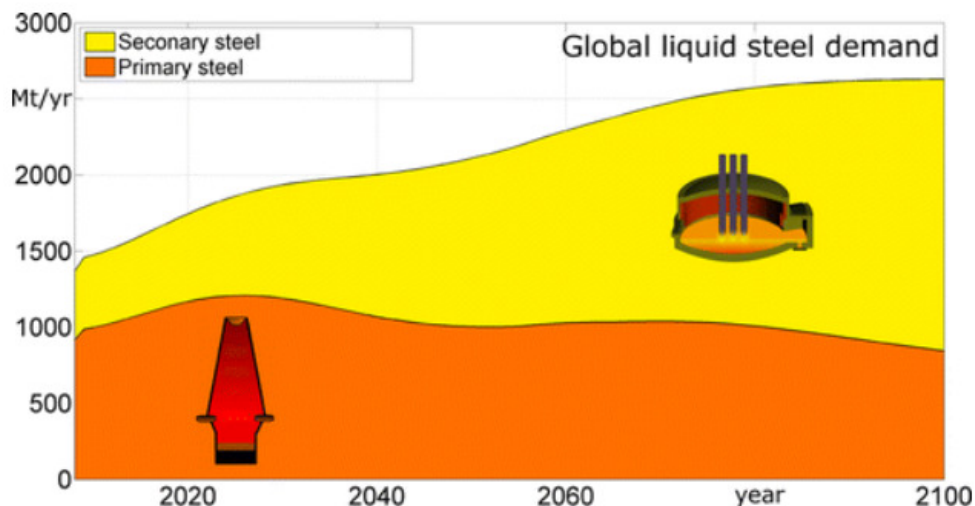
Figure 1.1: Global liquid steel demand. Primary steel represents the production from the BF-BOF route, and secondary steel via the scrap-based EAF route.
(Pauliuk *et al.*, 2013)

Figure 1.1 illustrates the forecast production contributions of the two main routes (the blast furnace ironmaking-basic oxygen furnace steelmaking (BF-BOF) integrated route and the electric arc furnace (EAF) route) to crude steel production until the end of the current century. The EAF route, recycling scrap steel into new products, will substantially increase its share. However, the BF-BOF integrated route, producing liquid steel from virgin materials, maintains a strong contribution to overall production (71.5 % in 2017 (World Steel Association, 2018)) throughout this time scale; as such its continued improvement is a necessity for progression within the industry. Steel production via the BF-BOF route involves the necessary manufacture of coke in coke oven plants. Cokemaking is costly and environmentally unfriendly therefore reducing the dependence upon coke has economic and environmental benefits for the BF-BOF route. Pulverised coal injection (PCI) is a technology that does just that and has therefore become a key part of modern blast furnace ironmaking. PCI involves injecting large volumes of fine coal particles into the raceway of a blast furnace.

The steel industry is competitive and established steel-producing countries are currently facing increased competition from developing countries where production costs are inherently lower, yet production capabilities are improving with the introduction of modern technology. This enhances the need for developed steel producers to continue to improve efficiency and to establish the most environmentally friendly methods possible as a differentiating aspect of their product.

There is a need to improve the efficiency and productivity of the blast furnace ironmaking process for economic reasons, and to reduce carbon emissions for environmental reasons. By assisting the raw materials selection process for blast furnace PCI this project is related to both these issues. The aim of this work is to develop a novel technique for characterising coal with respect to blast furnace coal injection.

Different coal types may vary a great deal in their properties and therefore also in their suitability for blast furnace injection. Various technical parameters are used to inform the selection of coals and it is important for blast furnace operators to

be able to evaluate the likely performance of prospective injection coals. A thorough understanding of all aspects of coal behaviour during blast furnace injection is necessary in this regard, as is the ability to measure the relevant coal properties and understand how these will affect blast furnace performance. Aside from technical factors the varying market values of different coals is also a key consideration in terms of selecting coals in order to make the most efficient and economic use of blast furnace PCI technology.

1.2 Problem formulation

Blast furnace operators are required to evaluate potential injection coals and make decisions on which coals to purchase in order to use PCI effectively and economically. This requires the use of tools that can predict the relative performance of different coals under blast furnace PCI conditions. A feature of coal behaviour under these conditions is the thermoplastic swelling of individual coal particles, however standard laboratory tests of coal thermoplasticity are designed to replicate cokemaking heating conditions and little is known about the effects of coal thermoplasticity on blast furnace performance. Due to its controlled environment, high heating rates (relative to a laboratory environment) and in-situ observation capabilities a high temperature confocal scanning laser microscope (HT-CSLM) offers a potential novel technique to evaluate the thermoplastic properties of a coal and provide information about how effectively that coal will perform as a PCI coal.

1.3 Thesis structure

A brief introduction to this topic and the objective of this work are covered in this current chapter (chapter 1). In the following chapter (chapter 2) the technical background of the project is presented; the role of the blast furnace within the steelmaking process is explained as well as environmental and economic challenges that it faces. The blast furnace itself is described in more detail, with a focus on the role that injecting auxiliary reducing agents (particularly coal) play in tackling those challenges. Identification of the most suitable coals for blast furnace injection is essential for achieving the maximum benefits economically, environmentally and technically, therefore some criteria currently used for coal

selection are discussed, as are the potential effects of coal thermoplasticity. Thermoplasticity is a factor that has not attracted much research with specific regard to blast furnace injection to date, yet the thermoplastic phenomenon of single particle swelling is likely to play a role in the way a blast furnace injection coal behaves and so the literature on the thermal swelling of coal particles is reviewed; including extrinsic and intrinsic factors influencing the swelling properties of coal particles, methods of measurement, modelling work and implications of the swelling process. Chapter 2 concludes with a summary of the unresolved issues arising from the review, which leads on to the formulation of the research approach (chapter 3). In chapter 3 the objectives of the work are presented along with associated hypotheses to be interrogated, the approach to interrogating each hypothesis is then described briefly. Further detail of the experimental methods employed is given in chapter 4.

Four result chapters then follow: Chapter 5, 'Development of technique', describes the development of the HT-CSLM technique for measuring the swelling ratio of individual coal particles; chapter 6, 'Effect of heating rate', investigates the effect of heating rate on the transient maximum swelling ratio of coal particles; chapter 7, 'Effect of particle density', investigates how segregating coal particles according to density affects swelling properties, and whether the Gieseler fluidity and rate of mass loss from density-segregated samples are key to their swelling properties; chapter 8, 'Effect of particle size', investigates the effect of particle size on the swelling properties of coal particles; and the final results chapter, chapter 9, 'Drop tube furnace tests', compares swelling results from the HT-CSLM and DTF (drop tube furnace) techniques and also allows swelling behaviour to be related to conversion and char reactivity results. The thesis concludes by drawing together the conclusions of all results chapters, re-visiting the hypotheses and making suggestions for further work (chapter 10).

2 Technical background

2.1 Blast furnace ironmaking and environmental challenges

The role of the blast furnace in the steelmaking process is explained below along with challenges it faces in the form of environmental pressure and alternative routes to steelmaking.

The blast furnace represents the long-established primary route to producing iron for steelmaking and is predicted to remain the predominant route until around 2040 (Pauliuk *et al.*, 2013) (Figure 1.1). After this time larger amounts of steel are predicted to be produced via the scrap-based electric arc furnace route (labelled secondary steel in Figure 1.1) than the blast furnace route (labelled primary steel in Figure 1.1). This is largely due to the increasing availability of scrap steel, as in-use steel comes to the end of its useful life. Meanwhile direct reduction methods may have the potential to provide another significant alternative to the blast furnace route in future. However, because the total global demand is predicted to rise, the absolute quantity of steel produced by the blast furnace route is shown to remain relatively constant so that the blast furnace is predicted to remain a significant route to steelmaking until 2100 and beyond.

Figure 2.1 illustrates the position of the blast furnace in the overall process of crude steel production. Also indicated are the scrap-based electric arc furnace (EAF) and direct reduction (DR) routes. The role of the coke ovens (CO), whose relevance to this project is explained in section 2.2, can also be seen.
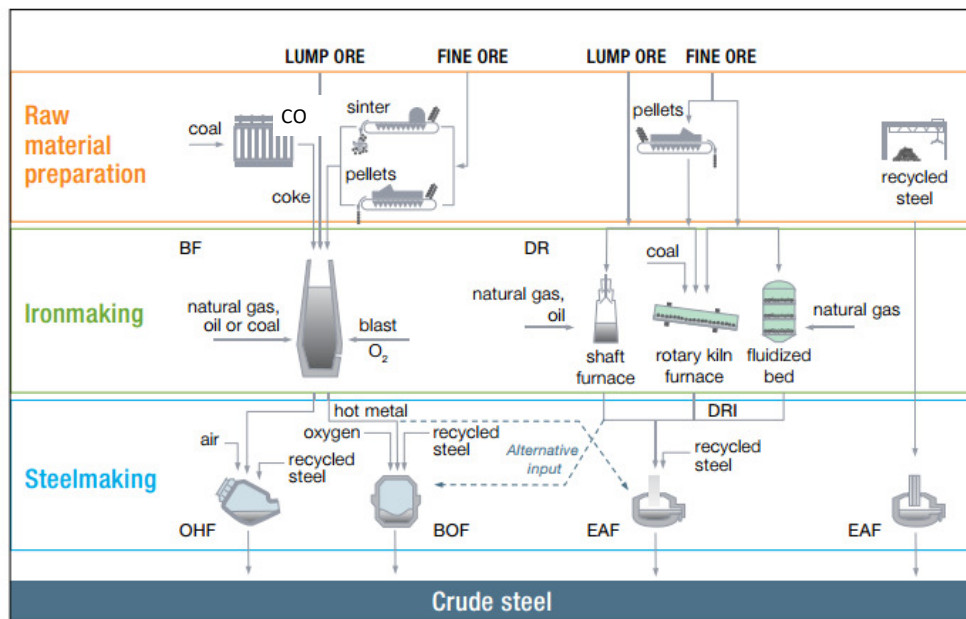
Figure 2.1: Flow diagram of crude steel production. CO = Coke Oven, BF = Blast Furnace, DR = Direct Reduction, DRI = Directly Reduced Iron, OHF = Open Hearth Furnace, BOF = Basic Oxygen Furnace, EAF = Electric Arc Furnace. (World Steel Association, 2018)

The reason that scrap-recycling and direct reduction may be seen as attractive alternatives to the blast furnace is due to the highly energy intensive nature and high carbon emissions of the blast furnace route. A modern integrated steel plant emits about 1.8 tons of carbon dioxide per ton of steel, most of which is associated with ironmaking (Smith, 2017). The blast furnace itself accounts for about 70 % of the total emissions from the integrated BF-BOF steel manufacturing process, whist this figure rises to 75-80 % when the associated processes of cokemaking, pelletising and sintering are included (Wang *et al.*, 2009).

The increased pressure in terms of environmental impact and competition from alternative steelmaking routes will make it necessary for blast furnaces to continue evolving to improve efficiency, productivity and environmental impact. The effective use of auxiliary reducing agents, in particular coal, will help to achieve this.

2.2 The blast furnace process

The blast furnace process is described below with emphasis on the tuyere and raceway zones.

The aim of the blast furnace process is to liberate iron from its oxides (iron ore). The iron produced by the blast furnace will be converted to steel in the subsequent steelmaking process (Figure 2.1).

The blast furnace itself is an industrial reaction vessel in which a counter-current flow of materials is established with solid and molten materials (the burden) moving down the furnace and gaseous species moving upwards (Figure 2.2). The burden, charged to the top of the furnace, comprises primarily of layers of iron ore and coke (coal carbonised in a coke oven). Flux material is also added, usually incorporated into the other burden materials. The burden descent takes several hours whereas the ascent of gases takes seconds.
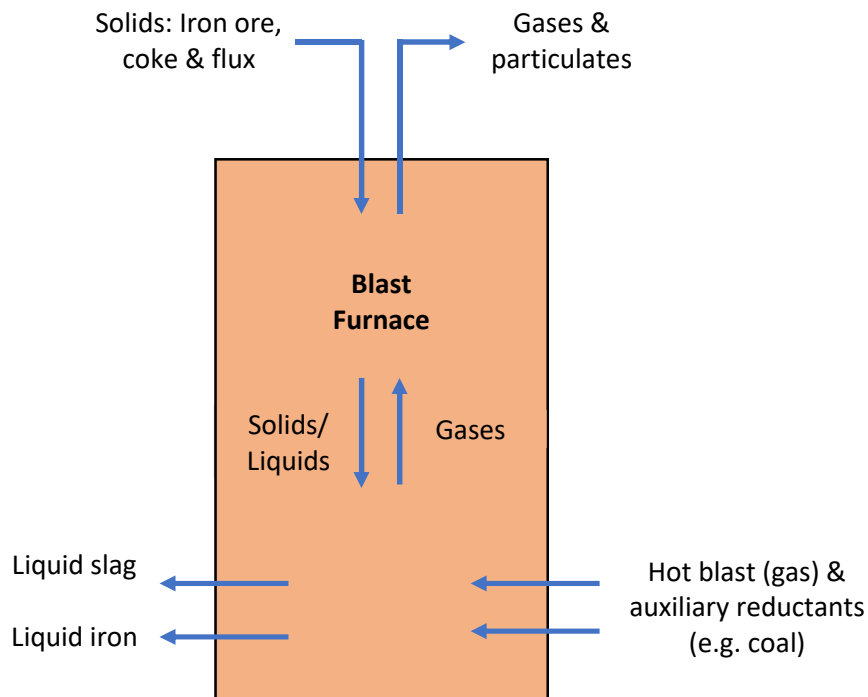
Figure 2.2: Simplified schematic diagram of blast furnace process.

Blast furnace size varies significantly. In the EU-15 (the 15 member countries of the European Union between 1 January 1995 and 30 April 2004) and the NAFTA

(North American Free Trade Agreement) countries the most common blast furnace hearth diameters are 8-13 m. In Japan and South Korea blast furnace hearth diameters are predominantly >14 m. In China small blast furnaces with hearth diameters < 8 m are most common; although it should be noted that the total number of blast furnaces in China is much greater than in the other areas mentioned and so the absolute number of larger furnaces in China is large in comparison to those other areas (Lungen, 2015).

Coke plays a vital role in the blast furnace process as it performs the following functions:

- A fuel providing heat for the process.
- A reducing agent to chemically reduce iron oxides to iron.
- A permeable physical structure supporting the burden and allowing molten material to percolate to the bottom of the furnace.
- A dust filter for uprising gas.
- A carbon source to carburise iron.

The flux material combines with elements of the ore to create the by-product slag.

Near the base of the furnace hot oxygen-enriched air is introduced at high pressure through openings called tuyeres (Figure 2.3). This 'blast' enables the combustion of coke to occur, creating heat and reducing gases (carbon monoxide and hydrogen), which go on to reduce iron oxide to iron. A void, or area of low coke density, within the furnace adjacent to the tuyere opening is created, this is called the raceway.

Gases percolate up through the furnace participating in chemical reactions (see section 2.4) and are captured as they exit the top of the furnace. Meanwhile the molten iron and slag are tapped separately from near the base of the furnace below tuyere level.

Iron ore (lump, pellets, sinter),

flux, coke

Gas, dust

Stockline

Iron ore, flux

Coke

Cohesive zone

Fluid zone

Raceway

Bustle pipe

Oxygen-
enriched air,
pulverised coal

Slag and
molten iron

Stack

Bosh

Hearth

Tuyere

Deadman
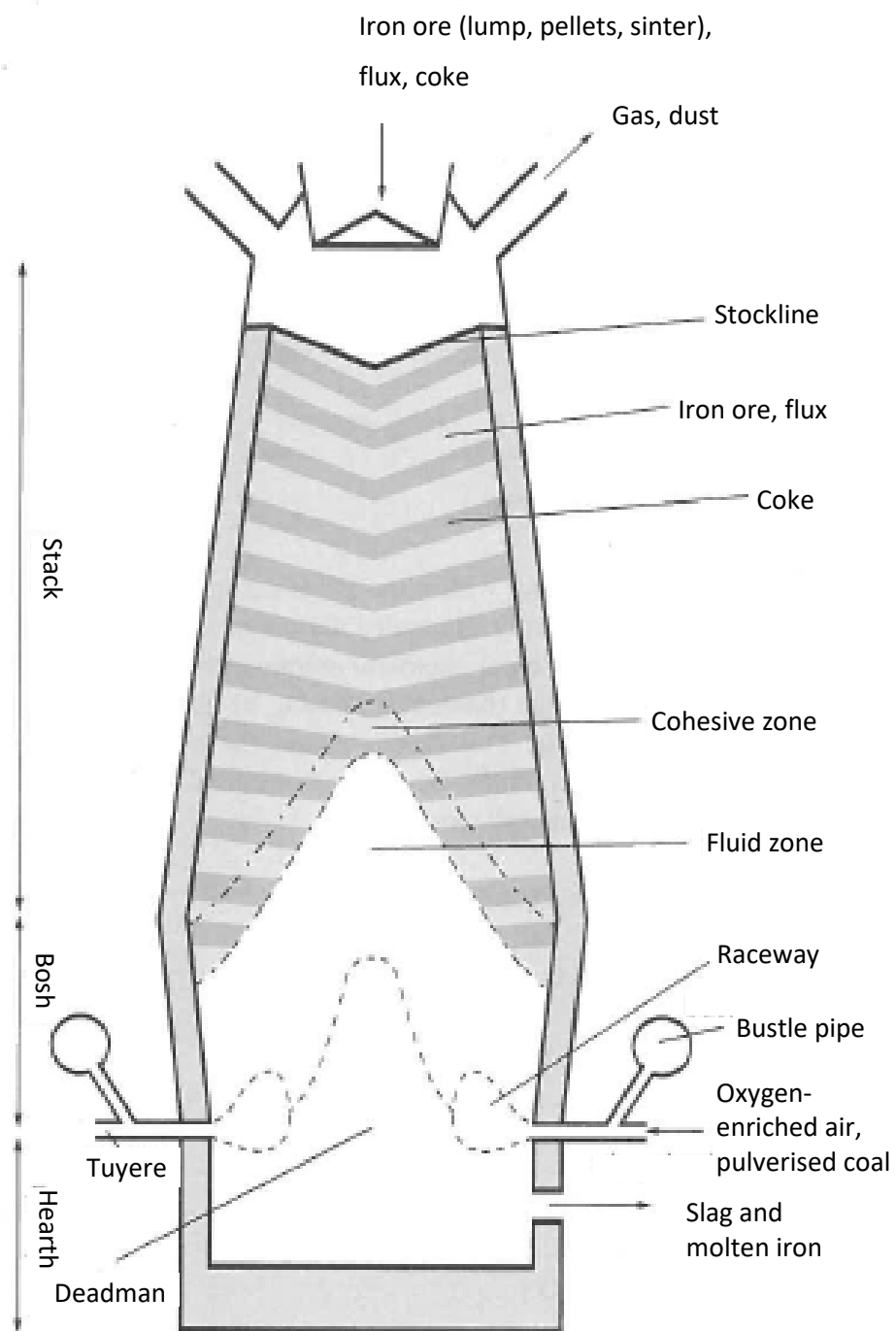
Figure 2.3: Blast furnace cross section. (Carpenter, 2006)

2.3 The use of auxiliary reducing agents

This section describes how auxiliary reducing agents are used to reduce the quantity of coke required, bringing economic, technical and environmental benefits.

As mentioned in chapter 1 the steel industry is facing challenges in the form of environmental pressure and competition from alternative steelmaking routes. Reducing the necessity for coke in the blast furnace process addresses both of these issues.

As discussed in section 2.2 coke is a necessity for the blast furnace, however the cokemaking process itself is costly and environmentally unfriendly. Coke oven plants must be maintained and eventually replaced, many are already operating beyond their original design-life (Carpenter, 2006). In addition, good quality cokemaking coals command a premium price, which increased steeply in the early 2000s due to the effect of Chinese economic expansion.

It is therefore advantageous to find ways of reducing the quantity of coke required in the ironmaking process, i.e. reducing the coke rate (quantity of coke required to make 1 ton of iron). One way of achieving this is by using auxiliary reducing agents; these provide an alternative source of reducing gases thereby lowering the requirement on coke as a reducing agent.

Auxiliary reducing agents are materials injected into the raceway zones through the tuyeres of a blast furnace (Figure 2.4). Materials such as oil, coal (granular or pulverised), natural gas and plastics (Murai *et al.*, 2015) have been used as auxiliary reducing agents, undergoing conversion to reducing gases within the tuyere and raceway. A slightly different case is the injection of hot reducing gas, which is already in its desired form at the point of injection. Hot reducing gas may be produced by treatment of recycled gas from the top of the blast furnace (Soskovets *et al.*, 2014).
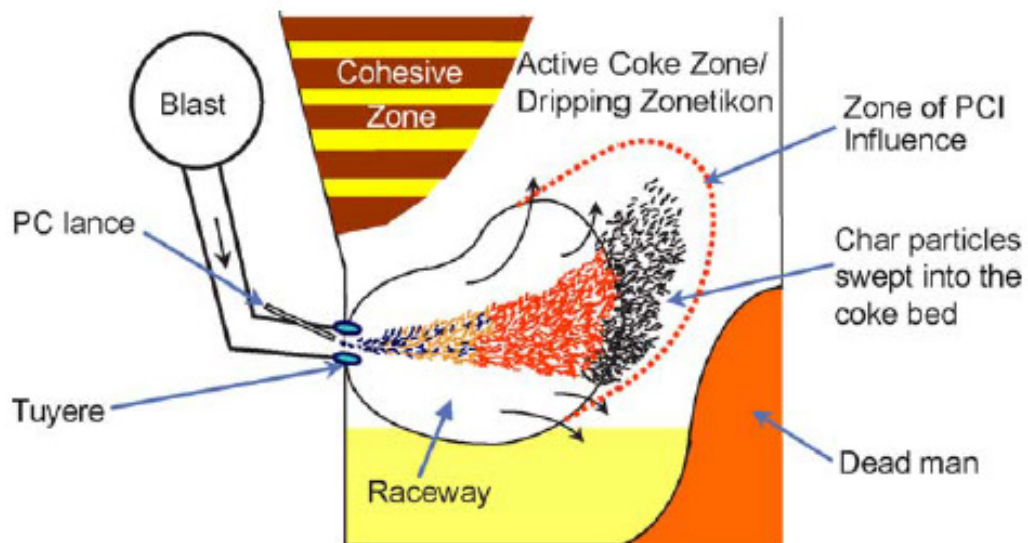
Figure 2.4: Tuyere and raceway section of blast furnace. (Mathieson *et al*., 2005)

The use of auxiliary reducing agents has become an important part of modern blast furnace operation as demonstrated by the graph produced by the Association of German Steel Manufacturers (VDEh), reproduced overpage as Figure 2.5, showing consumption of reducing agents of the blast furnaces in Germany. The consumption of coke decreased sharply in the 1950s and 1960s and has generally continued to decrease at a slower rate since then. Meanwhile the use of oil as a reducing agent became popular in the late 1960s and 1970s. The increasing price of oil relative to coal meant that coal became the predominant auxiliary reducing agent from the 1980s onwards.

Such is the trend towards coal as the preferred auxiliary reducing agent that in 2014/2015 'almost all the blast furnaces in the EU-15 are operated with coal injection' (Lungen, 2015). Some blast furnaces in 2013 achieved coal injection levels of about 270 kg/thm (ton of hot metal) with coke rates as low as 270 kg/thm. In 2015 the lowest carbon dioxide emissions from reductants were in the range of 1570 kg/thm (Lungen, 2015).

From the 1950s to around 1980 there was a significant decrease in the total consumption of reducing agents (i.e. coke + coal + oil + others). Since then the total consumption has been relatively consistent, indicating that further reductions have proved difficult to achieve.

This project concentrates on coal as an auxiliary reducing agent rather than oil or any other materials.
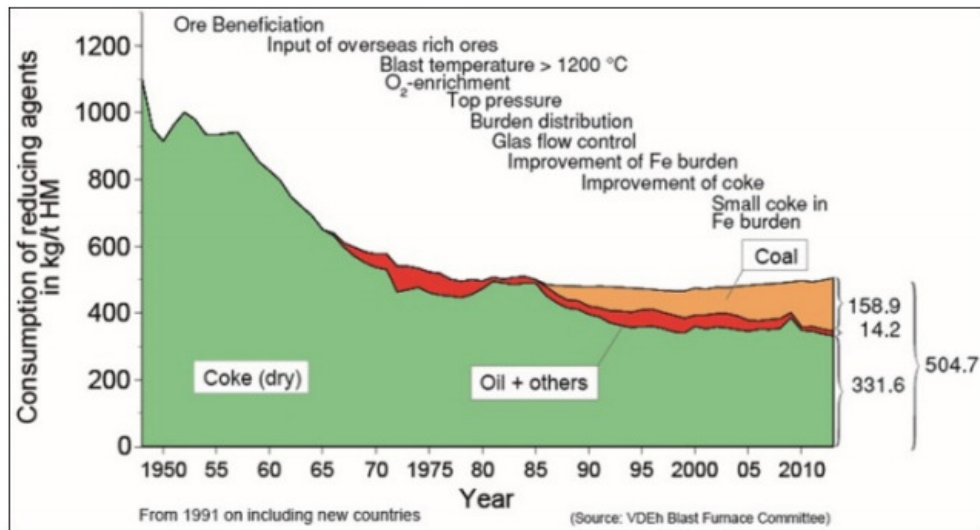
Figure 2.5: Consumption of reducing agents of the blast furnaces in Germany.
Figure produced by Stahlinstitut VDEh. (Lungen, 2015)

Although coke cannot be replaced altogether, for the reasons discussed in Section 2.2, reducing the coke rate by using coal as an auxiliary reducing agent injected through the tuyeres has the following benefits:

- Increased rate of production as, with less coke, there is a greater capacity within the furnace available for iron.
- Reduction in raw material costs. A wider range of coals can be used for injection in comparison to cokemaking. In addition, a reduced demand on the cokemaking process may allow more cost-effective coking blends to be used.
- Reduction in emissions from the cokemaking process.
- Extension of coke oven battery life.

Along with the benefits of reducing the coke rate the use of auxiliary reducing agents provides greater flexibility in blast furnace operations as injection rates can be modified quickly in response to changing conditions (Carpenter, 2006). The use of pulverised coal also increases the hydrogen content in the raceway, with the benefit that hydrogen acts as a reducing agent (see section 2.4).

2.4 Chemical reactions and conditions in the blast furnace

This section details the chemical reactions and conditions within the blast furnace that are of most relevance to this work.

The net effect of blast furnace chemical reactions is the reduction of iron oxide to iron by coke (carbon), which is oxidised to carbon dioxide. This is achieved by a series of reactions described below.

Iron oxide, in the form of haematite (Fe_2O_3) or magnetite (Fe_3O_4) in the iron ore, and subsequently wustite (FeO), is reduced to iron (Fe). The reducing agents are carbon monoxide and hydrogen present in the ascending gas as shown by reactions 2.1-2.6 (Carpenter, 2006).

$$3Fe_2O_3 + CO \rightarrow 2Fe_3O_4 + CO_2 \qquad \text{(Reaction 2.1)}$$

$$3Fe_2O_3 + H_2 \rightarrow 2Fe_3O_4 + H_2O \qquad \text{(Reaction 2.2)}$$

$$Fe_3O_4 + CO \rightarrow 3FeO + CO_2 \qquad \text{(Reaction 2.3)}$$

$$Fe_3O_4 + H_2 \rightarrow 3FeO + H_2O \qquad \text{(Reaction 2.4)}$$

$$FeO + CO \rightarrow Fe + CO_2 \qquad \text{(Reaction 2.5)}$$

$$FeO + H_2 \rightarrow Fe + H_2O \qquad \text{(Reaction 2.6)}$$
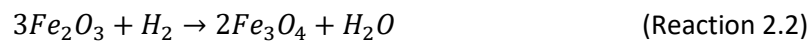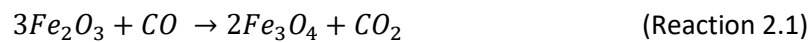
Reactions 2.1-2.6 begin in the stack section of the blast furnace (Figure 2.3) when the materials reach about 500 ^{o}C. They are exothermic therefore generate heat. The reducing gases can be regenerated by the reactions of carbon dioxide and water vapour with coke (Reactions 2.8 and 2.10). Further down the stack, when the temperature reaches 900-950 ^{o}C, direct reduction of iron oxides can occur. Although referred to as 'direct', due to the immediate consumption of coke, this is a two-step process illustrated by reactions 2.7-2.9. The iron oxides have an approximate stoichiometry of 2 iron atoms to 1 oxygen atom, they initially react with carbon monoxide to produce carbon dioxide, which is immediately

consumed by reaction with coke (carbon). Overall, this is endothermic, i.e. consumes heat energy (Geerdes *et al.*, 2009).

$$2\ FeO_{0.5} + CO\ \rightarrow 2\ Fe +\ CO_2 \qquad \text{(Reaction 2.7)}$$

$$+\qquad C +\ CO_2\ \rightarrow 2CO \qquad \text{(Reaction 2.8)}$$

$$\text{Total:}\ \ 2\ FeO_{0.5} + C\ \rightarrow 2\ Fe + CO \qquad \text{(Reaction 2.9)}$$
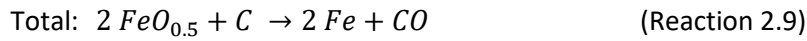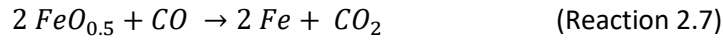
Lower down the furnace, in the cohesive zone, the iron ore begins to soften at around 1100 °C. Below this is the fluid zone in which temperatures are around 1500 °C and the iron ore has melted further. Below the fluid zone are the raceway zones, where the hot, oxygen-enriched blast enters the furnace at around 1100 °C and 180-250 m/s, with 21-25 % oxygen (or even higher at high coal injection rates) (Geerdes *et al.*, 2009).

Combustion of coke (Reaction 2.10) (exothermic) with blast oxygen in the raceway creates temperatures of around 2200 °C, making the raceway the hottest part of the furnace. Due to the abundance of coke the carbon dioxide produced by combustion is reduced to carbon monoxide by the Boudouard (aka solution loss) reaction (Reaction 2.8). Water vapour is reduced to hydrogen (Reaction 2.11). Reactions 2.8 and 2.11 are endothermic, the heat produced by reaction 2.10 allows them to proceed. By these reactions the reducing gases are produced, which reduce iron oxide in the stack.

$$C +\ O_2\ \rightarrow\ CO_2 \qquad \text{(Reaction 2.10)}$$

$$C +\ H_2O\ \rightarrow CO +\ H_2 \qquad \text{(Reaction 2.11)}$$

When coal is injected through the tuyeres it provides an additional source of carbon, which also undergoes Reactions 2.8 and 2.9. It is also a source of hydrogen therefore the quantity of reducing gases is increased.

The injected coal particles experience heating rates of 10^5-10^6 K/s, pressure of around 0.5 MPa and a turbulent environment within the raceway. The distance from the tuyere opening to the back of the raceway is 0.7-2.0 m and the particles have a residence time of 10-40 ms within the raceway (Carpenter, 2006).

There are more chemical reactions and processes occurring within the blast furnace, such as slag forming reactions, which are not detailed here.

2.5 Limitations of blast furnace coal injection

The use of blast furnace coal injection is beneficial as described in sections 2.3 and 2.4, but there are factors that limit the extent to which it can be used. When high rates of coal injection are employed it can lead to issues that adversely affect the blast furnace process.

A particularly important aspect of stable blast furnace operation is permeability; this describes the ability of gases to flow up the furnace and molten liquids to permeate downwards. Stable blast furnace operation depends upon good permeability and an evenly distributed flow. In turn, productivity depends on stability. The factors limiting coal injection are often linked to permeability requirements as discussed below. Information below is from Carpenter (2006):

Coal burnout – Incomplete combustion of coals results in char, which can accumulate in the coke bed outside the raceway, reducing permeability. Char may also be carried out of the furnace in the top gas and require removal before the gas can be recycled.

Raceway adiabatic flame temperature (RAFT) – Aka theoretical flame temperature (TFT). This is a value calculated from an energy balance of the raceway. The RAFT should be maintained within an optimum range; high enough to heat the burden and melt the ore but not so high as to cause solidification of slag. Coal injection causes a decrease in RAFT, which may need to be compensated for by increasing blast temperature or oxygen enrichment.

Oxygen enrichment – At high coal injection rates a sufficient amount of oxygen must be present in the blast and must mix sufficiently with the coal to allow combustion of the coal. Otherwise incompletely combusted char and low flame temperatures may result.

Coke quality – Low coke rates, associated with high coal injection rates, put a greater demand on the quality of coke present in the furnace. This coke experiences a higher physical load and longer residence time within the furnace. Fine material from coke degradation can reduce permeability.

Pressure differential – This is the difference between the blast pressure and the pressure at the top of the furnace. This drives the ascent of gases within the furnace. Coal injection can cause an increase in the pressure differential over the burden, leading to increased gas velocity resulting in heat loss, reduced productivity and reduced stability.

Heat flux ratio – This is the ratio of the heat capacity of the solid to the heat capacity of the gas. At high coal injection rates, the speed of burden descent decreases, lowering the heat flux ratio, which raises the temperature of the ascending gases resulting in heat loss.

Volume of molten material – Low coke rates mean a greater volume of molten material is present in the furnace. This can affect permeability and contribute to uneven distribution of gas and liquid flow. Ash from injected coal contributes directly to slag volume.

Blast furnace performance indicators are monitored to ensure coal injection does not become detrimental to blast furnace operation. However, assessment of coal performance is not a straight forward matter as it is often difficult to isolate the effect of the injection coal from other factors. Direct measurements or sampling from the raceway are very difficult due to the challenging conditions described in section 2.4. Researchers have therefore sought to replicate raceway conditions using pilot and laboratory scale test rigs to carry out research in controlled conditions and to provide an off-line means of assessing injection coals (Li *et al*., 2014 and Mathieson *et al*., 2005).

2.6 Selection of coals

Different coals have different properties as a result of the coal formation process, which has taken place over geological timescales. For example:

- Differences in the organic material deposited at the very beginning of the coal formation process.
- Differences in the conditions to which this material is exposed (for example, degree of degradation prior to burial, depth of burial, temperature experienced etc.)
- Differences in any inorganic material present within the coal.

The degree of metamorphism (or coalification) of the material as it progressively makes a transition from peat, through bituminous coal, to anthracite is referred to as the coal rank, i.e. the greater the degree of metamorphism the higher the rank (Suarez-Ruiz & Crelling, 2008). Increasing coal rank is characterised by decreasing volatile matter and moisture, and an associated increase in carbon content.

These different properties make certain coals more desirable than others; the most desirable coals command a higher price. It may be beneficial to use a blend of coals to create an injection blend with the desired characteristics. Selection of coals is important in order to optimise the cost effectiveness of coal injection. Some of the most important factors influencing the choice of coals are listed below. Information is from Greenslade & Paskins, (2014):

Experience

Experience of injecting a coal on plant will ultimately decide whether that coal is deemed suitable for PCI or not. Positive experiences, including those from other plants, will lead to a coal being favoured for selection. It is likely that new coals will be trialled on plant to assess their performance.

Strategic factors

Cost – As a key aim is to reduce the overall cost of iron production, the cost of coals is a key factor in selection.

Supplier – The supplying company must have the ability to reliably supply coal in the required quantities. Where the coal is from may have implications in terms of stock levels and logistics. The integrity and ethics of the supplying company may also be considered.

Technical factors

Replacement ratio (RR) – This is an estimate of how many kilograms of coal are required to replace one kilogram of blast furnace coke. The replacement ratio of a coal can be calculated using Equation 2.12 based on Proximate and Ultimate analyses of the coal. This formula may be adapted at each plant depending on local conditions. The replacement ratio is an important consideration as it will be more beneficial to replace as much coke as possible. High carbon content and low ash content go hand in hand with high replacement ratio.

$$RR = 2 \times C + 2.5 \times H - 2 \times H_2O - 86 + 0.9 \times A \qquad \text{(Equation 2.12)}$$

Where *RR* = replacement ratio, *C* = Ultimate carbon content of coal, *H* = Ultimate hydrogen content of coal, *H₂O* = Proximate moisture content of coal, and *A* = Proximate ash content of coal (Geerdes *et al.*, 2009).

Coal burnout – The burnout (aka conversion or combustion efficiency) of a coal, usually expressed as a percentage, is the degree to which the carbon is converted to gas, carbon monoxide or dioxide, under specific test conditions. A high burnout under conditions pertaining to the raceway is desired. Low burnout is likely to indicate that a higher proportion of unburnt char will exit the raceway, potentially contributing to operational problems as described in section 2.6. High burnout is generally associated with high volatile matter (see section 2.8.2) therefore a blast furnace plant may operate with injection coals within a specified volatile matter range. Various experimental methods of measuring burnout have been used (see section 2.7), however a standard test method has not evolved. It should be noted that there is a compromise between burnout and RR; high volatile matter tends to result in higher burnout but lower RR (due to lower carbon content).

Char reactivity – Coal char is the solid remains of the coal following partial conversion. This is distinguished from soot, which is solid material that has condensed from the gas phase following devolatilisation from the coal. During blast furnace injection coal will devolatilise, with the gaseous volatile species reacting much more quickly with available oxygen than the solid char. Following devolatilisation, char may be consumed by heterogeneous reactions; the

Boudouard reaction with carbon dioxide (Reaction 2.9), or reaction with any available oxygen from the blast (Reaction 2.8). It is generally considered desirable for char reactivity to be high so that reducing gases are rapidly created and to minimise the mass of char material exiting the raceway into the coke bed, where it may reduce permeability, or becoming entrained in the rising gases and exiting the top of the furnace, where it is not able to fulfil its purpose as a reducing agent. On the other hand, a potentially negative impact associated with the endothermic nature of char reactions has been recently proposed (Steer *et al.*, 2018) and is discussed in section 2.12.2. The reactivity of the char will be determined by a combination of the coal properties and the conversion conditions. A variety of methods have been employed by researchers to measure char reactivity, which are based on a measurement of the mass loss of a char sample against time under controlled conditions. Results may be presented as apparent reactivity (for example, unit mass per unit time) or intrinsic reactivity (for example, unit mass per unit time per unit surface area), the latter involves the necessary measurement of surface area (usually by the Brunauer–Emmett–Teller method).

Sulphur, phosphorus and alkali metal content – It is desirable for these to be low, not for combustion reasons but to avoid compromising the ironmaking process in general.

Ash content – At high injection rates the injected coal can become a significant source of ash in the blast furnace. Coals with low ash content, <10 %, are generally favoured (Carpenter, 2006). Low ash contents contribute to a higher RR.

Explosivity – Plants may have specific limits on coal explosivity to meet safety requirements. For example, the K_{st} (dust deflagration index) and limiting oxygen concentration (LOC) test.

Material Handling – This is a serious practical consideration for PCI injection, coals that are difficult to crush or have a tendency to block pipelines are not desirable. Tests such as the Hardgrove Grindability Test may be used as a guide in this respect.

A particular coal property that does not appear to attract much attention with specific regard to blast furnace injection is the thermoplastic behaviour of coal. Particles of coals that possess thermoplastic properties may swell when subjected to heat. This phenomenon is likely to impact upon the blast furnace process in various ways: For example, the increase in particle volume and potential increased likelihood of agglomeration may lead to blockages in conveying systems or to a reduction in blast furnace permeability. The decrease in char density may affect the way in which char particles are transported through the furnace and their potential to fragment. On the other hand, the increase in surface area may promote a more rapid initial burnout of the coal and an enhanced reactivity of the char particles. An improved knowledge of how the thermoplastic properties of coal influence the blast furnace process would help to inform the selection of blast furnace injection coals.

2.7 Introduction to coal devolatilisation and thermoplasticity

As described above, certain coals in the bituminous range possess thermoplastic properties enabling them to swell during heat treatment. (Coal swelling can also occur by sorption of a gas or solvent (Murata *et al*., 2008), however this review focuses on the thermal swelling of coal.) Coal thermoplasticity is vital to the blast furnace ironmaking process as it enables the manufacture of coke in coke ovens from raw coal. However, the heating conditions experienced by coal particles when injected into the tuyere of the blast furnace (described in section 2.4) are very different to those within a coke oven (Loison *et al*., 1989), therefore it is important to understand the effects of coal thermoplasticity with regard to blast furnace coal injection. Significant research has been carried out on the unrestricted swelling of individual coal particles at a variety of heating rates and pressures, which is relevant to the blast furnace coal injection process. This research (reviewed in the following sections), which includes experimental and modelling work, has improved fundamental understanding of the coal swelling process, the variations in swelling behaviour between different coal types, the effect of heating environment and the impact swelling has upon char properties.

The thermoplastic swelling of coal particles occurs within the context of coal devolatilisation. The coal devolatilisation process and the development of thermoplasticity are described below.

2.7.1   Coal devolatilisation

Coal devolatilisation is the removal of volatile material from the coal at elevated temperatures. During devolatilisation coal is transformed into three types of product (Solomon *et al.*, 1988):

- Gases, for example, methane, ethane, hydrogen, carbon dioxide and carbon monoxide.
- Tars, which are larger, complex molecules evolved as gaseous products but condensable at room temperature (Yu *et al.*, 2007).
- Char, which is the remaining solid residue.

Devolatilisation is described as the second step of combustion; preceded by evaporation of water and followed by gas-phase volatile matter oxidation and heterogeneous oxidation of the solid char (Figure 2.6) (Wu, 2005). It is therefore the defining feature of the early stages of coal combustion. In an inert atmosphere, where volatile and char materials are not oxidised, devolatilisation can be referred to as pyrolysis.
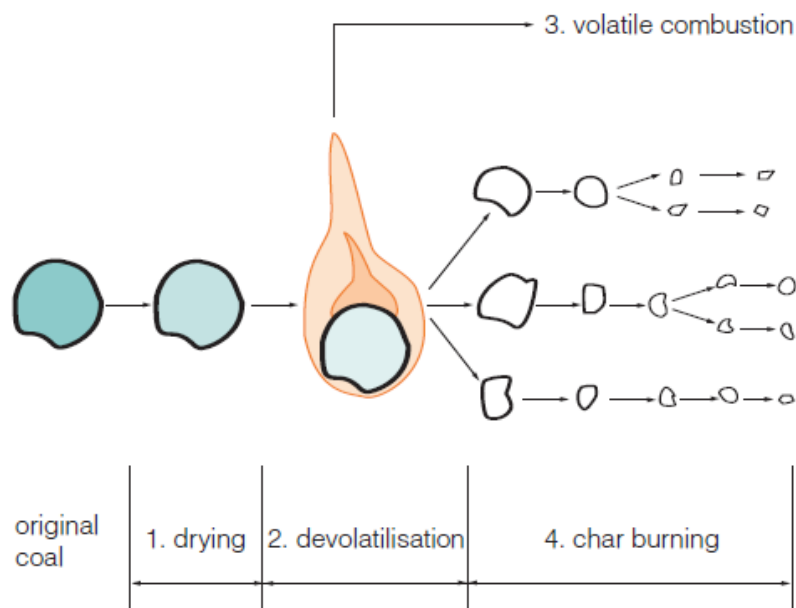
Figure 2.6: Four stages of pulverised coal particle combustion. (Wu, 2005)

Coals are described as having a volatile matter content, which is defined by the volatile matter test (ISO 562:2010), part of the Proximate Analysis of a coal (ISO 17246). The volatile matter test essentially involves heating 1 g of coal, sieved to <212 µm, to 900 °C in an inert atmosphere and holding at 900 °C for 7 minutes in a crucible with a lid. The mass loss associated with this process is defined as the volatile matter content of the coal (after taking account of any mass loss due to water evaporation). This is an empirical test, i.e. the result is imposed on the coal by the test conditions. Much work has been carried out to investigate the effect of heating conditions on coal devolatilisation (Alonso *et al.*, 1999; Hayhurst & Lawrence, 1995; Ross *et al.*, 2000; Tian *et al.*, 2016 and Wall *et al.*, 2002).

The precise mechanism of devolatilisation is complex and involves many reactions, which have been summarised by authors (Saxena, 1990; Solomon *et al.*, 1988; Solomon *et al.*, 1992 and Yu *et al.*, 2007). Saxena, (1990), stated that devolatilisation commences with the rupturing of the weakest C-C bonds, which are those at the bridges between ring systems, particularly aromatic ring systems. A certain amount of energy is required to break these bonds therefore devolatilisation begins at around 400 °C. As the temperature increases the following types of reaction take place in stages (Saxena, 1990): Cracking reactions (Reaction 2.13) produce highly reactive free radical species, which can combine to produce gaseous molecules (Reactions 2.14 and 2.15). Hydrogen free radicals may also stabilise larger hydrocarbon free radical species to produce tar molecules (Reaction 2.16). Condensation reactions (Reactions 2.17 and 2.18) create cross-links between large groups to create the char structure with the elimination of water or hydrogen molecules. Oxides of carbon are produced from carboxyl groups by Reaction 2.19.

Cracking: $\qquad R - CH_2 - R' \rightarrow R - CH_2 \cdot + \cdot R'$ $\qquad$ (Reaction 2.13)

Saturation: $\qquad \cdot CH_3 + H \cdot \rightarrow CH_4$ $\qquad$ (Reaction 2.14)

$\qquad \cdot OH + H \cdot \rightarrow H_2O$ $\qquad$ (Reaction 2.15)

Tar production: $\qquad R - CH_2 \cdot + H \cdot \rightarrow R - CH_3$ $\qquad$ (Reaction 2.16)

Condensation: $\qquad R - OH + H - R' \rightarrow R - R' + H_2O$ (Reaction 2.17)

$$R - H + H - R' \rightarrow R - R' + H_2 \qquad \text{(Reaction 2.18)}$$

Oxide formation: $R - COOH \rightarrow R - H + CO_2$ \qquad (Reaction 2.19)
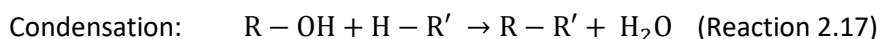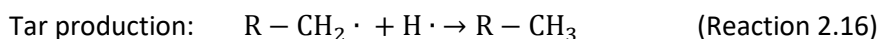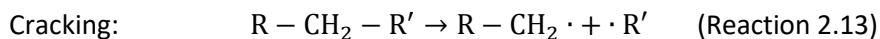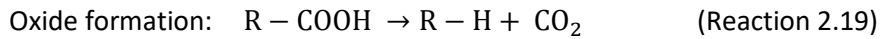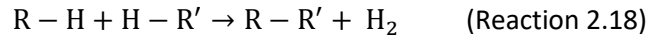
2.7.2 Coal thermoplasticity

During devolatilisation certain coals may develop thermoplasticity, i.e. the material becomes pliable due to the effect of heat. These coals may be referred to as softening coals or caking coals; during heating they pass through a thermoplastic temperature range, which is defined by a softening temperature at which plasticity develops and a re-solidification temperature at which the structure becomes solid once more. The thermoplastic temperature range and the extent of plasticity is dependent upon the coal type and the heating conditions. Features of thermoplasticity include (Coetzee at al., 2014):

- Softening
- Fusing
- Porosity development
- Swelling
- Shrinking
- Re-solidification

The concept of the metaplast is commonly used to explain the thermoplastic behaviour of softening coals. The metaplast is a metastable plastic intermediate (Saxena, 1990), which facilitates thermoplastic behaviour. It is formed from the reactive coal macerals[*] by condensation reactions to produce gases (for example, carbon dioxide and water vapour) and larger molecules of various sizes in a liquid phase (Yu *et al.*, 2007), which collectively constitute the metaplast. During the thermoplastic stage the coal can be considered to consist of metaplast, solid char (including mineral matter), and gases, which may be entrapped within the structure prior to release. The metaplast may be consumed either by evaporation of the lighter molecules to yield tar, by reactions to yield gases, or by cross-linking

---

[*] Macerals are the organic components of coal, they are the fossilised remains of different types of organic plant material. They are differentiated by the percentage reflectance of light from a polished surface of the coal sample during petrographic analysis. An introduction to coal macerals is given in Appendix A.

reactions to yield solid char. In this way the coal/char structure re-solidifies with progressive heating. Figure 2.7 illustrates the role of the metaplast in the pyrolysis process of softening coal.
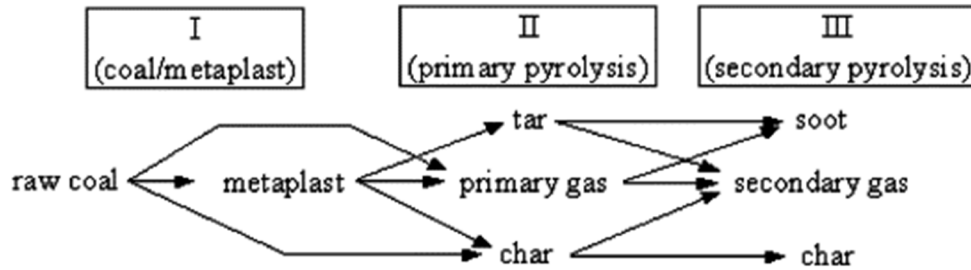
Figure 2.7: Schematic illustration of pyrolysis process of softening coal (Yu *et al.*, 2007).

Several standard laboratory tests have been developed to quantify the thermoplastic behaviour of coals. These are empirical tests developed for the analysis of coking coals. Therefore, the experimental conditions, for example a heating rate of typically 3 K/min, are linked to the cokemaking process. These tests include:

- The free swelling index (FSI), also known as crucible swelling number (CSN) – Subjectively measuring the change in volume of the ground coal after heating in a crucible and comparing the resulting coal cake with a series of standard images (ISO 501:2012).
- Gieseler plastometer test – Measuring coal fluidity as defined by the rate of revolution of a stirrer at constant torque, immersed in a packed volume of ground coal in a crucible during heating (ISO 10329:2008(E)). The rate of revolution is measured in terms of dial divisions per minute (ddpm).
- Ruhr dilatometer test – Measuring contraction and expansion of a 'pencil' (compacted cylinder of ground coal) as it is heated in a cylindrical retort (ISO 23873:2010).
- Caking index – Measuring the resistance to breakage of a cake of coal formed between the subject coal and an anthracite (ISO 15585:2006).

2.8 The coal particle swelling process

The swelling of individual, unconstrained, coal particles at high heating rates and pressure is of particular relevance to the blast furnace coal injection process. Below, the process of coal particle thermal swelling is described, as observed by experimental studies and predicted by modelling work.

2.8.1   Experimental studies

The swelling process is driven by the generation of gaseous volatile matter within a softened coal structure that can undergo plastic deformation. Thermal decomposition of the coal structure produces gaseous volatile matter (Reactions 2.12-2.14), which can become trapped within the coal structure. Evidence is seen in the form of pores, which remain in the char structure after re-solidification (Coetzee at al., 2014). Swelling is a common feature of the early stages of devolatilisation of a bituminous coal; Tsai & Scaroni, (1987), found that swelling began as soon as the vitrinite macerals softened and could begin with very little or no mass loss.

Measurement of swelling is usually reported in terms of a swelling ratio (SR), this is the size of the swollen coal particle divided by the original size of the particle as shown by Equation 2.20. The particle size is determined by some experimental measurement, which may be by volume (Coetzee *et al.*, 2014; Fu *et al.*, 2007), diameter (Strevoz *et al.*, 2005; Yu *et al.*, 2003) or area (Coetzee *et al.*, 2014 and Gao *et al.*, 1997).

$$Swelling\ Ratio\ (SR) = \frac{Size\ of\ swolen\ particle}{Original\ size\ of\ particle} \qquad \text{(Equation 2.20)}$$

A typical pattern of swelling for a coal particle is to increase in size to a maximum swelling ratio before shrinking to a final constant swelling ratio during re-solidification as shown in the example in Figure 2.8.
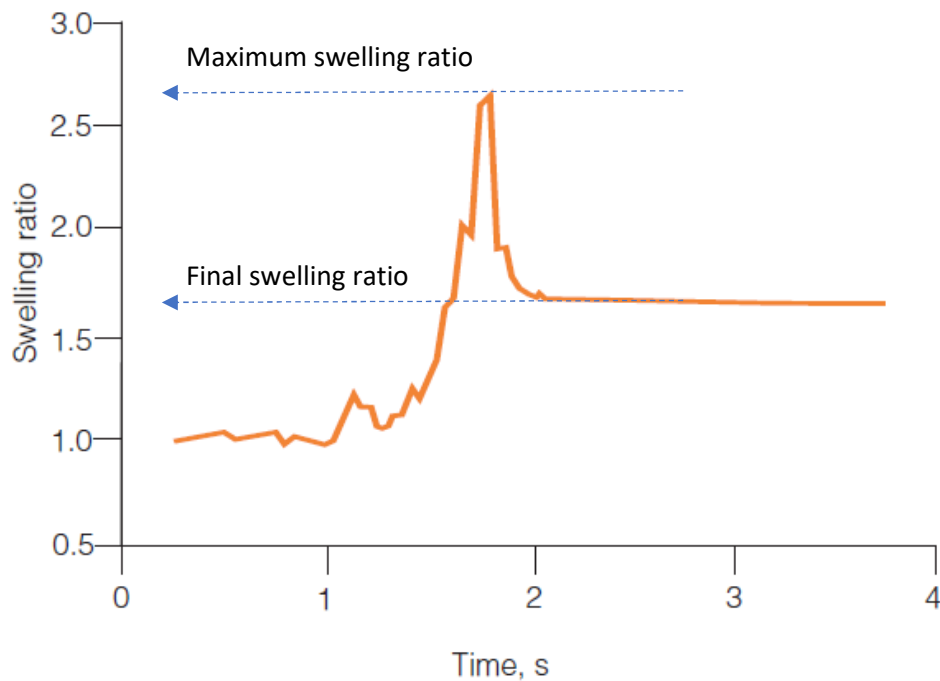
Figure 2.8 Changes in swelling ratio of a coal particle during heating observed by Yu *et al.*, (2003).

Tsai & Scaroni, (1987), observed that maximum swelling occurred during active devolatilisation, i.e. a significant amount of mass loss occurred after the particles passed through their maximum swelling ratio. The degree of shrinkage after maximum swelling was proportional to the extent of maximum swelling, i.e. the greater the size increase the greater the subsequent decrease. A small degree of shrinkage prior to swelling has also been noticed on occasions (Strevoz *et al.*, 2005), which has been attributed to closure of pores or deformation upon initial softening.

It has been observed that the transition to maximum swelling ratio and then to final swelling ratio occurs via a series of oscillations in particle size. Researchers using the Single Particle Reactor (Yu *et al.*, 2002 and 2003) observed this oscillation phenomenon (Figure 2.9). This behaviour was explained in terms of bubble formation and rupture; bubbles of accumulating gaseous volatile matter expand the particle, then rupture, releasing the volatile matter and causing rapid shrinkage before re-forming. This process may repeat numerous times before re-solidification of the particle. Highly swollen particles appeared almost transparent, implying that the outer fluid shell is very thin, and the particle is

highly porous. It is suggested that the wall strength of these swollen particles determines how large they can swell, and that high fluidity and low surface tension will therefore inhibit swelling by enabling more frequent bubble ruptures.

(a)
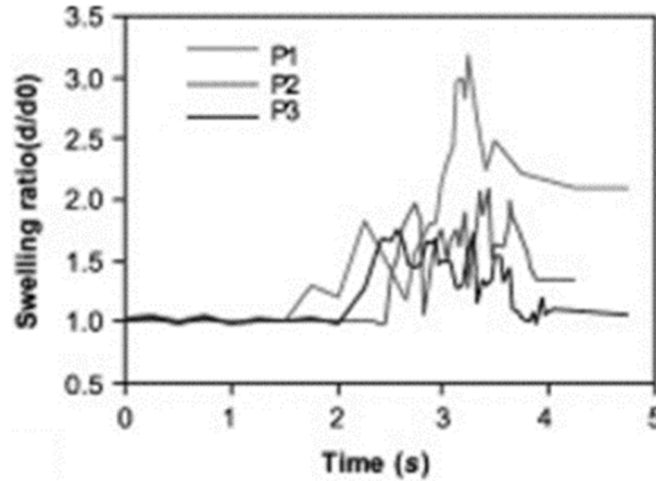
(b)
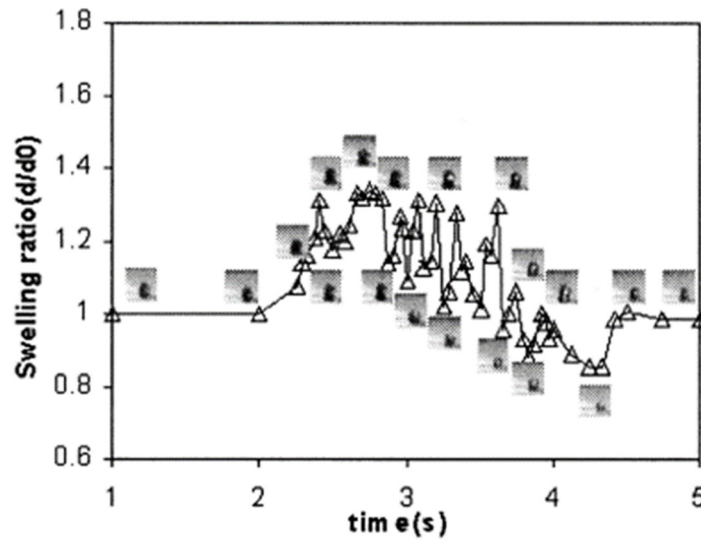
Figure 2.9: Changes in swelling ratio of individual particles during heating in the Single Particle Reactor illustrating oscillating swelling ratio as reported by (a) Yu *et al*., (2003), and (b) Yu *et al*., (2002).

Research revealing transient changes in particle size during the swelling process, i.e. a maximum swelling ratio and the oscillating nature of particle size (Gao *et al*, 1997; Yu *et al*., 2002 and 2003), demonstrates that analysis of char material after

a final swelling ratio has been reached cannot fully describe the transient physical changes that occur during swelling.

Yoshizawa *et al*., (2006), used a drop tube furnace to measure the swelling behaviour of eleven coals at a range of seven furnace temperatures between 400 °C and 1500 °C (Figure 2.27). The authors mentioned that one coal showed apparent 'resulting' behaviour at the higher temperatures, having also shown a peak in swelling at a furnace temperature of 800 °C (the peak at 800 °C was typical of coals in the study). It was also noted that this was not a continuous measurement, however it would seem, based on the evidence of continuous measurements by other researchers, that coal particles exhibit one maximum peak in swelling and that re-swelling of char particles is not a genuine phenomenon.

2.8.2　Modelling Studies

Progress has been made in modelling the swelling behaviour of coal particles. Yu *et al*., (2002), developed a model of the swelling process that predicted the heterogeneous nature of char structures present within a coal sample. The swelling process is responsible for the development of the physical char structure. Given that a variety of char structures exist within the same coal sample under the same heating conditions, there must be differences in the ways in which different particles swell.

A multiple bubble model was used by Yu *et al*. and transient swelling ratios could be calculated. Bubble coalescence was not considered. Coal Proximate and Ultimate analysis data were the initial inputs to the model to differentiate between coal types. The model proposed a mechanism of char structure evolution (Figure 2.10) whereby dense chars develop into cenospheres as volatile matter diffuses into and enlarges macro-pores, this creates a foam-type structure with many separate pores, the enlargement of central pores and the rupture of small pores at the particle surface causes the char to become progressively more cenosphere-like in structure. The final char structure depends upon the point in this evolution at which the particle re-solidifies.
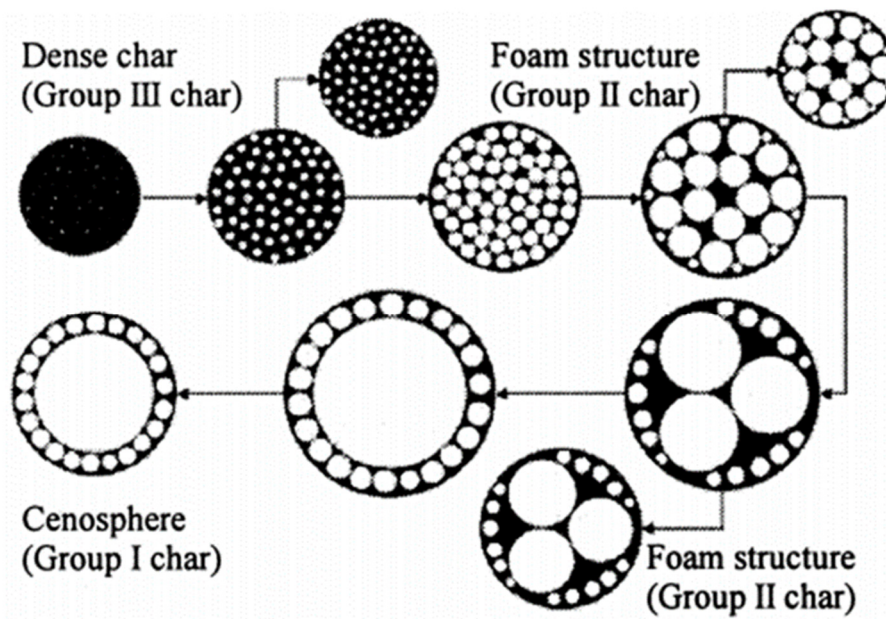
Figure 2.10: Char structure evolution mechanism proposed by Yu *et al*., (2002).

The final char structure was calculated by Yu *et al*. using a combination of the porosity and number of bubbles after devolatilisation, which were outputs of the model. For example, chars with porosity >80 % and one bubble were defined as cenospheres, whereas chars with porosity <50 % and a large number of bubbles were defined as dense chars. The model was applied to different density fractions of a coal sample and char types were predicted for each fraction. For example, the heaviest particles were predicted to be dense chars, the lightest particles were predicted to be cenospheres and an intermediate density fraction was predicted to produce foam-like chars. The distribution of char structures throughout the whole coal sample was calculated based on the mass of each density fraction. Modelled results were compared with image analysis results of drop tube furnace chars and there was good agreement in terms of predicting final swelling ratio, porosity and char type distribution.

Yang *et al*., (2014), produced a very detailed piece of modelling work to model the transient swelling behaviours of coal particles. They built on previous modelling work by combining a multiple bubble model with a single bubble model and considered the effect of internal particle pressure in what they defined as the pre-plastic phase. In the early stages of devolatilisation, before the development of

plasticity, internal pressure builds up within the particle due to volatile matter evolution. The internal pressure at this early stage of the process was found to be an important consideration in modelling the swelling behaviours of coal particles. The work aimed to model the process of bubble formation, coalescence and rupture. Three stages of devolatilisation were considered: the pre-plastic stage, the plastic stage and the re-solidified stage:

Pre-plastic stage – The particle is assumed to be spherical and isotropic with no fragmentation or thermoplastic deformation occurring during pyrolysis. The raw coal particle contains a very small amount of porosity.

Plastic stage – At the beginning of the plastic stage macro-pore structure collapses due to the flow of metaplast and the pore volume is converted to bubbles. The particle is assumed to contain one central bubble with many surrounding bubbles. This structure is assumed based on the establishment of a pressure gradient within the particle in the pre-plastic state whereby the pressure is greatest at the centre of the particle, which favours the growth of pores in the core of the particle and the closure of pores to form bubbles nearer the edge. The movement of gases towards the centre is favoured whilst the metaplastic material is pushed away from the centre. As plasticity develops this disrupts the pressure gradient and the internal pressure becomes uniform.

Re-solidified stage. The particle is assumed to have a constant size in the re-solidified state.

During the plastic stage the formation and growth of bubbles is modelled. Firstly, the viscosity of the coal material is calculated based on the metaplast content i.e. the greater the metaplast content the lower the viscosity. The formation of the central bubble is considered, as are the radius and number of surrounding bubbles, the growth rate of bubbles, the change in bubble number and the rupture rate of surrounding bubbles. The single bubble model is applied as the number of bubbles approaches 1. During the single bubble stage, the bubble ruptures when the internal pressure reaches a specified value and releases volatile matter. It is assumed that the shell closes and shrinks under surface tension to form a new bubble, at environmental pressure, in which further volatile

matter then accumulates and the bubble swells again. The shrinkage of the particle following maximum swelling is described in terms of frequent ruptures of the central bubble followed by rapid shrinkage due to surface tension, with insufficient volatile matter generation to swell the bubble in between shrinkages.

The results of the modelling work were compared with literature results. Predicted yields of char, gas and tar agreed well with experimental values from literature, helping to validate the model. Calculated final swelling ratios of eight high-volatile bituminous coals correlated reasonably well with experimental values over the range of 0.9-2.1 (experimental final swelling ratio) (Figure 2.11), although there was a greater degree of deviation from the experimental results at the higher end of the range. Two experimental values in particular appeared to be significantly lower than the calculated values. The degree of scatter in the results shows that it is difficult to precisely predict the differences in swelling ratio between different coal types.
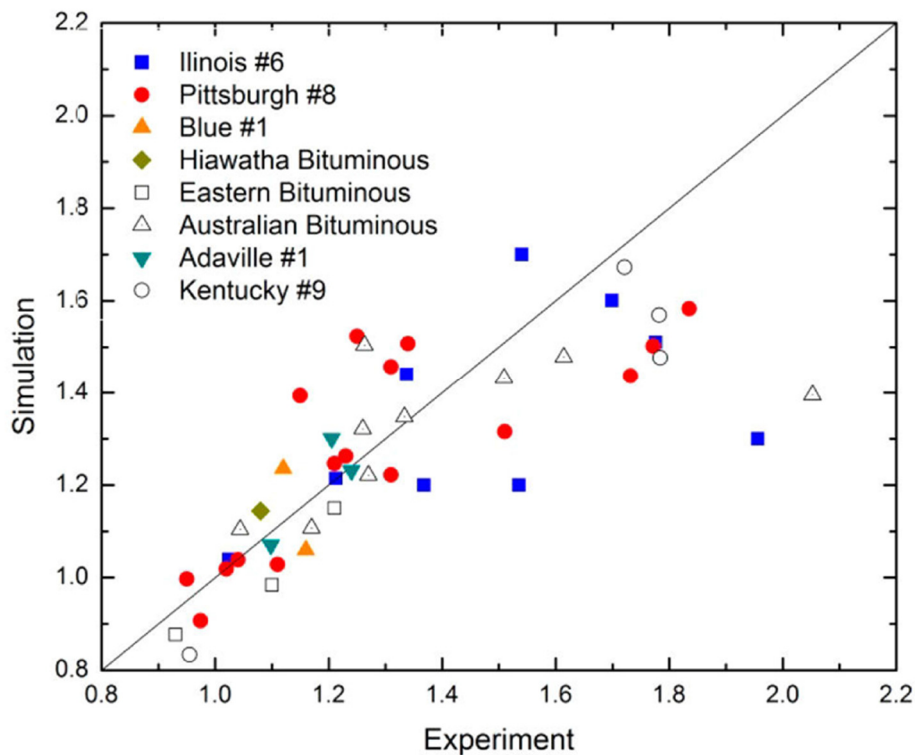
Figure 2.11: Comparison of the predicted final swelling ratio of coal particle with experimental data from literature. (Yang *et al.*, 2014)

The transient maximum swelling ratio is predicted by the model and compared with some experimental data (Figure 2.12). Although most of the experimental data points agree with the calculated values there are no experimental data points available at the point of maximum swelling ratio predicted by the model therefore it is difficult to know how accurate the prediction of transient maximum swelling ratio is.
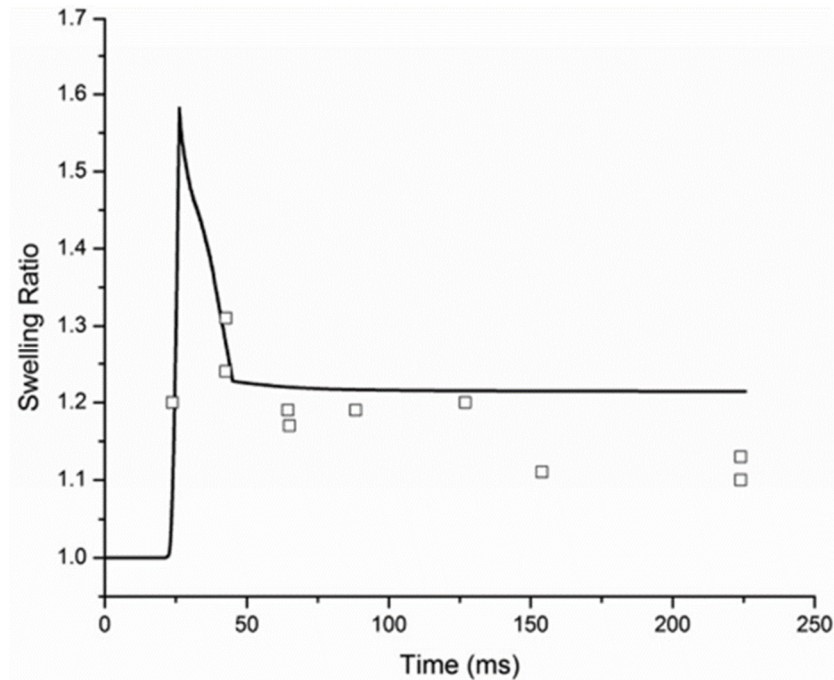
Figure 2.12: Comparison of the predicted change in swelling ratio of Illinois No. 6 bituminous coal (solid line) with experimental results (squares). (Yang *et al.*, 2014)

The average internal pressure within the particle is calculated to increase sharply due to volatile matter generation (Figure 2.13). This happens as the swelling ratio starts to increase, however average internal pressure peaks before swelling ratio peaks, then sharply decreases again to a very low value at the point where maximum swelling ratio is attained. After the peak in internal pressure the particle is still able to continue swelling so long as the internal pressure is greater than the external pressure. The particle swelling ratio begins to decrease when the internal pressure becomes sufficiently low.
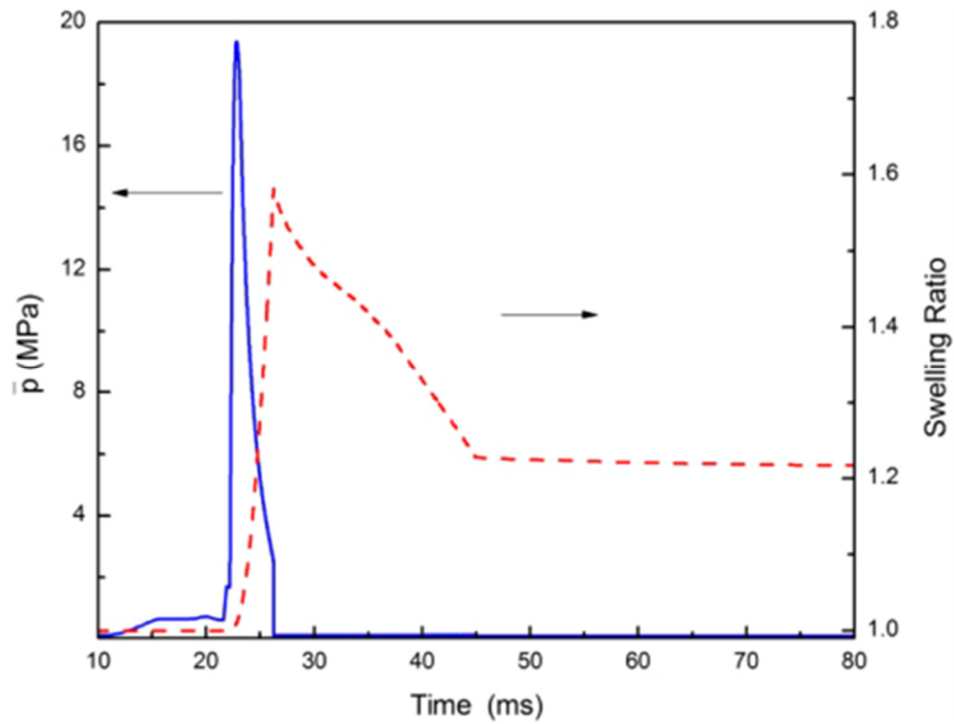
Figure 2.13: Predicted changes in average internal pressure and swelling ratio for Illinois No. 6 bituminous coal particles during the Fletcher experiment referenced within the source. (Yang *et al*., 2014)

The changes in the number of bubbles and the central bubble size were calculated. At the beginning of the plastic stage the number of bubbles is at its highest (Figure 2.14) and the expansion of surrounding bubbles contributes most to the early increase in swelling ratio. However, the number of bubbles rapidly decreases as bubbles rupture at the surface and coalesce with the central bubble, the radius of the central bubble increases rapidly and becomes the dominant factor in the swelling of the particle to maximum swelling ratio.
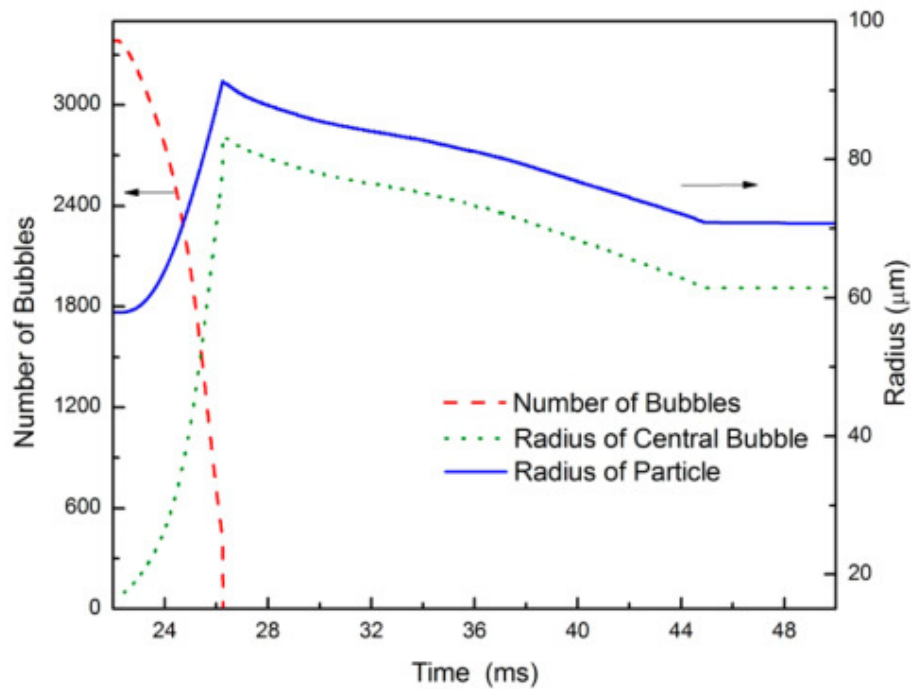
Figure 2.14: Predicted changes in the number of bubbles, central bubble size, and particle size for Illinois No. 6 bituminous coal particles in the Fletcher experiment referenced within the source. (Yang *et al*., 2014)

2.8.3 Summary of the coal particle swelling process

The process of thermal swelling of discrete coal particles is caused by the generation of gaseous volatile matter, specifically the light gases, to form bubbles within a softened coal structure. An increase in internal pressure drives the expansion of the bubbles and therefore the swelling of the particle. The heterogeneity of char structures observed within the same sample is explained in terms of the structure of the particle at the point of re-solidification; some char particles have a multiple bubble structure whereas others have progressed to a cenosphere-like structure in which many of the bubbles have coalesced to form one main central bubble. The composition of a particle in terms of maceral content determines how far in the process that particle progress before re-solidification. The growth and rupture of bubbles, in particular a large central bubble, explains the transient maximum swelling ratio that particles pass through before shrinking to a final swelling ratio, and the oscillations in swelling ratio

34

observed as a particle swells and shrinks. Oscillations in swelling ratio are caused by repeated bubble growth and rupture. The maximum swelling ratio represents the point at which the rate of evolution of light gases begins to decrease and therefore the internal pressure is no longer sufficient to drive continued bubble expansion. (The rate of evolution of gas composed of heavier tar molecules increases at this point, so the overall rate of mass loss is increasing even though the rate of light gas evolution is decreasing.) At this stage bubble rupture causes the shrinkage of particles. A final swelling ratio is reached when the particle re-solidifies.

It should be noted that swelling is not the only process that results in changes in coal particle size during heating. Fragmentation causes a reduction in particle size whilst agglomeration results in a particle size increase. Chen *et al.*, (2007), reported swelling, fragmentation and agglomeration processes all occurring during their drop tube furnace studies. Researchers working on this subject must be careful not to mistake agglomeration for swelling.

There is a lack of experimental data regarding the transient swelling ratios of particles heated at high heating rates and pressures, against which model predictions can be verified.

It has been suggested that the surface tension of the plastic coal particle is likely to influence the rate of bubble rupture and therefore the swelling properties of the particle, however no method has been found to directly measure this surface tension.

2.9 Methods used to investigate coal particle swelling

In this section the experimental methods used to measure coal particle swelling are reviewed. An important distinction is whether the method allows the transient swelling ratio to be measured or the final swelling ratio. Therefore, the methods are divided into two categories: Those enabling measurement of final swelling ratio only and those enabling the measurement of transient swelling ratios.

2.9.1   Measurement of final swelling ratio only

A variety of furnaces have been used to measure the final swelling ratio of coal particles. These experiments involve the measurement of particle size of the raw coal before heat treatment and measurement of the particle size of the quenched char after heat treatment. The final swelling ratio can be defined as the swelling ratio at the end of the experimental procedure. Pieces of apparatus such as drop tube furnaces (DTF) (Gale *et al.*, 1995 and Yu *et al.*, 2002), a flat flame burner (Gale *et al.*, 1995) and laminar entrained flow reactors (similar to a DTF) (Fletcher, 1993) have been used for this purpose.

These methods allow measurement of swelling under high heating rates (for example, 10^4 K/s has been estimated for the DTF) and the processes generally produce quantities of char allowing various analytical procedures to be performed on them. The ability to vary residence time within the furnaces can enable some investigation of the progressive nature of the swelling process (Tsai & Scaroni, 1987), however the transient swelling behaviours cannot be continuously observed. The fact that coal particles generally pass through their maximum swelling ratio early in the devolatilisation process means that very short residence times are necessary in these furnaces to sample particles prior to maximum swelling.

2.9.2   Measurement of transient swelling ratios

Methods of analysis allowing the continuous observation of transient coal particle swelling processes generally take the form of a particle placed within some form of heating apparatus and being observed by a camera.

An electric furnace (Fu *et al.*, 2007), an infra-red furnace (Toishi *et al.*, 2013) and a coal ash fusibility furnace (Coetzee *et al.*, 2014) have all been used for low heating rate work (3-10 K/min) using relatively large particle sizes (2-20 mm).

The Single Particle Reactor (SPR), a captive piece of equipment, has been used extensively for coal particle swelling research at higher heating rates, higher pressures and using smaller particle sizes (Strevoz *et al.*, 2005; Yu *et al.*, 2002 and Yu *et al.*, 2003). Individual particles are heated by means of a platinum strip whilst

being monitored by video camera. Heating rates reported in open literature are between 10 K/s and 300 K/s (Yu *et al.*, 2003). The SPR has been modified to enable the swelling of particles under elevated pressures to be measured (Strevoz *et al.*, 2005). Particle sizes used in these pieces of work are 63-90 μm (where stated).

Work has been carried out using carbon dioxide laser to heat coal particles (Gao *et al.*, 1997). This method allows a higher maximum heating rate than the SPR of up to 120 000 K/s, whilst a particle size of 100-355 μm was used. The heating rate is not constant throughout the procedure as illustrated in Figure 2.16.

These methods enable a greater insight into the process of coal swelling and have revealed the transient behaviours described previously. They enable the swelling of a single particle to be optically observed in real time and the maximum swelling ratio to be measured. The frequency and amplitude of bubble oscillations has also been measured by fast fourier transform analysis (Strevoz *et al.*, 2005). Heating rates are not as high as in the furnaces described in section 2.9.1, meanwhile the feature of analysing individual particles means that there is very little char material produced for further analysis. Due to the heterogeneity of coal it would also be necessary to repeat the test a number of times in order to obtain a representative sample average. The smallest particle sizes to have been used and reported in the open literature are 63-90 μm (Yu *et al.*, 2002 and 2003).

The methods described in section 2.9 are listed in Table 2.1 (in chronological order with most recent first) along with some features of the work.

Reference	Heating Apparatus	Heating Rate	Peak Temp	Pressure	Gaseous Environment	Swelling Measurement Method	Measurement of Maximum swelling ratio?	No. of Coals	Particle Size	Density separation?
Coetzee *et al.*, (2014)	Coal ash fusibility furnace	7 K/min	700 °C (Furnace temp)	0.1 Mpa	Nitrogen	Volume ratios by XCT and mercury submersion and area ratios by image analysis	Yes (by continuous imaging)	3	16 - 20 mm	No
Toishi *et al.*, (2013)	Infrared furnace equipped with camera	10 K/min	700 °C Max. (Furnace temp.)	0.1 Mpa	Nitrogen	Area ratio by image analysis	Yes (by continuous imaging)	2	2 mm	No
Fu *et al.*, (2007)	Electric furnace equipped with camera	3 K/min	1000 °C (Furnace temp.)	0.1 MPa	Argon	Volume ratio by calculation from image analysis	Yes (by continuous imaging)	2	2.0 x 1.9 mm - 20.0 x 10.8 mm	No
Strevoz *et al.*, (2005)	Pressurised Single Particle Reactor	200 K/s	1000 °C (Furnace temp.)	0.1 - 5.0 MPa	Nitrogen	Diameter ratio by measurement from image analysis	Yes (by continuous imaging)	1	Not specified	Yes
Yu *et al.*, (2003)	Single Particle Reactor	10 - 200 K/s	Assumed 1000 °C (furnace temp.) based on Strevoz *et al.*, (2005)	0.1 MPa	Assumed to be nitrogen based on Strevoz *et al.*, (2005)	Diameter ratio by measurement from image analysis	Yes (by continuous imaging)	2	63 - 90 µm	Yes

Yu et al., (2002)	Drop Tube Furnace (DTF) and Single Particle Reactor (SPR)	100 K/s in SPR, not specified for DTF	1300 °C in DTF (furnace temp.), assumed 1000 °C in SPR (furnace temp.) based on Strevoz et al., (2005)	0.1 MPa	Assumed to be nitrogen in SPR based on Strevoz et al., (2005), assumed to be nitrogen in DTF	Diameter ratio by measurement from image analysis (SPR) and from Malvern laser sizer (DTF)	Yes (in SPR by continuous imaging)	2	63 - 90 µm	Yes
Gao et al., (1997)	Particle heated directly by CO2 laser	2600 - 12000 K/s	460 - 690 °C (calculated max. particle temp.)	0.1 MPa	Nitrogen	Area ratio by image analysis	Yes (by continuous imaging)	3	100 - 355 µm	No
Gale et al., (1995)	A High Pressure Controlled Profile Drop Tube Reactor (HPCP) and a Flat Flame Burner (FFB)	2×10^4 -7 x 10^4 K/s	Aprox 1000 - 1600 K (calculated particle temperatures)	0.1 MPa	100 % nitrogen or helium in HPCP. Vitiated air in FFB (18 % H_2O, 4 % O_2, 7.5 % CO_2 and 70.5 % N_2)	Measurement of bulk density (tap density technique) combined with measurement of mass loss (Ti tracer technique) to estimate particle size before and after processing	No	2	63 - 75 µm	No

Fletcher, (1993)	Two laminar, entrained flow reactors. One electrically heated, the other heated by a flat flame.	10^4 K/s in electric reactor. 10^5 K/s in flat flame reactor	1200 K (Calculated max. particle temp.)	0.1 MPa	100 % N2 in electric reactor. 6 - 12 molar % oxygen in flat flame reactor	Measurement of bulk density (tap density technique) combined with measurement of mass loss (mineral tracer technique using silica, aluminium, titanium, and total ash) to estimate particle size before and after processing	No	5	106 - 125 µm	No
Lee *et al.*, (1991)	A High Pressure Entrained Flow Furnace (HEF) and an Atmospheric Pressure Entrained Flow Furnace (AEF)	10^4 K/s	1189 K (Furnace temp.)	0.1 MPa in AEF. 0.8 - 3.73 MPa in HEF	N2	Optical microscopy combined with image analysis	No	1	Mean diameter 62 µm	No
Tsai & Scaroni, (1987)	Entrained flow reactor	Not reported	1200 K (Furnace and	0.1 MPa	Pyrolysis and combustion	Measurement of bulk density (tap density technique)	Yes (by quenching at a	1	Mean diameter 112 µm	Yes

			secondary gas temp.)			combined with measurement of mass loss (ash tracer technique) to estimate particle size before and after processing	variety of residence times)			

Table 2.1: Comparison of the experimental techniques used in the cited literature to measure coal particle swelling.

2.10　The influence of coal properties on swelling ratio

In this section the influence of coal properties (particle size, volatile matter, particle density and standard thermoplastic indices) in determining the swelling of coal particles is reviewed.

2.10.1　Particle size

A number of studies have investigated the effect of particle size on final swelling ratio and some information is available regarding the effect of particle size on transient coal swelling behaviour. However, the latter aspect is not comprehensively covered in the published literature for the range of particle sizes used in this project.

The final swelling ratio of coal particles has been reported to increase with decreasing particle size (Yu *et al*., 2005). Particle size fractions were separated by sieving and subjected heat treatment in a drop tube furnace. The results were attributed to a greater concentration of vitrinite in the smaller particles. This highlights a complication when investigating particle size effects, which is that sieved size fractions tend to differ in terms of their composition. Therefore, the underlying reason for the different swelling behaviours can be the composition of the particles rather than their size. Steer *et al*., (2015b), crushed equivalent samples of five coal types to three different size specifications, so that the three samples of each coal would contain the same overall composition. The results showed a trend of greater swelling with smaller size specifications.

Fu *et al*., (2007), used pieces of coal much greater in size than those used in this current work; the smallest pieces used by Fu *et al*., were 2.0 mm diameter by 1.9 mm height. The larger the piece of coal the greater the maximum swelling ratio and final swelling ratio (Figure 2.15). This pattern was consistent between two coal types; however, it may not be applicable to the range of sizes associated with PCI and the maximum heating rate used by Fu *et al*., was 3 K/min i.e. much slower than the heating rates associated with PCI.
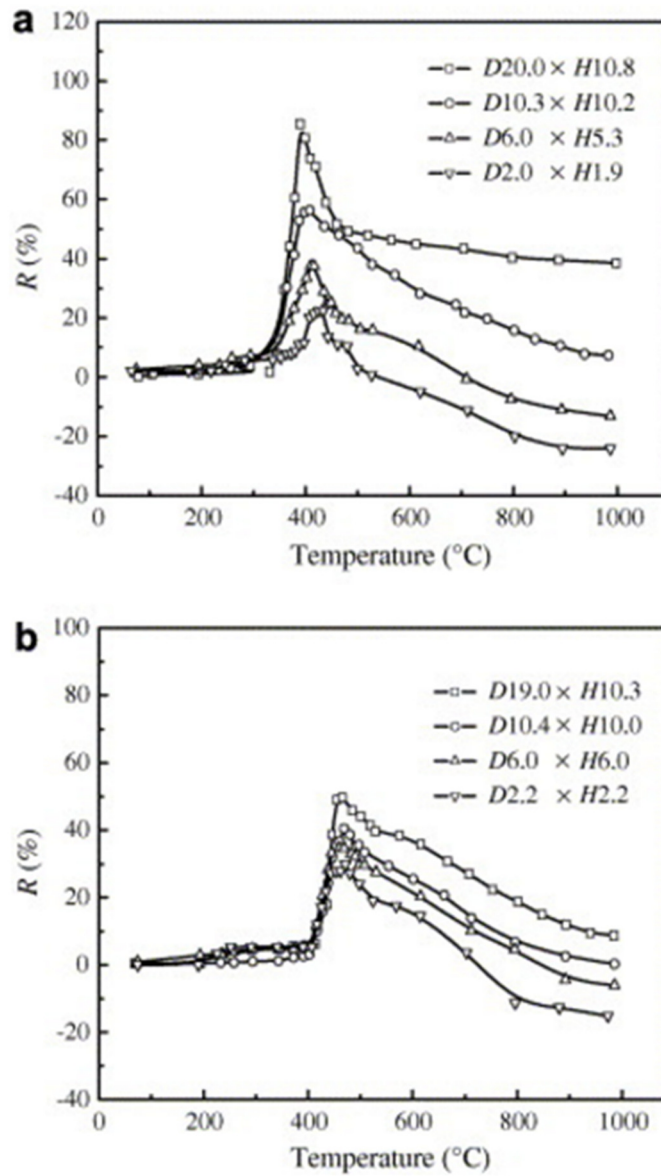
Figure 2.15: Volumetric swelling and shrinkage curves of raw coals with different sizes (units of mm), using two different coal types: (a) 25.87 % volatile matter (db) and (b) 13.39 % volatile matter (db). (Fu *et al*., 2007)

Gao *et al*., (1997), found that increasing the particle size from 149 μm to 335 μm diameter decreased the maximum swelling ratios yet increased the final swelling ratios of two coal types when heated using a carbon dioxide laser. The temperature of maximum swelling increased for the larger particle sizes (Figure 2.16). These results are in contrast to those of Fu *et al*., (2007), in which both the maximum and final swelling ratios were affected in the same way by particle size.

However, the particle sizes used by Gao *et al.*, were much smaller and the heating rates much greater.

(a)
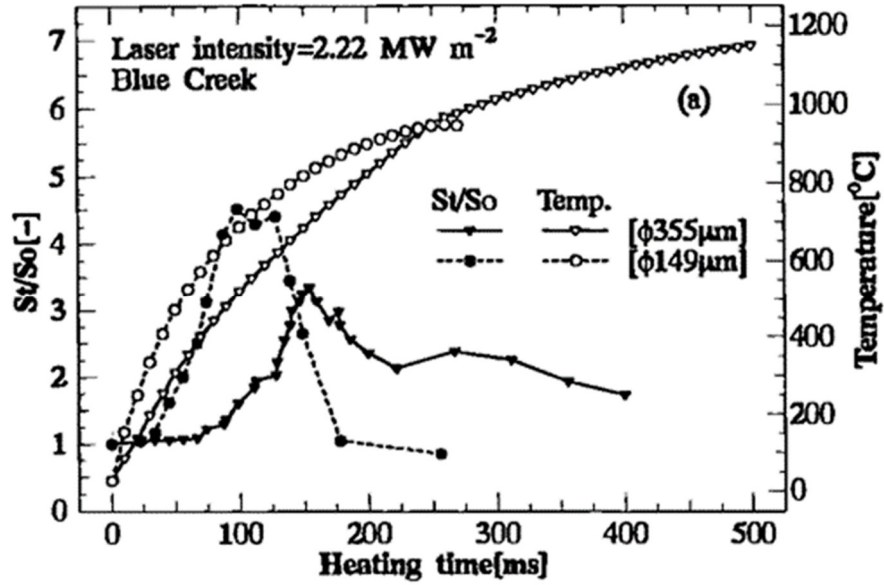
(b)
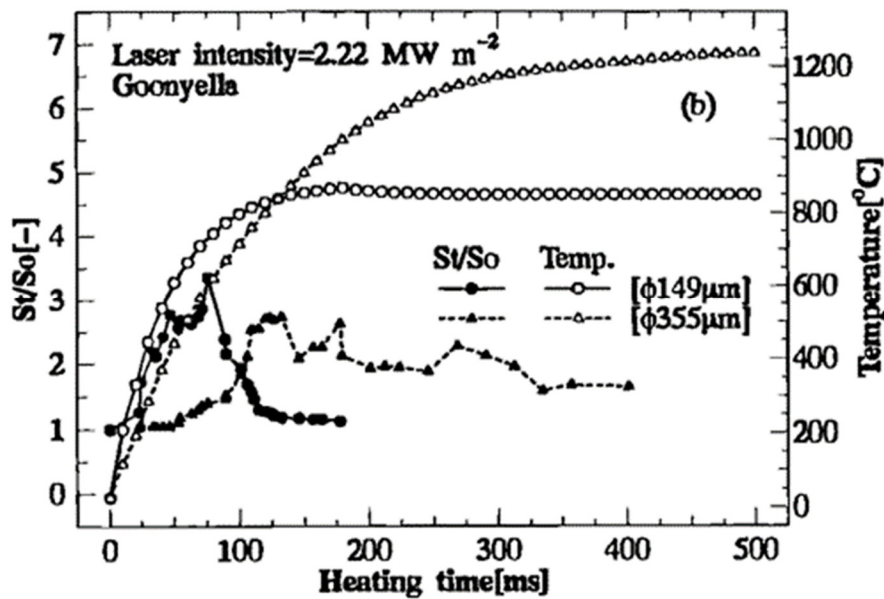
Figure 2.16: Effect of particle size on the swelling ratio and temperature profile of particles of (a) Blue Creek coal, 27.5 % volatile matter (db), and (b) Goonyella coal, 24.6 % volatile matter (db). (Gao *et al.*, 1997)

The particle size affected the predicted maximum heating rate experienced by particles in the work of Gao *et al*. The 149 μm particles experienced a maximum

heating rate of 1.1 x 10^4 K/s, whilst for the 335 μm particles that figure was lower, 8.4 x 10^3 K/s. It was also observed by Gao *et al.*, that the duration of plasticity was approximately doubled for both coals by the increase in particle size, however the effect on interval time between oscillations was different for the two coals. For Blue Creek coal the interval time was generally increased at the larger particle size whereas for Goonyella coal the interval time was generally decreased.

The particle size range used in the current project is just below that used by Gao *et al.*, (1997).

Gao *et al.*, explained their results in terms of the transfer of gas and metaplast. The diffusion of gas and metaplast being easier within smaller particles than larger ones before a re-solidified shell forms; enhancing maximum swelling ratio but decreasing final swelling ratio. Gao *et al.*, suggested that the larger the particle the more difficult it becomes for gas evolved at the centre to exit the particle; therefore, the formation of a large bubble is favoured. The different behaviours of the two coals with respect to the effect of particle size on interval time between oscillations was used to highlight the effect of coal type, i.e. the development of viscosity or surface tension was different between the two coals.

Gao *et al.*, stated that 'it is generally believed that the smaller the particle size, the lower the plasticity coal will retain, or that fine grinding of coal decreases all of the physical phenomena that are associated with plasticity.' However, they pointed out that this information was obtained at low heating rates using packed-bed samples, which means the results of such experiments can not necessarily predict the behaviour of single coal particles heated at high heating rates.

Yu *et al.*, (2003), referred to work in which observations of coal particle swelling in a DTF showed that smaller particle sizes led to a greater maximum swelling ratio, whilst the final swelling ratio was independent of particle size. This is consistent with the findings of Gao *et al.*, (1997), to an extent (although Gao *et al.*, actually observed a lower final swelling ratio for the smaller particles). Gale *et al.*, (1995), also referred to work which apparently demonstrated an increase in swelling with decreasing particle size although it was not specified whether this was a maximum swelling ratio or final swelling ratio. The original sources referenced by

Yu *et al.*, and Gale *et al.*, could not be found so the details of these pieces of work are not known, including what particle size ranges were used.

Yang *et al.*, (2014), included in their model of coal particle swelling an influence factor representing the initial volume of the coal particle. Solid and metaplast phases are scattered throughout the particle, if the distance between two groups of metaplast is large enough then they are prevented from trapping pore volume to form bubbles. In larger particles the metaplast can be more easily divided therefore the larger the particle radius the lower the influence factor in the number of bubbles formed. Therefore, according to the model, the smaller particles will swell more. This explanation seems to contradict the explanation of Gao *et al.*, (1997), that gaseous volatile matter is more easily trapped by larger particles.

The available information does not present a clear relationship between particle size and swelling. It appears that the effect of particle size may depend upon the size range in question. It may also be the case that the effect on maximum swelling ratio is different to the effect on final swelling ratio. The final swelling ratio has been found to increase with decreasing particle size, however this is attributed to increasing vitrinite concentration rather than to the particle size itself.

2.10.2   Volatile matter

Studies on coal swelling involving multiple coals show that different coals frequently show different swelling behaviours under the same experimental conditions, demonstrating that swelling properties are dependent upon coal type. As coal swelling is driven by the formation of bubbles of evolving volatile matter it may be expected that a relationship exists between coal volatile matter and swelling properties, however such a relationship is not apparent from the open literature.

One of the pieces of work reviewed included a suite of eleven coals (Yoshizawa *et al.*, 2006), enabling direct comparison of these coals under the same heating conditions. A drop tube furnace was used to measure the final swelling ratio of all

coals across a range of furnace temperatures. No relationship between coal volatile matter and swelling was observed, as illustrated by Figure 2.17, which shows the maximum observed final swelling ratio (irrespective of furnace temperature) plotted against coal volatile matter.
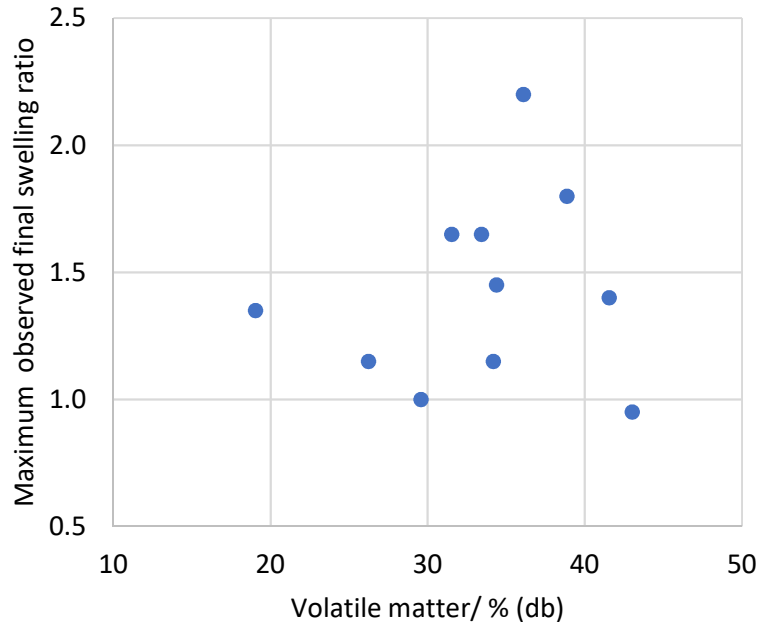
Figure 2.17: Maximum observed final swelling ratio of coals studied by Yoshizawa *et al*., (2006), versus coal volatile matter.

Fletcher *et al*., (1993), included five coals in their study but the Proximate volatile matter figures were not given. The carbon and hydrogen contents of the coals were provided but there was no correlation between a higher H/C ratio, which can be associated with higher volatile matter, and final swelling ratio.

Figure 2.18 shows a compilation of results from several works in which two or three types of coal were used and maximum swelling ratio was measured by continuous monitoring; maximum swelling ratio is plotted against volatile matter (db). In the results of Yu *et al*., (2003), and Toishi *et al*., (2013), a higher volatile matter coal swells more than a lower volatile matter coal, although this is inconclusive as only two coal types were studied in each case. In the work of Fu *et al*., (2007), the difference between coal types is dependent upon particle size; for the largest particles (20 x 10 mm) the higher volatile matter coal swells more but for the smallest particles (2 x 2 mm) the lower volatile matter coal swells

marginally more. Fu *et al*., (2007), also noted that the higher volatile matter coal began swelling at a lower temperature. In studies where three coal types were used (Gao *et al*., 1997, and Coetzee *et al*., 2014) no correlation was found between volatile matter and swelling. The experimental conditions vary greatly between the pieces of work cited in Figure 2.18, however the different coal types within each study were tested under the same conditions and all the cited results were generated at atmospheric pressure.

Figures 2.17 and 2.18 do not provide positive evidence for a relationship between final or maximum swelling ratio and coal volatile matter.
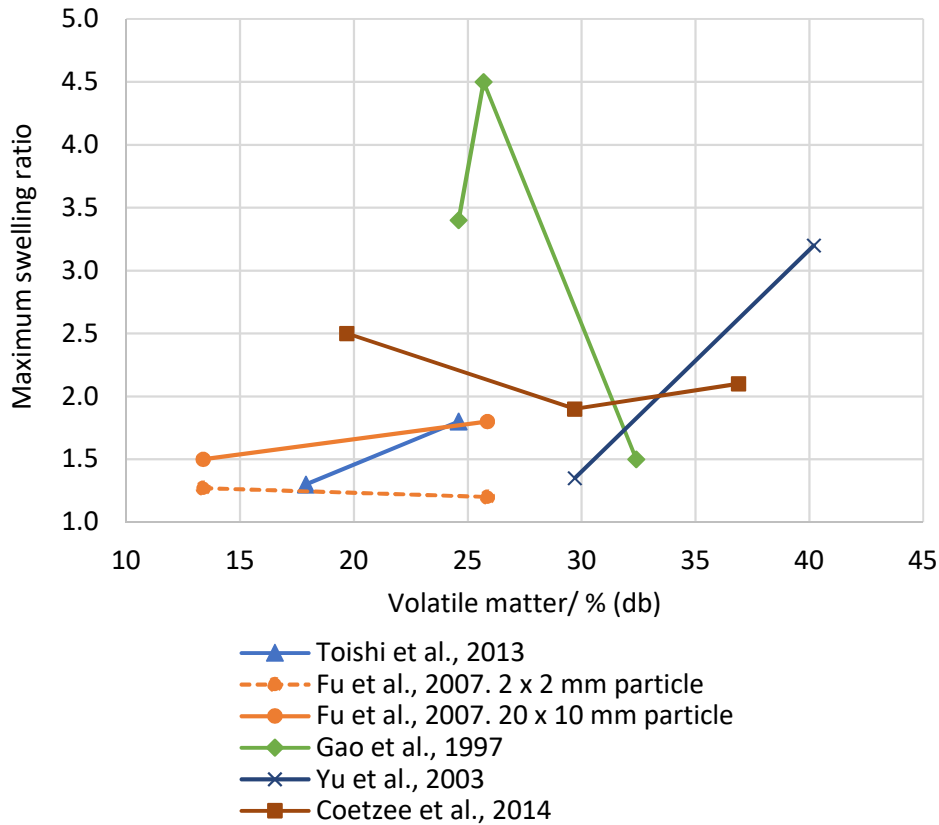
Figure 2.18: Maximum swelling ratio versus volatile matter (db) of parent coal at atmospheric pressure. Data sourced from references cited within the figure.

Chen *et al*., (2007), calculated final swelling ratio using particle size distribution measurements, which showed a higher volatile matter coal swelling more than a lower volatile matter coal. Cross-section SEM images of coal and char particles

showed the pores of the higher volatile matter coal were more developed than those of the lower volatile matter coal at 1000 $^{\circ}$C.

Barriocanal *et al*., (2003), showed that Gieseler maximum fluidity peaks at around 32-34 % volatile matter (db), and as particle swelling has been linked to Gieseler maximum fluidity (Gao *et al*., 1997) (see section 2.10.4.2) it might be expected that particle swelling would show a similar trend in relation to volatile matter. The data presented by Barriocanal *et al*., illustrate a fairly wide degree of scatter in the relationship, which might also be expected for particle swelling.

Nomura & Thomas, (1996), investigated why three different coals, which seemed to be very similar in terms of their rank and characterisation data, produced very different properties in terms of the swelling pressure they exerted during cokemaking. Their results showed that the coal exerting the greatest swelling pressure had its highest rate of volatile matter release per unit temperature during a temperature range where the cross-link density within the coal structure was high (Figure 2.19).
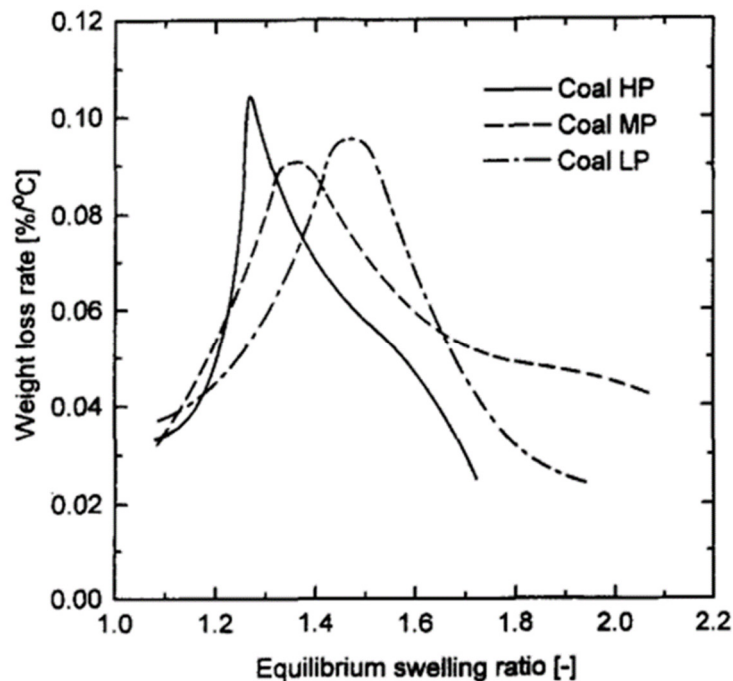
Figure 2.19: Rate of mass loss with respect to temperature versus equilibrium swelling ratio for three coals: HP = high coking pressure, MP = medium coking pressure and LP = low coking pressure. (Nomura & Thomas, 1996)

Note that in this figure the equilibrium swelling ratio, obtained by sorption of pyridine, is used as a measure of the cross-link density, i.e. the lower the equilibrium swelling ratio the higher the cross-link density. This high cross-link density resisted the flow of gaseous volatile matter. The coal exerting the lowest swelling pressure had its highest rate of volatile matter release per unit temperature during a temperature range where the cross-link density was relatively low, which allowed gases to escape more easily. The degree of swelling pressure was not a function of the rate of volatile matter release per unit temperature alone but depended upon the macromolecular structure of the coal at the temperature at which the rate of volatile matter release was highest.

Yang *et al*., (2014), modelled the swelling behaviour of two coals, the lower volatile matter coal was predicted to have a higher final swelling ratio at all heating rates at 0.1 MPa (Figure 2.30). The relative swelling ratios of the two coals were determined by a balance between the effects of internal pressure driving swelling on one hand yet causing bubble rupture on the other. The higher volatile matter coal had a higher yield of light gas therefore a higher internal pressure, but it also had a higher frequency of bubble rupture, which resulted in the lower swelling ratio. Above 0.2 MPa, however, the higher volatile matter coal was predicted to swell more (Figure 2.34). Increasing the ambient pressure reduced the frequency of bubble rupture for both coals but the effect was greatest for the higher volatile matter coal. As the difference in frequency of bubble rupture between the two coals became smaller the difference in internal pressure became the differentiating factor, i.e. higher volatile matter coal swelled more. Therefore, it was predicted that changes in ambient pressure could determine which coal had the greatest final swelling ratio (the effects of ambient pressure are reviewed in section 2.11.4).

The available information does not provide a trend in terms of the relationship between Proximate volatile matter content and coal particle swelling. There is no evidence of a correlation between greater volatile matter and greater swelling ratios despite the fact that the evolution of volatile matter drives the swelling process. This indicates that factors other than Proximate volatile matter content are critical. As mentioned in Section 2.9 it is the yield of light gases rather than

total volatile matter that is most important for swelling. The timing of volatile matter release during the pyrolysis process and the coal's physical properties during volatile matter release are important factors in determining the swelling properties of a coal, whilst ambient pressure is also predicted to influence whether one coal swells more than another.

2.10.3   Particle density – maceral and mineral content

Several works have investigated coal particle swelling behaviour in relation to mineral and maceral[*] content. Separation of coal particles with different mineral and maceral contents is generally achieved by separating according to density, which can be done using sink/float or centrifugation techniques. The three major maceral groups differ in density in the order inertinite > vitrinite > liptinite, i.e. the denser particles will be richer in inertinite whilst the less dense particles will be richer in liptinite. Mineral matter is generally denser than all macerals therefore the presence of mineral matter within coal particles will increase the particle density.

Tsai & Scaroni, (1987), carried out experiments in an entrained-flow reactor using coal samples separated by size and density. This produced a test sample with a narrow particle size range (mean diameter 112 µm) and broadly separated according to maceral type and mineral content. They observed that vitrinite-rich particles had the highest swelling ratio and that swelling tended to decrease with increasing inertinite concentration (Table 2.2 and Figure 2.20). Increasing liptinite concentration did not particularly increase swelling (liptinite was the minor maceral component). Therefore, they concluded that the amount of vitrinite was responsible for the overall swelling behaviour. Surface area measurements by carbon dioxide adsorption showed a greater reduction in surface area for the inertinite-rich samples, consistent with low thermoplasticity and low swelling of inertinite.

---

[*] See Appendix A for an explanation of macerals.

	A1	A2	A3	A4
Liptinite/ vol. % (daf)	18	11	14	-
Vitrinite/ vol. % (daf)	62	71	53	-
Inertinite/ vol. % (daf)	20	18	33	-
Ash/ wt. % (db)	4.3	3.1	11.4	52.3

Table 2.2: Composition of coal samples associated with Figure 2.20. Labels A1-A4 denote increasing density of samples. (Tsai & Scaroni, 1987)
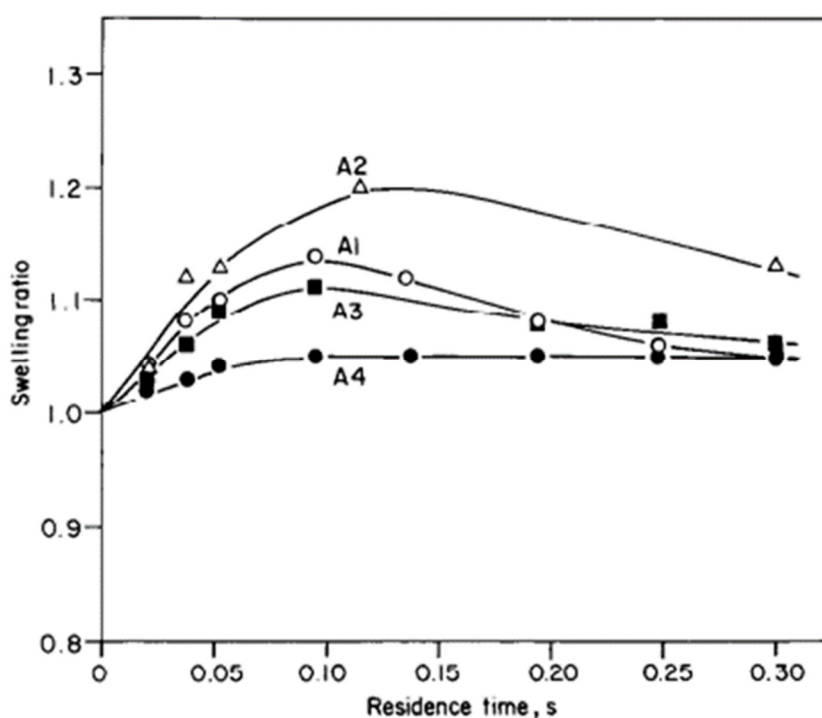
Figure 2.20: Effect of maceral composition on the swelling ratio of coal particles during pyrolysis at different residence times in an entrained-flow reactor: A1 = liptinite rich; A2 = vitrinite rich; A3 = inertinite rich; A4 = mineral rich. (Tsai & Scaroni, 1987)

Yu *et al.*, (2003), separated a 63-90 μm coal sample into five density fractions. Lighter fractions, containing more vitrinite and liptinite showed a greater swelling ratio and more intensive bubble formation in Single Particle Reactor experiments than heavier fractions, which contained more inertinite and mineral matter. Figure 2.21 shows results for three of the density fractions whilst Table 2.3 shows the petrographic and mineral compositions (where the information is available). Note that the concentration of liptinite appears high, due to the fact that not all

density fractions are presented. The lightest fraction also had a plastic phase much longer in duration than the heavier density fractions, this was attributed to its higher liptinite content. Mineral matter was considered not to contribute to swelling therefore higher mineral concentrations supressed swelling of the denser coal particles in which it was most prevalent.

	F 1.25	F 1.35	F 1.50
Liptinite/ vol. % (daf)	-	59.2	46.6
Vitrinite/ vol. % (daf)	-	35.4	42.6
Inertinite/ vol. % (daf)	-	5.4	10.8
Ash/ wt. % (db)	-	10.8	15.5

Table 2.3: Composition of coal samples associated with Figure 2.21. Labels denote sink-float density fractions increasing in density from F 1.25 to F 1.50 (F = floats). See Section 4.3 for explanation of sink-float technique. (Yu *et al.*, 2003)
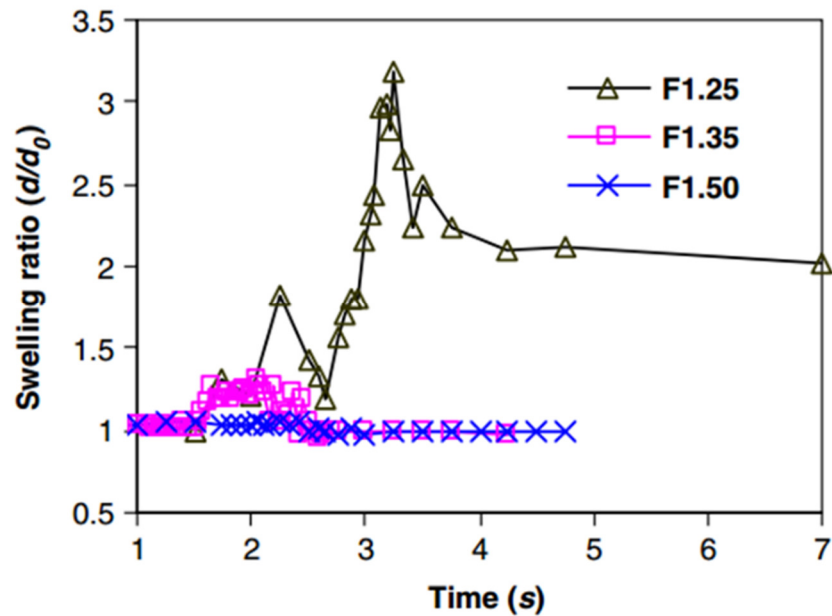
Figure 2.21: Transient swelling ratios of the observed particles from three density fractions of a coal of 40 % volatile matter (db) at a heating rate of 100 K/s. (Yu *et al.*, 2003)

Two coals were included in the study by Yu *et al.*, (2003), data in Table 2.3 and Figure 2.21 refers to the higher volatile matter coal of 40 % volatile matter (db). There was more variation between density fractions in this coal because, with

increasing coal rank, differences between chemical compositions of maceral groups decrease. This meant that for the lower volatile matter coal (29.7 % (db)) the swelling of the F 1.50 particles was not greatly different to the swelling of the F 1.25 particles. Therefore, of the heavier (F 1.50) fractions of both coals, that of the lower volatile matter coal swelled the most even though the higher volatile matter coal showed much more swelling in general.

Yu *et al*., (2003), examined the char structures produced by the different density fractions. The lighter fractions produced more swollen char particles with a high degree of porosity enclosed within a thin wall with flow textures on the surface observed by scanning electron microscope (SEM). The heavy fractions, in contrast, were more likely to show little or no change in morphology on heating and produce char particles with open pores or cracks on the surface.

Maceral groups have different fluidities in the order liptinite > vitrinite > inertinite (Lee *et al*., 1991) i.e. the lighter macerals have the greater fluidity. Maximum Gieseler fluidity has been linked to greater swelling ratios (Gao *et al*., 1997), this is discussed in section 2.10.4.2. Therefore, the greater fluidity of the lighter macerals is likely to contribute to their greater swelling. Although liptinite has a greater fluidity than vitrinite, the fluid properties of the vitrinite are likely to determine the overall swelling behaviour of the coal, as vitrinite tends to be present in greater proportions than liptinite.

Distribution of macerals amongst coal particles can explain the heterogeneous nature of swelling within the same coal sample (Lee *et al*., 1991). Segregation of macerals can occur during pulverisation of coal; relatively soft vitrinite tends to concentrate in smaller particles whereas harder inertinite remains in the larger particles.

Strezov *et al*., (2005), observed that low-density particles show a greater degree of bubble formation, rupture, swelling and contraction than higher density particles at atmospheric pressure. They also showed a greater tendency to shrink a little before swelling. These observations were attributed to the higher proportion of vitrinite in these particles and agree with the results of Yu *et al*., (2003), and Tsai & Scaroni, (1987). The particles of low-mid density showed a

greater degree of uniformity in their swelling behaviour than the denser particles. The denser particles had the higher concentrations of inertinite and mineral matter, however they still had a concentration of 33 % vitrinite overall. Therefore, it was considered likely that some dense particles had sufficient vitrinite to cause significant swelling and therefore lead to the heterogeneous behaviours seen within that group. It was suggested that the greater proportion of inertinite in the denser particles would cause these particles to have a higher viscosity than the lighter particles, which would hinder swelling, contraction and oscillations of bubble formation and rupture. This was backed up by the fast fourier transform measurement of transient oscillations of coal particles as bubbles formed and ruptured during swelling. The amplitude of oscillations narrowed as particle density increased.

To summarise the effect of coal particle density, the density is determined by the mineral and maceral content. The cited research demonstrates that the maceral content of coals is a significant factor in determining the swelling properties. The lighter the particles the greater their swelling is likely to be due to the higher concentrations of vitrinite and liptinite, whilst the heavier particles, containing more inertinite and mineral matter will swell less. Mineral matter does not contribute to swelling. The vitrinite maceral group controls the swelling of coal particles, rather than liptinite, because vitrinite is the predominant constituent.

2.10.4   Particle swelling in relation to standard tests of coal thermoplasticity

The swelling of coal particles is a feature of coal thermoplasticity. Three standard tests of the thermoplastic properties of coals are the Gieseler plastometer, Ruhr dilatometer and free swelling index tests, as described in section 2.7.2, however the conditions under which these tests are carried out are different to the experimental conditions under which individual particle swelling is measured in the literature cited in Table 2.1. For example, under the standard laboratory tests the bulk properties of volumes of ground coal are measured during heat treatment, therefore particles are not behaving independently of each other. The particle size range used is larger than the typical size range of PCI, and also the

heating rates used are very low as they are based on those of cokemaking (3 K/min). Fu *et al.*, (2007), showed that the swelling of a coal cake was different to the swelling of a solid lump of the same coal: The coal cakes showed significant shrinkage, but little swelling compared to the lump coal, and the processing of coal into cakes also moderated differences between the two coal types studied. Some pieces of work have provided data that enable comparisons to be drawn between the thermoplastic properties, as determined by standard tests, and the swelling of discrete coal particles. These are reviewed in this section.

2.10.4.1 Free swelling index

The results of the free swelling index (FSI) test may be expected to correlate with data on individual coal particle swelling. Fletcher *et al.*, (1993), studied five coals with a range of FSI values in two different reactor types at oxygen concentrations of 0 %, 6 % and 12 %. The general trend was for coals with a higher FSI to be associated with higher final swelling ratios (Figure 2.22). The relationship was not exact; for example, the coal with a FSI of 6.5 produced a higher final swelling ratio than the coal with FSI 7.5, and the two coals with a FSI of 0 gave differing final swelling ratios.
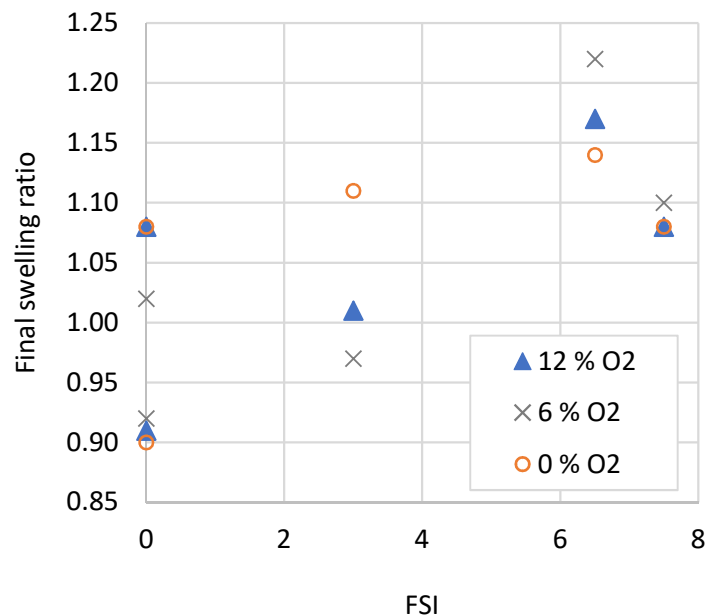
Figure 2.22: Relationship between FSI of parent coal and final swelling ratio of five coals heated in a flat flame, entrained flow, laminar flow reactor at oxygen concentrations of 0 %, 6 % and 12 %. (Fletcher *et al.*, 1997)

Coatzee *et al*., (2014), also observed a trend of increasing maximum swelling ratio with increasing FSI within a suite of three coals (Figure 2.23), in their work a low heating rate of 7 K/min and large particle sizes (16-20 mm) were used. These results indicate that, although a coal with a higher FSI may be more likely to show higher individual particle swelling, the FSI cannot precisely predict the swelling behaviour of individual particles. It is also apparent that a coal with a FSI of 0 can show swelling properties under conditions that differ to those of the FSI standard test. Similarly, Lee at al., (1991), observed that a coal with a FSI of 1 swelled considerably in a high pressure entrained flow reactor.
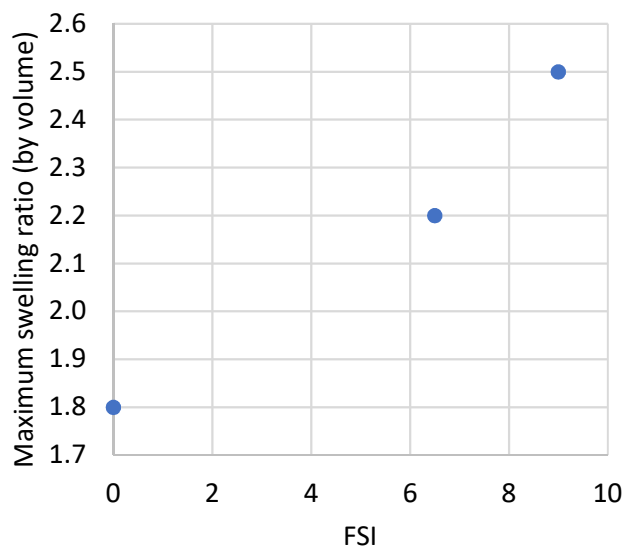
Figure 2.23: Relationship between FSI of parent coal and maximum swelling ratio (by volume) of large coal particles. (Coatzee *et al*., 2014)

2.10.4.2   Gieseler fluidity

The Gieseler Plastometer test gives a measure of the plasticity (or fluidity) of a packed coal bed as it is heated. As it is necessary for the structure of a coal particle to undergo deformation as it swells it might be expected that a higher maximum Gieseler fluidity would facilitate greater swelling. Indeed Gao *et al*., (1997), observed this trend using a suite of three coals (Figure 2.24) heated by a carbon dioxide laser system. This trend was observed at four different laser intensities; the greater the laser intensity the lower the maximum swelling ratio. The effect of increasing laser intensity on reducing the swelling ratio is greatest

for the coals with higher maximum Gieseler fluidity. Gao *et al.*, supposed that higher fluidity can reduce bubble rupture thereby enabling increased swelling. This seems contrary to the suggestion by Yu *et al.*, (2002), who suggested that high fluidity would inhibit swelling by facilitating more frequent bubble ruptures however it may be the case that there is an optimum range of fluidity for particle swelling, above and below which particle swelling decreases.

Gao *et al.*, (1997), suggested that the swelling ratio under the experimental conditions may be anticipated from maximum Gieseler fluidity, although it seems the analysis of a greater number of coals would be needed in order to verify this.
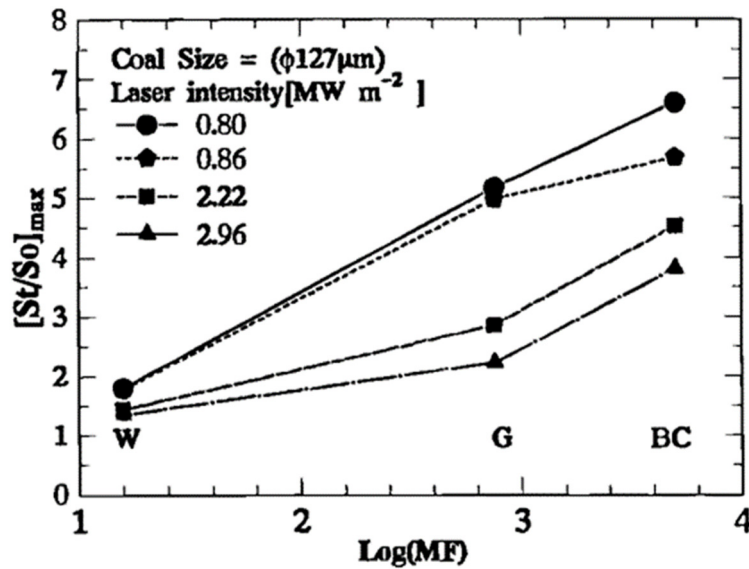
Figure 2.24: Relationship between swelling ratio and maximum Gieseler fluidity of three coals: W = Witbank, 32.4 % volatile matter (db), G = Goonyella, 24.6 % volatile matter (db) and BC = Blue Creek, 25.7 % volatile matter (db). (Gao *et al.*, 1997)

2.10.4.3 Ruhr dilatation

The Ruhr dilatometer test measures the contraction and dilation of a pencil of crushed coal (particle size <212 μm). Coatzee *et al.*, (2014), compared swelling of large (16-20 mm) coal particles at 7 K/min with standard Ruhr dilatometer results. A coal that showed no Ruhr contraction or dilation did show significant swelling properties under the experimental conditions (Figure 2.25a). Meanwhile particles of a coal that showed Ruhr contraction and dilation exhibited swelling and

shrinkage within more-or-less the same temperature range as the Ruhr plastic range (Figure 2.25b). The temperature of maximum swelling ratio corresponded well with the temperature of maximum Ruhr contraction.

(a)

(b)
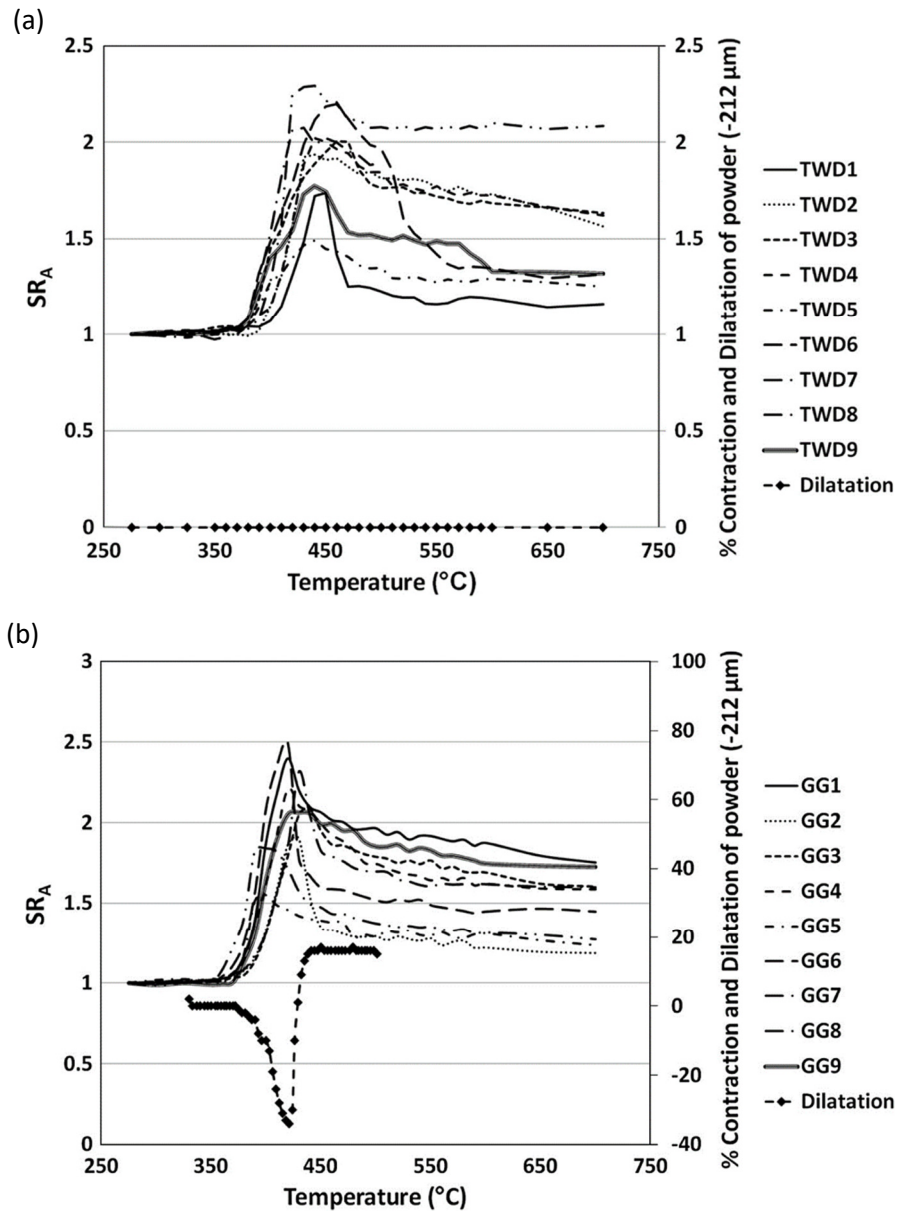
Figure 2.25: Swelling behaviour of nine large individual coal particles during heating plotted alongside Ruhr dilatation of parent coal for two coal types: (a) TWD = 29.7 % volatile matter (db) and (b) GG = 36.9 % volatile matter (db). (Coatzee *et al.*, 2014)

2.10.4.4   Summary

The available evidence suggests that standard thermoplastic properties tests can provide an indication as to the swelling behaviour of individual coal particles under heating conditions that are different to the standard test conditions; for example, coals with higher FSI and maximum Gieseler fluidity are likely to exhibit greater single particle swelling properties (as opposed to the bulk swelling of a packed volume of particles) at heating rates greater than those associated with the standard tests. Meanwhile the Ruhr plastic temperature range corresponds to the temperature range in which particle swelling and shrinkage takes place. These relationships are not unsurprising as the swelling of coal particles is a feature of coal thermoplasticity. Nevertheless, it is also evident that there are limitations associated with using the results of standard tests to predict single particle swelling behaviour under non-standard experimental conditions. For example, there are several examples of coals showing little or no thermoplastic properties under standard test conditions yet showing swelling behaviour under different experimental conditions, where heating rates are greater.

2.10.5   The effect of oxygen and sulphur content on coal swelling

The influence of oxygen and sulphur contents within the coal structure has not been investigated specifically in relation to individual coal particle swelling, however these constituents have been linked to coal thermoplastic properties in general. Oxygen within the coal structure is considered to reduce fluidity (Coetzee *et al.*, 2014), i.e. higher oxygen contents are linked to lower Gieseler maximum fluidity values. Mochizuki *et al.*, (2013), found a correlation between increasing organic sulphur content and decreasing maximum Gieseler fluidity; they also observed that addition of sulphur containing compounds to a raw coal reduced the maximum Gieseler fluidity of the coal. They suggested that organic sulphur may act as a hydrogen acceptor, bonding to (or 'trapping') transferable hydrogen which has previously been correlated with high maximum fluidity (Kidena *et al.*, 1996).

If it is assumed that a higher maximum fluidity can be approximated to a higher maximum swelling ratio (Gao *et al.*, 1997) then it can be expected that higher oxygen and organic sulphur contents of coals will contribute to lower swelling ratios.

2.10.6   Summary of the influence of coal properties on swelling

Different coals often exhibit different swelling characteristics under the same experimental conditions, demonstrating that coal properties play an important role in determining swelling behaviour. The variables of particle size and Proximate volatile matter content do not seem to produce clear relationships with swelling, however the relationship between particle density and swelling is clear. i.e. less dense particles swell more than denser particles. Particle density is controlled by maceral and mineral content, with the lighter vitrinite and liptinite macerals contributing to swelling. Of these maceral groups vitrinite is typically the much larger component therefore it is the vitrinite that governs the swelling behaviour. The heavier inertinite macerals contribute only a limited amount to swelling whilst mineral matter, which is the densest component, does not contribute.

Standard coal thermoplastic properties tests, Gieseler Plastometer, Ruhr Dilatometer and Free Swelling Index, can provide an indication of the likely extent of single particle swelling behaviour but not, it seems, a precise prediction.

2.11   The influence of heating environment on coal swelling

In this section the effect of the heating environment on coal particle swelling is reviewed. Research work has covered the following variables: Gas composition, temperature, heating rate and pressure.

2.11.1　Gas composition

Much of the work related to investigating thermal swelling of coal particles has been conducted under inert atmospheres, i.e. pyrolysis conditions, which eliminates the influence of factors such as interactions between the coal and external gases. However, some work has investigated the difference between pyrolysis and combustion conditions and also the effect of the presence of gases other than oxygen.

Tsai & Scaroni, (1987), found that during combustion in an entrained flow reactor the pattern of swelling was similar to that during pyrolysis, however the extent of maximum swelling and the rate of shrinkage were greater during combustion. The greater swelling ratio was attributed to the extra heat from volatile combustion causing more rapid pyrolysis, therefore the effect of combustion is effectively a result of increased heating rate. Whereas the apparent faster shrinkage was thought to result from a more severe fragmentation and collapse of thin walled cenospheres under internal burning.

Fletcher, (1993), also investigated the difference in swelling between a pyrolysis environment and a combustion environment. He concluded that the degree of swelling at the heating rate >10^4 K/s was not affected by the gas phase oxygen concentration and suggested that differences reported previously (references within Fletcher, 1993) may have been due to partial oxidation of char subsequent to pyrolysis. A further suggestion by Fletcher was that differences in swelling behaviour of a coal in different instruments would be due to heating rate and/or the presence of post-flame combustion gases other than oxygen.

2.11.2　Temperature

It is difficult to specifically assess the effect of temperature on coal particle swelling because the effects of temperature and heating rate are so closely related. Particles generally swell somewhere between 400 °C and 500 °C under low heating rates (3-7 K/min) (Coetzee *et al*., 2014 and Fu *et al*., 2007) and at higher heating rates (1000s of K/s) maximum swelling temperatures of 700-800 °C

have been observed (Gao *et al*., 1997). The rate at which particles are heated has been a more pertinent subject for research.

Gale *et al*., (1995), did, however, comment on the effect of maximum calculated particle temperatures in an entrained flow reactor and a flat flame burner. Trends in swelling ratio and porosity with respect to particle temperature were dependent on coal type. Both coals studied were high-volatile bituminous; one showed a general trend of decreasing swelling ratio and porosity with increasing temperature whilst the other coal showed a slight decrease in swelling ratio but an increase in porosity with temperature. The authors acknowledged that it was difficult to separate the effects of particle temperature and heating rate.

Lu *et al*., (2000), provided the swelling results of three coals studied using a drop tube furnace operated at three different temperatures (Figure 2.26). Residence times were 1 second. A greater degree of swelling was shown by all three coals at the lowest furnace temperature of 900 °C. The lower swelling at higher furnace temperatures was attributed to greater fragmentation at these temperatures.
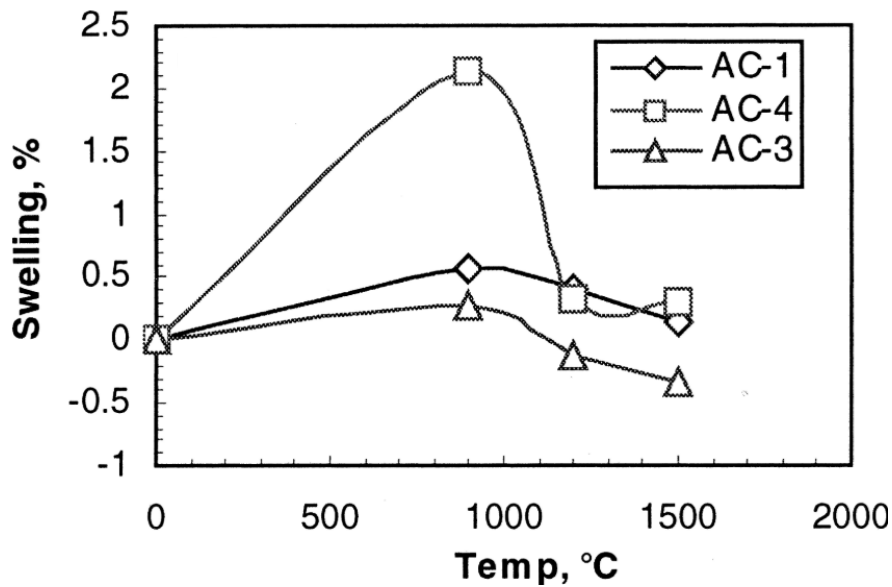
Figure 2.26: The final swelling ratios of char particles of three coals heated in a drop tube furnace at three temperatures. Coal AC-1 = 34.5 % volatile matter (db), coal AC-3 = 15.1 % volatile matter (db) and coal AC-4 = 24.6 % volatile matter (db).

(Lu *et al*., 2000)

Yoshizawa *et al.*, (2006), similarly used a drop tube furnace to measure the final swelling ratio of eleven coals at eight furnace temperatures between 400 °C and 1500 °C Figure 2.27). In this case the optimum furnace temperature for observing swelling was 800 °C, comparable to the optimum observed by Lu *et al.*, 2000.
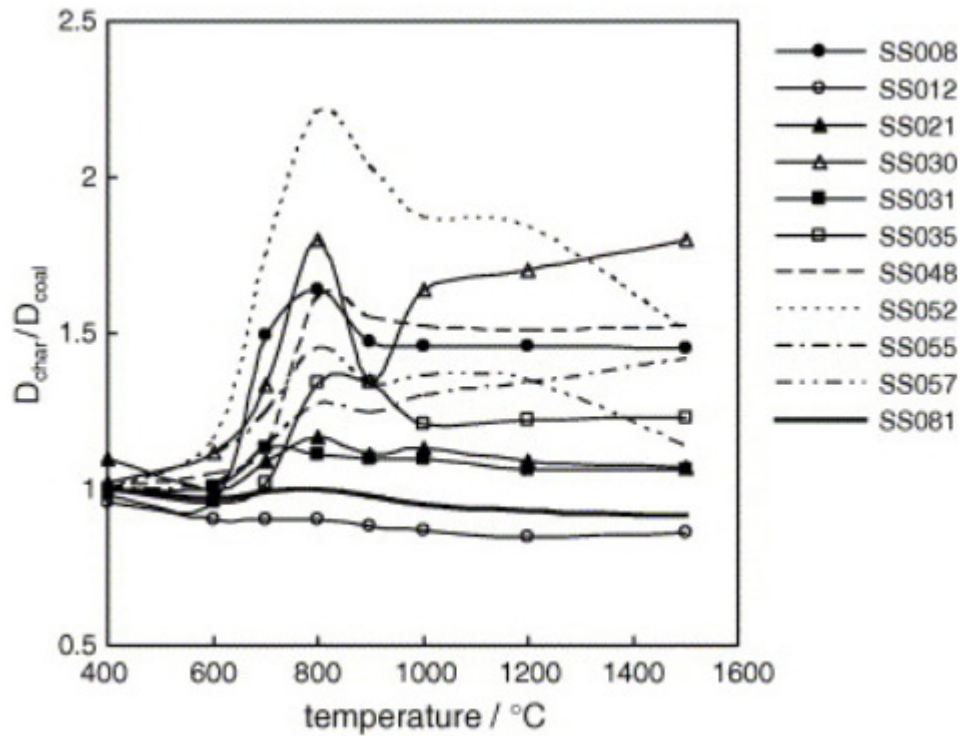
Figure 2.27: The final swelling ratios of eleven coals heated in a drop tube furnace at eight temperatures. (Yoshizawa *et al.*, 2006)

Chen *et al.*, (2007), also commented that SEM cross-section images of coal and char particles showed more pronounced development of pores as the furnace temperature increased.

2.11.3   Heating rate

The influence of heating rate on particle swelling has been covered by several pieces of experimental work and efforts have been made to model these effects.

Increasing the heating rate initially has the effect of increasing swelling ratio, however there is an optimum heating rate above which swelling ratio decreases. Gale *et al.*, (1995), referenced various previous experimental studies, some of

which showed an increase in swelling ratio with heating rate, whilst others showed a decrease. They combined their own experimental results, which showed a decrease in final swelling ratio with respect to heating rate between 2 x 10^4 K/s and 7 x 10^4 K/s, with those of Zygourakis, (1993), which showed an increasing swelling ratio between 0.1 K/s and 10^3 K/s. The result suggested that final coal swelling ratio passes through a maximum with respect to heating rate. This maximum was between 10^3 K/s and 2 x 10^4 K/s. Porosity measurements mirrored this pattern. Shurtz *et al.*, (2011), subsequently added to the evidence of decreasing final swelling ratio with increasing heating rate above about 10^4 K/s (Figure 2.28). They described the increasing swelling behaviour below this temperature as Regime 1, and the decreasing swelling behaviour above this temperature as Regime 2. The residence times of the various techniques vary, but in all cases final swelling ratio is measured.

The heating rate associated with blast furnace coal injection is estimated to be 10^5-10^6 K/s (Carpenter, 2006), which is at the very upper limit of the range covered by Figure 2.28. Based on this evidence it could be assumed that the swelling of coal particles during blast furnace coal injection is relatively low, however the elevated pressure within the blast furnace would act to increase swelling (see section 2.11.4).
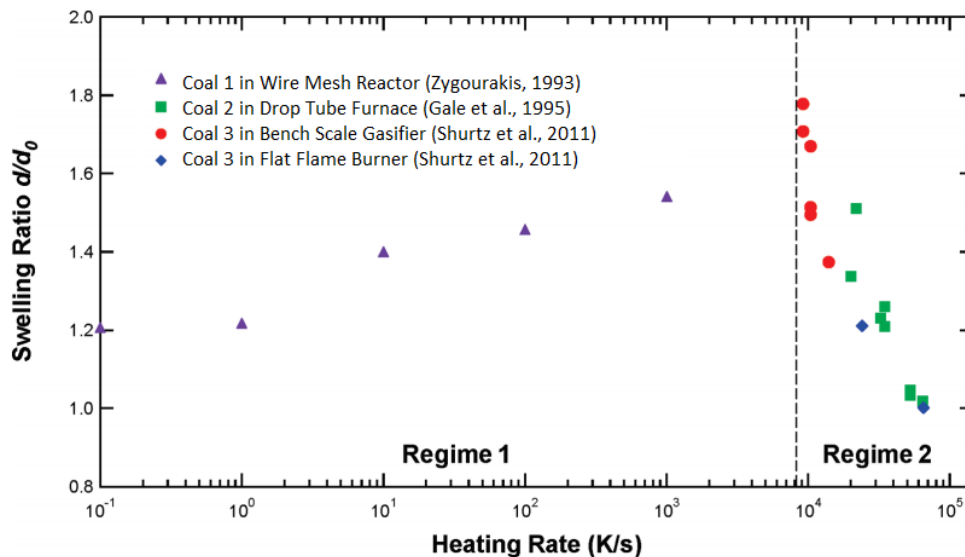
Figure 2.28: Swelling ratio versus maximum particle heating rate for three coals. Bench Scale Gasifier was similar to a Drop Tube Furnace. (Shurtz *et al.*, 2011)

It should be noted that although a heating rate of 10^5-10^6 K/s is often referenced for coal particles undergoing PCI, an original source for this estimate has not been found during this current work.

Gale *et al.*, (1995), attributed the initial increase in swelling with respect to heating rate to an increased volatile matter yield, and the subsequent decrease to the rate of volatile matter release being faster than the relaxation time involved in the expansion of the particle. At high heating rates the particle rapidly re-solidifies very soon after gaseous volatile matter evolves (Shurtz *et al.*, 2011). An increased influence of internal temperature gradients at the highest heating rates was also suggested. The very low degree of swelling at the lowest heating rates was explained in terms of volatile matter being able to escape the particle before significant internal pressure could build up.

Gao *et al.*, (1997), performed experiments using a carbon dioxide laser system to heat individual coal particles. By changing the laser intensity, the calculated maximum heating rate experienced by the particles was varied. It was found that an increase in maximum calculated heating rate from 2.6 x 10^3 K/s to 1.2 x 10^4 K/s brought about a decrease in maximum swelling ratio (Figure 2.29) and final swelling ratio for three coal types.
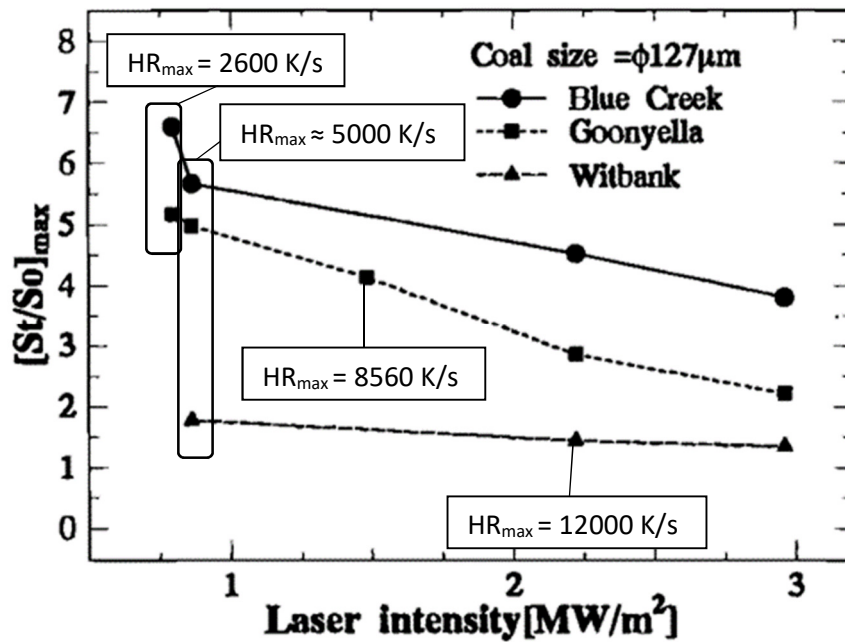
Figure 2.29: Effect of laser intensity on the maximum swelling ratios of three types of coal. Calculated maximum heating rates are labelled. (Gao *et al.*, 1997)

This result is broadly in line with the work of Gale *et al*., (1995), and Shurtz *et al*., (2011), as the heating rates used were close to the transition between Regimes 1 and 2. This suggests that the optimum heating rate for coal swelling may be slightly lower than depicted in Figure 2.28. The decrease in final swelling ratio upon increasing maximum heating rate from 2.6 x 10^3 K/s to 1.2 x 10^4 K/s (Gao *et al*., 1997) was from ~4-5 to ~1. Swelling Ratios of 4-5 are much greater than those reported by Shurtz *et al*., (2011), in Figure 2.28. The temperature of maximum swelling increased with increasing laser intensity as did the frequency of bubble rupture. It should be noted that the increase in laser intensity also resulted in an increase in peak temperature experienced by the particles as well as the increased maximum heating rate.

Yu *et al*., (2003), found that increasing the heating rate from 10 K/s to 100 K/s and then to 200 K/s enhanced the swelling behaviour observed, this agrees with the work of Zygourakis, (1993), and Gale at al., (1995). There was a great difference between the swelling behaviour at 10 K/s and 100 K/s; at the lower heating rate fewer particles swelled, the maximum swelling ratio was reduced, and less bubbling was observed. At 200 K/s some particle movement driven by volatile gas release was observed.

Yu *et al*., (2003), reported that increasing heating rate increased the percentage of porous char morphologies. They attributed this to increased fluidity and devolatilisation rate at higher heating rates, along with a shift in devolatilisation to a higher temperature range and increased volatile matter yield by suppression of secondary reactions. These secondary reactions allow reactive volatile matter to crack and leave some mass remaining within the particle.

Yu *et al*., (2003), cited an increased fluidity at higher heating rates. This has been shown to be true for low heating rates (0.7-7.2 K/min) (Yu *et al*., 2007), however a study using a specially designed high temperature, high heating rate plastometer (Fong *et al*., 1986) indicated that maximum fluidity slightly decreased with increasing heating rate from 75 K/s to 450 K/s, which is closer to the range investigated by Yu *et al*., (2003). An increase in the extent of the fluid temperature range and an increase in the softening and re-solidifying temperatures were also

apparent as heating rate increased (Fong *et al*., 1986), which may be influential with regard to swelling behaviour.

Yang *et al*., (2014), included an investigation into the effects of heating rate in their modelling work. Their model predicted a peak in final swelling ratio occurring at heating rates of around $1.5 \times 10^4 – 2.0 \times 10^4$ K/s for the two coal types in their study at 0.1 MPa (Figure 2.30). Their model was unable to calculate swelling ratios at heating rates below 10^3 K/s when a central single bubble is assumed. The model results agreed well with experimental results at heating rates above 10^4 K/s, including those of Gale *et al*., (1995). Comparative experimental data for small particles was unavailable between heating rates of 10^3 K/s and 10^4 K/s.
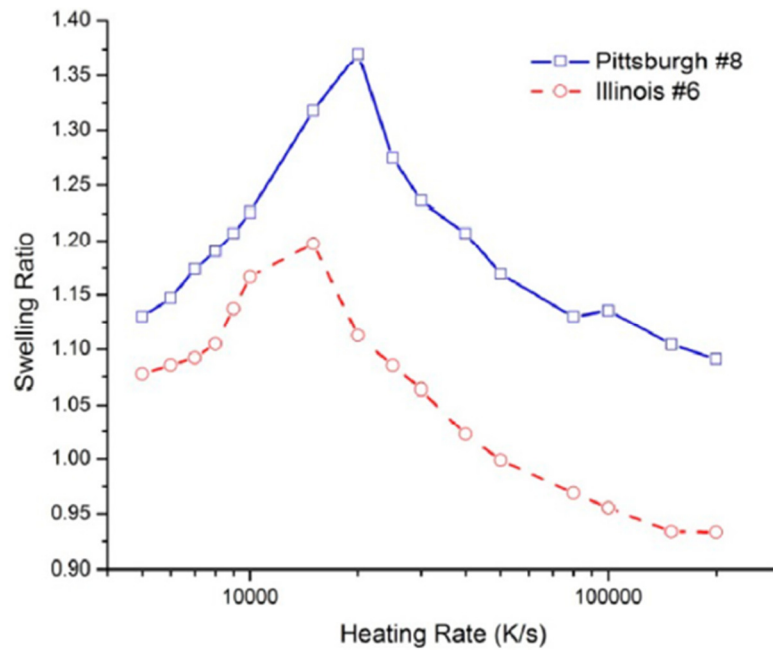
Figure 2.30: Change in final swelling ratio of two coal types versus heating rate at an ambient pressure of 0.1 MPa for a particle 60 μm in diameter. (Yang *et al*., 2014)

Yang *et al*., (2014), described the change in final swelling ratio with heating rate in terms of the internal pressure within the particle and the initial number of surrounding bubbles. As the heating rate increases the internal pressure increases, which increases the driving force for swelling but also increases the frequency of bubble rupture, which favours shrinkage. The duration of the

internal pressure peaks also decreases with increasing heating rate, this decrease in plastic deformation time reduces the swelling. Increasing the heating rate increases the initial internal pressure at the beginning of the plastic stage, this initially favours a greater number of surrounding bubbles, which has the effect of increasing final swelling ratio, but after a certain heating rate it is the size of the central bubble that increases at the expense of the total bubble number, which decreases (Figure 2.31). In addition, the increasing size of the central bubble causes the shell thickness to decrease, which assists the flow of bubbles out of the particle, reducing the bubble number.
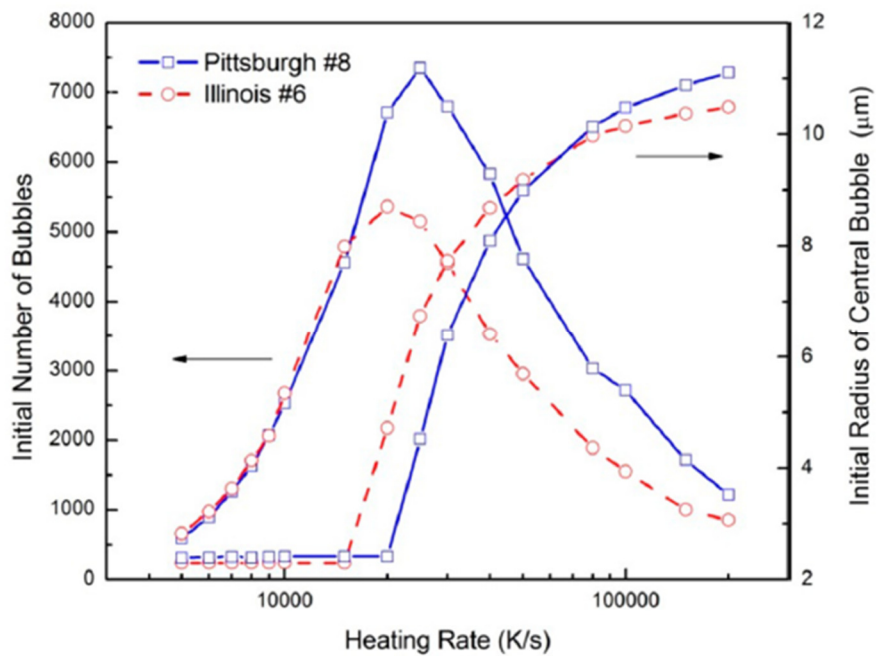
Figure 2.31: Initial number of bubbles and initial radius of the central bubble in the plastic stage at various heating rates and an ambient pressure of 0.1 MPa. (Yang *et al.*, (2014)

The influence of heating rate on several interconnected factors is complex therefore a sensitivity analysis was performed by Yang *et al.*, (2014), under a variety of computational conditions. The results indicated that, at 0.1 MPa, the initial number of bubbles in the plastic stage was the dominant factor in the increasing and then decreasing pattern of swelling ratio with increasing heating rate. The initial bubble number in the plastic stage is controlled by the initial

pressure in the plastic stage therefore the initial pressure in the plastic stage was shown to be an important factor in determining final swelling ratio.

To summarise, the evidence from experimental and modelling work is that increasing the heating rate has the effect of initially increasing swelling ratio then decreasing swelling ratio. The initial increase has been attributed to an increasing rate and yield of volatile matter evolution, resulting in a greater driving force for swelling; to an increased fluid temperature range, and also to an increased initial internal pressure within the particle at the beginning of the plastic stage, which leads to a larger initial number of bubbles, which favours swelling. The decrease in swelling ratio at higher heating rates is attributed to the rate of volatile matter release becoming faster than the relaxation time involved in the expansion of the particle, the increased rupture frequency of the central bubble and the decreased duration of the internal pressure peak.

The heating rate at which swelling ratio peaks is estimated to be between 10^3 K/s and 2×10^4 K/s at 0.1 MPa, but the precise heating rate is likely to be coal type dependent as indicated by Figure 2.30. Modelling work by Yang *et al*., (2014), also predicts that ambient pressure will have a significant impact upon the value of the optimum heating rate (see section 2.11.4).

2.11.4   Ambient pressure

The effects of ambient pressure on coal particle swelling have been investigated experimentally and by modelling. Lee *et al*., (1991), investigated the effect of pressure on the swelling of coal particles under rapid pyrolysis conditions using a high pressure entrained-flow furnace. Their results showed that there was an optimum pressure for maximum swelling, which was the result of two opposing effects (Figure 2.32). Increasing the pressure from 0.1 MPa to 0.8 MPa caused an increase in swelling attributed to increased fluidity brought about by the retention of volatile matter, which acted as a plasticising agent. Increasing the pressure from 0.8 MPa to 2.2 MPa caused a decrease in swelling attributed to a second effect becoming dominant – the resistance to expansion. Wu *et al*., (2000), used a pressurised drop tube furnace and found that increasing the pressure from 0.1 MPa to 1.5 MPa resulted in an increase in final swelling ratio (Figure 2.32). Chars

produced at high pressures were also found to be more likely to have high internal and surface porosity, with thin walls. Both these studies were carried out under inert, or close to inert, conditions.
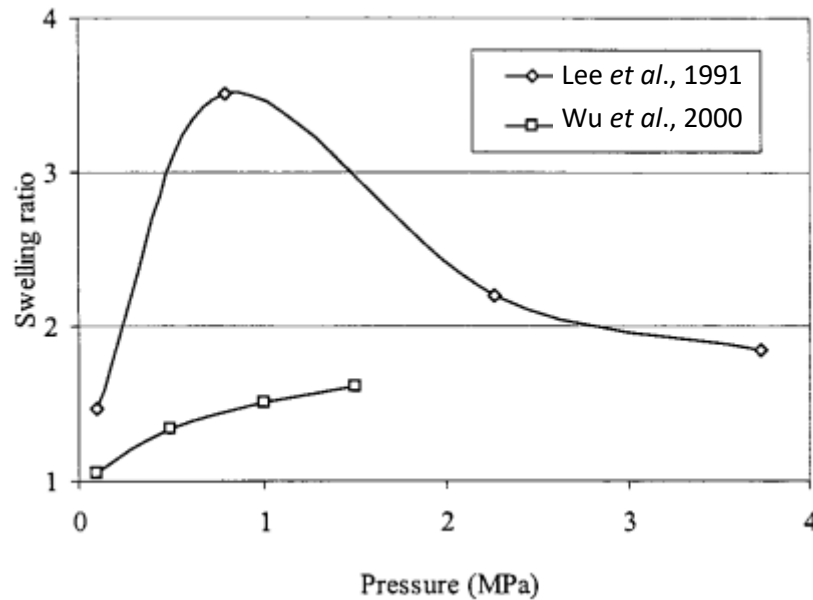
Figure 2.32: Effect of pressure on swelling ratio; results of two studies. (Wu *et al*: 2000)

Strevoz *et al*., (2005), using a pressurised Single Particle Reactor with a heating rate of 200 K/s, reported an optimum pressure of 1 MPa in terms of both maximum swelling ratio and final swelling ratio (Figure 2.33). This value is close to the value of 0.8 MPa reported by Lee at al., (1991), despite the differences in heating rate between the two pieces of work. The authors (Strevoz *et al*., 2005) also noted a reduction in the particle oscillations (oscillations brought about by bubble growth and rupture) with increasing pressure. There was also some variation in how increasing pressure affected particles of different density. For example, at 1 MPa the lightest particles had the greatest final swelling ratio followed by the mid-density particles, with the heaviest particles showing a minimal final swelling ratio. However, at atmospheric pressure the mid-density particles had the highest final swelling ratio and the heavier and lighter particles both had a low final swelling ratio. This was a result of the much greater degree of shrinkage of the lightest particles after swelling at atmospheric pressure.

(a)
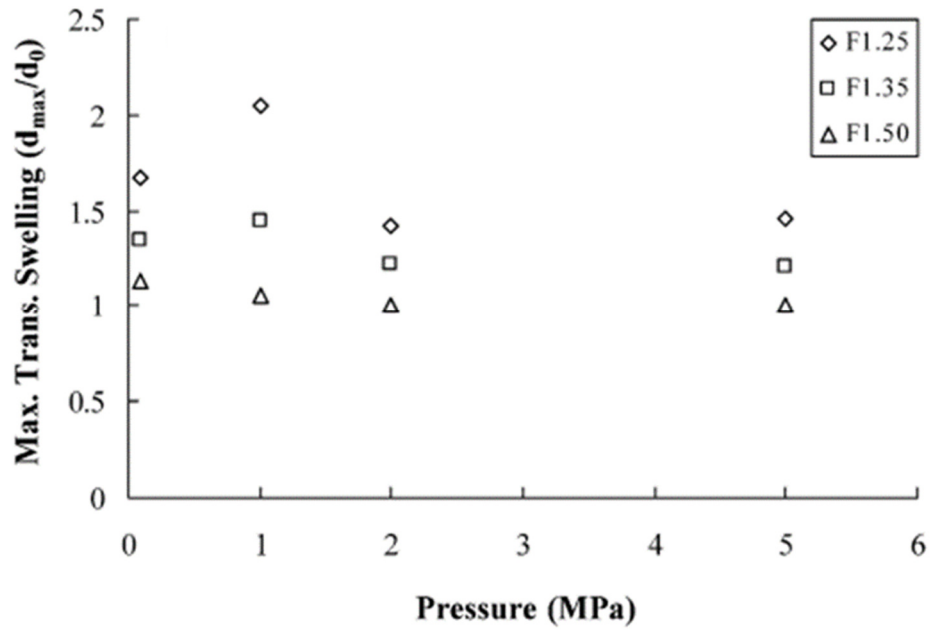
(b)
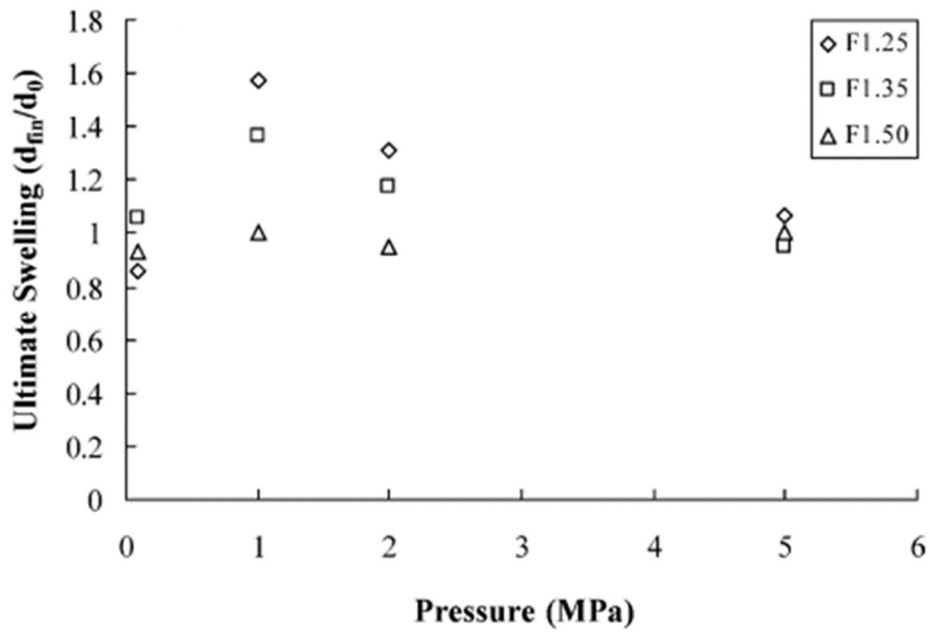
Figure 2.33: Comparison between the maximum transient swelling ratio (a) and final swelling ratio (b) for density fraction coal particles under different ambient pressure conditions. (Strevoz et al., 2005)

Strezov et al., (2005), described the effect of increasing pressure in terms of altering the vapour/liquid equilibrium so that the higher molecular weight

material remains as liquid within the particle rather than evaporating, i.e. similar to the retention of volatile matter described by Lee *et al*., (1991). Strevoz *et al*. also considered that increasing pressure could potentially close pores and resist the egress of volatile matter from the particle.

Increasing the pressure affected when in the pyrolysis process the majority of swelling occurred. At 0.8 MPa the majority of swelling occurred late in the devolatilisation process when the rate of weight loss was low, however at 2.2 MPa the majority of swelling occurred early in devolatilisation when the rate of weight loss was high. At the higher pressure the resistance to expansion meant that swelling was only able to occur when the build-up of pressure within the particle was highest, i.e. when the rate of weight loss was high.

The effects of pressure are likely to be coal-type dependant. Kahn & Jenkins, (1986), found that that the effect of pressure on coal swelling behaviour in a high-pressure micro-dilatometer as a function of coal rank was highly variable and that the maximum swelling parameter at 2.9 MPa showed little correlation with properties measured at standard pressure.

Yang *et al*., (2014), included an investigation into the effects of ambient pressure on final swelling ratio in their modelling work. The trend of increasing and then decreasing final swelling ratio with increasing ambient pressure was observed in the model results, with the peak appearing at 0.3-0.4 MPa for the two coals studied at a heating rate of 10^4 K/s (Figure 2.34). Although this value for optimum ambient pressure is lower than the values given by Lee at al., (1991), and Strevoz *et al*., (2005), this may be due to the fact that only a limited number of ambient pressures were used in those pieces of work. Figure 2.34 suggests that whilst ambient pressures of 0.8 MPa and 1.0 MPa would indeed have produced the highest swelling ratios of the pressures studied by Lee *et al*., and Strevoz *et al*., they may not necessarily have represented the true optimum. Therefore, the results of Yang *et al*., are in fact consistent with the two previous works. The results of Wu *et al*, (2000), are not consistent however, as they appear to indicate an optimum at or above 1.5 MPa.

The calculated results agreed reasonably well with most experimental results from literature cited by Yang *et al*., however there was an exception for one coal, which attained a much higher swelling ratio (>3.5) in the experimental results than was predicted (~1.6). This coal was heated at a slower rate than the other two modelled coals and it was suggested that a combination of lower heating rate and higher ambient pressure would lead to an increased likelihood of more than one central bubble forming. In this case the single central bubble model would have limitations.
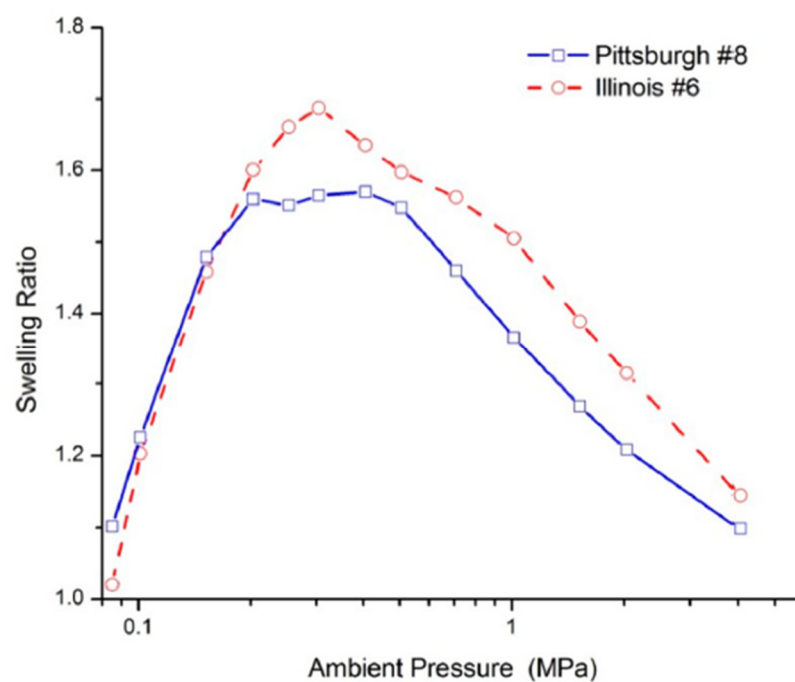
Figure 2.34: The change in final swelling ratio of two coals with ambient pressure at a heating rate of 1×10^4 K/s. Pittsburgh #8 VM = 38.8 % (daf), Illinois #6 VM = 44.27 % (daf). (Yang *et al*., 2014).

Yang *et al*., (2014), explained the effects of ambient pressure in terms of the difference between the internal pressure and the ambient pressure. Increasing the ambient pressure reduces this pressure difference, which has different competing effects. Initially the reduction in pressure difference reduces the frequency of bubble rupture and therefore increases swelling ratio. Volatilisation is also restricted by higher ambient pressures, which increases the metaplast content of the coal, this increases plasticity and extends the duration of the plastic stage, contributing to an increased swelling ratio. On the other hand, reducing the

pressure difference also reduces the driving force for swelling, thereby decreasing the swelling ratio, and if the ambient pressure is high enough it has the effect of restricting the particle swelling. Increasing ambient pressure reduces both the initial internal pressure at the beginning of the plastic stage and also the number of bubbles, these effects decrease the swelling ratio.
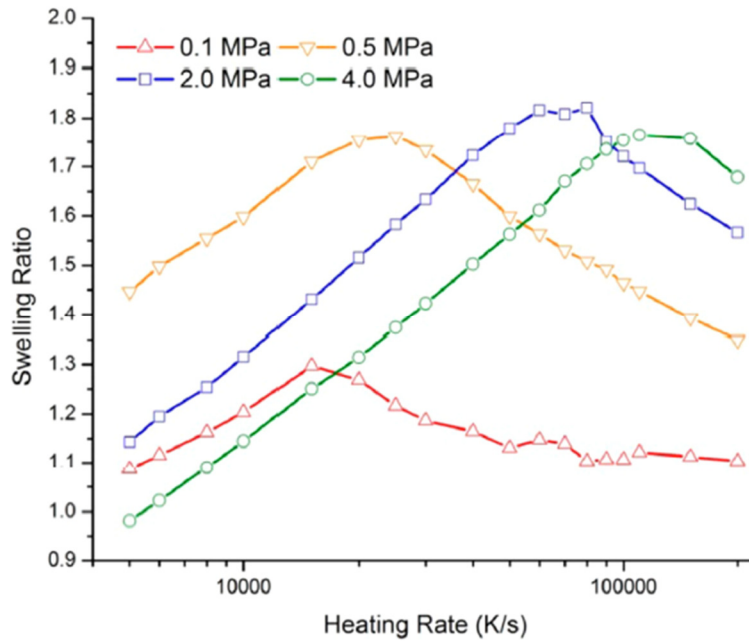
Figure 2.35: Predicted final swelling ratios at various heating rates and various ambient pressures for a 60 μm diameter particle of Illinois No. 6 bituminous coal. (Yang *et al*., 2014)

The variables of ambient pressure and heating rate both have the effect of first increasing and then decreasing swelling ratio as they themselves increase. Modelled results of Yang *et al*., (2014), show that increasing ambient pressure increases the peak in swelling ratio with respect to heating rate, and shifts it to higher heating rates (Figure 2.35). At higher ambient pressures the change in swelling ratio with the increase in heating rate is larger, which is due to the effect of increasing ambient pressure lowering bubble rupture frequency, this opposes the effect of increasing heating rate which would otherwise increase rupture frequency. This enables the increasing internal pressure to drive further swelling.

To summarise, the evidence from experimental and modelling work is that increasing the ambient pressure has the effect of initially increasing, then

decreasing swelling ratio. The optimum ambient pressure is predicted to be around 0.3-0.4 MPa at a heating rate of 10^4 K/s and the value of the optimum ambient pressure is predicted to increase as heating rate increases. The value is also likely to be coal-type dependent. The initial increase in swelling ratio has been attributed to increased fluidity/plasticity brought about by retention of volatile matter, and a decrease in the frequency of central bubble rupture. The decrease in swelling ratio at higher ambient pressures is attributed to the opposition to particle expansion by the external pressure, and a decreased initial internal pressure at the beginning of the plastic stage, which reduces the number of bubbles thereby reducing swelling ratio.

In the blast furnace raceway, coal particles experience pressures of 0.5 MPa (Carpenter, 2006). Yet, much experimental work investigating coal properties in relation to PCI is carried out at atmospheric pressure. This is understandable, given the cost and complexity of undertaking experiments under high-pressure conditions. The literature reviewed here highlights one reason, i.e. particle swelling, why the relative behaviours of coals at atmospheric pressure may not necessarily be extrapolated to behaviours at blast furnace pressure. The swelling behaviour, and therefore char properties, of a certain coal type may be affected to a greater extent by increasing pressure than another coal type.

2.11.5 Summary of the influence of heating environment on coal swelling

The heating environment has a significant effect on the swelling properties of coal particles. The maximum swelling ratio and final swelling ratio pass through a maximum with respect to increasing heating rate and to increasing ambient pressure. At 0.1 MPa the optimum heating rate is estimated to be between 10^3 K/s and 2 x 10^4 K/s. At a heating rate of 10^4 K/s the optimum pressure is predicted to be around 0.3-0.4 MPa. The effects of heating rate and ambient pressure are also interconnected i.e. increasing the heating rate increases the value of the optimum swelling pressure. The presence of oxygen in the atmosphere may increase swelling by increasing the heating rate due to combustion.

2.12 Consequences of coal swelling

In this section the consequences of coal particle swelling are reviewed. These include devolatilisation rate, char properties, ash formation and NO_x formation.

2.12.1 Devolatilisation rate

Combustion of volatile gases is the first step of the combustion process after water evaporation, therefore the rate of devolatilisation governs the initial rate of combustion of coal particles. Since rapid conversion rates are required for blast furnace coal injection it is useful to understand how the coal swelling process is related to the rate of devolatilisation.

The mechanism of mass transfer of volatile gases from a devolatilising coal particle is influenced by the thermoplastic properties of the coal. For non-softening coals the mechanism is by diffusion through the pore system, whereas the pores of softening coals initially become blocked as fluidity develops, in this case gas transfer occurs by bubble growth and rupture as described in section 2.8. Therefore, the swelling process is intrinsically linked to conversion.

A correlation between maximum expansion rate and burning time of single pulverised coal particles was established showing that burning time decreases with increasing maximum expansion rate (Yu *et al.*, 2003). This implies a faster rate of conversion for particles that swell faster. This is supported by Howard (1981) (reference within Yu *et al.*, 2007), who reported a higher range of *Q-Factor*[*] values for highly swelling coals (*Q* = 1.5-1.8) compared to lesser swelling coals (*Q* = 1.3-1.5), with the effect being strongest for bituminous coals. On the other hand, Stubington & Linjewile, (1988), presented evidence that suggested higher FSI values correlated with longer devolatilisation times, although this was attributed to the greater degree of fragmentation of the lower swelling coals within the study rather than an inhibiting effect of swelling.

---

[*] *Q-Factor* is the ratio of devolatilisation measured during a specific process in question to the standard Proximate volatile matter, i.e. it is a measure of the effectiveness of devolatilisation during the specified process.

Muto *et al*., (2016), numerically modelled a pulverized coal jet flame and compared scenarios in which particle swelling and shrinkage were considered and when they were not considered. The results indicated that the swelling and shrinkage of particles did not significantly affect the gas temperature distribution of the flame. However, the simulated results did suggest greater carbon conversion up to 120 mm from injection for particles where swelling and shrinkage was considered (Figure 2.36). Muto *et al*., did not discuss this in-depth, but related the increased conversion to swelling being the dominant process up to 120 mm. This simulation suggests that swelling coals will burn out at a higher initial rate than lesser-swelling coals.
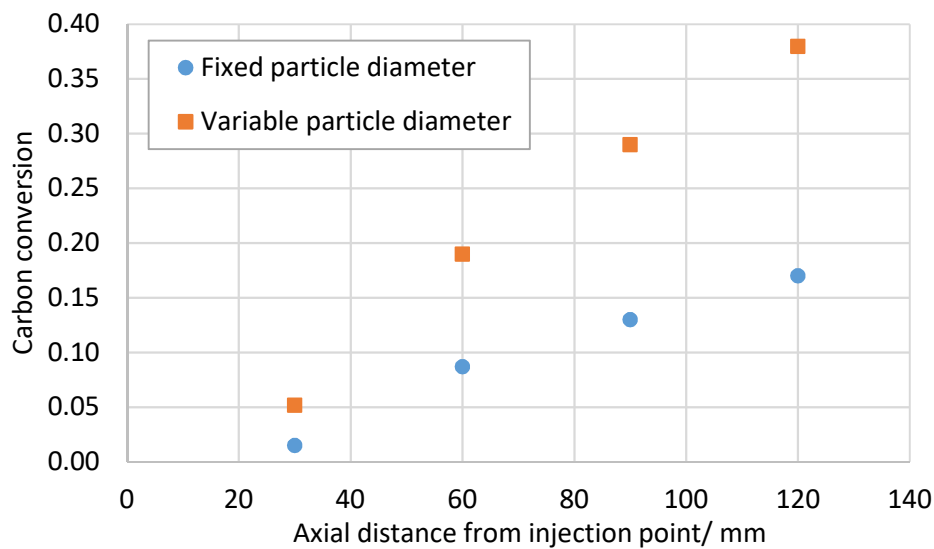
Figure 2.36: Estimated average carbon conversion (max. conversion = 1.0) of pulverised coal particles as a function of axial distance from injection assuming a fixed particle diameter and a variable particle diameter (Muto *et al*., 2016).

The evidence presented above suggests that swelling coals may be converted at a faster rate than lesser-swelling coals. However, in the experimental results of Coetzee *et al*, (2014), no correlation was observed between degree of swelling and mass loss within a suite of three coals studied at low heating rates. Similarly Steer *et al*., (2015b), did not find a correlation between swelling and drop tube furnace burnout within a suite of four coals. This indicates that any influence of swelling on the initial conversion rate is not necessarily straight-forward to identify and that other factors may be influential.

2.12.2   Char properties

The development of char particle morphology is intrinsically linked to the swelling of the particle, and is of great importance to the properties of the char. The size of the char particle and the internal structure formed from a swelling coal is dictated by the formation and behaviour of bubbles rather than by the pore structure of the parent coal particle (Yu *et al.*, 2007). The size, surface area and pore structure of the char are then important in determining the overall reactivity of the char (Menéndez *et al.*, 1993).

Char reactivity by heterogeneous oxidation can occur in any of three regimes as illustrated by Figure 2.37 (Wu, 2005). The regime under which a char reacts is dictated by a temperature-dependent balance between the rate of diffusion of the reactive gas to the reaction site and the rate of the chemical reaction between gas and char. The three regimes and the influence of the char morphology within each are described below:

I. *Regime I*. At relatively low temperatures the overall rate of reaction is lowest and the rate determining step is the heterogeneous chemical reaction between the char and the gas. Gas molecules are readily available to react with any available char surface. Under Regime I increasing the total surface area available for reaction increases the rate of the chemical reaction.

II. *Regime II*. At higher temperatures the overall rate of reaction is faster, the chemical reaction occurs faster and the rate limiting step becomes the rate at which the gas can diffuse into the particle to access the large internal surface area. Under Regime II increasing the accessibility of the internal surface area to reactive gases increases the overall rate of reaction. In this regard the absence of large 'feeder pores' at the char surface has been linked to lower rates of char reactivity (Hippo & Walker, 1975).

III. *Regime III*. At even higher temperatures the overall rate of reaction is fastest. The rate of the chemical reaction is so fast that the gas reacts at the surface of the particle before it is able to access the internal pore

structure. Under this regime the rate limiting step is the rate of diffusion of gas to the char surface. Increasing the overall size of the particle can increase the overall reaction rate by decreasing the time required for gas to diffuse to the particle surface.
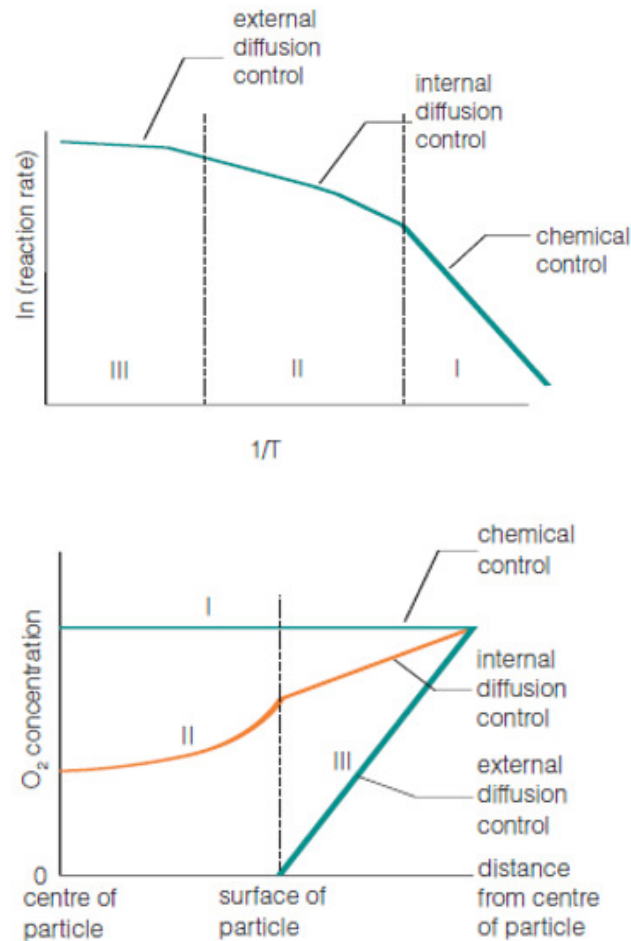
Figure 2.37: Reaction regimes of char oxidation. (Wu, 2005)

Laboratory tests on char reactivity are typically carried out under Regime I conditions so that the rate of the heterogeneous chemical reaction between gas and char is measured. This measurement is influenced by the total char surface area as described above, therefore in order to eliminate this influence from the results researchers may include measurements of the char surface area (usually by BET method) to produce a figure for intrinsic char reactivity (i.e. reactivity ÷ surface area) (Zeng *et al.*, 2005). This intrinsic reactivity can also be influenced by the swelling process; Yoshizawa *et al.*, (2006), found that stacking of aromatic ring systems within the char was greatest at heat-treatment temperatures where

swelling also peaked, leading to the conclusion that the thermoplastic expansion of the particle facilitated increased aromatic stacking. It was suggested that this, in turn, may result in a decreased intrinsic reactivity of the organic material. Russel *et al.*, (2000), described a greater effect of thermo-deactivation of char particles from a highly fluid bituminous coal in comparison to a low volatile matter, high rank coal when heated at high temperatures. This thermo-deactivation is the result of greater ordering of the carbon structure and led to a reduced char reactivity. This work again suggests lower intrinsic char reactivity associated with swelling coals.

As described above swelling can increase the reactivity of char particles. Steer *et al.*, (2018), found a tendency for the more highly reactive chars produced in a drop tube furnace to react more endothermically with carbon dioxide during reactivity tests in a simultaneous thermal analysis instrument. Greater char reactivity is generally considered to be beneficial to the blast furnace process, yet this endothermic reactivity was proposed to have a potentially negative effect, where the possible local temperature reduction caused by the endothermic reaction of char particles outside the raceway may lead to blast furnace instability.

One consequence of coal swelling may be an increased level of particle agglomeration during the heating process. Sexton *et al.*, (2018), studied the phenomenon of agglomeration in relation to the blast furnace process. A greater tendency to agglomerate was observed for coals with a higher caking index. Chen *et al.*, (2007), also observed that of the two coals they studied using a drop tube furnace agglomeration was more pronounced for the coal which showed the higher degree of swelling. Agglomeration was considered to potentially adversely affect blast furnace performance due to the increased potential for reduced burden permeability, however Sexton *et al.*, (2018), found that the agglomerated char particles had a greater reactivity than the non-agglomerated chars, even when the two forms of char were powdered to minimise differences in morphology.

The fragmentation of coal char particles at high temperatures during the latter stages of combustion has been linked to the char morphology (Yu *et al.*, 2007). Wu *et al.*, (2000), observed that increasing the pressure in a pressurised drop tube furnace resulted in a greater final swelling ratio, a greater percentage of char particles with high internal porosity and a greater degree of fragmentation. Dakič *et al.*, (1998), worked with an experimental fluidised bed test rig and also linked fragmentation to swelling. They suggested that when swelling was low the pore system remained open therefore internal pressure did not build up to result in fragmentation, also when swelling was greatest the expansion of the particle acted to alleviate the increasing internal pressure. However, there was a middle-range where fragmentation appeared to be more prevalent. In this range thermoplasticity caused pores to close yet the swelling was not great enough to alleviate the increasing internal pressure, resulting in fragmentation. The result of fragmentation is to decrease particle size and further increase the surface area available for reaction, with the freshly exposed surfaces potentially having a more reactive surface chemistry than the pre-existing surfaces (Steer *et al.*, 2015b), and also to affect the formation of ash particles (see below).

2.12.3 Ash and NO$_x$ formation

The formation of ash is affected by the swelling of coal particles. Swelling itself, and subsequent fragmentation of the resulting thin-walled cenospheres, helps to prevent the coalescence of mineral matter during conversion, leading to smaller ash particles (Wu *et al.*, 1999).

A lower degree of conversion of char nitrogen to nitrogen monoxide has been observed for chars with greater swelling properties due to the increased heterogeneous reduction of nitrogen monoxide on the char surface (Arenillas *et al.*, 1999).

2.13 Summary and unresolved issues

The steel industry is the second biggest industry in the world and the quantity of crude steel produced annually is predicted to continue rising to meet the needs of a growing world population. Blast furnace ironmaking represents the long-

established primary route to producing iron for steelmaking and is predicted to remain the predominant route until around 2040. After this time increasing amounts of steel are likely to be produced via the scrap-based electric arc furnace route, yet the blast furnace will remain a significant route until 2100 and beyond.

Blast furnace ironmaking is an energy intensive process and a significant source of carbon emissions. Therefore, increased pressure in terms of environmental impact and competition from alternative steelmaking routes will make it necessary for blast furnaces to continue improving their efficiency, productivity and environmental impact.

The effective use of auxiliary reducing agents, predominantly coal in modern blast furnace ironmaking, will help blast furnaces meet these challenges by reducing the dependence upon coke within the blast furnace. Auxiliary reducing agents are materials injected into the blast furnace through the tuyeres, they are converted to reducing gases within the raceway zones, thereby lowering the requirement on coke as a reducing agent. As a result, a lower coke rate may be used (less coke per ton of iron) which has environmental, economic and technical benefits.

Different coals have different properties and market values therefore selecting the most cost-effective coals for blast furnace injection is important. However, assessment of coal performance is not a straight forward matter as it is often difficult to isolate the effect of the injection coal from other factors. Direct measurements or sampling from the raceway are very difficult due to the challenging conditions. It is therefore necessary to be able to predict the behaviour of an injection coal using the results of pilot scale and laboratory scale tests and mathematical modelling.

The thermoplastic properties of coal are likely to affect the performance of blast furnace injection coals due to the thermal swelling of coal particles. The increases in particle volume and surface area, and the decrease in particle density resulting from the swelling process are likely to impact upon the conveying of the material into the raceway, the conversion within the blast furnace and the transport of char particles through the furnace.

Research on coal particle swelling has demonstrated that the unrestrained swelling behaviour of discrete particles is not necessarily anticipated by the standard tests of coal thermoplasticity such as free swelling index, Ruhr dilatometer and Gieseler plastometer, which use packed volumes of coal particles and low heating rates. Extrinsic factors such as heating rate, pressure and gas composition influence swelling, as do intrinsic factors such as maceral and mineral composition. Real-time imaging of swelling coal particles has revealed the process of bubble growth and rupture, by which swelling occurs, and the existence of the transient maximum swelling ratio. The swelling of coal particles is predicted to increase the rate of burnout at low residence times and is intrinsically linked to the char properties. Ash chemistry, char particle size and the evolution of NO_x are also shown to be affected by the swelling of coal particles.

Although modelling work has successfully predicted many of the features of coal particle swelling observed in laboratory tests, there is still a degree of inaccuracy when it comes to predicting the swelling behaviour of different coals based on their properties. This indicates that there are some properties of the coal, which influence swelling in a way that is not yet fully understood. For example, the surface tension of the plastic coal particle during heating is anticipated to affect the rate of bubble growth and rupture, however no experimental methods have been applied to directly measure the surface tension. The effects of particle size and volatile matter have not been conclusively researched, and although some comparisons have been drawn with the results of standard thermoplastic tests (for example some correlation with FSI and with Gieseler fluidity has been observed) these only include a small number of coals (generally 3).

Knowledge of coal particle swelling properties has not been widely applied to the blast furnace PCI situation, so that it is not known what the impact of particle swelling will be on the overall process. A full understanding of the implications of coal thermoplasticity with regard to blast furnace PCI is necessary for a complete evaluation of a potential PCI coal.

3 Formulating the research approach

The aim of this project is to develop a novel technique to characterise coal for blast furnace coal injection. The thermoplastic swelling properties of discrete coal particles has been identified as a variable characteristic of coals, which is likely to impact upon blast furnace performance. The exact manner in which coal particle swelling affects the blast furnace is not fully understood. The HT-CSLM has been identified as a potentially suitable method for the analysis of the transient swelling properties of discrete coal particles due to the closely controlled heating environment and optical imaging capabilities of the equipment. The project will interrogate known extrinsic and intrinsic factors influencing the swelling behaviour of coal to offer robust testing of this novel characterisation test. Swelling has been chosen due to the scarcity of existing knowledge regarding the effect it has on blast furnace performance, and its potential to influence coal conversion, char reactivity, extent of agglomeration and blast furnace permeability. The overall aim will be explored through a hypothesis driven approach, which has been broken down in the following section to clearly state the interrogated influences and why they are chosen. Each hypothesis is followed by the method of interrogation.

Hypothesis 1 – The swelling of individual coal particles can be measured using the HT-CSLM.

Objective 1 – Develop a method of measuring coal particle swelling using the HT-CSLM, which will form the basis of a novel technique for characterising coal for blast furnace coal injection. The swelling of discrete coal particles has been reported in the literature using methods involving some heating apparatus combined with optical imaging, as described in chapter 2, therefore the HT-CSLM has been identified as potentially a suitable method for this type of measurement.

Approach to Hypothesis 1 – Measurements of coal particle swelling during heating will be conducted by image analysis of HT-CSLM videos recorded at 15

frames per second. Relevant coal samples will be provided by Tata Steel and crushed to a particle size range consistent with blast furnace PCI grades. A suite of four coal samples will be tested to assess the applicability of this technique across a range of coal types. Results will be compared to those of standard tests of coal thermoplasticity, i.e. Gieseler fluidity and Ruhr dilatometer to show whether information is revealed by the HT-CSLM technique, which would not otherwise be apparent from the standard techniques.

Hypothesis 2 – Increasing heating rate increases the transient maximum swelling ratio of coal particles.

Objective 2 – Use the HT-CSLM to investigate the effect of heating rate on transient coal particle swelling ratios. The effect of heating rate has been studied previously, mainly with regard to final swelling ratio, therefore this investigation provides a means of testing the technique and providing improved knowledge of the effect of heating rate on maximum swelling ratio.

Approach to Hypothesis 2 – This work will make use of the ability of the HT-CSLM to heat samples at closely controlled heating rates of up to 700 K/min, which is the limit of the equipment. This limit means that swelling should occur under Regime 1 (see Figure 2.28), in which final swelling ratio has been found to increase with increasing heating rate. The effect of increasing heating rate on the transient maximum swelling ratio of coal samples will be investigated. Four coal types will be used in this work to see if effects are common across this range of coal types.

Hypothesis 3 – Lighter coal particles attain a greater maximum swelling ratio than denser particles of the same coal.

Objective 3 – Use the HT-CSLM in conjunction with coal density separation to investigate the effect of particle density on maximum swelling ratio. The density of coal particles has previously been shown to affect swelling behaviour due to differences in maceral and mineral contents between density fractions, therefore this investigation provides a means of testing the HT-CSLM technique.

Approach to Hypothesis 3 – Density separation will be carried out using a sink-float centrifugation technique. The swelling behaviour of the density fractions will be measured by HT-CSLM. Two coals will be selected for this study from the suite of four coals. The density fractions will also be characterised by Proximate, Ultimate, petrographic, Gieseler fluidity and thermo-gravimetric (TGA) analyses.

Hypothesis 4 – Coal swelling behaviour can be related to Gieseler fluidity and TGA mass loss.

Objective 4 – Based on the knowledge that swelling is driven by the evolution of volatile matter and facilitated by the thermal softening of the coal structure, investigate whether the Gieseler fluidity and mass loss (as measured by TGA) of a coal sample can be related to its HT-CSLM swelling behaviour.

Approach to Hypothesis 4 – The Guiseler fluidity of the four coal types will be measured in the standard way. The mass loss of coal samples during devolatilisation will be measured by TGA. The swelling behaviour of the coals will be measured by HT-CSLM at the same heating rate as used for TGA. The data will be analysed to show relationships between the development of Gieseler fluidity, the rate of volatile matter evolution (as measured by mass loss) and the swelling ratio. A similar approach will be taken with density-separated fractions of two of the coals. Density separated fractions of a coal are likely to have different swelling, fluidity and rate-of-mass loss characteristics.

Hypothesis 5 – The maximum swelling ratio of coal particles increases with increasing particle size within the size range associated with blast furnace PCI.

Objective 5 – Use the HT-CSLM to investigate the effect of particle size on transient coal particle swelling ratios within the particle size range associated with blast furnace PCI. Coal particle size is known to affect certain characteristics such as devolatilisation and has the potential to affect maximum swelling ratio by means of increased volatile matter residence time and increased influence of temperature gradients within the particle.

Approach to Hypothesis 5 – Three particle size fractions of two coals will be analysed by HT-CSLM to investigate the effects of particle size on coal swelling.

The test samples will not only be categorised by particle size but also by density, i.e. a narrow density fraction of each particle size will be used to minimise the effect of variables such as mineral and maceral composition, which can vary according to particle size within the overall crushed sample.

Hypothesis 6 – The swelling ratio observed by HT-CSLM correlates with that observed after drop tube furnace (DTF) treatment.

Objective 6 – Use a DTF to 'scale-up' the HT-CSLM experiments, i.e. determine whether the swelling ratio observed by HT-CSLM correlates with that observed after DTF treatment at a much higher heating rate. Moving to the higher heating rates associated with the DTF is known to increase the final swelling ratio of coal particles, this investigation will determine whether the relative swelling behaviours of the four selected coals is consistent between the two techniques.

Approach to Hypothesis 6 – A DTF will be used to heat the four coals in an environment closer to that of the blast furnace raceway than was possible in the HT-CSLM. The coal particles will be subject to much higher heating rates in the DTF than in the HT-CSLM and will be 'injected' into a moving gas stream rather than heated within a crucible. Particle size analysis will enable the swelling ratio after DTF processing to be measured. The order of swelling of the four coal types in the two techniques can be compared.

Hypothesis 7a – The rate of coal conversion is enhanced by particle swelling.

Hypothesis 7b – The rate of char reactivity is enhanced by particle swelling.

Objective 7 – Use the results of DTF tests to evaluate whether coal particle swelling affects rates of coal conversion and char reactivity, which are considered important for effective PCI operation. Some previously published modelling work has suggested that model coal particles with swelling have higher rates of conversion at low residence times than identical particles with no swelling. This work will provide some experimental evidence regarding the influence of swelling on conversion. The reactivity of char particles has previously been shown to be influenced by char surface area therefore high levels of swelling are expected to increase char reactivity.

Approach to Hypotheses 7a and b – DTF test work will produce quantities of char much greater than those produced by HT-CSLM, therefore it will be possible to measure the degree of conversion and the char reactivity of each DTF char sample. Along with the swelling data described under Hypothesis 5 it will be possible to assess whether the greater swelling of certain samples is associated with higher levels of conversion or char reactivity.

4 Experimental methods

4.1 Coal selection

Four coals, referred to as A, B, C and D, have been selected for inclusion in this project. The coals have been provided by Tata Steel, IJmuiden. A and B have been used as injection coals within Tata Steel Europe, whilst C and D have been selected to provide a comparison. The coals form two pairs; A and B are lower volatile matter coals (14-18 % (daf)) whereas C and D are higher volatile matter coals (~36 % (daf)). Each pair consists of a coal being known to have swelling behaviour (B and D) and another being considered to have little or no swelling behaviour (A and C).

Coal A has been used frequently as a pulverised injection coal and is considered a reliable injectant in terms of facilitating stable blast furnace operation. The use of coal B in pulverised coal injection has been associated with a lack of blast furnace stability and is also known to cause material handling problems at the plant. Coals C and D have been used in cokemaking blends rather than as injection coals and have been included to provide a contrast to the lower-volatile coals A and B.

Characterisation data of coals A-D is shown in Table 4.1. With the exception of the petrographic data all results are the average of a minimum of two duplicate tests. The instruments used to generate the data are listed in Table 4.2 along with the relevant standards. Further detail is available in Appendix B i.e. petrographic reflectance histograms, Ruhr dilatometer graphs, Gieseler plastometer graphs and ash chemistry results.

	Coal A	Coal B	Coal C	Coal D
Proximate analysis				
Moisture/ % (ad)	1.9	0.8	3.6	1.4
Volatile matter/ % (db)	14.4	18.4	36.4	36.3
Ash/ % (db)	9.0	6.6	4.6	5.5
Fixed carbon/ % (db)(diff)	76.6	75.1	59.0	58.1
Ultimate analysis				
Carbon/ % (daf)	88.1	88.7	81.2	83.9
Hydrogen/ % (daf)	4.4	4.8	5.4	5.7
Nitrogen/ % (daf)	2.2	1.2	1.6	1.5
Sulphur/ % (daf)	0.4	0.8	0.4	1.2
Oxygen/ % (daf)(diff)	5.3	5.4	11.9	9.0
Petrographic analysis				
Liptinite/ %	0.0	1.9	4.0	4.1
Vitrinite/ %	76.1	72.0	56.8	75.5
Inertinite/ %	23.9	26.2	39.2	20.3
Vitrinite reflectance, Ro (max.)	1.6	1.5	0.8	0.8
Ruhr dilatometer data				
Softening temp./ °C	†	433	404	372
Max. contraction temp./ °C	†	468.5	499	417
Re-solidification temp./ °C	†	495	No re-solidification	450
Max. contraction/ %	†	-10	-19	-15
Max. dilation/ %	†	12	Contraction only	46
Gieseler plastometer data				
Softening temp./ °C	†	450	408	393
Solidification temp./ °C	†	495	438	469
Plastic range/ °C	†	45	30	77
Max. fluidity/ ddpm	†	7	2	3433
Max. fluidity temp./ °C	†	477	424	432
Free swelling index (FSI)	1	8	3-4	8

† Coal A produced no contraction or dilation in the dilatometer and no plasticity in the plastometer.

Table 4.1: Coal characterisation data for coals A-D.

	Instrument	Standard
Proximate analysis	Leco TGA 701	ISO 17246
Ultimate analysis	Leco TruSpec CHN + S	ISO 17247
Petrographic analysis	Leica Q550IW automated image analysis system	
Rhur dilatometer	RB Automazione DL 4000	ISO 23873
Gieseler plastometer	RB Automazione PL 2000	ISO FDIS10329
Free swelling index	Results provided by Tata Steel following in-house testing	ISO 501
Ash chemistry	Thermo Scientific ARL Perform'X Sequential XRF	ISO/TS 13605
Particle size analysis	Malvern Mastersizer (Chapters 5-8) Retsch Camsizer (Chapter 9)	

Table 4.2: Instruments used for coal characterisation and particle size analysis.

4.2 Coal crushing

Coal preparation involved air-drying and crushing the samples to a size specification considered typical of blast furnace PCI, i.e. 80 % below 75 µm. Un-washed coal samples of approximately 3-4 kg were received. These uncrushed samples contained lumps of up to 5 cm in some cases, therefore the particle size was first moderated by crushing the largest pieces, using pestle and mortar, before passing the whole sample through a disc mill to produce a coarsely crushed sample. This coarsely crushed sample was then further crushed using a Tema mill in batches of 75 g (this was found to constitute approximately 1/3 of the working volume of the Tema mill). For each coal a 'calibration' of the Tema mill was first carried out so that a single pass through the Tema mill would reduce 75 g portions of the coarsely crushed sample to the desired specification. Particle size distribution graphs, produced using a Malvern Mastersizer, of coals A-D are shown in Figure 4.1. The milling times necessary to achieve these similar size distributions are shown in Table 4.3. These residence times illustrate differences in grinding performance between the coals.

Coal ID.	Time in Tema mill/ s
Coal A	30
Coal B	10
Coal C	43
Coal D	96

Table 4.3: Residence time within Tema mill required to crush 75 g of different coal types to ~80 % < 75 μm.
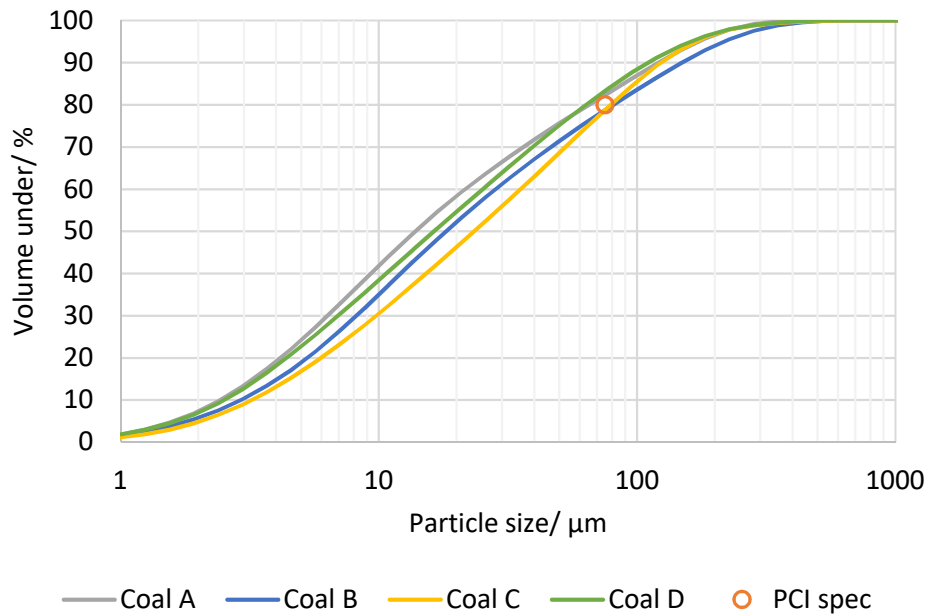
Figure 4.1: Particle size distributions of coals A-D after crushing to a nominal PCI specification using Tema mill.

A comparison was made between the Mastersizer and the technique of wet sieving to measure particle size distribution. Five different samples were analysed using both techniques and the results were in good agreement.

After crushing to 80% < 75 μm, as described above, each coal sample was divided into narrow size fractions by wet sieving to reduce the variability in characteristics within each sample that can be caused by segregation (Cloke *et al*., 2002; Tian *et al*., 2016). Wet sieving was used rather than dry sieving due to its greater efficiency at separating very small particle sizes. The sieves used had the following aperture sizes: 38 μm, 53 μm, 63 μm, 75 μm, 90 μm and 125 μm. This produced

six size fractions as the smallest material (<38 μm) was removed in the waste water.

Detailed characterisation data relating to the separated sieve fractions is available in Appendix C. This includes the particle size distribution within each separated sieve fraction of coals A-D (measured by Malvern Mastersizer), the Dv(0.5) values (the diameter below which 50 %, by volume, of the sample exists), Proximate and Ultimate analysis data and petrographic reflectance distribution graphs.

4.3 Separation by density

Certain coal samples were separated by density to investigate differences between density fractions. This was achieved by a sink-float centrifugation technique (ISO 7936: 1992(E)) using caesium chloride solutions of different concentrations as the separating media. Particles denser than the separating medium sink, and are termed 'sinks', whilst particles less-dense than the medium float, and are termed 'floats'. Five density fractions were thus obtained as shown in Table 4.4. Densities shown here are all relative to 1 L of water having a density of 1 kg/L.

Density of medium in which particles sink/ kg/L	Density of medium in which particles float/ kg/L	Sample ID.
Not determined	1.2	F1.2
1.2	1.3	S1.2-F1.3
1.3	1.4	S1.3-F1.4
1.4	1.7	S1.4-F1.7
1.7	Not determined	S1.7

Table 4.4: Definitions of density fractions used in this work.

4.4 Measurement of coal swelling

Measurement of the swelling of individual coal particles was made by analysing videos obtained from a high temperature confocal scanning laser microscope (HT-CSLM) (Figure 4.2). The HT-CSLM heating chamber is gold-plated, ellipsoidal in shape and heated using a halogen lamp. A platinum crucible containing the sample was placed on a stage at one focal point, with the halogen lamp located at

the other focal point. The ellipsoidal shape and highly reflective coating focused infra-red radiation from the lamp onto the sample. In this way the sample was heated evenly and at closely controlled heating rates of up to 700 K/min. Meanwhile the gas within the chamber remained relatively cold, which helped to prevent contamination and reduce the potential for oxidative processes. The system also enabled rapid quenching of the sample.

1. Charge-Coupled Device
2. 405 nm laser
3. Beam splitter
4. Sample crucible
5. Stage assembly
6. Thermocouple
7. Gold-plated chamber
8. Bulb
9. Argon inlet
10. Argon outlet
11. Path of laser beam
12. Path of radiation
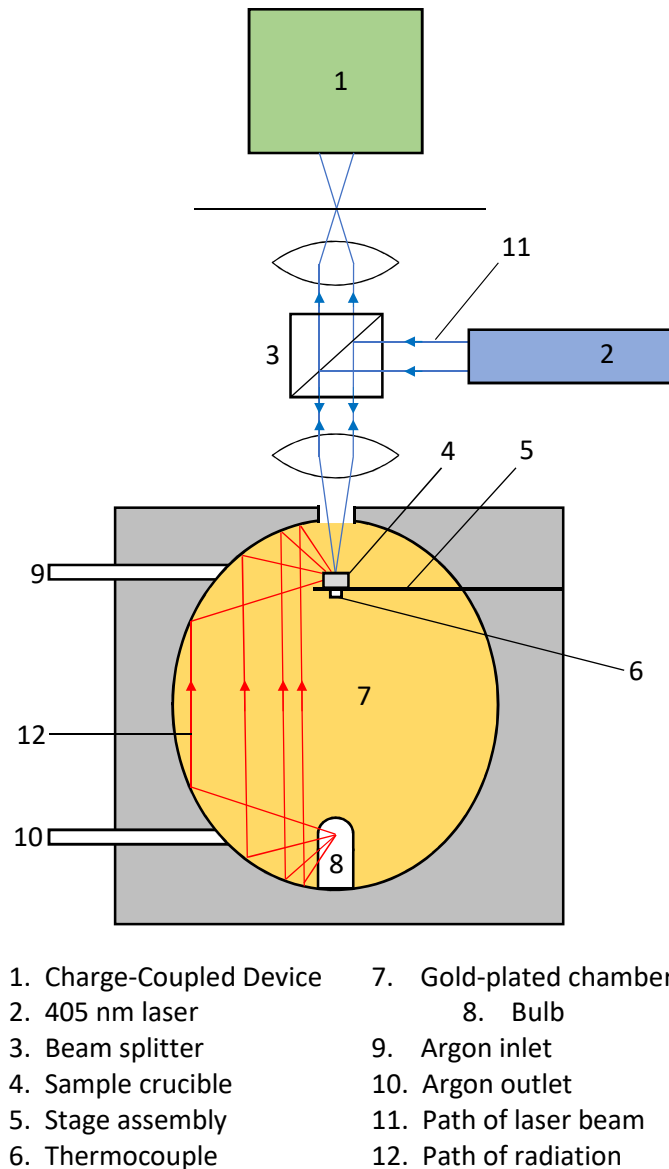
Figure 4.2: Schematic diagram of high temperature confocal scanning laser microscope (HT-CSLM).

The test sample was prepared by placing a small quantity of dispersed particles of the coal in the crucible and adding a drop of isopropanol. The isopropanol

prevented the particles being blown out of the crucible during evacuation and re-filling of the chamber and evaporated during the initial heat-up procedure. The crucible was placed on an aluminium oxide spacer on the sample stage within the chamber (to prevent the Pt crucible and Pt stage fusing at high temperatures), which was then evacuated by connecting to a rotary vacuum pump for a few seconds before being filled with argon. The argon was of N6 purity and the oxygen concentration was further reduced by passing through heated copper and magnesium turnings. The test was performed under a steady 200 mL/min flow of argon to sweep away gaseous products of devolatilisation and provide an inert atmosphere. The pressure within the chamber, which was kept just above atmospheric pressure, was controlled by a valve at the gas outlet.
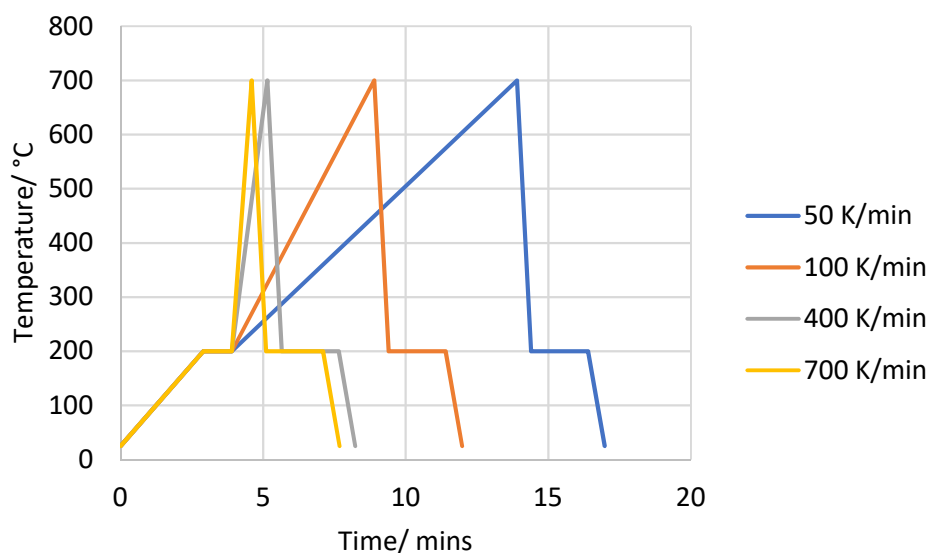
Figure 4.3: The programmed heating profiles used on the HT-CSLM during this work.

The programmed heating profiles used in this work are illustrated in Figure 4.3. A typical heating profile included an initial pre-heating stage, in which the crucible was heated to 200 °C at 60 K/min and held for 1 minute to condition the bulb, the isopropanol evaporated during this stage. The field of view was selected during this 1 minute hold period and the microscope was focused. The crucible was then heated at a closely controlled rate during the active test stage. Heating rates of 50 K/min, 100 K/min, 400 K/min and 700 K/min were used during the active test stage in this work. Once the peak temperature of 700 °C was attained (which was

found by preliminary experiments to cover the temperature range of particle swelling) the crucible was rapidly cooled at 1000 K/min (nominal rate) down to 200 °C. This temperature was held for 2 minutes to maintain the condition of the bulb before cooling to ambient temperature at 300 K/min. The temperature measurement was from a thermocouple attached to the base of the platinum stage.
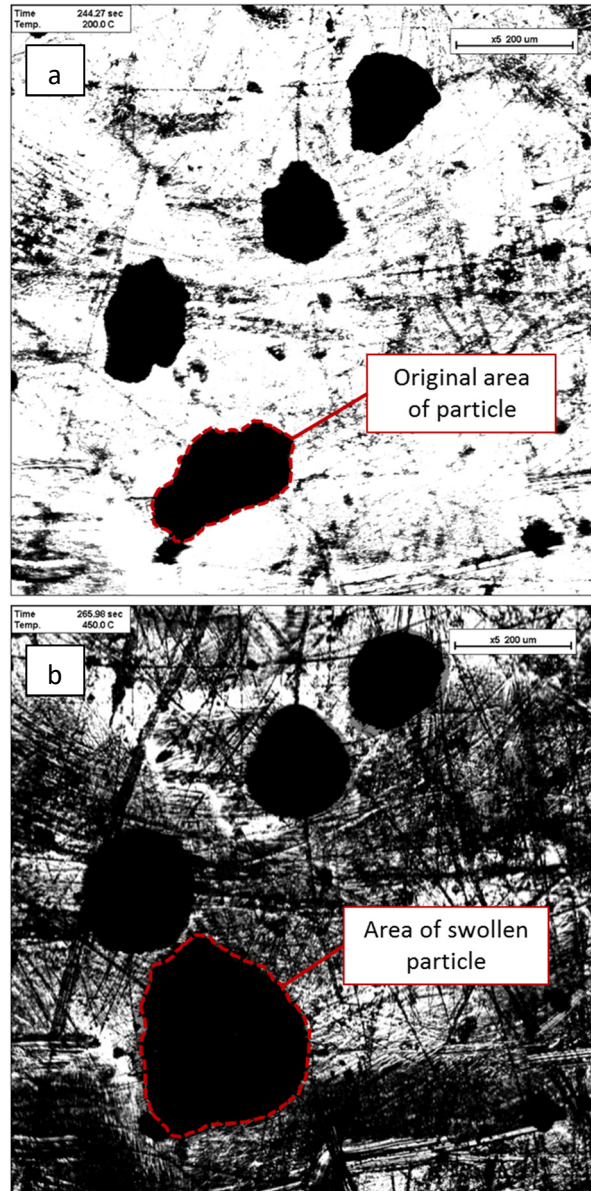
Figure 4.4 Images from HT-CSLM video showing how the area covered by a particle increased when heated from 200 °C (a) to 450 °C (b) at 700 °C/min.

The laser microscope is designed to give a clear view of a narrow focal plane, in this work the microscope was focussed on the inside surface of the crucible base

so that the coal particles appeared in silhouette. The sample was captured on a monochromatic video in real time during the test and analysis of video stills using ImageJ software enabled the changing size of particles to be monitored in terms of their 2-dimentonal area as illustrated in Figure 4.4. The swelling ratio of a particle at temperature = t (SR_t) is defined by Equation 4.1 where A_0 is the area of the particle at the beginning of the active test heating stage (i.e. at 200 °C) and A_t is the area of the particle at temperature = t.

$$SR_t = \frac{A_t}{A_0} \qquad \text{(Equation 4.1)}$$

4.5 Simultaneous thermal analysis

Simultaneous thermal analysis (STA) involves thermogravimetric analysis (TGA) and differential scanning calorimetry (DSC) conducted simultaneously. TGA is the measurement of changes in the mass of a test sample as a function of temperature. DSC is the measure of the energy required to maintain the test sample at a pre-determined temperature. Both measurements are carried out against an empty reference crucible.

STA of coal samples was primarily carried out to obtain the TGA data, providing information on the changing mass of a coal sample during heating, which could then be related to the changing average swelling ratio of a sample of the same material obtained by HT-CSLM. DSC data was also obtained, which was useful in identifying a chemical reaction associated with one of the coals.

STA was carried out using a Netzch STA 409 PC Luxx instrument with a vertical design and a maximum heating rate of 50 K/min. The inert gas used was argon of N6 purity. To mitigate for changes that are unrelated to the sample itself, a blank 'correction' test was carried out using an empty crucible as the sample crucible, the results of the blank crucible were subtracted from the test results. The sample starting mass was 10-11 mg and a 3-step heating profile was used as shown below:

1. Dynamic heating from 20 °C to 900 °C at 50 K/min under argon (30 mL/min)

2. Isothermal heating at 900 °C for 30 minutes under argon (30 mL/min)

3. Isothermal heating at 900 °C for 40 minutes under air (25 mL/min)

Step 1 enabled comparison with HT-CSLM data (HT-CSLM tests that were carried out at 50 K/min) and allowed the moisture content of the sample to be calculated. Step 2 enabled the volatile matter content of the sample to be calculated under conditions analogous to those of the standard test for volatile matter. Step 3 enabled the ash content of the coal to be calculated. The flow rate of air was set differently to that of argon to mitigate for differences in buoyancy between the two gases.

Similar tests were carried out using a Setaram Setsys Evolution TGA instrument in which a heating rate of 100 K/min was possible, to assess the benefits of testing at the higher heating rate. Tests were performed using heating rates of 50 K/min and 100 K/min in Step 1. Slightly different hold times were used in Steps 2 and 3, and the inert gas used was helium. A sample mass of 10-11 mg was also used for this work.

4.6 Scanning electron microscopy

A *FEI* Quanta Field Emission Gun 650 SEM was used to obtain images of char particles. Samples were prepared by either mounting the particles on a carbon stub or transferring the platinum crucible directly from the HT-CSLM into the SEM.

4.7 Drop tube furnace tests

Drop tube furnaces (DTF) have been applied to the study of blast furnace injection coals as a means of measuring coal conversion at high heating rates and temperatures (Du *et al*., 2010; Kalkreuth *et al*., 2005; Li *et al*., 2014; Sahu *et al*., 2014; and Steer *et al*., 2015a and 2015b;). In other work a pressurised DTF has been used to research the gasification of coal (Katjitani *et al*., 2002) at up to 2 MPa. The precise design of different DTFs may vary but the general features are the same; the furnace is a vertical heated tube, with a gas flow from top to bottom. The sample is fed into the top of the furnace and char is collected from the bottom.

The DTF was used in this work to provide a heating environment closer to that of the blast furnace raceway than that provided by the HT-CSLM, to see if swelling results were consistent between the HT-CSLM and the DTF. Calculation of conversion (by ash tracer method) and char reactivity tests also enabled swelling data to be compared with conversion and char reactivity data, which was not possible with HT-CSLM chars due to the small quantities of char material produced.

The DTF used in this work is illustrated in Figure 4.5 and consists of a 1 m ceramic vertical tube (internal diameter 5.2 cm). The internal void was heated by radiation to 1100 °C. Thermocouples at the top, middle and bottom of the furnace allowed the temperature to be controlled zonally. Coal was fed into the top of the tube by means of a screw feeder and conveyed into the furnace by a carrier gas, nitrogen, at 0.5 L/min, via a feeder tube of 6 mm internal diameter.

1. Void
2. Cylindrical ceramic tube
3. Screw feeder
4. Coal feed hopper
5. Thermocouples
6. Carrier gas
7. Secondary gas
8. Receiver probe
9. Cyclone & catch pot
10. Oxygen analyser
11. To off-gas cleaning
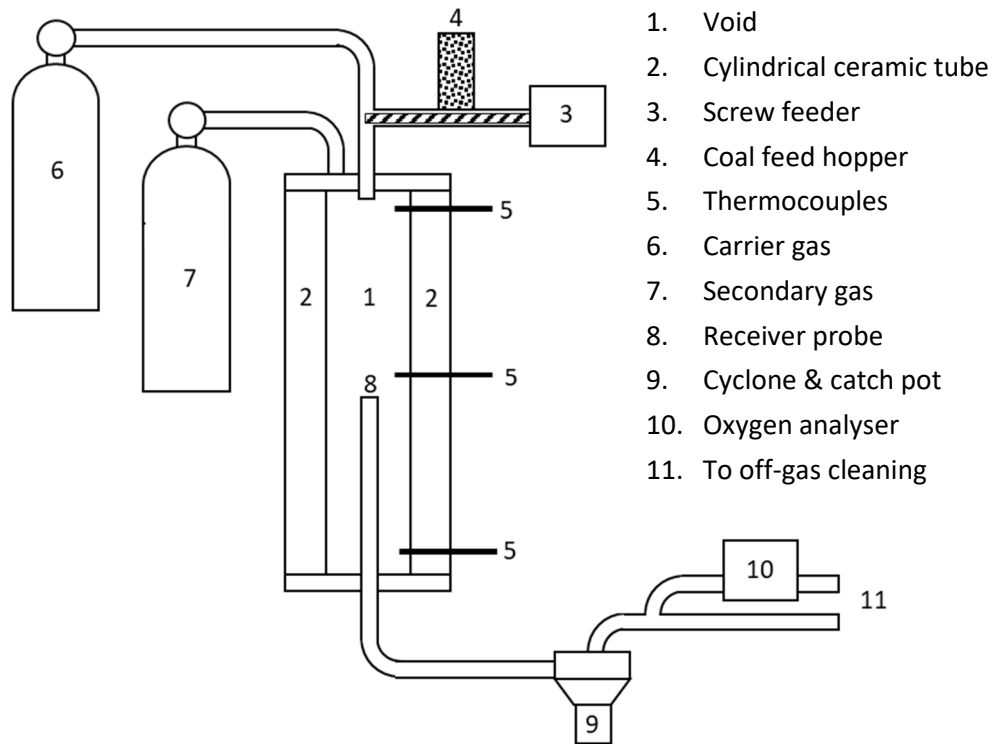
Figure 4.5: Schematic illustration of the drop tube furnace.

The heating rate experienced by coal particles is estimated to be >10^4 K/s (Du *et al.*, 2010). The feed rate of the coal was controlled by the speed of the screw-feeder and was approximately 15 g/hr in this work. The low feed rate promotes single particle reaction. A secondary gas (also nitrogen, with a small amount of air

in this work) was also fed into the top of the furnace at 20 L/min. Nitrogen was chosen to provide an essentially inert environment, so that heating conditions were consistent with the HT-CSLM in this respect. A combustion environment would have created an extra means by which particle size may change, due to consumption by oxidation. The addition of a small amount of air was controlled to create an oxygen concentration of approximately 1 %, this was done to prevent blockages caused by tar build-up. Measurement of oxygen concentration was by analysis of sampled off-gas.

A ceramically protected and water-cooled receiving probe with an internal diameter of 6 mm was inserted into the bottom of the furnace on the central axis to receive char particles. The vertical position of the probe can be altered to vary coal particle residence time. In this work the position was constant to create a residence time of 35 ms. This short residence time was chosen in order to sample the particles during the early stages of devolatilisation. Char was collected in a cyclone for further analysis, whilst the off-gas was pumped through traps to extract tars and particulates. The rate at which the off-gas was pumped out of the furnace and the conveying and secondary gases were fed in were balanced so that laminar flow through the furnace was established and a slight positive pressure was maintained within the furnace.

4.8 Char reactivity

Char reactivity tests were carried out to measure the reactivity of chars produced by DTF tests towards carbon dioxide of 99.5 % purity. The same Netzch STA used for TGA and DSC measurements was used for char reactivity tests. The procedure is based on the isothermal method used by Gu *et al*., (2008). Measuring the reactivity of char towards carbon dioxide involved two steps as follows:

1. Dynamic heating from 20 °C to 900 °C at a rate of 50 K/min under carbon dioxide (60 mL/min).
2. Isothermal heating at 900 °C for 10 hrs (or 20 hrs) under carbon dioxide (60 mL/min).

Subtraction of a blank 'correction' test was used (as described in section 4.5) to improve accuracy. In most cases ten hours was found to be a suitable length of time to allow a relatively stable minimum mass to be achieved, however the most unreactive char samples required 20 hrs. The minimum mass was assumed to represent the ash content of the test portion therefore char reaction was deemed to be complete when the sample mass reached a minimum. The initial sample mass was approximately 2.5 mg. Char samples were subject to reactivity tests as collected from the DTF, i.e. no additional devolatilisation of the chars was carried out. Some tests were repeated using char samples, which had been crushed to a fine powder by pestle and mortar, to moderate the variable of char surface area, these are identified in the text. Char conversion, as a percentage, at time = t, is defined by Equation 4.2:

$$Conversion_t = 100\ \% \times \left(\frac{W_0 - W_t}{W_0 - W_{min}}\right) \qquad \text{(Equation 4.2)}$$

Where W_0 is the initial sample mass, W_t is the sample mass at time = t and W_{min} is the minimum sample mass. The reactivity of the char is represented by the Reactivity Index, which has units of %/min and is defined by Equation 4.3:

$$Reactivity\ Index = \frac{50\ \%}{t_{0.5}} \qquad \text{(Equation 4.3)}$$

Where $t_{0.5}$ is the time (in minutes) at which char conversion is at 50 %. Duplicate tests were carried out and Reactivity Index values are reported as an average of duplicate tests.

4.9 Horizontal tube furnace and mass spectrometry

A horizontal tube furnace connected to a mass spectrometer was used to monitor gaseous devolatilisation products of coal samples. A Carbolite HTF-1600/50 tube furnace with an internal diameter of 75 mm and length of 1200 mm was connected to a Hiden HPR 20 mass spectrometer. A coal sample of 1 g was placed in a ceramic sample boat in the centre of the tube, the tube was sealed and a flow of argon at 200 mL/min carried gaseous devolatilisation products to the mass

spectrometer. The tube was heated to 1000 °C at 100 % power. A high temperature capillary arm, set to its maximum temperature of 450 °C, was used to convey gasses from the tube furnace to the mass spectrometer, to minimise condensation of gas species prior to the mass spectrometer. The resulting heating rate of the tube was calculated using time and temperature measurements and was found to decrease from ~30 K/min during the early stages of heating to ~7 K/min in the latter stages. The mass spectrometer was programmed to analyse the following gases: Methane, ethane, hydrogen, carbon dioxide, carbon monoxide, water vapour, argon and nitrogen. The sum concentration of these gasses was set to 100 %, therefore the figures presented are relative to the sum total of these gasses. The argon concentration before heating was measured to be 96-97 % by the mass spectrometer. Data is presented following adjustments to account for the time delay between gas evolution within the furnace and detection at the mass spectrometer, and to account for the measured changes in furnace heating rate throughout the experiments.
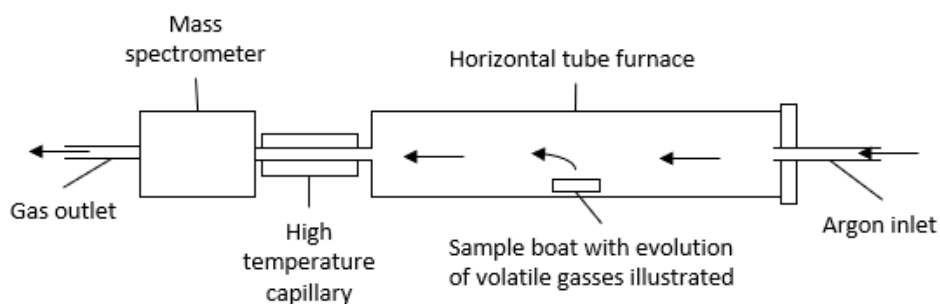
Figure 4.6: Schematic illustration of the experimental set up used for mass spectrometry measurements.

5 Development of technique

5.1 Introduction

The thermal swelling of coal particles is a potentially important factor in understanding the behaviour of coals during blast furnace coal injection. The standard laboratory tests of coal thermoplasticity have been developed for cokemaking, they involve heating of packed volumes of coal particles at low heating rates (3 K/min) (described in section 2.7.2). In this chapter a novel technique has been developed, which has greater relevance to blast furnace coal injection, using an HT-CSLM to directly observe the transient swelling behaviours of a number of discrete coal particles during heating. An inert atmosphere, maximum heating rates of 700 K/min and peak temperatures of 700 °C are applied as described in section 4.4. The HT-CSLM has been used in numerous research projects for a variety of purposes (Barnes *et al*., 2018; Hechu *et al*., 2017; Slater et.al, 2017; Spooner *et al*., 2017a and 2017b) including the observation of pyrolysis of a carbon source (Bharadwaj *et al*., 2004). Four different coals (A-D) with a range of characteristics are included in this chapter, the reasons for selecting these coals has been discussed in section 4.1. This chapter aims to demonstrate the suitability of the HT-CSLM technique for measuring coal particle swelling and differentiating between coal types. It is expected that a transient maximum swelling ratio and oscillations of bubble growth and rupture will be observed by the HT-CSLM. The similarities and differences between results of the HT-CSLM technique and standard thermoplasticity test results (Gieseler plastometer, Ruhr dilatometer and free selling index) are discussed, meanwhile TGA and mass spectrometry data also places the HT-CSLM swelling results within the overall context of devolatilisation.

Hypothesis to be investigated is Hypothesis 1 - The swelling of individual coal particles can be measured using the HT-CSLM.

5.2 Experimental

The coal preparation procedure has been described in section 4.2. The samples used in this chapter are the >125 µm sieve fractions obtained by wet sieving following Tema mill crushing. The Proximate, Ultimate and petrographic data for these sieve samples are shown in Table 5.1. Petrographic reflectance distribution histograms are available in the Appendix C.

	Coal A	Coal B	Coal C	Coal D
Proximate analysis				
Moisture/ % (ad)	2.4	0.8	3.4	1.5
Volatile matter/ % (db)	12.2	18.2	39.4	37.2
Ash/ % (db)	12.2	9.1	4.8	6.2
Fixed carbon/ % (db) (diff)	75.6	72.7	55.8	56.6
Ultimate analysis				
Carbon/ % (daf)	88.2	88.1	81.2	83.9
Hydrogen/ % (daf)	3.9	4.7	5.5	5.7
Nitrogen/ % (daf)	2.1	1.2	1.8	1.5
Sulphur/ % (daf)	0.4	1.1	0.4	1.1
Oxygen/ % (daf) (diff)	5.8	6.0	11.2	7.8
Petrographic analysis				
Liptinite/ %	0.0	1.6	4.0	4.0
Vitrinite/ %	75.4	68.1	60.8	65.1
Inertinite/ %	24.6	30.3	35.2	30.9
Vitrinite reflectance, Ro (max.)	1.9	1.7	0.7	0.8

Table 5.1: Proximate, Ultimate and petrographic data of the >125 µm sieve fractions of coals A-D.

Particle size distributions, obtained by Malvern Master-Sizer, are shown in Figure 5.1. These data indicate that although the particles have been retained on the 125 µm aperture sieve there is still a proportion of particles that are smaller than 125 µm (>50 % in the case of coal D). This may be due to inherent inefficiency of the sieving process. For example, smaller particles 'piggy-backing' on larger particles (even though wet sieving was used to minimise this), or due to the different

measurement techniques, i.e. sieving selects particles according to whether their smallest profile is able to pass through the sieve apertures whereas the Matersizer uses laser diffraction to measure particle volume. HT-CSLM work was carried out using the 50 K/min and 700 K/min heating profiles shown in Figure 4.3.
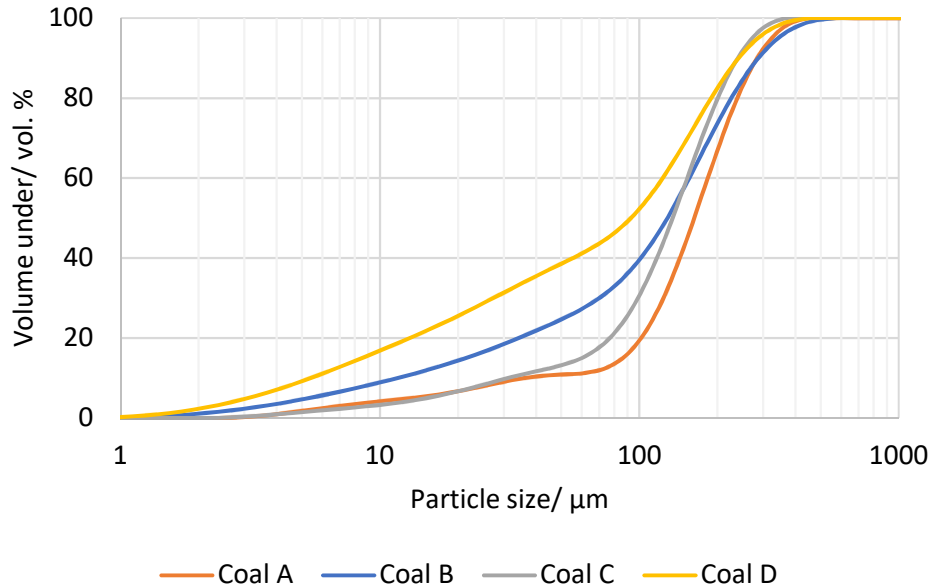
Figure 5.1: Particle size analysis of the >125 µm sieve fractions of coals A-D, which were used in this chapter.

5.3 Results and analysis

5.3.1 Measurement of coal particle swelling

The swelling profile of a particle of coal B on heating at 700 K/min in the HT-CSLM is shown in Figure 5.2. This particle exhibits the archetypal features of a swelling coal particle: Oscillations in size and a transient peak in swelling ratio followed by shrinkage to a final, more stable swelling ratio (there is a striking similarity between Figure 5.2 and Figure 2.8). Between 380 °C and 480 °C the swelling ratio increases in a series of oscillations, which can be attributed to the formation, rupture and re-formation of bubbles of evolving volatile matter within the softened coal structure. After passing through a peak swelling ratio at 480 °C the re-formation of bubbles no longer increases the particle size and bubble ruptures serve to decrease the swelling ratio. From 520 °C the particle has a more stable final swelling ratio of around 1.9.
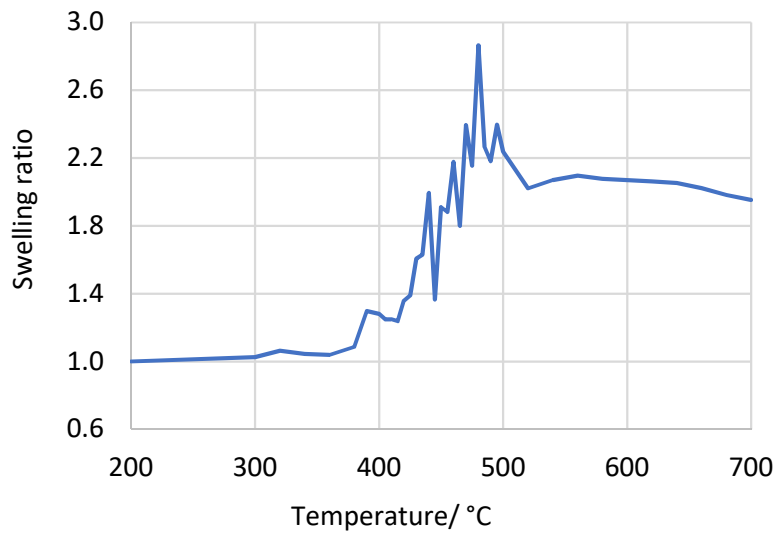
Figure 5.2: The swelling profile of a particle of coal B heated at 700 K/min in the HT-CSLM.

Still images from the HT-CSLM of the particle represented in Figure 5.2 are shown in Figure 5.3. These images are captured at selected temperatures to illustrate the particle immediately before rapid heating (200 °C), immediately prior to a bubble rupture (440 °C), immediately after bubble rupture (445 °C), at the point of maximum swelling (480 °C) and finally when oscillations of bubble formation and rupture are finished (600 °C).
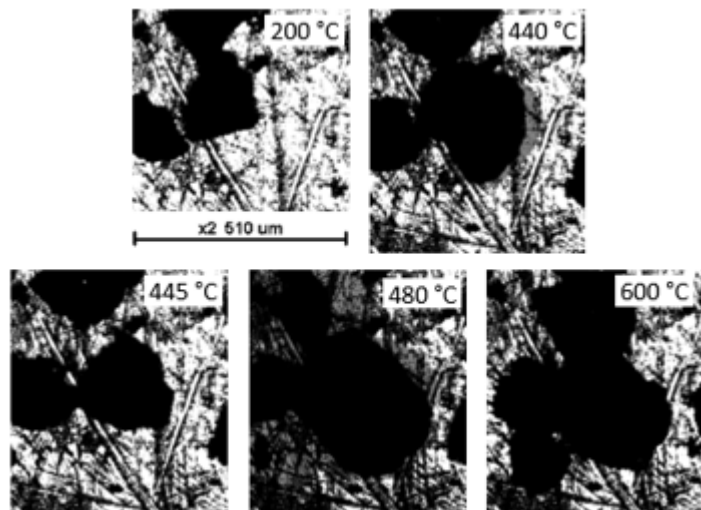
Figure 5.3: Images of the particle (centre) represented in Figure 5.2, taken from the HT-CSLM at five different temperatures.

Scanning electron microscopy (SEM) images of swollen char particles from coal B have also been obtained as shown in Figure 5.4. Figure 5.4 (a and b) shows the morphology of particles that were rapidly quenched from 450 °C (close to the temperature of maximum swelling ratio), which exhibit a swollen structure. Holes in the outer surface of these particles can be seen, which may be the result of bubble ruptures. Particles that have been quenched from 700 °C are shown in Figure 5.4 (c and d), these have the shrivelled appearance of particles that have shrunk from a swollen state. It should be noted that the SEM images in Figure 5.4 are typical morphologies observed for this sample, but they do not represent the morphology of every particle in the sample. Particles with different appearances were also observed and this indicates heterogeneity within the sample.

(a)

50 μm

(b)

50 μm

(c)

50 µm

(d)

100 µm
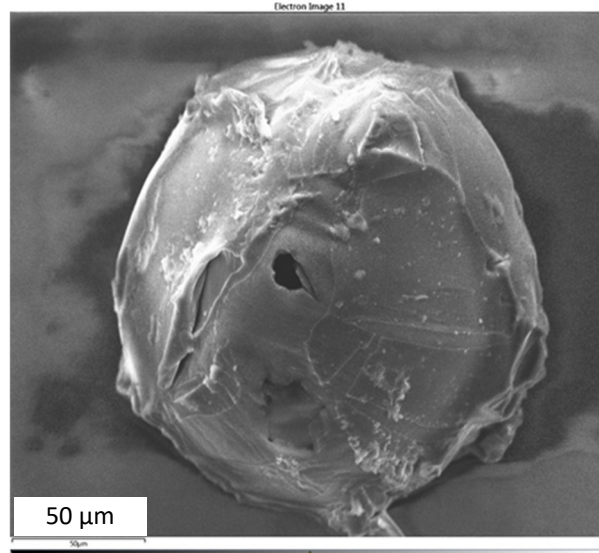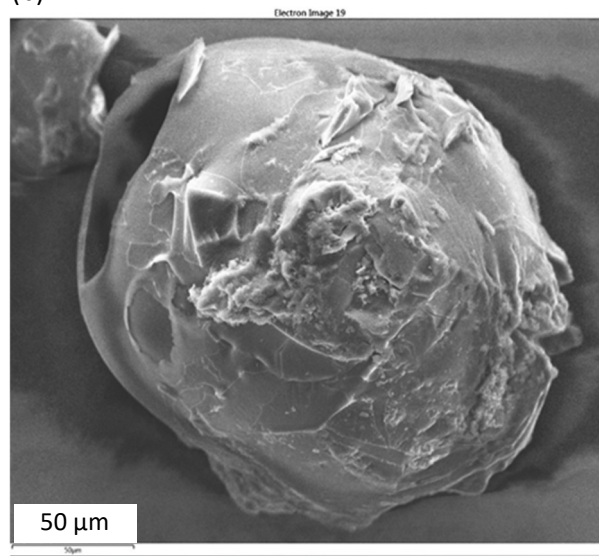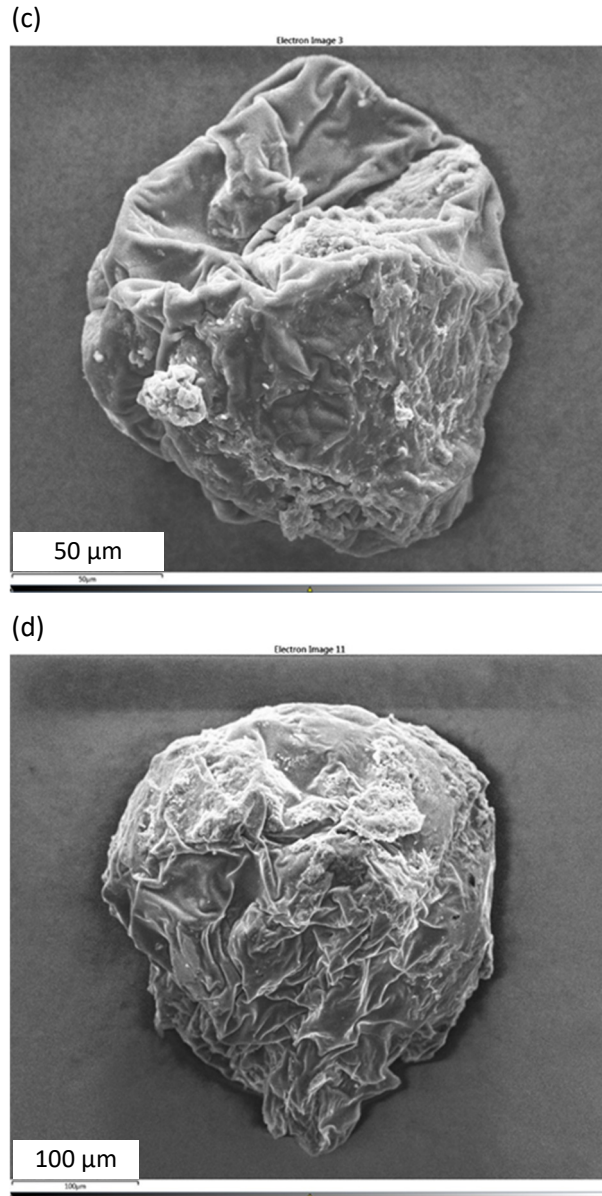
Figure 5.4: SEM images of particles of coal B after heating in the HT-CSLM to 450 °C (a and b) and 700 °C (c and d).

Twenty particles of coal B were tested by HT-CSLM and showed a variety of swelling profiles, one of these was shown in Figure 5.2, the remaining 19 are shown in Figure 5.5. They are roughly ordered by increasing swelling behaviour. Some particles show very little change in swelling ratio and end up with a swelling ratio close to 1 at 700 °C, for example, (a). The most severe fluctuations in swelling ratio can be seen in Figure 5.5s, this particle shows significant transient swelling yet shrinks back to a low swelling ratio at 700 °C. Conversely particles may retain a swelling ratio close to their maximum, for example, Figure 5.5m. Two

particles (Figure 5.5 l and m) briefly shrank to smaller than their original size (swelling ratio <1) following severe bubble ruptures. The highest transient swelling ratio observed was close to 2.9 (Figure 5.2).

(a)

(b)

(c)

(d)

(e)

(f)
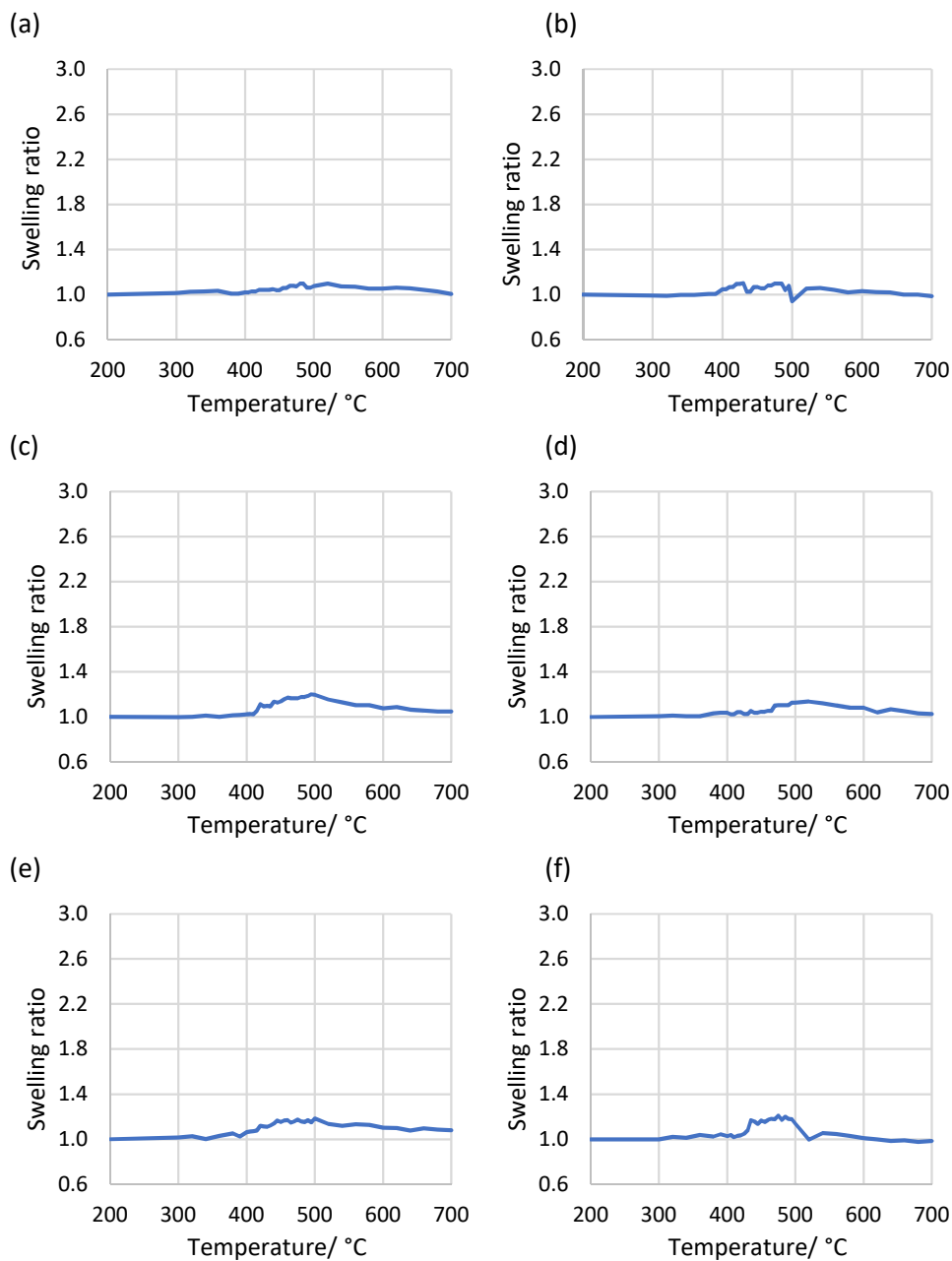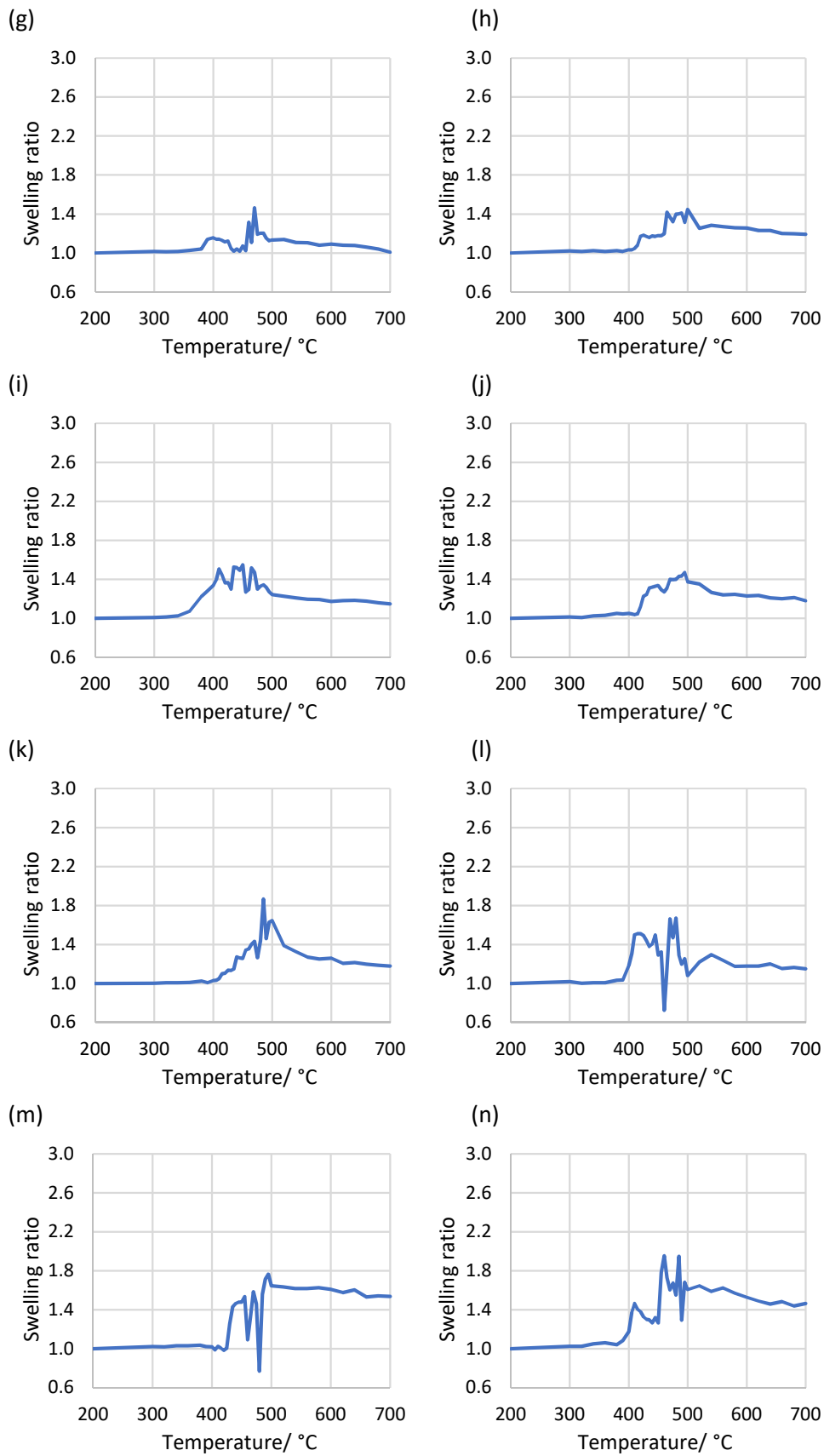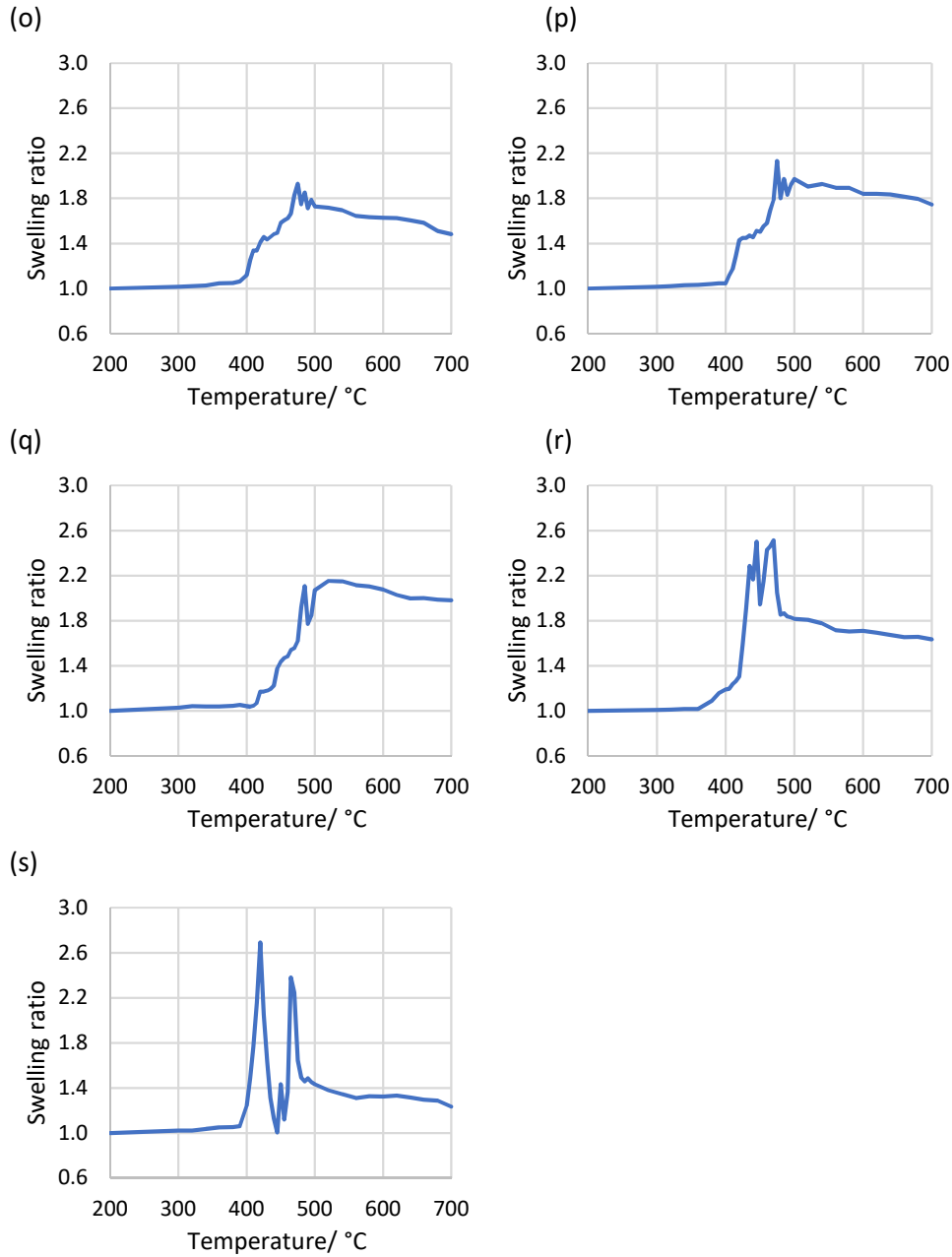
Figure 5.5: The changes in swelling ratio of particles of coal B, >125 µm, measured at 700 K/min.

Figure 5.6 demonstrates the degree of variability between particles. The mean swelling ratio of the coal B particles is plotted with error bars representing 1 standard deviation either side of the mean. Although there was significant variability in the magnitude of swelling between the particles, the temperature at which swelling began and the temperature of maximum swelling were consistent; 400 ±20 °C for swelling onset and 470 ±50 °C for maximum swelling ratio.
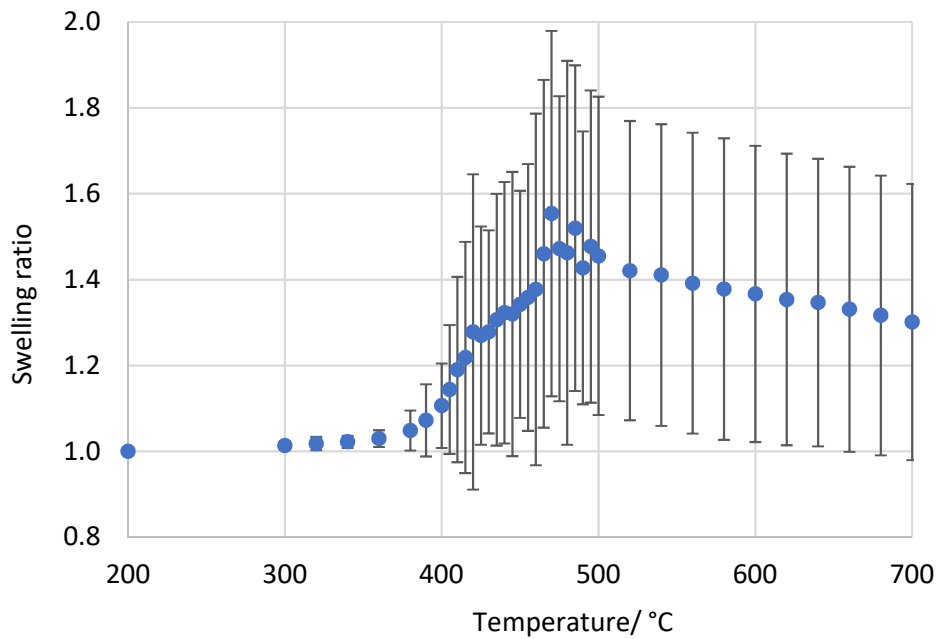
Figure 5.6: Mean swelling profile of 20 particles of coal B with error bars showing 1 standard deviation either side.

It is possible to observe agglomeration behaviour under HT-CSLM conditions, this is illustrated by Figure 5.7, which shows particles of coal B forming an agglomerate during heating at 700 K/min. When these instances occur, these particles are not included in the analysis because the particles are no longer individual. It is important to select a starting view under the HT-CSLM in which particles are disperse in order to avoid this situation. Exclusion of these particles may lead to non-representative results as the more highly swelling particles are more likely to be affected by agglomeration.
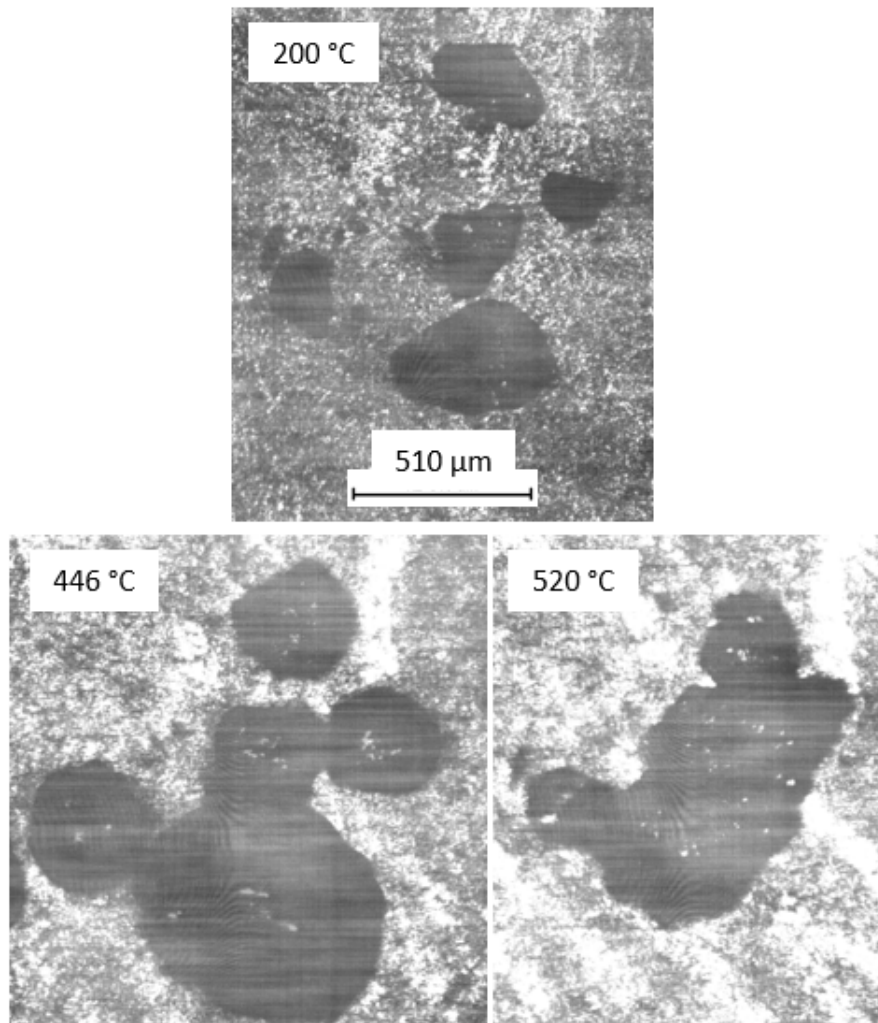
Figure 5.7: Illustration of agglomeration behaviour between particles of coal B during heating in the HT-CSLM at 700 K/min.

5.3.2   Different coal types

Figure 5.8(a) shows the mean swelling ratios of particles of coals A-C heated at 700 K/min in the HT-CSLM. The number of particles contributing to these mean swelling ratios are 30 for coal A, 20 for coal B and 20 for coal C. The different coal types swell to different extents. The swelling behaviour of coal B has been described above, meanwhile coal C begins significant swelling at 400 °C, about 20 °C higher than coal B. Initially the rate of swelling of coal C is similar to that of coal B, meaning that the swelling of coal C is broadly similar to coal B up to 440 °C. However, the duration of swelling of coal C is shorter than for coal B, peaking at 440 °C, 30 °C lower than coal B. The peak swelling ratio of coal C is lower than that

of coal B. The rate of shrinkage after reaching peak swelling ratio is similar for coals B and C. Figure 5.8(b) shows the same data, with error bars of 1 standard deviation either side of the mean illustrating the degree of overlap in swelling behaviours between the samples.

(a)

(b)
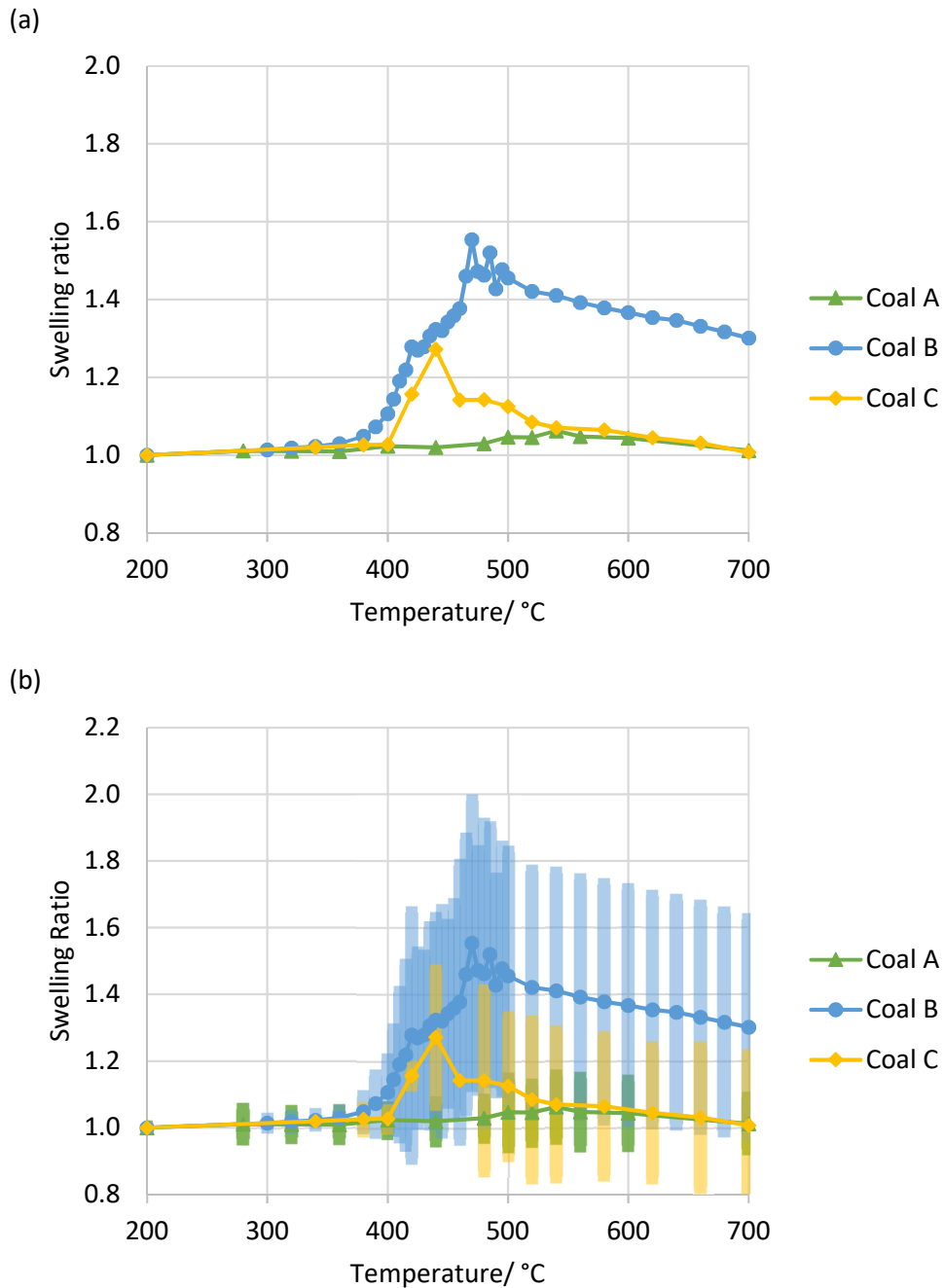
Figure 5.8: Mean swelling profiles of coals A, B and C when heated at 700 K/min by HT-CSLM (a), and with error bars illustrating 1 standard deviation either side of the mean (b).

Coal A has the lowest maximum swelling ratio, 1.06, of coals A-C and reaches its maximum swelling ratio at the highest temperature, 540 °C. The onset of swelling is at 400 °C, i.e. similar to coals B and C, however the rate of swelling is much slower. The rate of shrinkage of coal A after passing through its maximum swelling ratio is similar to that of coals B and C. Coals A and C finish the test with very similar swelling ratios between 540 °C and 700 °C.
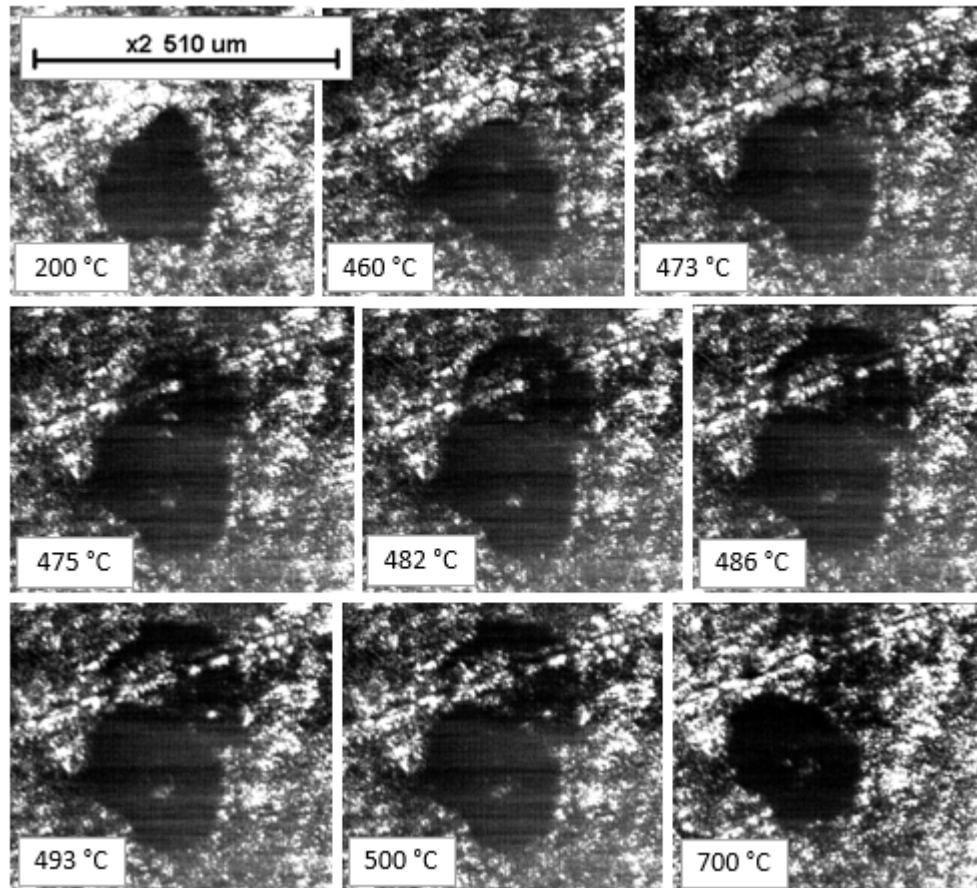
Figure 5.9: Images captured by HT-CSLM of a particle of coal C heated at 700 K/min illustrating the growth and rupture of a bubble.

Figure 5.9 illustrates the formation and rupture of a bubble from a particle of coal C, heated at 700 K/min in the HT-CSLM. A bubble begins to develop at 460 °C, bubble rupture is estimated to be at around 480 °C and leaves a residue visible on the crucible surface, which partially evaporates but is still visible at 700 °C. This process takes place shortly after the maximum swelling temperature of the coal C sample, during the temperature range of shrinking. The images indicate that not only gas, but also fluid material is ejected from the particle in this instance. This

phenomenon is not necessarily typical of this sample; however, it illustrates that this behaviour can occur and can be observed by HT-CSLM.

When particles of coal D were heated at 700 K/min in the HT-CSLM some particles lost their form and the softened material began to flow over the surface of the crucible. The result can be seen in Figure 5.10; these SEM images were obtained by moving the crucible from the HT-CSLM to the SEM after quenching. It is apparent that the material has become highly fluid and many bubbles have formed and burst prior to re-solidification. Figure 5.11 shows the apparent HT-CSLM swelling ratio of coal D, this is a mean of 9 particles. This has not been included in Figure 5.8 as the swelling ratio is not based on true particle size measurements, but the area covered by the fluid material. Therefore, the swelling ratio itself is not true. The characteristics of this behaviour are a rapid increase in swelling ratio as the material becomes fluid and an absence of the rapid shrinkage that typically follows immediately after the maximum swelling ratio. The maximum apparent swelling ratio attained is often high, a maximum of ~6 has been observed.

(a)

100 µm
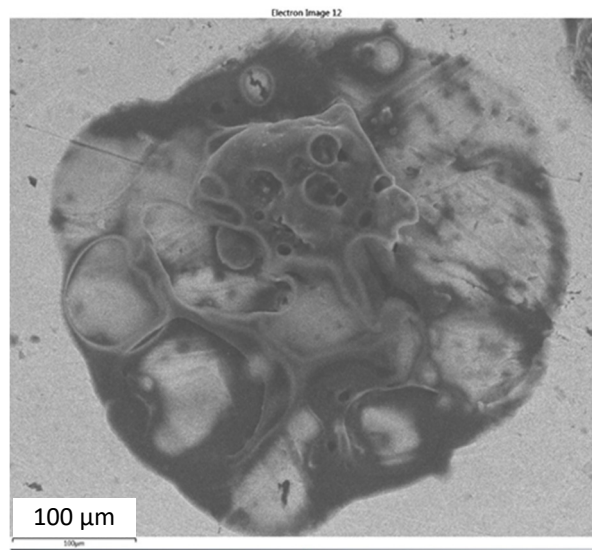
(b)
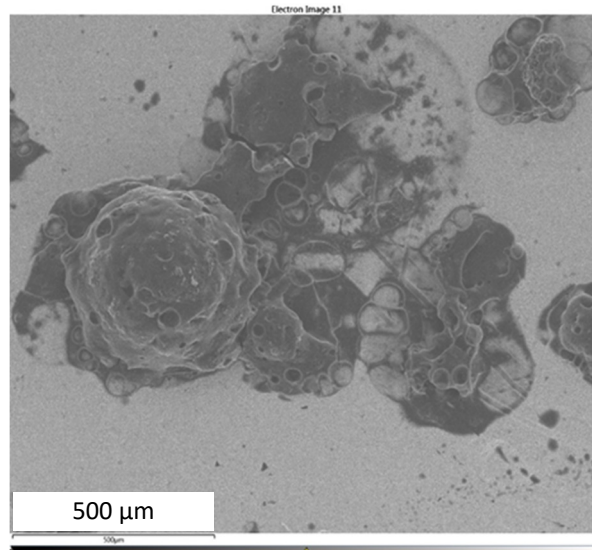
Figure 5.10: SEM images of particles of coal D after heating to 700 °C at 700 K/min in the HT-CSLM.

Figure 5.12 shows the characteristic appearance under HT-CSLM; at 440 °C the outer boundary of the particle has not receded, it is stuck to the crucible surface, inside this boundary is an area of residual material with the crucible surface showing through, and at the centre there is a dark area where a bulk of material remains. The image of residual material remaining on the crucible surface has similarities to the remains of the bubble rupture from a coal C particle in Figure 5.9. The distinction between the inner bulk material and the outer residual material is not always so clear, especially as the particle begins to become fluid. As with coals A-C variation was observed within the coal D sample; some particles showed little or no swelling, however where swelling occurred the pattern above was followed i.e. rapid increase in swelling ratio and a lack of shrinking after reaching maximum swelling ratio. Prior to this dramatic deformation a small degree of swelling is observed followed by some shrinkage immediately before deformation.
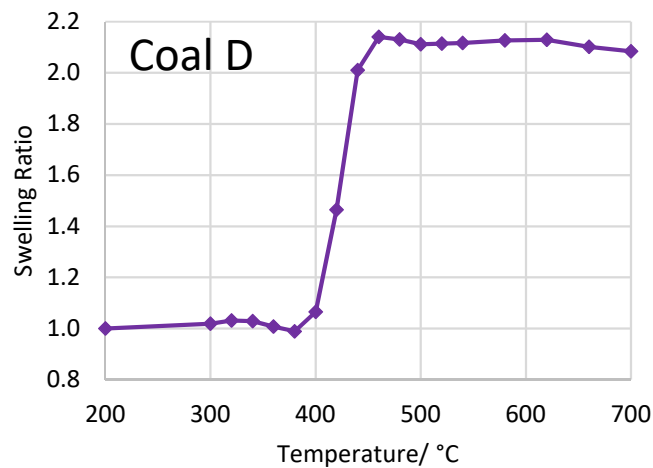
Figure 5.11: Mean swelling profile of coal D when heated at 700 K/min by HT-CSLM.
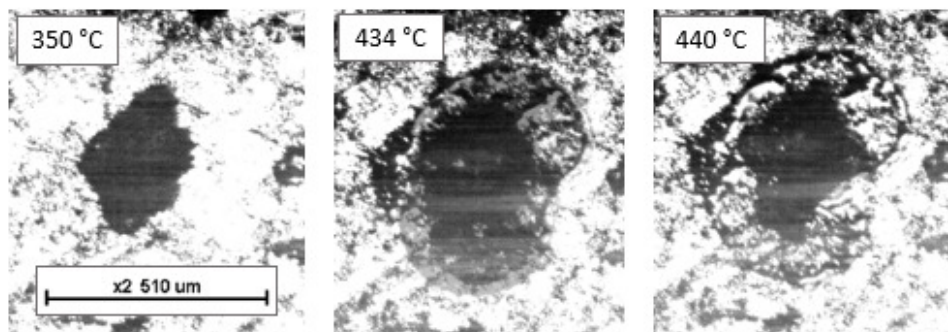
Figure 5.12: HT-CSLM images of a particle of coal D heated at 700 K/min illustrating the particle appearance before, during and after swelling (temperatures 350 °C, 434 °C and 440 °C respectively).

5.3.3 Comparison with standard fluidity, dilatation and free swelling index data

Figures 5.13 and 5.15 show the mean swelling ratio of coals A-D in comparison with the Gieseler fluidity and Ruhr dilatometer data (Note, the different scale of (d) compared to (a,b & c) in both cases. The HT-CSLM swelling data is from >125 μm sieved particles whereas the fluidity and dilatation data is from the whole parent coal. The fluidity and dilatation figures are also given in Table 4.1.

(a)

(b)

(c)

(d)
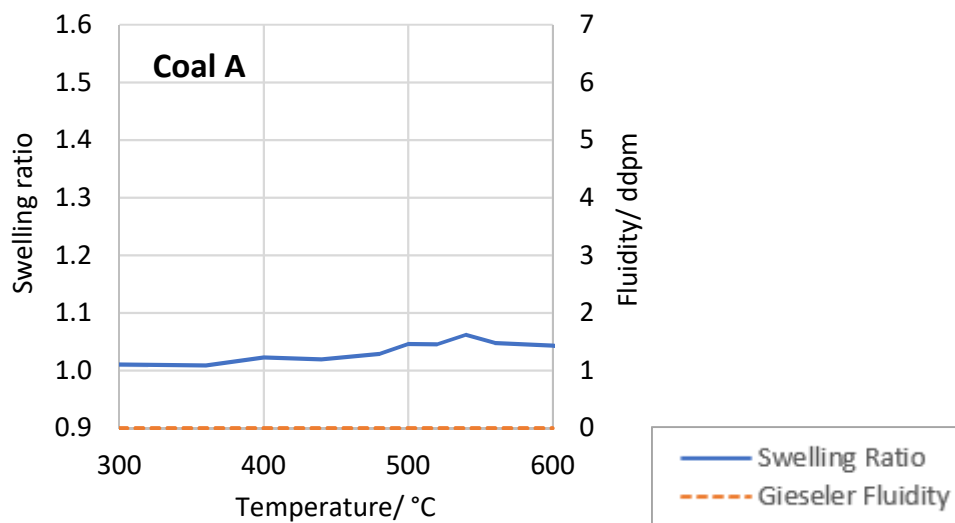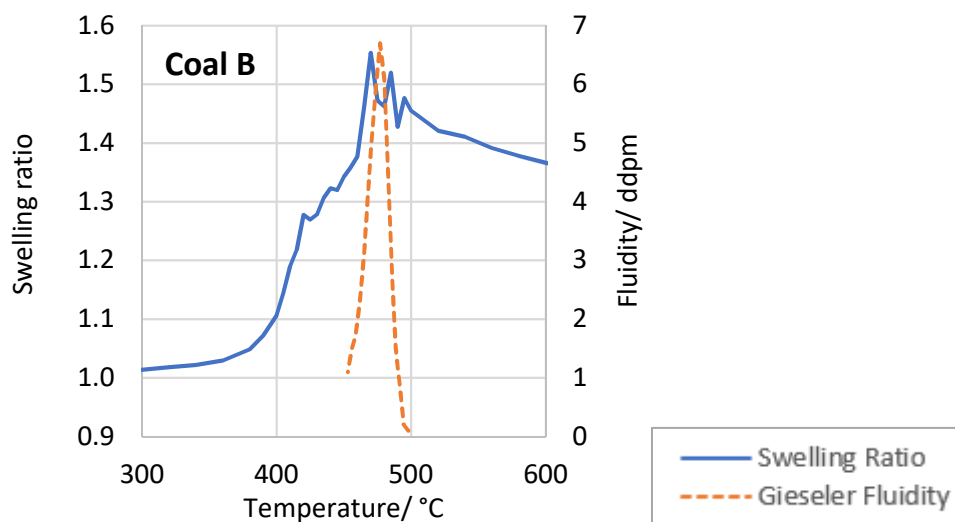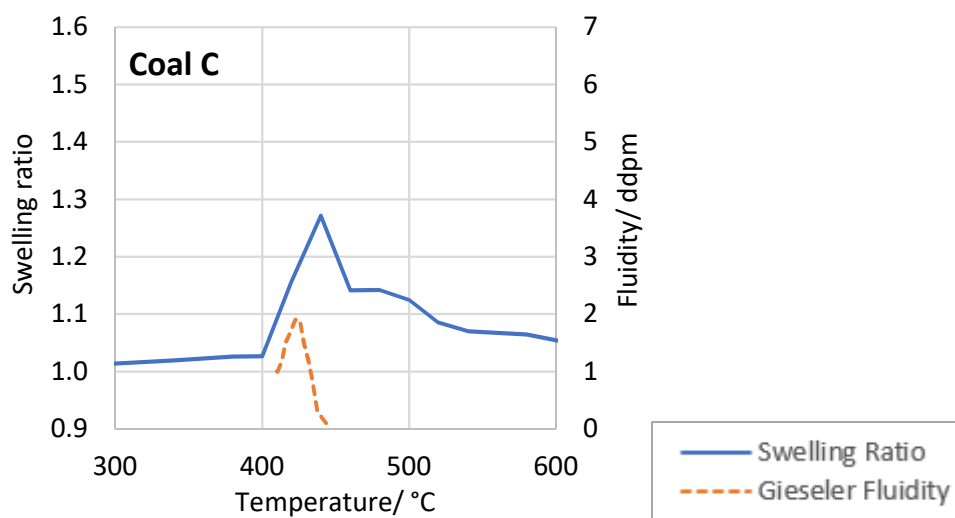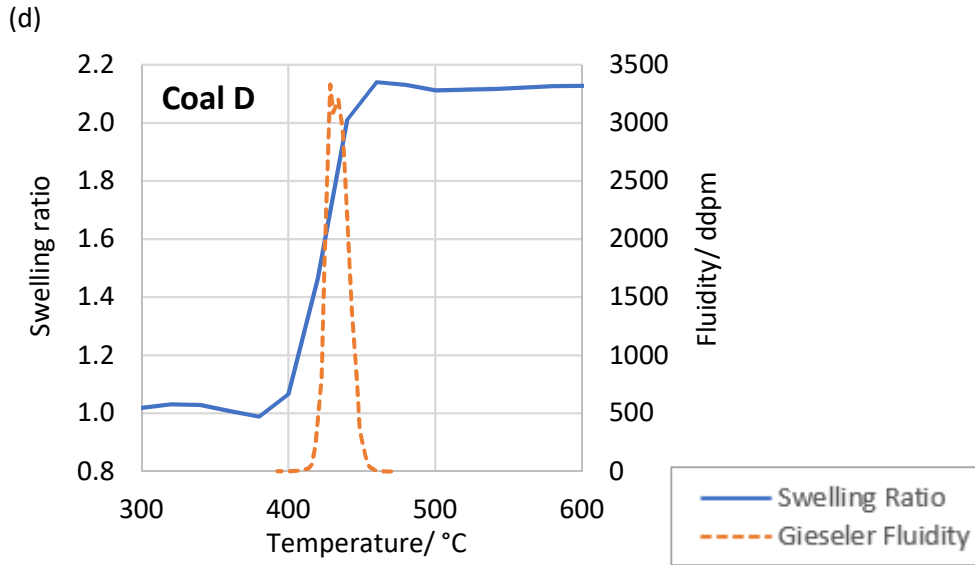
Figure 5.13: Mean HT-CSLM swelling profiles of coals A-D plotted against Gieseler Fluidity data. Note, the different scale of (d).

Coal A does not produce Gieseler fluidity or Ruhr dilatation, however it does produce a small degree of HT-CSLM swelling (Figures 5.13 and 5.15). The maximum swelling ratio of coals B and C occur at different temperatures (470 °C and 440 °C respectively), both broadly coincide with the respective temperatures of maximum Gieseler fluidity (477 °C and 426 °C respectively) (Figure 5.13). The maximum Gieseler fluidity value also correlates with the maximum swelling ratio for coals A, B and C at 700 K/min (Figure 5.14), albeit this represents a small range of fluidity values. When swelling ratio is measured at a heating rate of 50 K/min in the HT-CSLM maximum swelling ratio values are lower and the increase in swelling ratio with increasing fluidity is not as great, i.e. increasing fluidity has a greater effect when higher heating rates are applied. Chapter 6 deals further with the effect of heating rate.
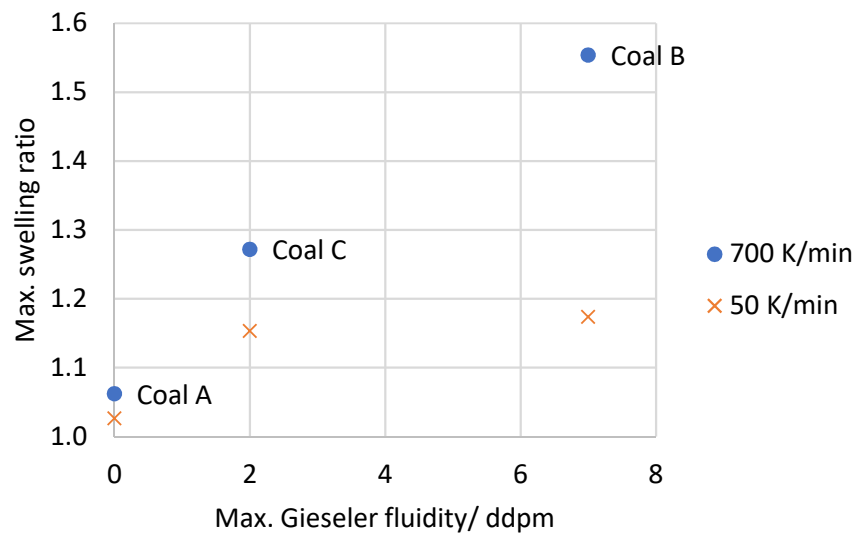
Figure 5.14: Maximum mean swelling ratio of coals A-C at 50 K/min and 700 K/min plotted against maximum Gieseler fluidity.

The temperature of Gieseler re-solidification for coal B (498 °C) coincides with the temperature at which swelling ratio oscillations stop occurring (Figure 5.13). The onset of swelling in the HT-CSLM, however, occurs at a lower temperature (between 300 °C and 400 °C) than the Gieseler softening temperature (453 °C), indicating that swelling can occur before fluidity is registered in a Gieseler test. There is a distinction between coal B and coals C and D in this respect, as there is little change in the swelling ratio of coals C and D in the HT-CSLM below their Gieseler softening temperatures.

As discussed above, coal D behaves differently to coals B and C in the HT-CSLM, the rapid increase in apparent swelling ratio of coal D as it deforms effectively corresponds to the Gieseler fluidity temperature range, which begins at 393°C (i.e. the particles lost their form soon after the Gieseler softening temperature was reached). This implies that the technique developed in this study may not be capable of measuring the swelling of coals with high fluidity. Coetzee *et al*., (2014), observed larger pieces of coal deforming in a similar way, in their case the parent coal had a maximum Gieseler fluidity of 1209 ddpm, the maximum Gieseler fluidity of coal D is 3433 ddpm.

In similar fashion to the Gieseler fluidity, the temperature of Ruhr re-solidification for coal B also coincides with the temperature at which swelling ratio oscillations

stop occurring (Figure 5.15), and similarly the onset of swelling in the HT-CSLM occurs at a lower temperature than the Ruhr softening temperature. The temperature of maximum swelling ratio coincides with the temperature of maximum contraction. Coetzee *et al.*, (2014), found a similar comparison between their transient swelling results and dilatation using much larger particle sizes and lower heating rates than were used here in the HT-CSLM.

(a)

(b)

(c)

(d)
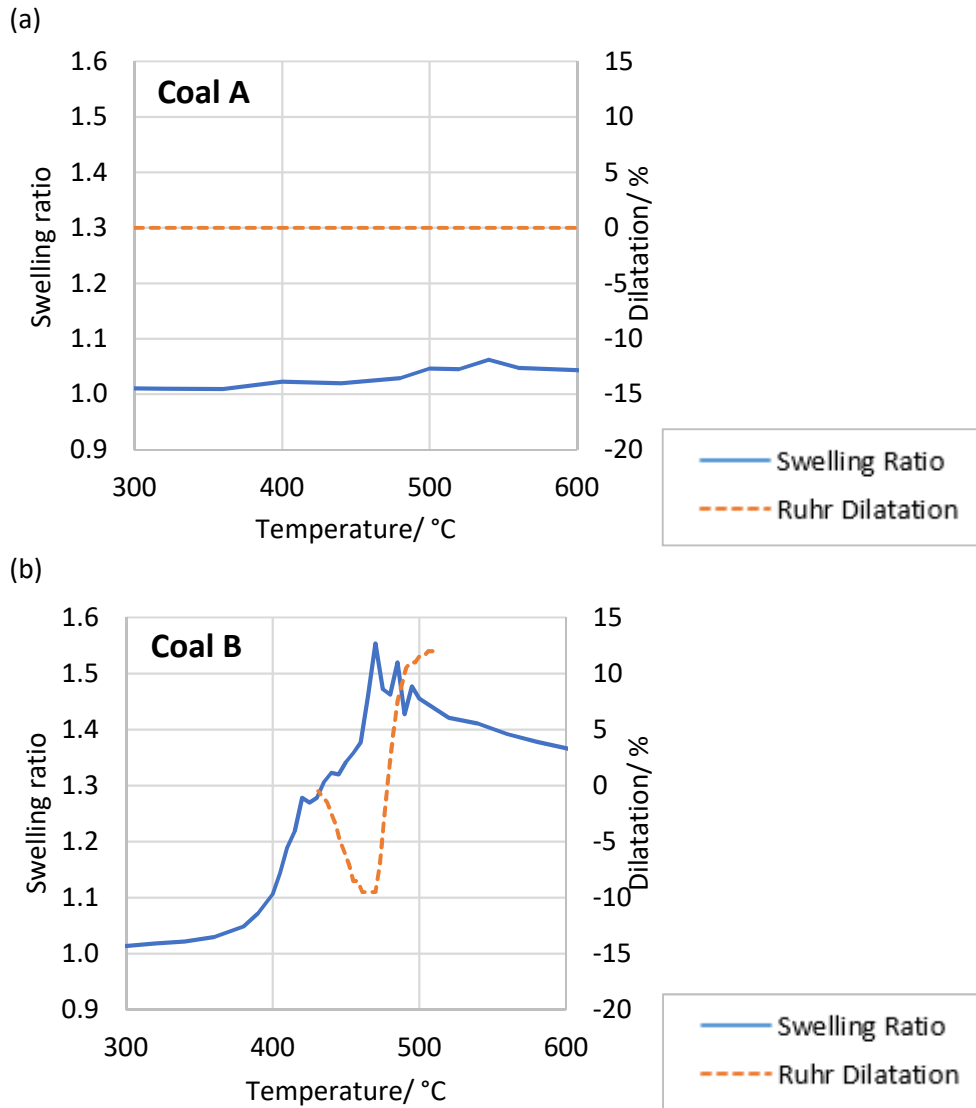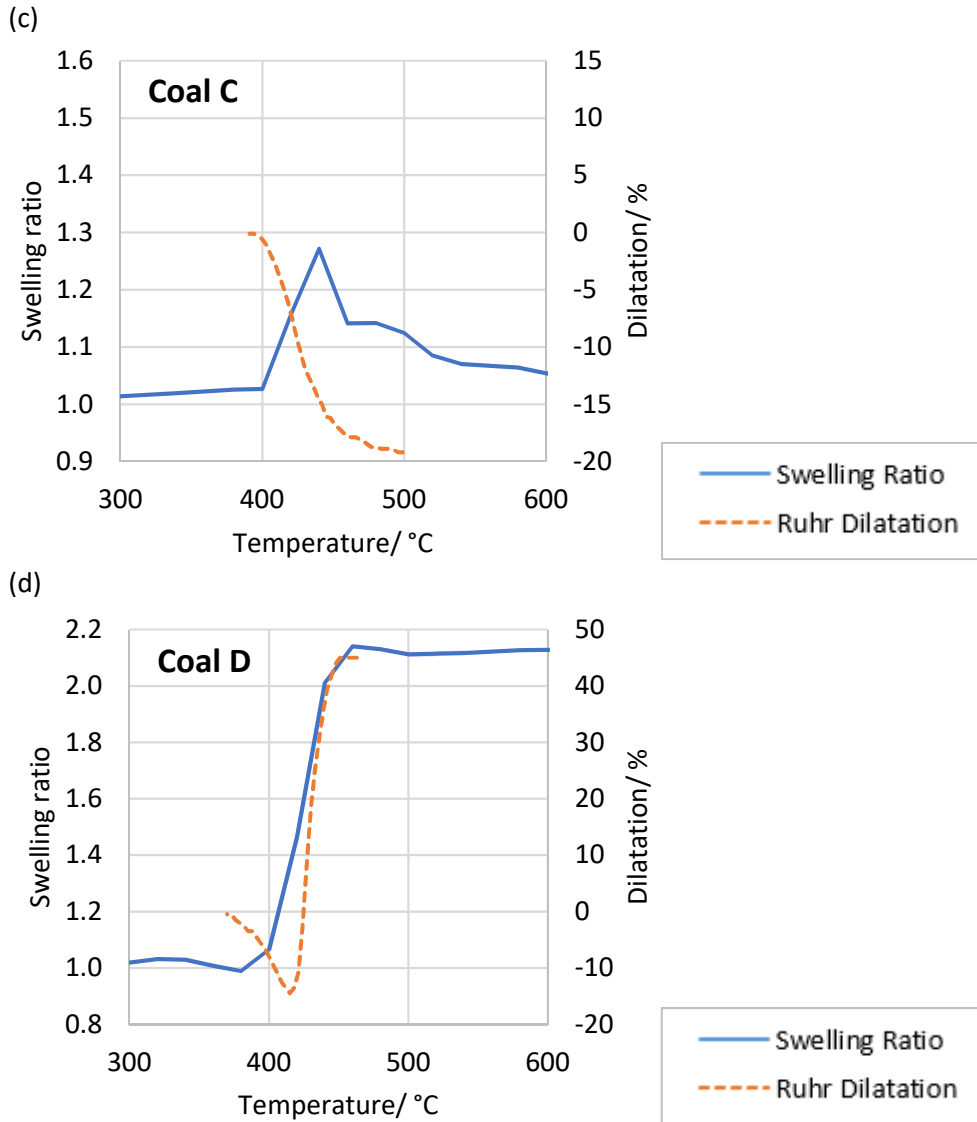
Figure 5.15: Mean HT-CSLM swelling profiles of coals A-D plotted against Ruhr dilatation data. Note, the different scale of (d).

Coal C shows contraction only in the Ruhr dilatometer (Figure 5.15 c). The onset of HT-CSLM swelling and Ruhr contraction occur at the same temperature, and the temperature of maximum swelling ratio coincides with a slowing in the rate of contraction. Coal C illustrates that a lack of Ruhr dilation does not necessarily indicate a lack of HT-CSLM swelling.

The softening behaviour of coal D in the HT-CSLM corresponds to the temperature range of Ruhr contraction and dilation. The apparent swelling ratio begins to

increase shortly after the Ruhr softening temperature is reached and stops increasing soon after the Ruhr re-solidification temperature is reached.

Figure 5.16 shows the HT-CSLM maximum swelling data for coals A-C plotted against the free swelling index (FSI) of the parent coals (data given in Table 4.1). The trend with regards to FSI is almost identical to that described for maximum Gieseler fluidity (Figure 5.14). For these three coals maximum fluidity correlates well with FSI.
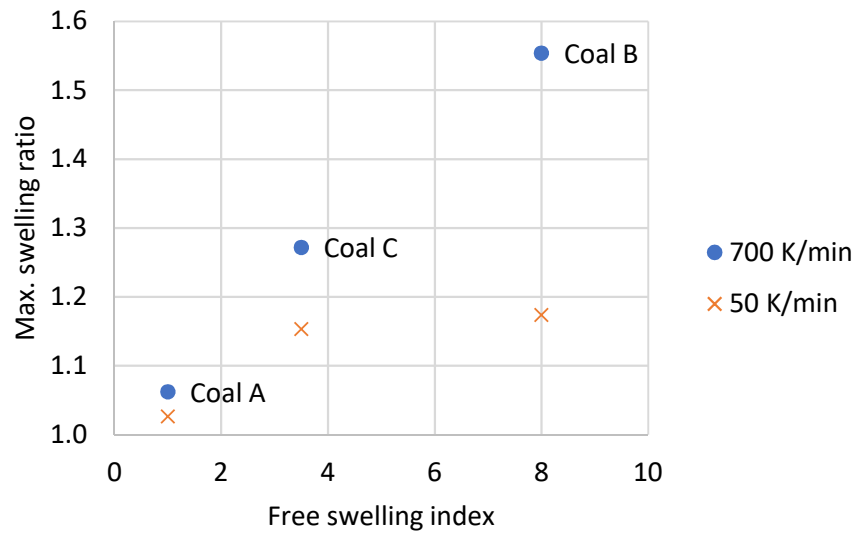
Figure 5.16: Maximum mean swelling ratio of coals A-C at 50 K/min and 700 K/min plotted against free swelling index (FSI).

5.3.4   Relationship between swelling and DTG

In Figure 5.17 the HT-CSLM swelling of coals A-D are compared with differential thermogravimetric (DTG) data, i.e. the rate of mass loss on heating, measured by TGA. The heating rate used in both instruments was 50 K/min. The number of particles contributing to the mean swelling ratio values in each case is 33 for coal A, 22 for coal B, 28 for coal C and 4 for coal D. Dashed orange lines represent the Gieseler fluid range of coals B-D.

(a)
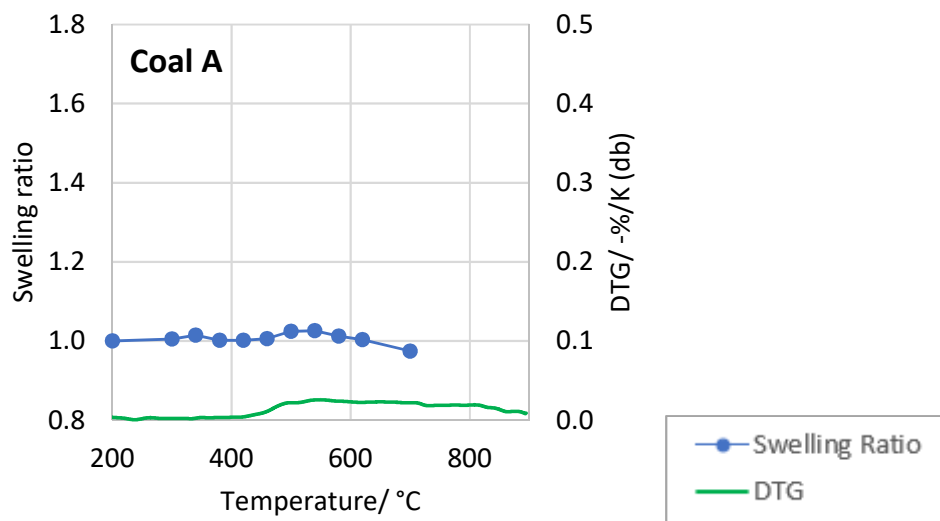
(b)
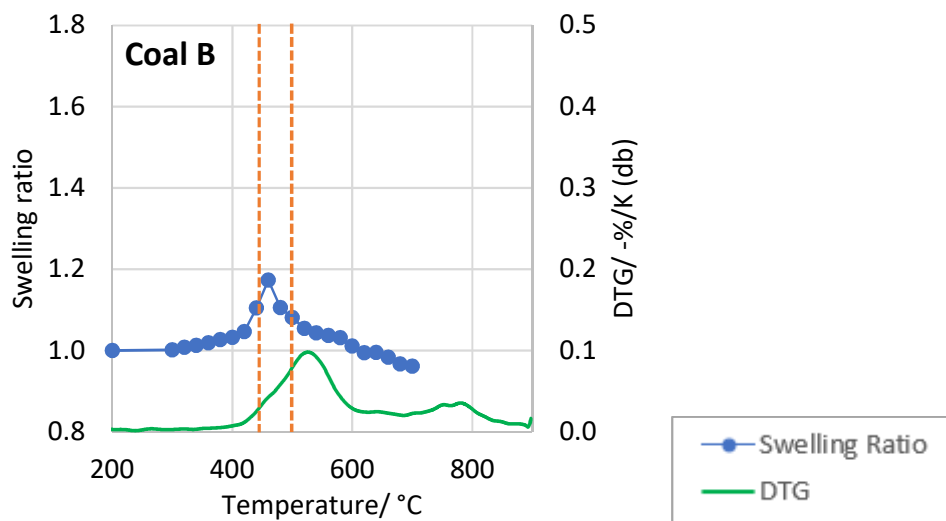
(c)
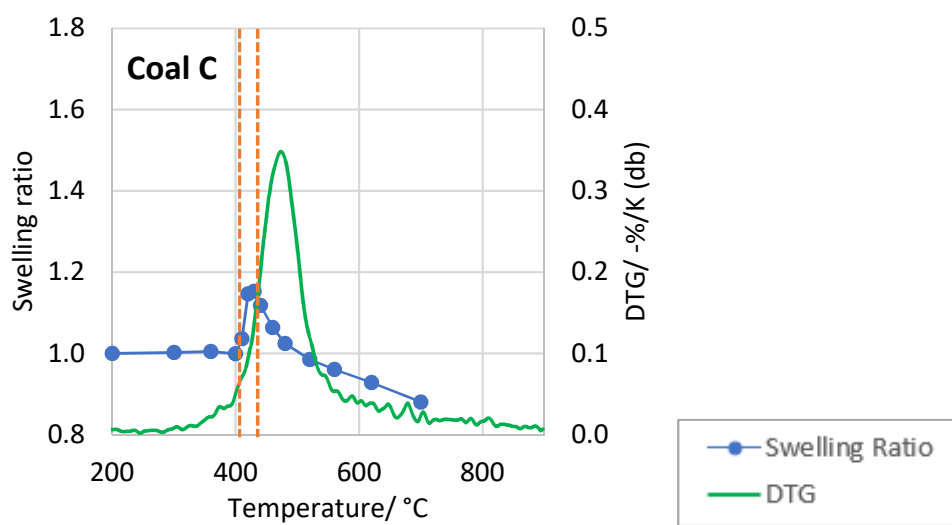
(d)
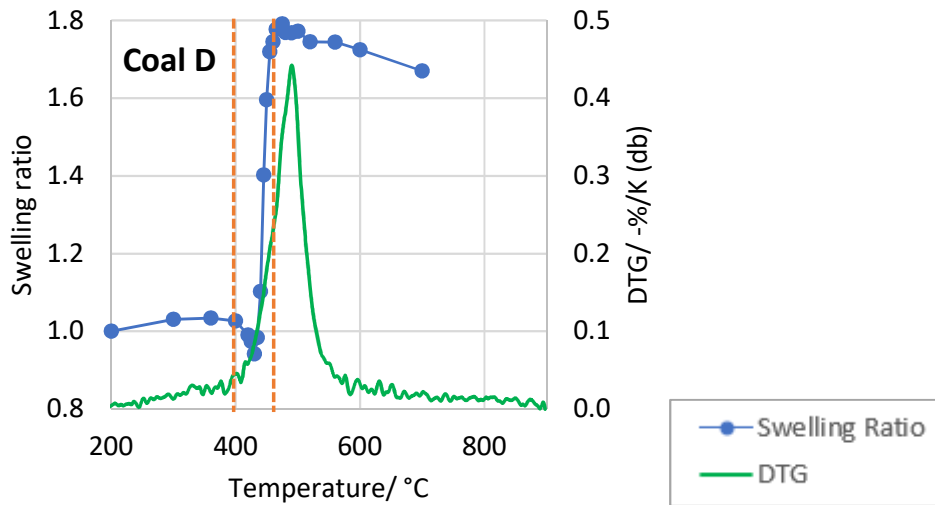
Figure 5.17: The mean HT-CSLM swelling ratios of coals A-D at 50 K/min plotted alongside DTG data at 50 K/min. Dashed orange lines represent fluid range.

As coal B is heated the swelling ratio begins to increase above 300 °C, before the rate of mass loss increases significantly at around 400 °C (Figure 5.17b). The peak swelling ratio is reached at 460 °C, a temperature when the rate of mass loss is increasing but before the maximum rate of mass loss is attained. The peak swelling ratio seems to coincide with a very subtle shoulder on the DTG graph i.e. the acceleration in mass loss decreases around the temperature of maximum swelling. Above the temperature of peak rate of mass loss, 530 °C, the rate of particle shrinking also decreases.

Coal A exhibits a broad devolatilisation profile with a poorly defined DTG peak at around 560 °C (Figure 5.17a). The onset of swelling and the onset of increasing rate of mass loss are both around 420 °C. The peak swelling ratio coincides with the peak rate of mass loss at 540 °C. As the swelling ratio decreases the rate of mass loss decreases gradually.

Coal C shows a clear peak in its DTG profile at around 480 °C (Figure 5.17c), this peak is greater in magnitude than that of coal B (-0.34 %/K compared to -0.01 %/K) but is at a lower temperature (480 °C compared to 530 °C); correspondingly the temperature of maximum swelling ratio is lower too (430 °C compared to 460 °C). As with coal B the swelling ratio peaks as the rate of mass loss is increasing,

and the rate of particle shrinkage decreases as soon as the rate of mass loss begins to decrease. Unlike coal B, swelling of coal C is not observed prior to the onset of significant mass loss.

Coal D has the highest peak rate of mass loss, -0.43 %/K, of the four coals and a narrow DTG profile. The deformation of coal D in the HT-CSLM begins at 420 °C, close to the onset of rapid mass loss. The deformation of coal D and the increase in rate of mass loss occur together, the apparent swelling ratio peaking at 475 °C and the DTG curve peaking shortly afterwards at around 490 °C.

5.3.5   Mass spectrometry of coal samples

A horizontal tube furnace coupled to a mass spectrometer (MS), as described in section 4.9, was used to analyse some of the gaseous products of devolatilisation from samples of coals A and B. Results are shown in Figure 5.18. Due to the estimation of the time delay between gas evolution within the furnace and detection at the MS, and potential temperature-lag between the furnace temperature and the sample temperature, the temperature measurements are subject to some uncertainty. Nevertheless, the results indicate that higher levels of hydrogen, methane and ethane are produced by coal B than coal A, reflecting the greater rate of mass loss of coal B within this temperature range. Gas evolution begins at lower temperatures for coal B (300-400 °C) than for coal A (400-500 °C), broadly corresponding to the temperatures at which swelling begins for these coals. For coal B the temperature of peak swelling ratio (460 °C at 50 K/min and 485 °C at 700 K/min) is in the temperature range where levels of methane and ethane are both close to their peak. When the sum of the concentrations of methane plus ethane is plotted against HT-CSLM swelling data (Figure 5.19) there is good agreement between the temperatures of maximum swelling and the temperature of maximum methane plus ethane concentration for coal B, which supports the concept that swelling is driven by the generation of light hydrocarbon gases in this case. This is not the case for coal A, for which the maximum rate of evolution of methane plus ethane occurs at higher temperatures (~640 °C) than the temperature of maximum swelling (540 °C).

(a)

(b)
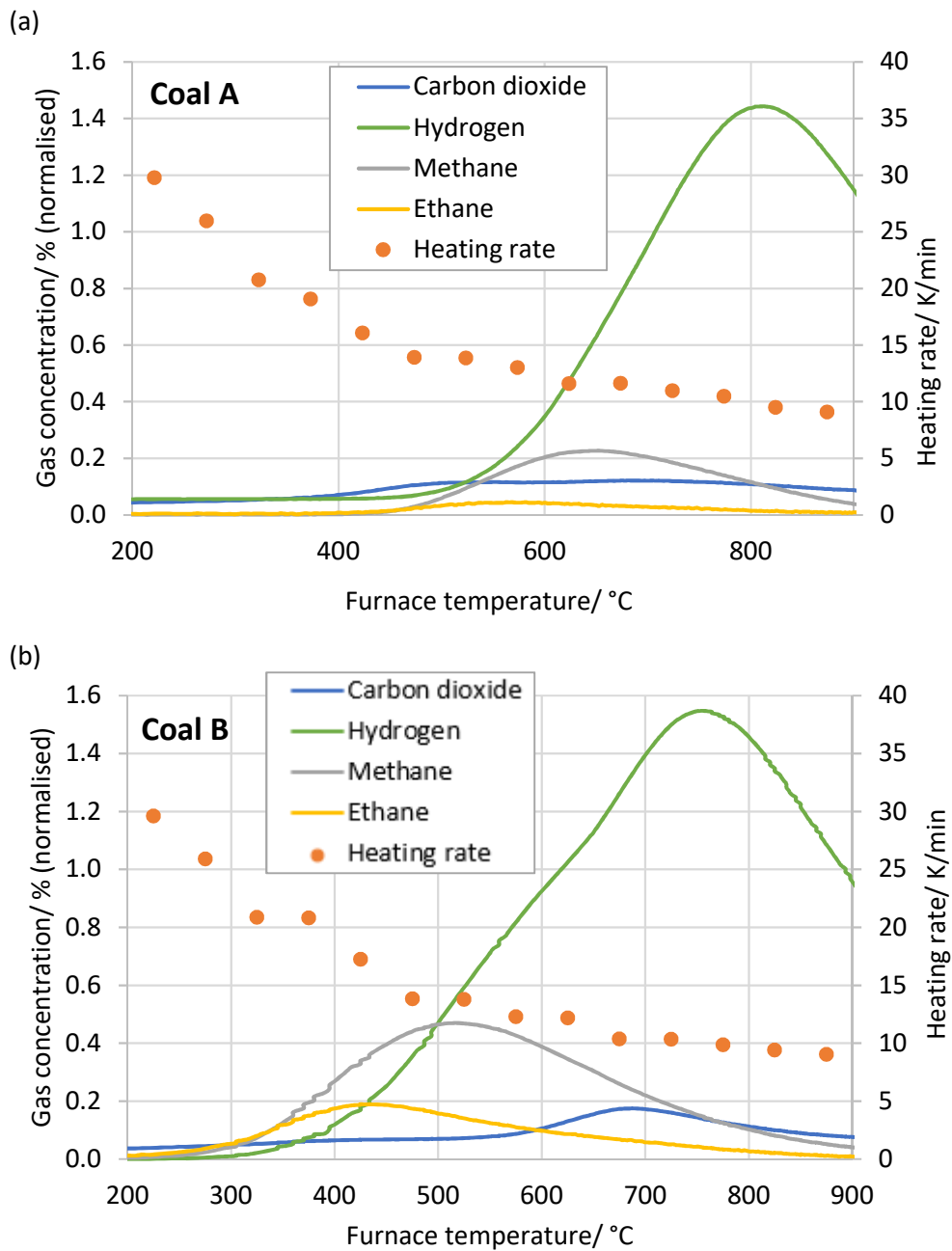
Figure 5.18: Mass spectrometry analysis of specified gaseous products of samples of coals A and B (a and b), >125 µm, upon heating in a horizontal tube furnace.

(a)

(b)
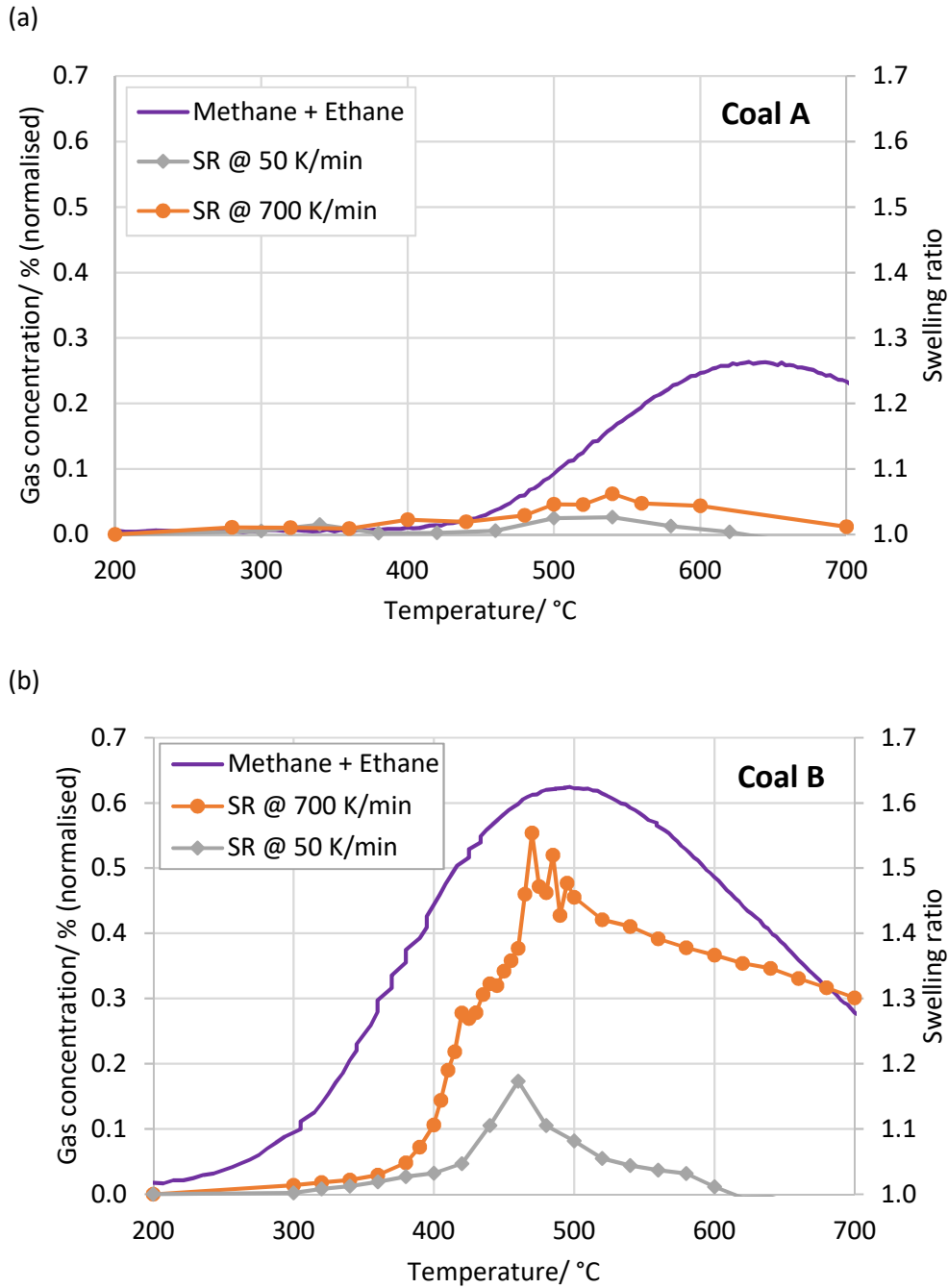
Figure 5.19: Combined mass-spectrometry results of methane plus ethane upon heating in a horizontal tube furnace plotted alongside HT-CSLM swelling data at 50 K/min and 700 K/min for coals A and B (a and b respectively), >125 μm.

5.4 Discussion

5.4.1 Measurement of coal particle swelling

The transient swelling behaviours of discrete coal particles have been directly observed using the HT-CSLM. Features of the swelling process, such as the oscillations of bubble formation and rupture and the existence of a transient maximum swelling ratio, which have previously been observed using equipment such as the Single Particle Reactor (SPR) (Yu *et al.*, 2003) and a carbon dioxide laser heating system (Gao *et al.*, 1997), are also observed using the HT-CSLM technique.

A feature of the HT-CSLM operation is the closely controlled heating rate, which is a difference between this technique and the two techniques mentioned above. Although the SPR and the carbon dioxide laser heating system are capable of higher heating rates than the HT-CSLM those heating rates are less closely controlled. For example, the heating rate in the SPR has been estimated by taking time and temperature measurements and has been varied by adjusted the power input. The heating rate experienced by particles in the laser heating system is calculated and is predicted to change throughout the duration of the test. The measured swelling ratios from these techniques are therefore typically presented as a function of residence time rather than temperature. In the HT-CSLM it is possible to accurately observe the temperature at which different features of the swelling process occur.

There is a great degree of variation in the extent of swelling between particles within the same sample. The smaller the particles used the greater the potential for the constituents of the coal to be separated into discrete particles. Previous work has shown that the different petrographic constituents of coals have different swelling properties (Yu *et al.*, 2003). It is therefore important that a sufficient number of particles from each sample are tested in order to obtain a representative average. The HT-CSLM is a useful technique in this regard due to the ability to observe several particles simultaneously.

5.4.2 Different coal types and comparison with standard fluidity, dilatation and free swelling index data

It is possible to distinguish the different swelling behaviours of different coal types using the HT-CSLM, a range of behaviours was observed within the suite of four coals studied. The Proximate, Ultimate and petrographic data do not appear to correlate with HT-CSLM maximum swelling ratios. As discussed in section 2.11, volatile matter evolution drives swelling yet the order of maximum HT-CSLM swelling ratio does not follow the order of Proximate volatile matter. For example, coal B has a higher maximum swelling ratio than coal C but a lower volatile matter content. Equally the maceral compositions do not anticipate swelling behaviour; the vitrinite and liptinite macerals are associated with swelling whereas the inertinite maceral inhibits swelling (Yu *et al.*, 2003), yet coal B has more inertinite and less vitrinite than coal A.

The Gieseler fluidity and Ruhr dilatation results of the parent coals have been compared with the HT-CSLM swelling results. There appears to be a relationship between the HT-CSLM swelling data and Gieseler fluidity data. There is agreement between maximum Gieseler fluidity temperature and maximum HT-CSLM swelling temperature and a correlation between the value of maximum Gieseler fluidity and maximum HT-CSLM swelling ratio. This relationship is affected by heating rate; at 700 K/min the effect of increasing fluidity is greater than at 50 K/min. A similar correlation with regard to swelling ratio and Gieseler fluidity has been observed by Gao *et al.*, (1997), although conversely in that study increasing the laser intensity (and therefore the maximum heating rate) decreased the maximum swelling ratio and reduced the effect of increasing fluidity. This may be explained by the possibility that the heating rates used by Gao *et al.*, (2600 K/s – 12000 K/s) fall within the region in which swelling ratio decreases with increasing heating rate; based on Figure 4.20 this may indeed be the case. The maximum Gieseler fluidity of the coals used by Gao *et al.* were greater than those of coals A-C; plotting the results of Gao *et al.* alongside the results of this work (Figure 5.20) suggests that the correlation between maximum Gieseler fluidity and maximum

swelling ratio extends from the higher fluidity coals studied by Gao *et al.* to the lower fluidity coals used in this work, although the heating rates associated with the two techniques are very different.
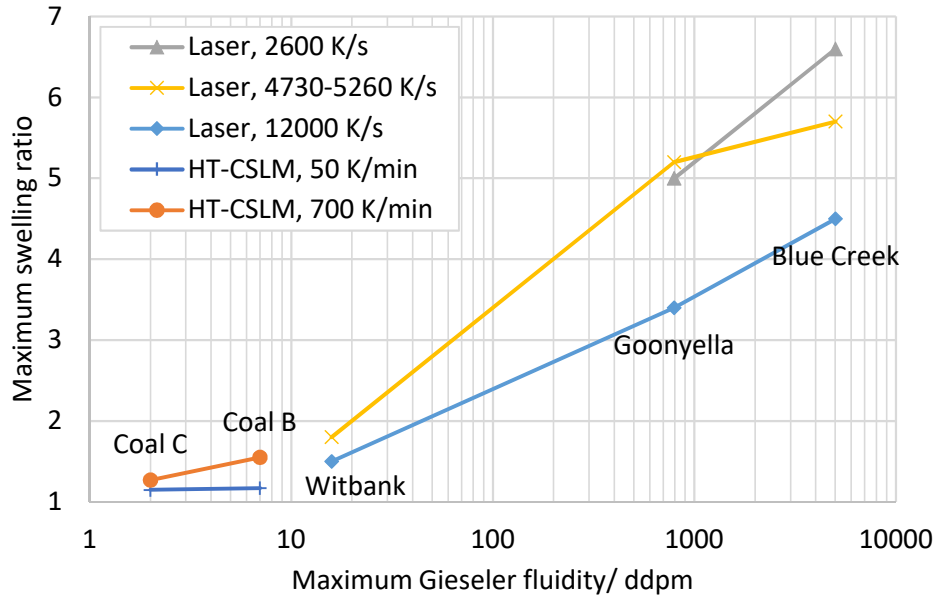
Figure 5.20: Maximum swelling ratio against maximum Gieseler fluidity for coals B and C heated by HT-CSLM (this work) and three specified coal types heated by laser (Gao *et al.*, 1997).

In the present work FSI values correlate with maximum swelling ratio values in almost exactly the same way that maximum Gieseler fluidity does. This reflects the fact that FSI and maximum fluidity correlate with each other for coals A-C, however these parameters do not necessarily correlate for all coals (for example, coal D) therefore if a wide range of coals were to be analysed by HT-CSLM it could be assumed that FSI and maximum fluidity could not both correlate with maximum swelling ratio. Coal A illustrates the ability for a coal with no Gieseler fluidity and no Ruhr dilatation to exhibit some swelling properties under HT-CSLM test conditions, therefore coals with no thermoplasticity under standard test conditions may swell during blast furnace injection.

Development of fluidity is necessary for swelling, it enables the structure of the coal to expand under the pressure of the evolving gaseous material. It appears that the cessation of bubble growth is associated with the loss of fluidity even though, at that point in the process, gaseous material is still being evolved at a

significant rate. Yet swelling is observed in the HT-CSLM at temperatures lower than the Gieseler softening temperature. This may be due to the differences in the experimental conditions between the Gieseler plastometer and the HT-CSLM. In the Gieseler plastometer the coal is closely compacted so that a small amount of plasticity development may not be sufficient to allow movement of the spindle. In the HT-CSLM each particle is physically unconstrained therefore a small degree of thermoplasticity may be more likely to result in swelling. Alternatively swelling may be measured in some particles even if the majority have not developed sufficient plasticity to swell. In this aspect the HT-CSLM technique is a better indicator of the thermoplastic behaviour of coal particles during blast furnace injection and indicates that swelling is likely occur during blast furnace injection at temperatures lower than the Gieseler softening temperature.

Greater fluidity allows greater swelling of coal particles, although the case of coal D suggests a limit above which high fluidity causes particles to lose their form and structure under HT-CSLM conditions. In this case the resistance to de-gassing of the particles appears to be low enough for bubble rupture to dominate, which does not facilitate the swelling of the particle by bubble growth.

5.4.3 Relationship between swelling, DTG and mass spectrometry

The swelling of coal particles is driven by the evolution of gaseous volatile matter, yet, as mentioned above, higher Proximate volatile matter content does not necessarily equate to greater HT-CSLM swelling ratio. The characteristics of the volatile matter and the pattern of its release may be factors in the swelling process. Coals A and B have roughly similar total volatile matter contents however the pattern of release is different. For coal A, which shows the lowest levels of HT-CSLM swelling at 50 K/min, the rate of mass loss never goes above about 0.03 %/K (daf), whereas for coal B the rate of mass loss reaches a peak rate of almost 0.10 %/K (daf). It may be that the rate of mass loss of coal A is not sufficient to drive swelling, alternatively it may be the lack of thermoplasticity in coal A that is preventing a more rapid release of volatile matter from the coal.

Coal B begins to swell before the rate of mass loss begins to increase significantly. This can be explained if volatile matter is initially restrained within particles, increasing the internal pressure and causing swelling without being released from the particle. When the internal pressure is sufficient to cause bubble rupture then gas is released, and mass is lost.

For coals B and C the peak rate in mass loss does not coincide with the peak swelling ratio, which occurs at a lower temperature. The peak swelling ratio of coal B does seem to coincide with a very subtle shoulder on the DTG graph where the acceleration in mass loss temporarily decreases a little. This feature is consistent with modelling work by Yang *et al.*, (2014), who modelled the devolatilisation and swelling of particles of Illinois No. 6 bituminous coal as per experimental work by Fletcher. The modelled results (Figure 5.21) predicted a maximum swelling ratio at 26 ms, which coincided with a temporarily slower predicted rate of mass loss. Before this time the rate of mass loss increased due to increasing gaseous volatile matter yield, and afterwards increasing tar yield caused a rapid rate of mass loss whilst the rate of gas evolution became lower.
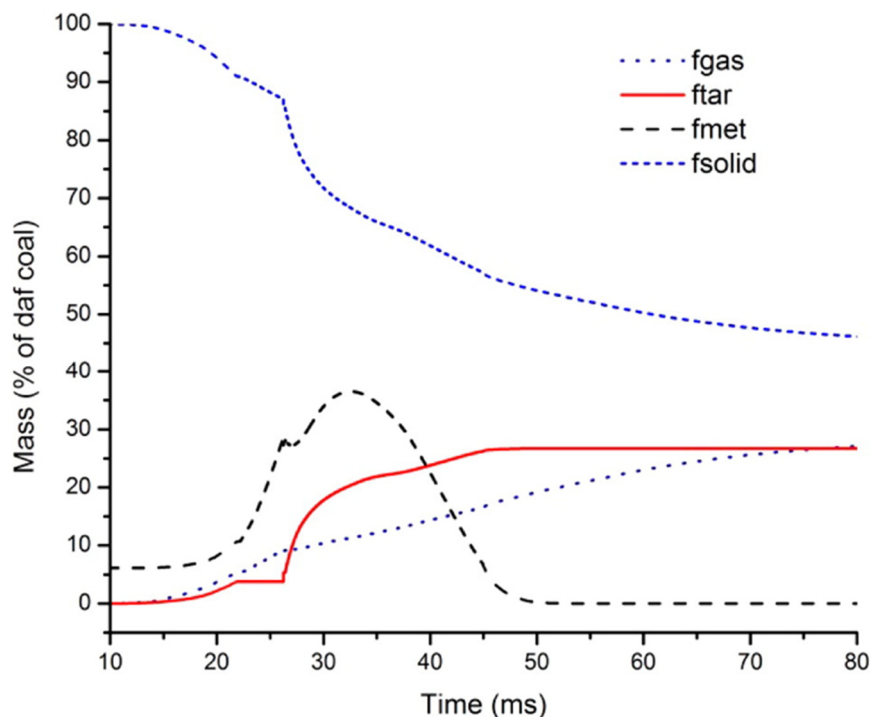
Figure 5.21: Predicted volatiles yield for Illinois No. 6 bituminous coal particles in the Fletcher experiment. (Yang *et al.*, 2014)

Although the coal modelled by Yang *et al*. is not necessarily the same as used in this work the modelling illustrates that peak swelling ratio represents the point at which the rate of light gaseous volatile matter evolution begins to decrease, and the rate of tar evolution begins to increase. The shoulder on the DTG graph is therefore likely to represent this transition between the volatile products. Light gaseous molecules such as hydrogen, methane, ethane and carbon dioxide (Wu, 2005) would produce more pressure than the same mass of heavy gaseous molecules, which may help to explain the decrease in swelling ratio after this point. This is supported by the MS results of coal B, in which the concentration of methane plus ethane peaks at a temperature close to the temperature of maximum swelling. The hydrogen concentration does not coincide with swelling; it peaks at a higher temperature (~760 °C) at which the fluidity of the coal would have been reduced. Hydrogen can be a product of condensation reactions associated with the formation of cross-links and the re-solidification process (Reaction 2.18).

The methane plus ethane MS peak of coal A occurs at a higher temperature than the maximum swelling ratio of coal A. This may help to explain the low swelling of coal A, i.e. these gases are evolved from coal A at temperatures where any small degree of fluidity has reduced.

The peak rate of mass loss (for coals B and C) occurs at a temperature at which the rate of particle shrinkage decreases. A reduction in the rate of volatile evolution should facilitate less frequent bubble ruptures and therefore a decrease in the rate of shrinkage. This is coupled with the reduction in Gieseler fluidity as the coal re-solidifies.

In the HT-CSLM, the STA and the horizontal tube furnace there will be a degree of time lag between the instrument recording a temperature and the coal sample reaching that temperature. This analysis assumes that this time lag is very similar between the instruments. However, the sample masses used were different (only a scattering of particles in the HT-CSLM, 10-11 mg in the STA and 1 g in the horizontal tube furnace) therefore the temperature lag may have been greater when greater sample masses were used.

5.5 Conclusions

The novel contributions made in this chapter are the novel application of the HT-CSLM to the field of coal particle swelling analysis, the observation of correlation between temperature of maximum swelling and the maximum Gieseler fluidity temperature, the observation of correlation between maximum swelling ratio and maximum Gieseler fluidity at low fluidity values.

Hypothesis 1 – The swelling of individual coal particles can be measured using the HT-CSLM, is accepted with the limitation that it may not be possible in the case of high fluidity coals that deform to the extent that material can no longer be described as a true particle.

The HT-CSLM has been used to measure the transient swelling properties of discrete coal particles up to 700 °C at 50 K/min and 700 K/min by direct observation. Pulverised coal particles retained on a 125 µm sieve have been analysed. The HT-CSLM is able to observe the same features of the swelling process as observed by different instruments in the literature. The HT-CSLM technique has the ability to observe several particles simultaneously and the closely controlled heating rate enables the temperature at which events occur to be accurately measured. Discrete, unconstrained particles can be observed, as opposed to packed volumes of particles, i.e. the heating environment is more like that of injection into the blast furnace.

HT-CSLM conditions can reveal swelling properties, which are not apparent from conventional methods of measuring thermoplasticity. A coal which shows contraction only in the Ruhr dilatometer has been shown to exhibit swelling under HT-CSLM conditions. Another coal with no conventional thermoplastic properties, i.e. no Gieseler fluidity, no Ruhr dilatation and a FSI of zero has been shown to exhibit swelling properties under HT-CSLM conditions. Swelling has also been observed in the HT-CSLM at temperatures lower than the Gieseler and Ruhr softening temperatures. Therefore, some information about the likely swelling behaviours of coal particles in the blast furnace can be obtained from the HT-CSLM technique, which may not be obtained from standard tests of coal thermoplasticity.

There is a relationship between the HT-CSLM swelling behaviour and Gieleser fluidity; The peak swelling ratio occurs at a similar temperature to the maximum fluidity temperature, and the greater the maximum Gieseler fluidity (within the range 0-7 ddpm) the greater the maximum HT-CSLM swelling ratio. When combined with the results of Gao *et al*., (1997), the correlation between maximum fluidity and swelling ratio appears to extend from coals with no fluidity to coals with very high fluidity (~5000 ddpm).

HT-CSLM swelling data obtained at 50 K/min is compared with DTG data obtained at the same heating rate. A common feature of the coals that swell at this heating rate is that the peak swelling ratio occurs during the rapid acceleration in mass loss associated with devolatilisation, and at a temperature lower than that of the peak rate of mass loss. The coal that showed the least HT-CSLM swelling at this heating rate also had a low rate of mass loss.

6 Effect of heating rate

6.1 Introduction

The use of HT-CSLM has been shown, in chapter 5, to be a suitable technique for direct real-time optical imaging of thermally swelling coal particles. Heating rates of 700 K/min and 50 K/min were applied in chapter 5. 700 K/min is the maximum heating rate that the HT-CSLM can be reliably operated at. A heating rate of 50 K/min was also applied to samples in order to draw comparisons with DTG data, which itself was collected at 50 K/min (the maximum operating heating rate of the STA instrument). Increasing the heating rate was found to increase the extent to which Gieseler fluidity affected swelling ratio. In this chapter the effect on coals A-D of increasing heating rate from 50 K/min to 700 K/min is investigated further. The effect of heating rate on coal particle swelling has been researched previously (Gale *et al.*, 1995; Gao *et al.*, 1997; Yang *et al.*, 2014; Yu *et al.*, 2003 and Zygourakis, 1993) although generally with regard to the final swelling ratio of particles. The HT-CSLM technique allows the effect of heating rate on the transient maximum swelling ratio to be investigated more closely.

Hypothesis to be investigated is Hypothesis 2 – Increasing heating rate increases the transient maximum swelling ratio of coal particles.

6.2 Experimental

Coals A-D are studied in this chapter. As in the previous chapter particles of pulverised coal retained on the 125 μm aperture sieve during wet sieving are used. Heating rates applied in the HT-CSLM are 50 K/min, 100 K/min, 400 K/min and 700 K/min as shown in Figure 4.3. The number of particles analysed for each coal at each heating rate is given in Table 6.1.

In chapter 5 coal B was shown to exhibit strong swelling behaviour under the HT-CSLM, coal A exhibited very weak swelling whilst the swelling of coal C was in between. Meanwhile the highly fluid behaviour of coal D prevented accurate measurement of its swelling behaviour.

	Coal A	Coal B	Coal C	Coal D
50 K/min	33	22	28	4
100 K/min	-	20	-	-
400 K/min	-	23	-	-
700 K/min	30	24	20	9

Table 6.1: The number of particles of each coal type analysed at each heating rate.

6.3 Results and analysis

Figure 6.1 illustrates the effect of heating rate on the swelling ratios of coals A-D between 50 K/min and 700 K/min. Coal B was studied at four different heating rates (Figure 6.1b & c). The mean swelling ratio begins to increase at around 350 °C and passes through a maximum at 460-470 °C before decreasing again. The temperature of maximum swelling ratio appears to be independent of heating rate. The value of the maximum swelling ratio increases with increasing heating rate, which is illustrated by Figure 6.2. The rate of particle swelling increases with heating rate, however the rate of particle shrinkage after passing through the maximum swelling ratio appears to be independent of heating rate. At 700 °C, the end of the test, the mean swelling ratios are still decreasing.

(a)
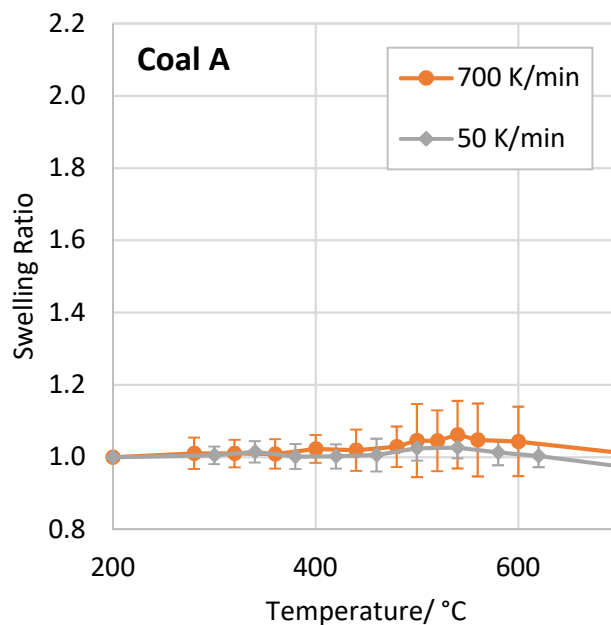
(b)
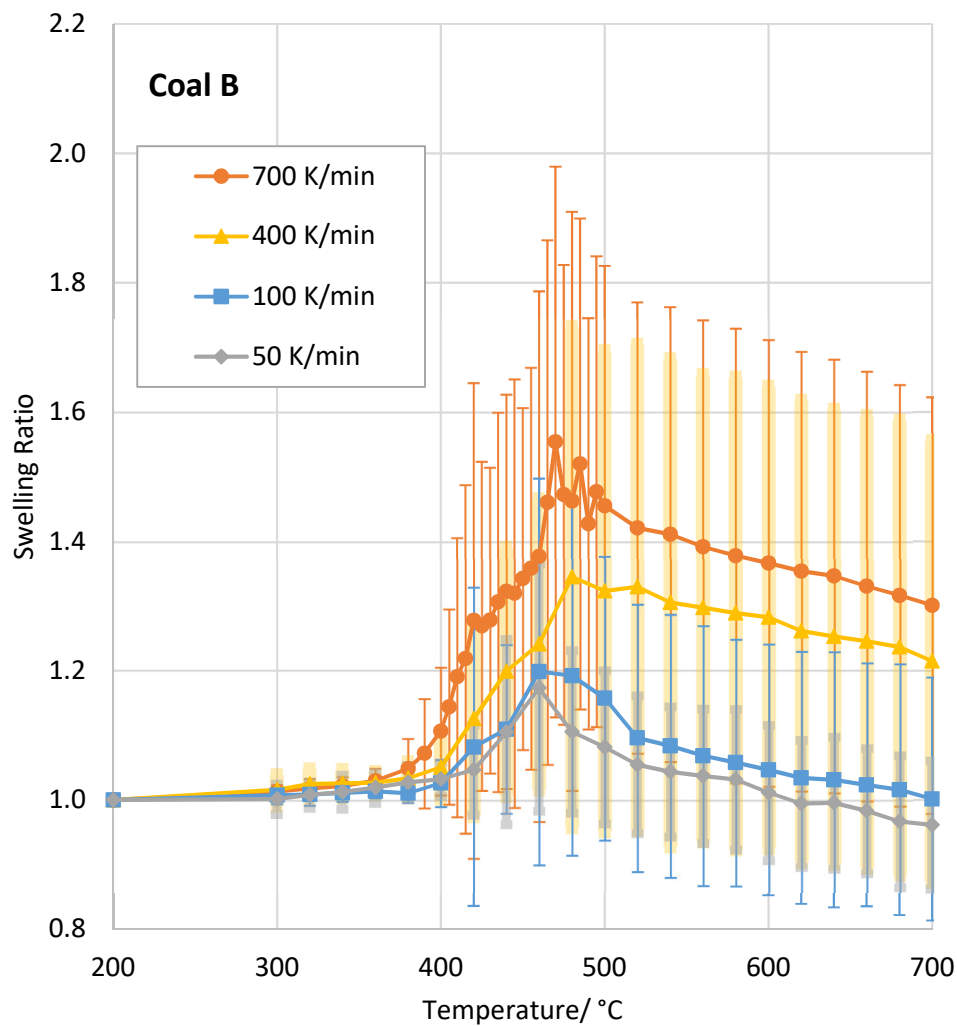
(c)
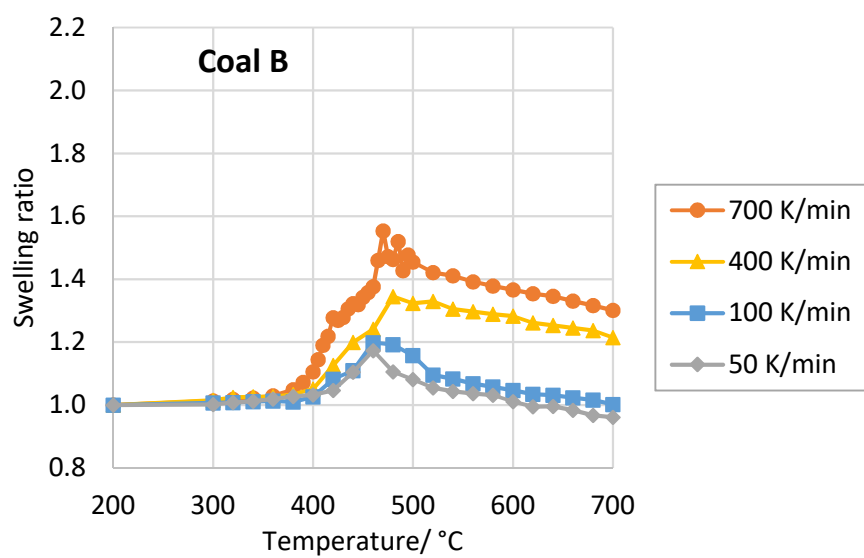
(d)
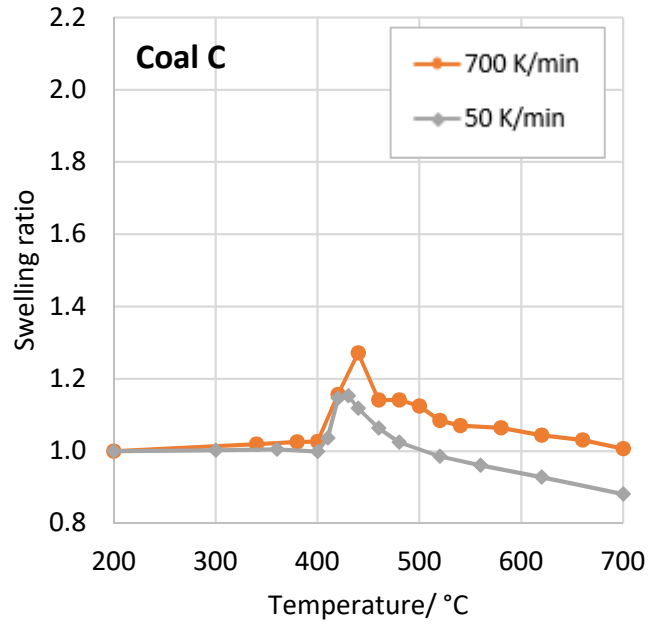
(e)
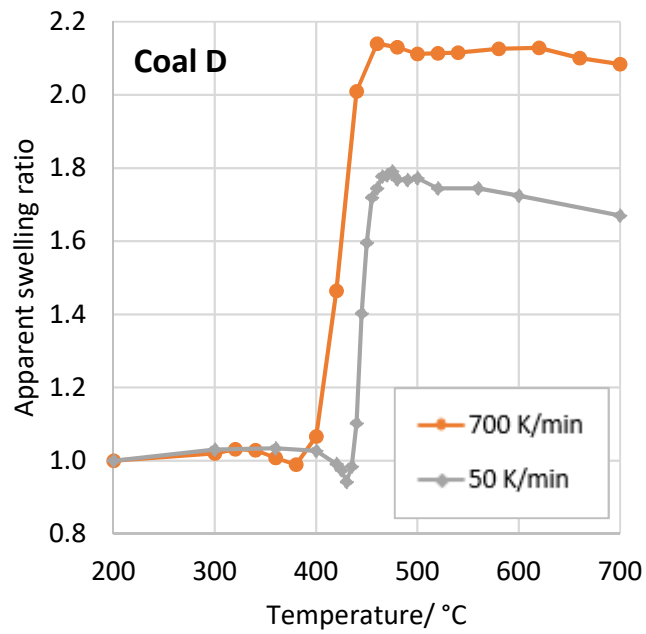
Figure 6.1: The mean swelling profiles of coals A-D at heating rates between 50 K/min and 700 K/min. Coal B is shown with error bars (b) and without error bars (c).

Coal A shows the weakest swelling behaviour of all four coals, however a maximum swelling ratio of 1.03 is observed at 50 K/min and 1.06 at 700 K/min, i.e. an effect of heating rate is detectable (Figure 6.1a). Coal C also shows the

effect of increasing maximum swelling ratio (from 1.15 to 1.27) with increasing heating rate from 50 to 700 K/min (Figure 6.1d). As with coal B, the maximum swelling temperature of coals A and C appear to be largely independent of heating rate.

Figure 6.2 shows the effect of heating rate on the maximum swelling ratios of coals A-C; the extent to which maximum swelling ratio increases with heating rate appears to be dependent upon coal type, the greater the maximum swelling ratio of a coal at a given heating rate the greater the effect of increasing heating rate.
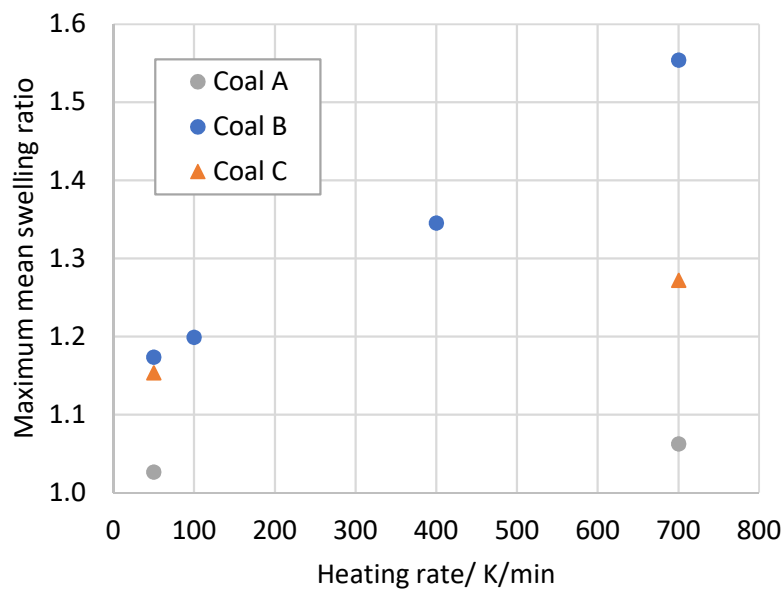
Figure 6.2: The maximum mean swelling ratio of coals B and C plotted against heating rate.

Despite the problems associated with measuring a true swelling ratio for coal D (discussed in chapter 5) the data for this coal is included in Figure 6.1e to illustrate that the highly fluid behaviour observed at 700 K/min is also observed at 50 K/min. This data is reported as an 'apparent swelling ratio' as it is not considered to represent a genuine reflection of the particle volume. The mean data in Figure 6.1e is based on a very limited number of particles, however there is a suggestion that deformation occurs to a greater extent at 700 K/min than at 50 K/min, and that the onset of deformation occurs at a lower temperature at 700 K/min. The temperature at which deformation ceases appears to be largely independent of heating rate.

The relative standard deviation (RSD) of swelling ratio values (the standard deviation in swelling ratio expressed as a percentage of the mean swelling ratio) were calculated at temperatures close to the maximum swelling temperature (typically ± 20 °C from the maximum swelling temperature), and average values calculated for coals A-C at each heating rate. RSD is used here as a measure of the relative variability in swelling ratio values within a sample, the RSD enables a better comparison of the variation in swelling ratio between samples than standard deviation as it accounts for the differing values of mean maximum swelling ratio between density samples. Table 6.2 shows the results, these show a general trend of increasing variability as heating rate, and therefore magnitude of maximum swelling ratio, increases. The exception is coal C, which shows slightly more variability at 50 K/min than at 700 K/min. It is also apparent that the more highly swelling coals tend to have a greater degree of variability than the lesser swelling coals, for example at 700 K/min the RSD increases as maximum swelling ratio increases.

	RSD at Max. swelling ratio/ %		
	Coal A	Coal B	Coal C
50 K/min	3.2	13.5	19.2
100 K/min	-	19.9	-
400 K/min	-	24.9	-
700 K/min	7.7	25.5	18.8

Table 6.2: Average RSD values at temperatures around maximum swelling ratio for coals A-C.

An STA instrument capable of heating rates up to 100 K/min was used to measure the pattern of mass loss of samples of coal B, >125 µm particles, at 50 K/min and 100 K/min to investigate whether differences in swelling behaviour associated with heating rate could be related to differences in the pattern of mass loss. The TG and DTG results are shown in Figure 6.3. The pattern of mass loss is very similar at the two heating rates. Up to 900 °C slightly more mass is lost at 50 K/min and the DTG peaks occur at lower temperatures. For example, the initial DTG peak occurs ~15 °C lower at 50 K/min. The peak rate of mass loss is slightly higher at 50 K/min.

(a)

(b)
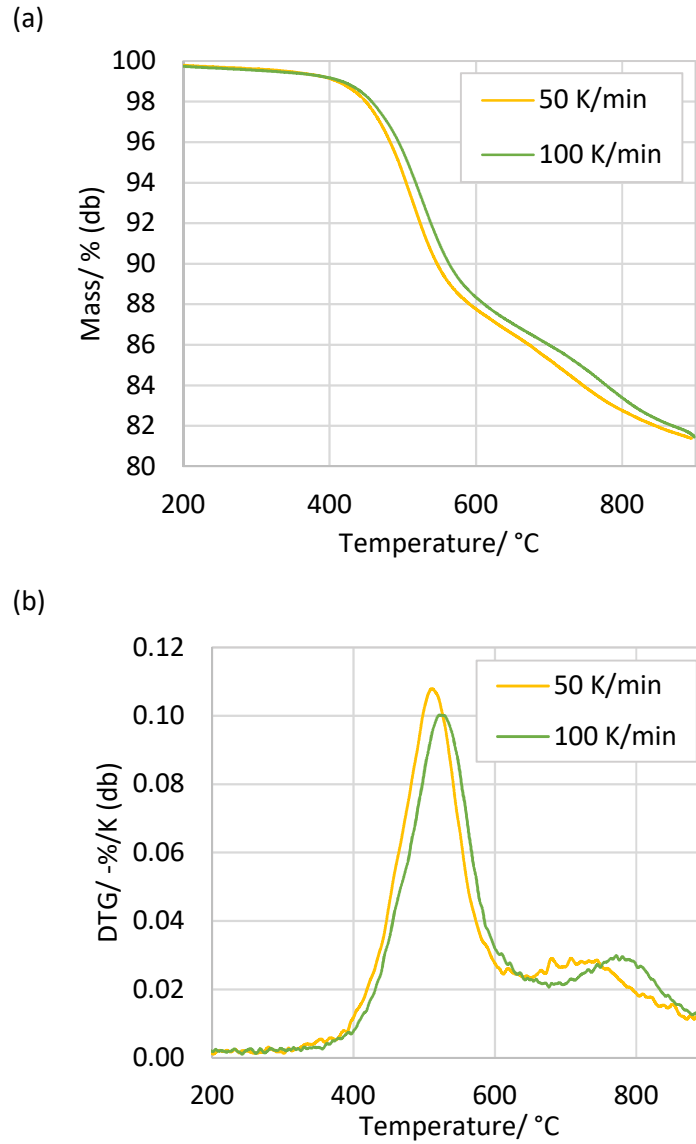
Figure 6.3: TG (a) and DTG (b) data from the heating of >125 μm particles of coal B at 50 K/min and 100 K/min.

6.4 Discussion

This work has demonstrated that the transient maximum swelling ratio of three coals (A-C) increases with regard to heating rate within the range 50-700 K/min. This increase in maximum swelling ratio is explained by the increased internal pressure within particles at higher heating rates. Low rates of heating enable volatile gases to escape the particles before sufficient pressure builds up to drive swelling.

Previous research investigating the effect of heating rate upon coal particle swelling has tended to deal with final particle swelling ratios. Only Yu *et al.*, (2003), using the Single Particle Reactor stated that there was a 'much smaller maximum swelling ratio' at a heating rate of 10 K/s than at 100 K/s, although the data was not published. The results of the current work agree with previously published results on final swelling ratio (although it should be noted that at 700 °C the mean swelling ratio of the samples was decreasing, i.e. had not reached a stable final value) and demonstrate that the trend also applies to the transient maximum swelling ratio. The gradient of increase in maximum swelling ratio with regard to heating rate is the same as that for final swelling ratio in this study. This is illustrated by Figure 6.4, which shows data for coal B.
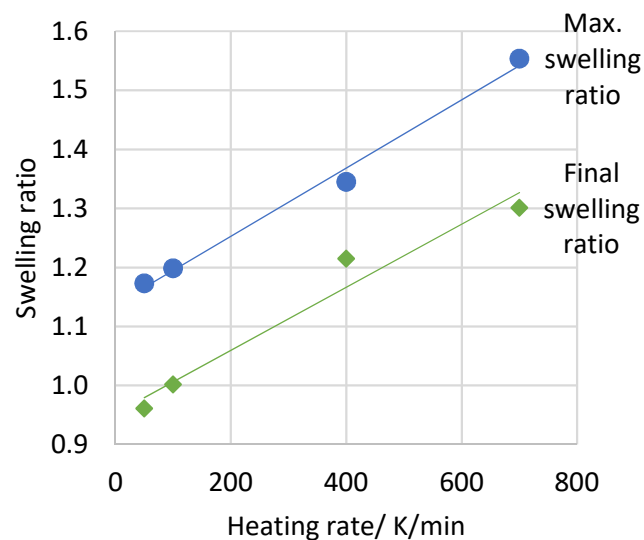
Figure 6.4: The effect of heating rate on maximum and final swelling ratio for coal B samples. Final swelling ratio measured at 700 °C.

Coal A shows no indication of thermoplasticity during Gieseler fluidity, Ruhr dilatometer and free swelling index (FSI) tests, which are all carried out under low heating rates (3 K/min is standard for Gieseler fluidity and Ruhr dilatation). Figure 6.2 implies that, if heated at 3 K/min, the maximum swelling ratio of coal A would be expected to be extremely low. The presence of swelling in coal A under HT-CSLM conditions implies some degree of fluidity, some fluidity may also exist at lower heating rates although it may be insufficient to enable movement of the spindle during a Gieseler test or enable Ruhr contraction. The reduced pressure

build-up within particles at lower heating rates would result in no Ruhr dilation and an FSI of zero.

In this study the temperature of maximum swelling ratio appears to be independent of heating rate. However, Gao *et al.*, (1997), used a laser heating system and found that the temperature of maximum swelling increased from ~460 °C to ~660 °C with increasing maximum heating rate from 2.6 x 10^3 K/s to 1.2 x 10^4 K/s respectively. A similar increase was observed for all three coals studied by Gao *et al*. (Figure 6.5). The magnitude and range of heating rates were much greater than those associated with the HT-CSLM in this current work. If the relationship shown in Figure 6.5 is applicable at the lower heating rates associated with the HT-CSLM (i.e. 700 K/min = 11.67 K/s) this would suggest that increases in the temperature of maximum swelling ratio are not clearly detectable over the range used in the HT-CSLM, i.e. increasing the heating rate by 650 K/s increases the temperature of maximum swelling by ~14 °C.
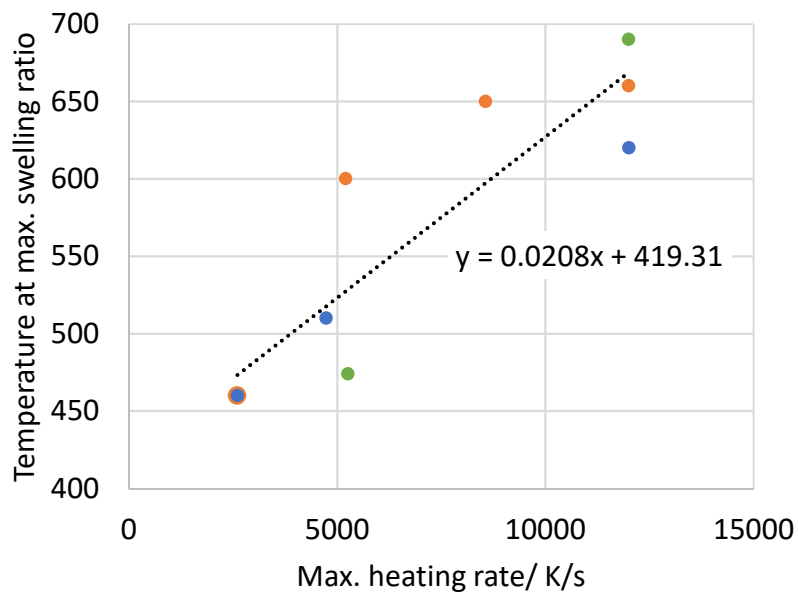
Figure 6.5: Effect of increasing maximum heating rate on the temperature of maximum swelling ratio in laser heating experiments by Gao *et al.*, (1997). Different colour markers represent different coal types.

6.5 Conclusions

The novel contribution made in this chapter is the experimental observation that the transient maximum swelling ratio increases with heating rate.

Hypothesis 2 – Increasing heating rate increases the transient maximum swelling ratio of coal particles is accepted.

Increasing the heating rate from 50 K/min to 700 K/min has been shown to increase the transient maximum swelling ratio and the rate of swelling, although this is coal dependent. The swelling onset temperature and the rate of shrinkage following peak swelling ratio appear to be independent of heating rate over the range of heating rates used in this study. It is likely that the temperature of peak swelling ratio does increase with increasing heating rate, but over the range of heating rates used in this study the effect is not clearly visible.

7 Effect of particle density

7.1 Introduction

The use of HT-CSLM has been shown to be a suitable technique for real-time optical imaging of thermally swelling coal particles, and the effect of heating rate on transient maximum swelling ratio between 50 and 700 K/min has been investigated. Within the same sample a variety of swelling behaviours is observed, as was noted in chapter 5. This illustrates the heterogeneity between particles within a sample. In this chapter density separation is used to separate particles according to maceral and mineral content, with the aim of demonstrating the origin of heterogeneous behaviour. Gieseler fluidity and DTG analysis of density fractions is also carried out to provide additional insight into differences between density fractions.

Hypotheses to be investigated are:

Hypothesis 3 – Lighter coal particles attain a greater maximum swelling ratio than denser particles of the same coal.

Hypothesis 4 – Coal swelling behaviour can be related to Gieseler fluidity and TGA mass loss.

7.2 Experimental

Coals A and B are studied in this chapter. Coal B was selected as it showed the greatest swelling behaviour of coals A-D; coal A was selected as it was considered to be an interesting material for further investigation due to its unusual petrography i.e. the double-peaked reflectance histogram shown in Figure 7.3a. As in the previous two chapters particles of pulverised coal retained on the 125 μm aperture sieve during wet sieving are used. Density separation, by sink-float centrifugation as described in section 4.3, was carried out following wet sieving. The heating rate applied in the HT-CSLM was 700 K/min as this has been shown to facilitate the greatest swelling behaviour (chapter 6). The number of particles analysed for each test sample is given in Table 7.1. For Gieseler fluidity

measurements of density fractions, the coal preparation is as described here therefore differing from the ISO Standard with respect to sample preparation.

Density Fraction	Coal A	Coal B
F1.2	29	27
S1.2-F1.3	31	20
S1.3-F1.4	36	11
S1.4-F1.7	26	18
S1.7	33	18

Table 7.1: The number of particles analysed by HT-CSLM in each test sample.

7.3 Results

7.3.1 Density separation

Density separation allowed the density distributions within the samples of coals A and B to be obtained, the mass percentages of each density fraction are shown in Table 7.2 and cumulative distributions are shown in Figure 7.1. The particles of coal A are, overall, denser than those of coal B. Approximately 80 wt. % of coal A particles fell within the density range 1.3-1.7 kg/L, whereas ~80 wt. % of coal B particles fell within the range 1.2-1.4 kg/L.

Density Fraction	Coal A	Coal B
F1.2	2	6
S1.2-F1.3	9	50
S1.3-F1.4	48	30
S1.4-F1.7	33	8
S1.7	9	6

Table 7.2: Mass % of each density fraction within coals A and B.
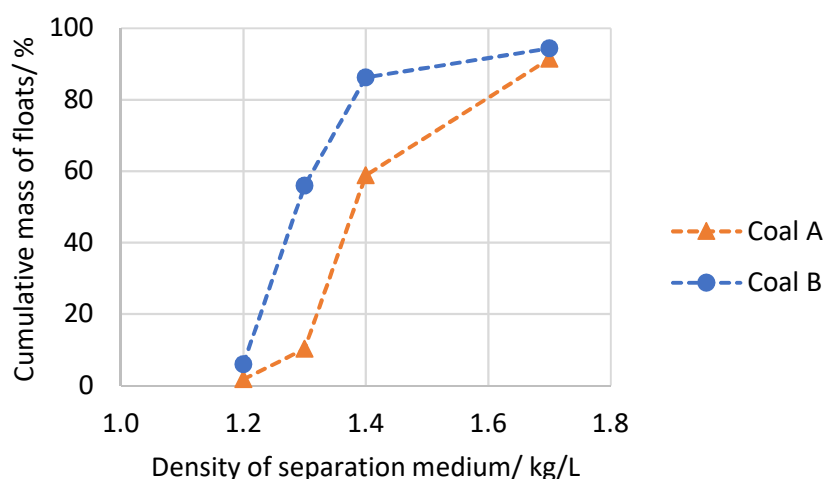
Figure 7.1: Cumulative density distribution of particles of coal A and coal B.

7.3.2 Proximate analysis of density fractions

Proximate analysis of each density fraction of coals A and B is given in Table 7.3 and presented graphically in Figure 7.2, these are calculated from Netzch TGA data. The general trends common to both coals are that ash content (db) is at a minimum in the S1.2-F1.3 fraction and increases with particle density, whilst the F1.2 fraction also has an ash content slightly greater than the S1.2-F1.3 fraction. The volatile matter (db) remains relatively constant across all density fractions although the S1.2-F1.3 and S1.7 fractions show slightly greater values than the other density fractions. The fixed carbon, by definition, constitutes the remainder of the samples and approximately follows an inverse pattern to the ash content.

A difference between the coals is that coal A shows a step-change in Proximate composition between S1.4-F1.7 and S1.7; whereas coal B shows a more gradual transition as particle density increases.

Coal		F1.2	S1.2-F1.3	S1.3-F1.4	S1.4-F1.7	S1.7
A	FC/ wt. % (db)	81.0	81.3	82.9	76.0	26.8
	VM/ wt. % (db)	11.8	15.3	11.0	9.2	15.3
	Ash/ wt. % (db)	7.2	3.4	6.0	14.7	57.9
B	FC/ wt. % (db)	75.9	80.3	76.2	55.2	27.7
	VM/ wt. % (db)	17.1	18.5	15.5	16.6	22.3
	Ash/ wt. % (db)	7.0	1.2	8.3	28.2	50.0

Table 7.3: Proximate analysis data of the density fractions of coals A and B.
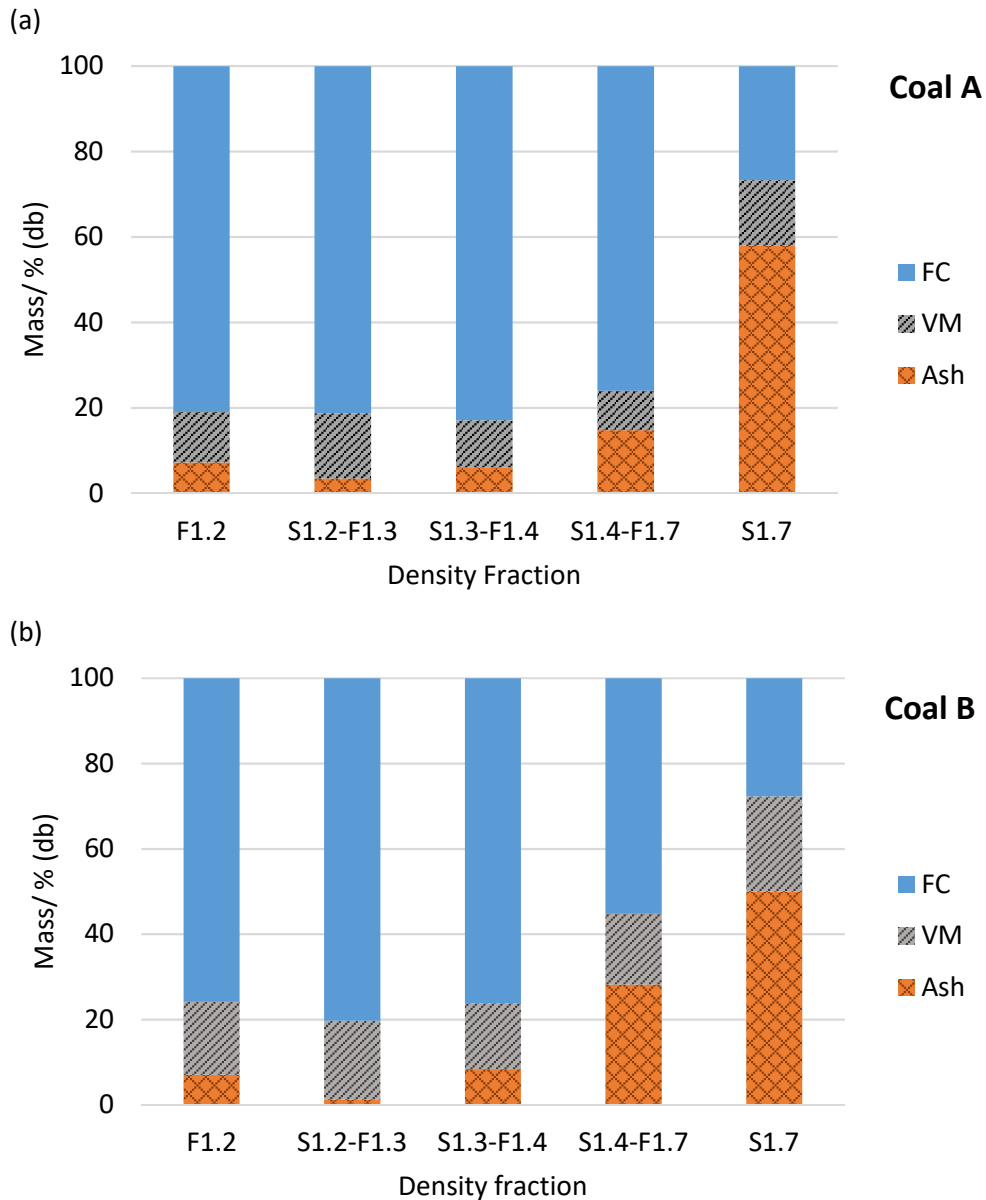
Figure 7.2: Proximate analysis of density fractions of coals A and B (a and b).

7.3.3 Petrographic analysis of density fractions

Petrographic analysis of each of the density fractions is shown in Figures 7.3-7.5. The reflectance distribution histograms for each coal (Figures 7.3 and 7.4) show that the reflectance distribution changes according to particle density.

Coal A (Figure 7.3) has an unusual petrography, there is a broad reflectance distribution which is double peaked (Figure 7.3a). There was insufficient material to analyse the F1.2 fraction of coal A. The S1.2-F1.3 particles appear to be

responsible for the peak at reflectance group 15 whilst the S1.3-F1.4 particles may be responsible for the second peak at reflectance group 20. As density increases the reflectance distribution seems to become broader, less distinct and shifting to higher reflectance values. The S1.7 particles have 58 % ash therefore the organic material present in these particles is likely to be that which happens to be connected to mineral matter. Figure 7.5a indicates that the levels of vitrinite are slightly greater than the levels of inertinite and differences in the vitrinite: inertinite ratio between the density groups are small. No liptinite is detected in coal A.

(a)

(b)

(c)

(d)

(e)
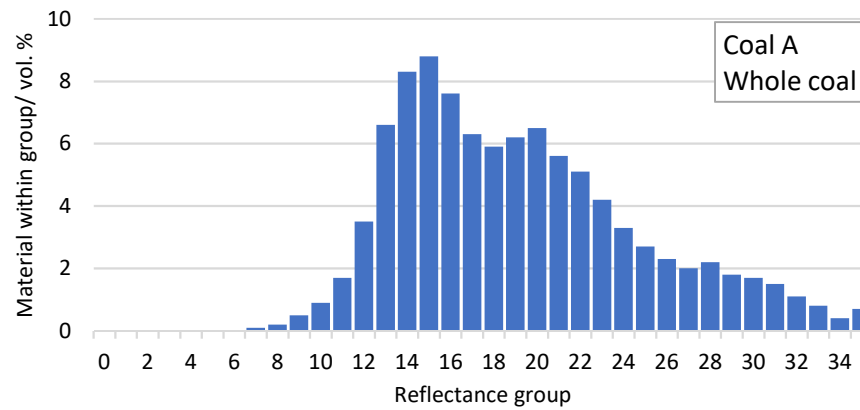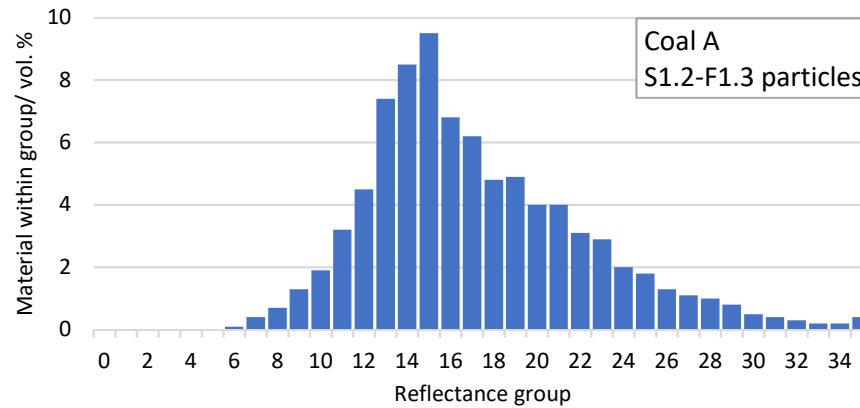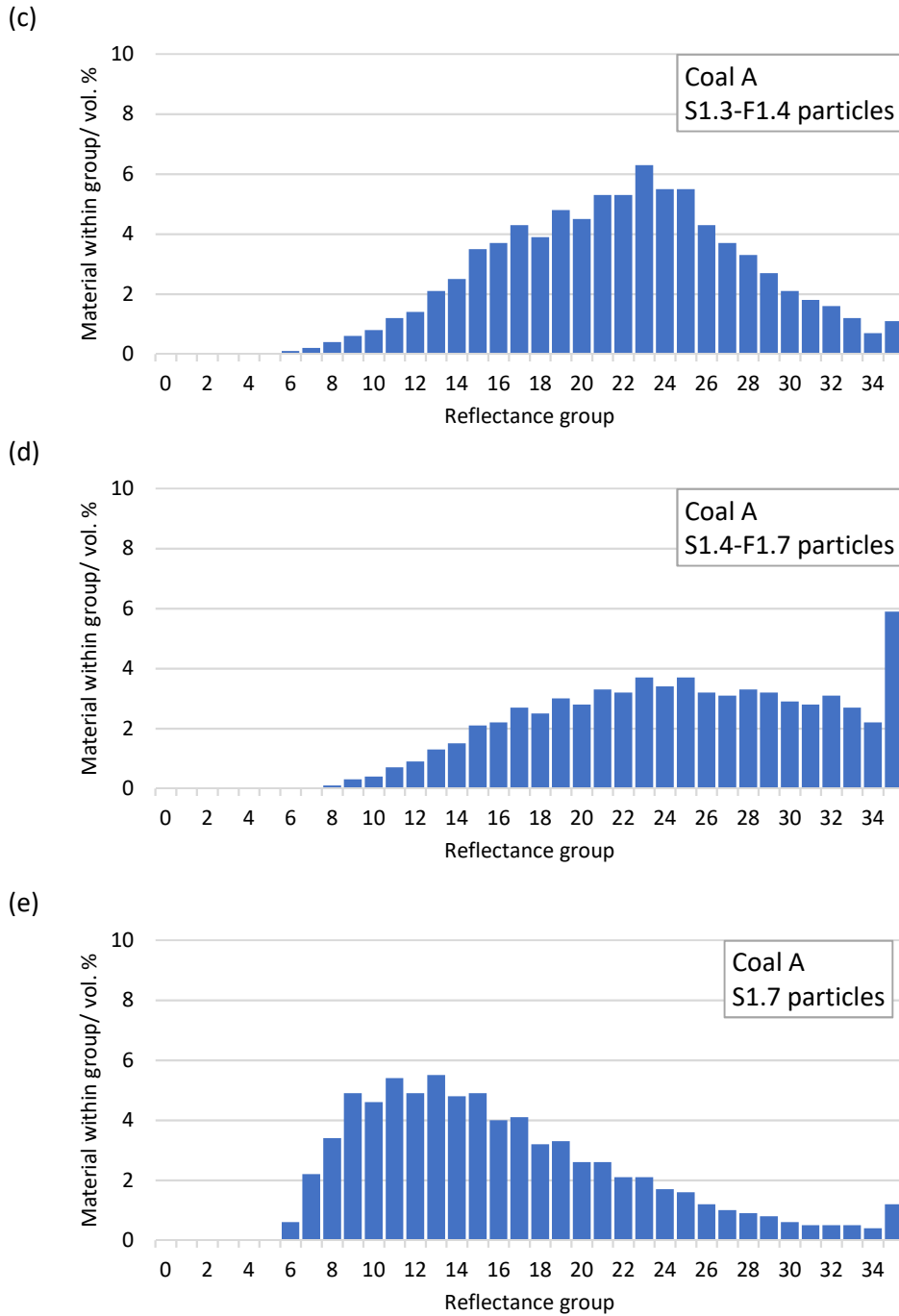
Figure 7.3: Petrographic reflectance distribution graphs of coal A (a) and
separated density fractions of coal A: S1.2-F1.3 (b), S1.3-F1.4 (c), S1.4-F1.7 (d),
S1.7 (e). Note: there was insufficient material available to perform petrographic
analysis on the F1.2 fraction of coal A.

In the case of coal B (Figure 7.4) particles of density below 1.4 are relatively
consistent in terms of their reflectance, which is closely centred around
reflectance groups 13-14. As particle density increases the reflectance distribution

becomes broader, and a greater percentage of material is observed at the higher reflectance values. Figure 7.5b shows a transition from ~80 % vitrinite to ~40 % vitrinite as density increases, meanwhile inertinite increases from ~20 % to ~50 %. Liptinite also increases from ~1 % to ~4 %.

(a)
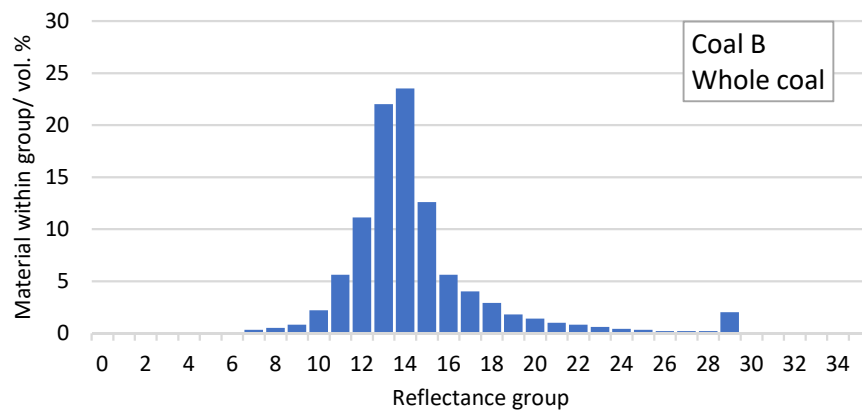
(b)
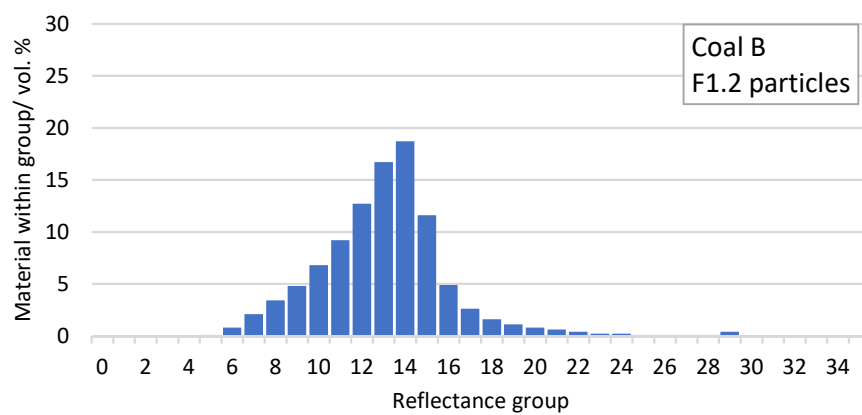
(c)
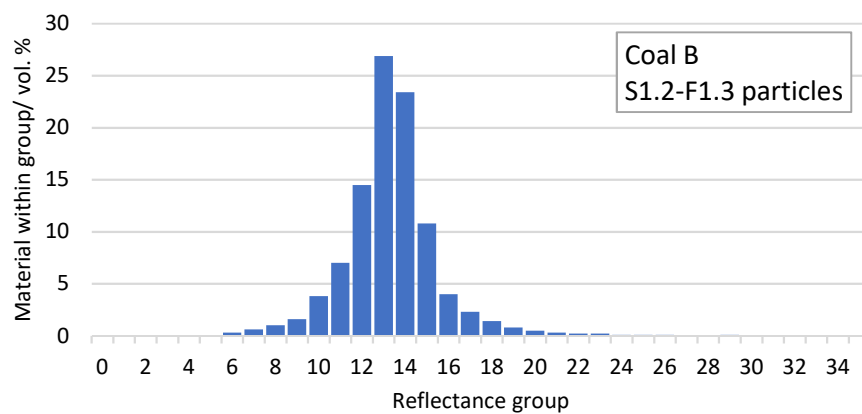
(d)
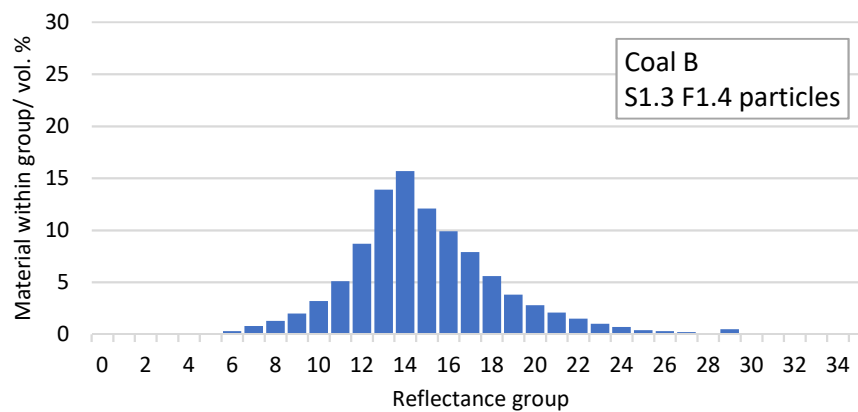
(e)
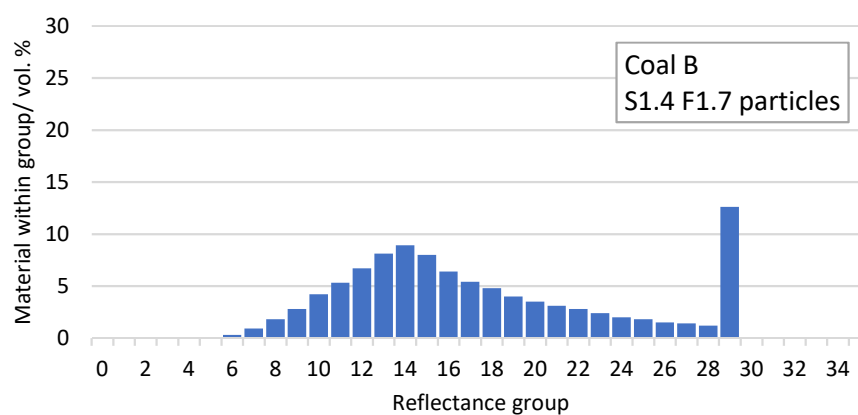
(f)
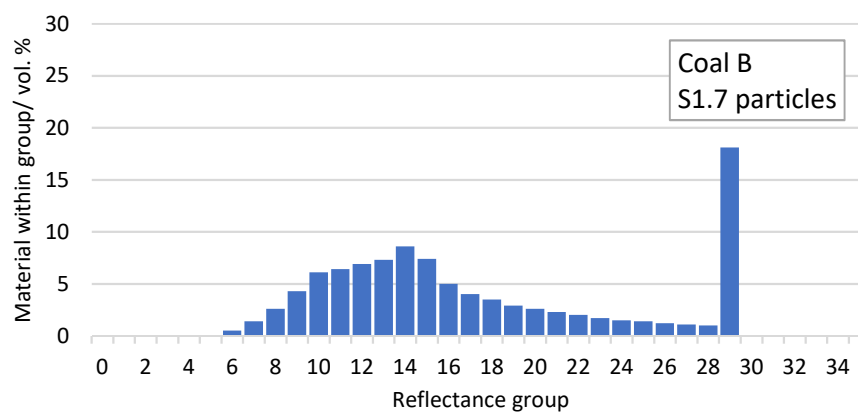
Figure 7.4: Petrographic reflectance distribution graphs of coal B (a) and separated density fractions of coal B: F1.2 (b), S1.2-F1.3 (c), S1.3-F1.4 (d), S1.4-F1.7 (e), S1.7 (f).

Coal		F1.2	S1.2-F1.3	S1.3-F1.4	S1.4-F1.7	S1.7
A	Vitrinite/ Vol. % (daf)	-	50.2	53.2	50.5	54.1
	Inertinite/ Vol. % (daf)	-	49.8	46.8	49.5	45.9
	Liptinite/ Vol. % (daf)	-	0	0	0	0
B	Vitrinite/ Vol. % (daf)	78.6	81.5	68.3	54.9	44.3
	Inertinite/ Vol. % (daf)	20.1	17.4	29.5	41.9	51.7
	Liptinite/ Vol. % (daf)	1.3	1.1	2.1	3.2	4.1

Table 7.4: Maceral composition of the density fractions of coals A and B.

(a)
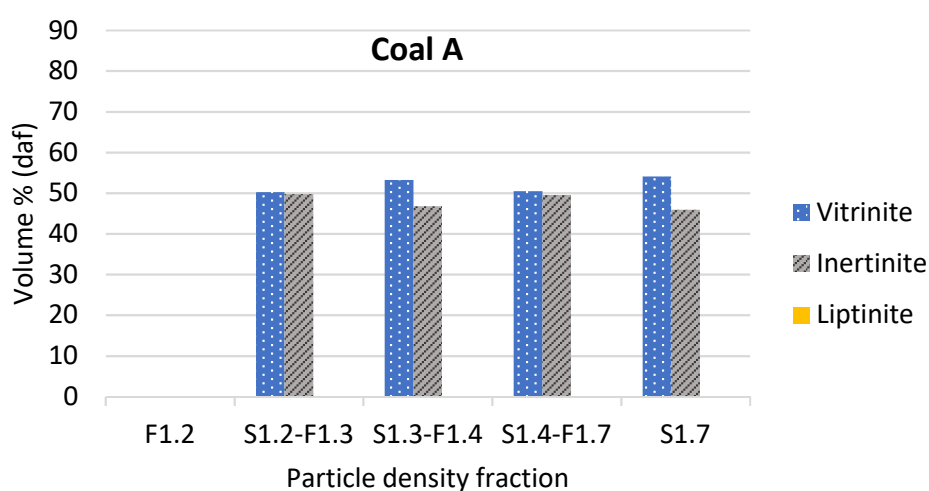
(b)
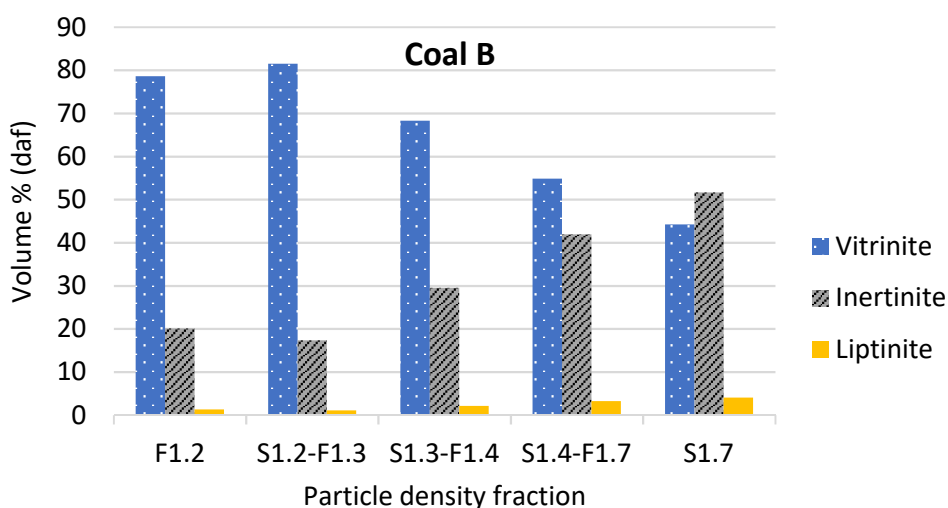
Figure 7.5: Composition of the different density fractions of coals A and B (a and b) by petrographic analysis.

7.3.4   Swelling of density fractions

The swelling properties of the density fractions of coals A and B were measured using HT-CSLM, results are shown in Figure 7.6. The swelling ratios shown here are mean values representing the number of particles given in Table 7.1. The levels of swelling for coal B are greater than those of coal A, the maximum swelling ratio of each density fraction of coal B is greater than the equivalent density fraction of coal A.

The general trend for both coals is that the lighter particles reach a greater maximum swelling ratio than the denser particles. The exception is in the case of coal A where the S1.2-F1.3 particles swell more than the F1.2 particles.

(a)

(b)
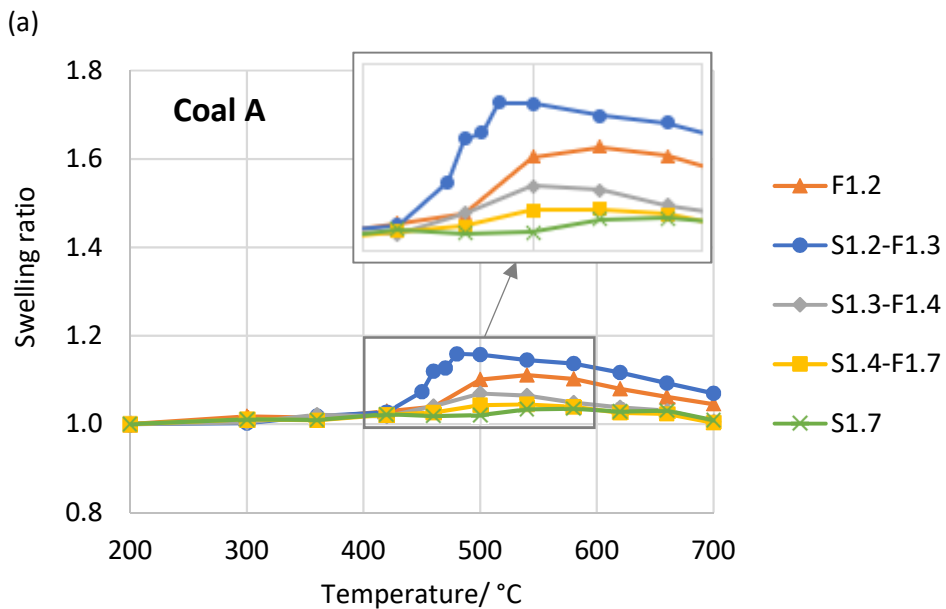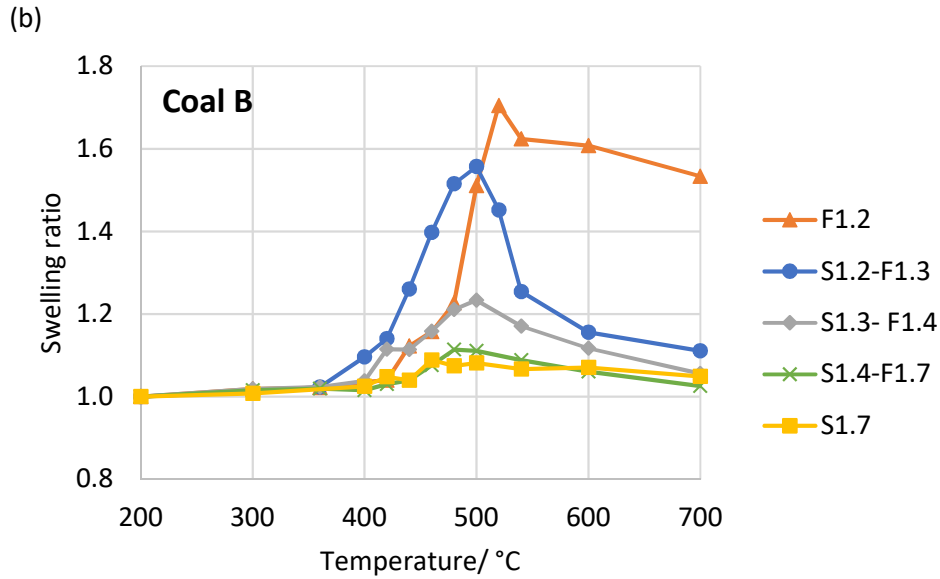
Figure 7.6: Mean swelling profiles of density fractions of coals A and B (a and b) measured using HT-CSLM.

The temperature range over which swelling occurs for coal A is largely independent of particle density, although there is some variation in the temperature of maximum swelling. This variation may be due to the broad nature of the swelling peaks of coal A. For coal B the temperature of maximum swelling appears to be largely unaffected by particle density, apart from the F1.2 particles, which reach a maximum swelling ratio at 520 °C, which is 20 °C higher than the other density fractions of coal B.

In order to check the continuity of results between this chapter and chapter 5, the swelling results of individual density fractions were used, along with the relative proportions of each fraction, to calculate the expected swelling profile of each coal prior to density separation. The weighting given to each density fraction is based on the mass percentage of that fraction within the total sample. The swelling results of each coal prior to density separation are presented in chapter 5, and these results are compared with calculated (reconstructed) results in Figure 7.7.

The calculated results of coal A are in good agreement with the measured results from chapter 5 (Figure 5.8), and the same is true for coal B up until the point of maximum swelling, after this the measured results show less shrinkage than the

calculated results. Figure 7.6b shows that it is the F1.2 particles of coal B that tend to maintain a high swelling ratio up until 700 °C therefore it may be that a disproportionately large number of these particles contribute to the >125 μm sample mean presented in chapter 5.

(a)

(b)
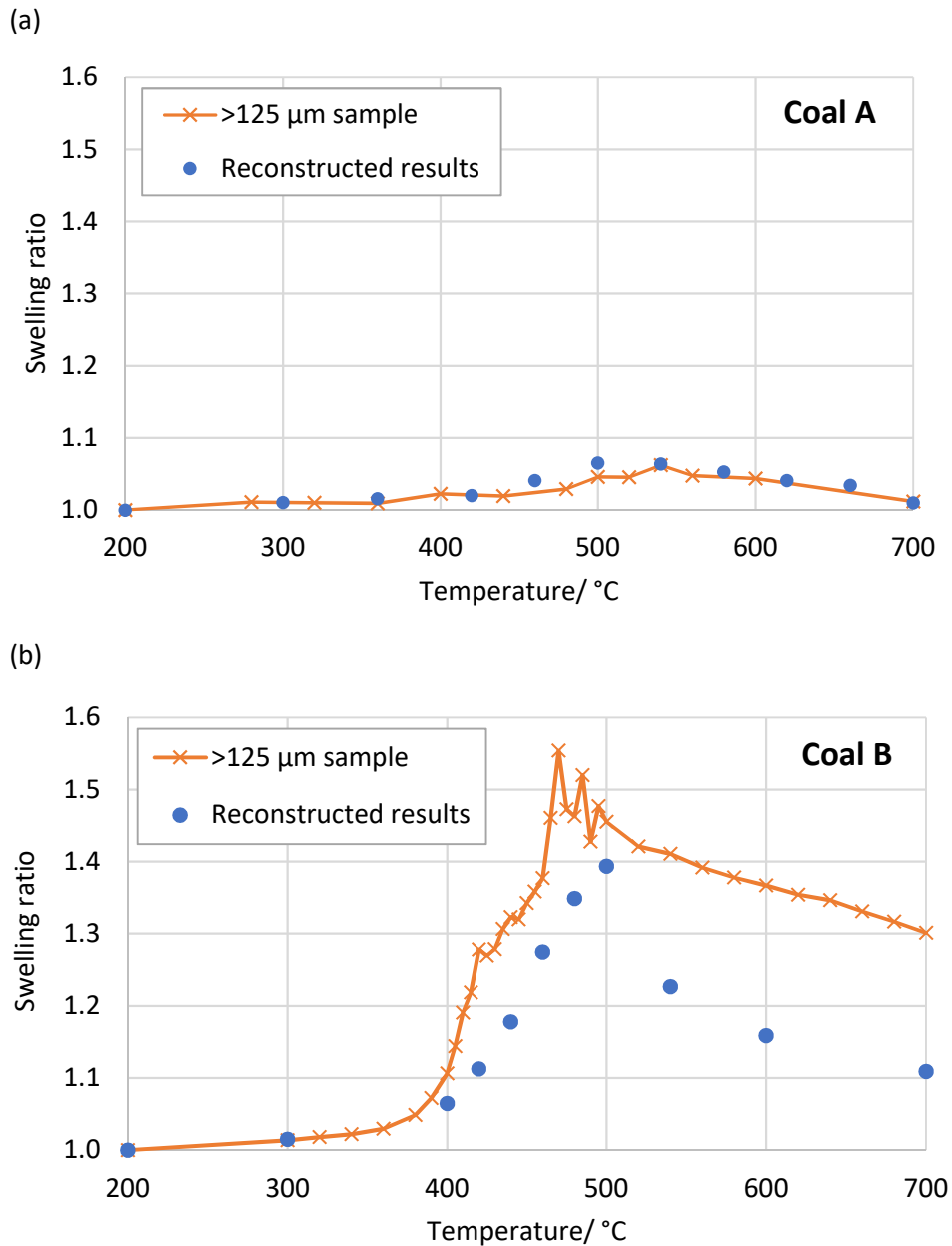
Figure 7.7: Comparison between the mean swelling profile of unseparated samples of coals A and B (a and b) (data from chapter 5) with calculated values based on results of density separated fractions of the coals.

An aim of density separation was to investigate the origin of the heterogeneous swelling behaviour described in chapter 5. In Figures 7.8 and 7.9, the variation in swelling behaviour within each density fraction of each coal is shown in the form of error bars representing 1 standard deviation either side of the mean. The trend is for greater standard deviation at higher swelling ratios. Overlays are included in the Figures to illustrate the substantial overlap between error bars. A similar figure (Figure 5.6) was presented in chapter 5 showing the standard deviation in swelling ratio for a sample of coal B, >125 µm, particles; this is reproduced in Figure 7.10, overlaid with the data for the S1.2-F1.3 density fraction of coal B (which has a similar swelling profile and maximum swelling ratio to the parent coal B sample). It can be seen that, contrary to expectation, there is no significant decrease in the standard deviation of swelling ratio values for the S1.2-F1.3 sample. In fact, the standard deviation values are greater than those of the parent sample around the temperature of maximum swelling.
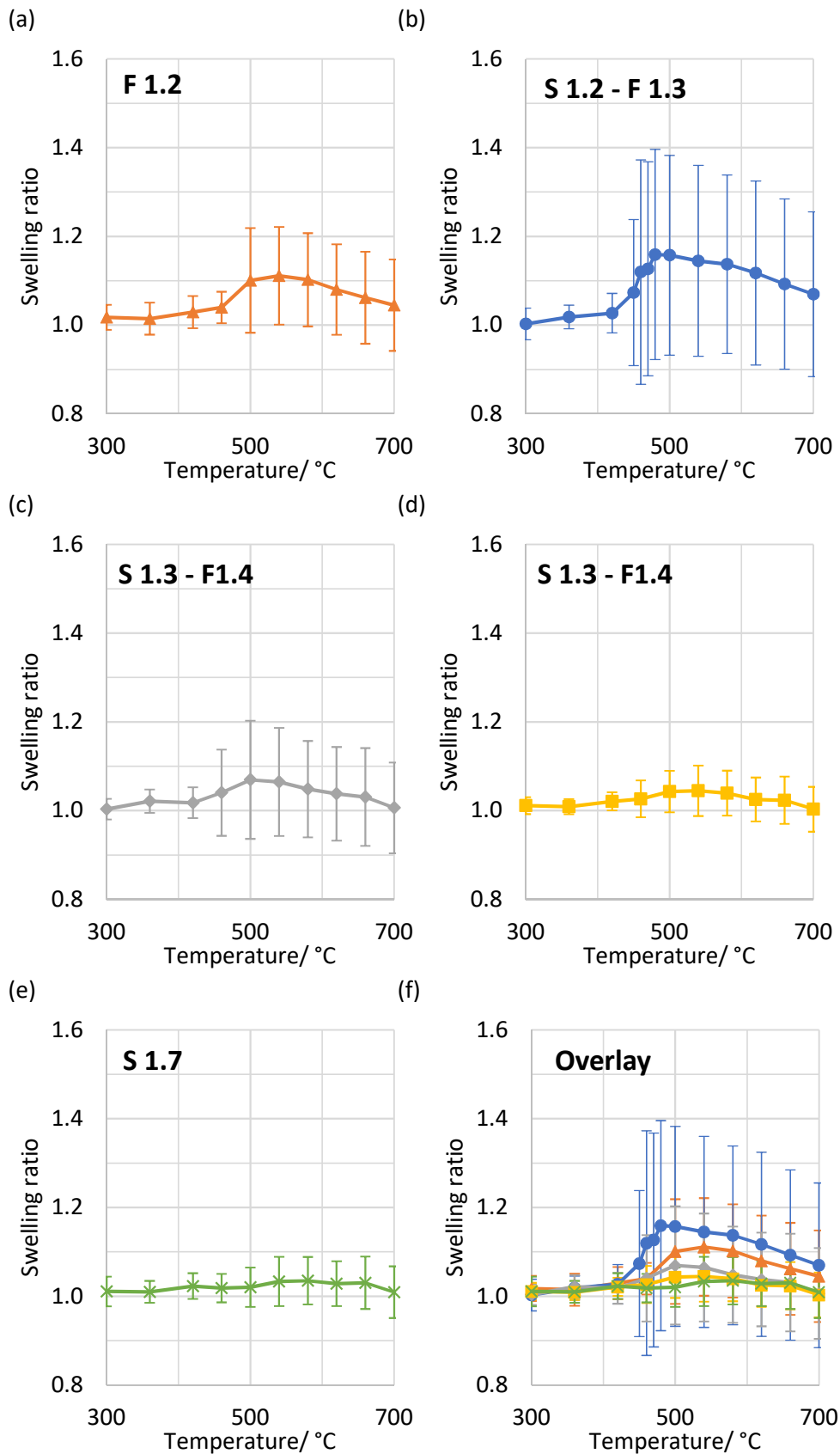
Figure 7.8: Mean swelling profiles of density fractions of coal A, >125 μm, with error bars representing 1 standard deviation either side of the mean.
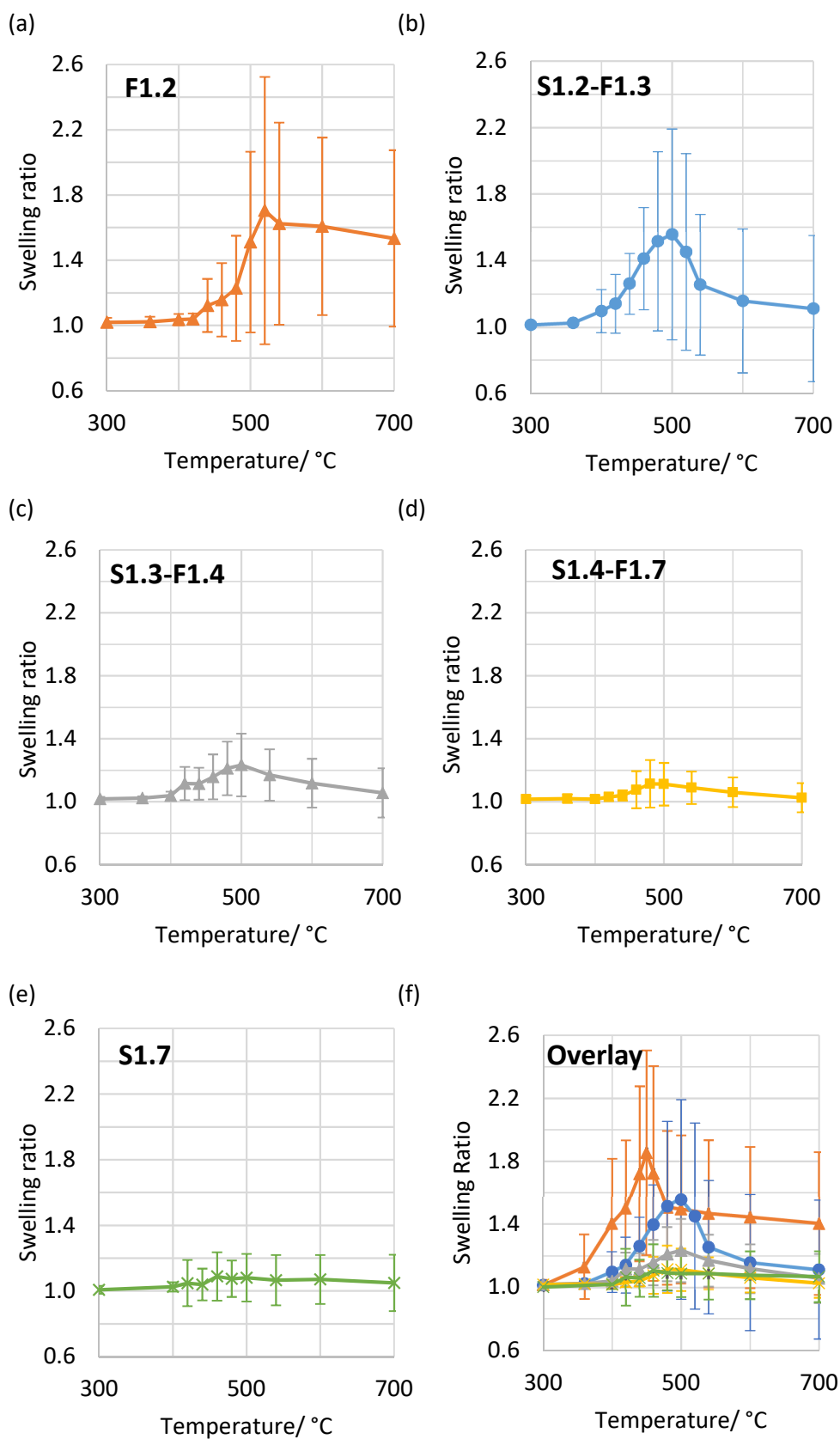
Figure 7.9: Mean swelling profiles of density fractions of coal B, >125 μm, with error bars representing 1 standard deviation either side of the mean.
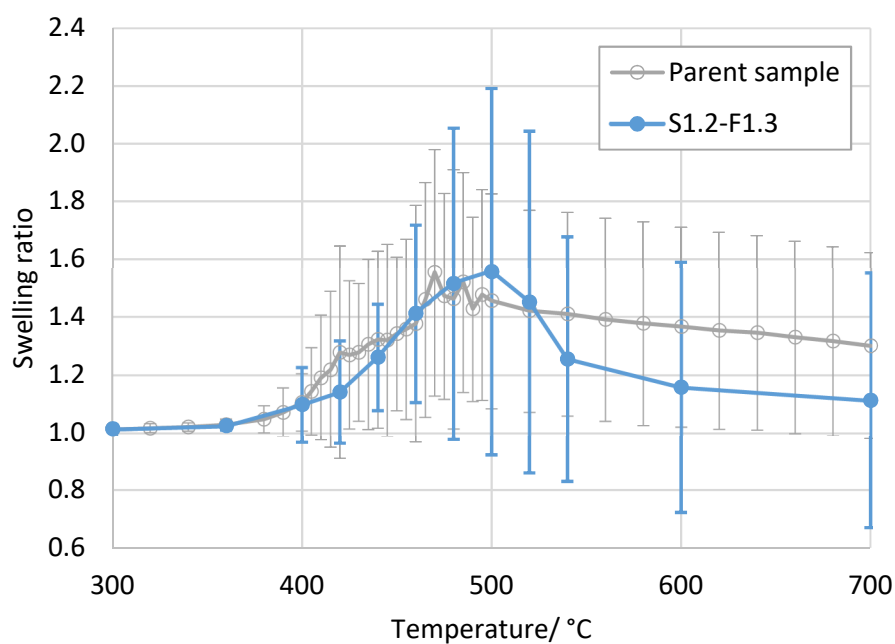
Figure 7.10: Mean swelling profiles of the coal B, >125 µm parent sample and the S1.2-F1.3 density fraction of this sample, with error bars representing 1 standard deviation either side of the mean.

	Sample	Max. swelling ratio	RSD at max. swelling ratio/ %
Coal A	Parent	1.0	7.7
	F1.2	1.1	10.0
	S1.2-F1.3	1.2	21.0
	S1.3-F1.4	1.1	11.1
	S1.4-F1.7	1.0	4.9
	S1.7	1.0	5.1
Coal B	Parent	1.6	25.5
	F1.2	1.7	41.0
	S1.2-F1.3	1.6	39.0
	S1.3-F1.4	1.2	15.1
	S1.4-F1.7	1.1	11.1
	S1.7	1.1	11.0

Table 7.5: Maximum mean swelling ratio and relative standard deviation in swelling ratio at temperature of maximum swelling for the coal B parent sample and density fractions of that sample.

Further data is presented in Table 7.5; here the relative standard deviation (RSD) (the standard deviation in swelling ratio expressed as a percentage of the mean swelling ratio) is given, along with maximum swelling ratio values for the >125 μm parent samples and the density fractions of coals A and B. Regarding the coal B data, there is a divide at density 1.3; density fractions below this value have a greater swelling ratio and also greater RSD values of 39-50 %. Density fractions above 1.3 have a lower swelling ratio and lower RSD values of 10-15 %. The value of RSD for the parent sample is in between, at 25.5 %. For coal A the density of 1.3 does not represent a clear divide as it does for coal B, however the trend of Increasing RSD with increasing swelling ratio exists, as does the fact that the RSD values of the three most highly swelling density fractions is greater than that of the parent coal sample.

7.3.5 DTG analysis of density fractions

Differential thermo-gravimetric (DTG) data of the density fractions is presented in Figures 7.10 and 7.11. The heating rate used to produce this data was 50 K/min, which is lower than the 700 K/min used in the HT-CSLM to produce the swelling data.

The rate of mass loss for all density fractions of coal A begins to increase as temperatures rise above 400 °C (Figure 7.11b). The S1.7 fraction shows the highest peak rate of mass loss, at around 490 °C. Of the remaining samples the F1.2 and S1.2-F1.3 fractions show peaks at ~530 °C, the S1.2-F1.3 peak being the higher. The S1.3-F1.4 and S1.4-F1.7 fractions have lower rates of mass loss and similar profiles to one-another, they exhibit indistinct peaks in their rates of mass loss at around 540 °C and 550 °C. The S1.3-F1.4 sample has a slightly higher rate of mass loss than the S1.4-F1.7 sample. Above ~700 °C the rates of mass loss of the samples converge.

The DTG profile of coal A prior to density separation does not show a clear peak at ~530 °C (Figure 7.11a) because it is dominated by the S1.3-F1.7 fractions, which account for ~84 % of the sample.
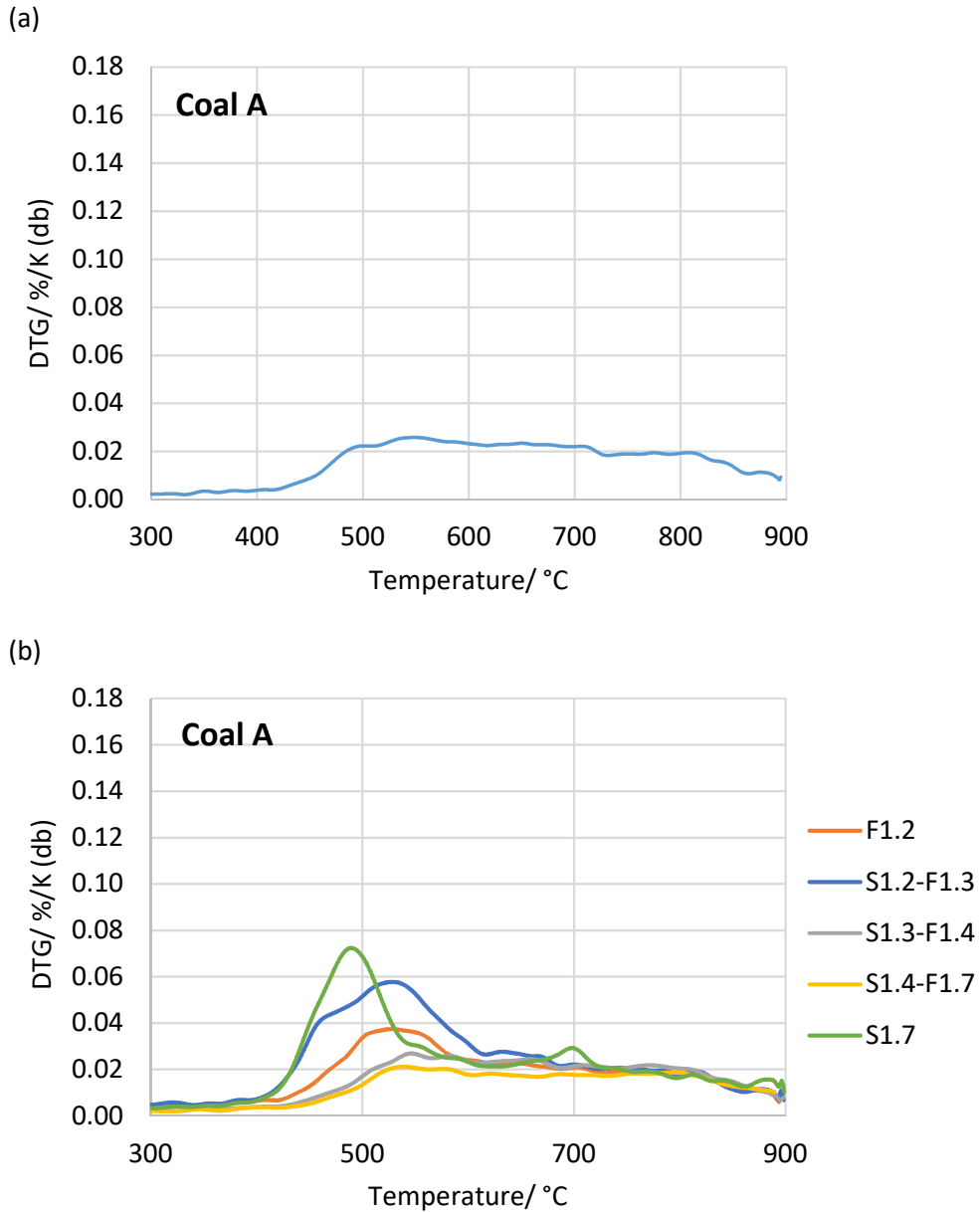
Figure 7.11: DTG analysis of non-density-separated coal A (a) and density fractions of coal A (b).

The DTG profile of coal B up to 900 °C is double peaked, with the major peak occurring at ~530 °C and a minor peak occurring at ~800 °C (Figure 7.12a). Density separation shows that whilst all density fractions contribute to the ~530 °C peak, it is the denser fractions, S1.4-F1.7 and S1.7, which produce the peak at ~800 °C, with the S1.7 fraction having the highest DTG peak at this temperature. (Figure 7.12b).

At ~530 °C the magnitude of peak rate of mass loss follows the order of decreasing density, with the exception that the F1.2 sample does not have the highest rate of mass loss but follows a pattern very similar to the S1.3-F1.4 fraction.

(a)
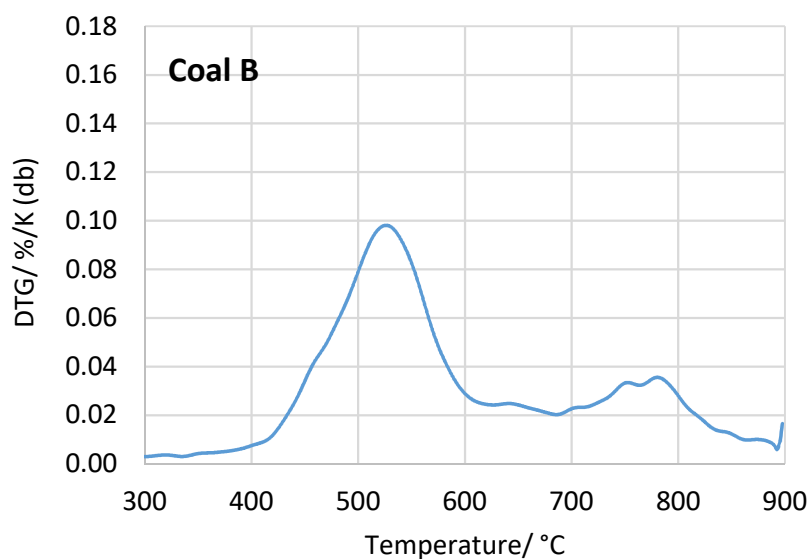
(b)
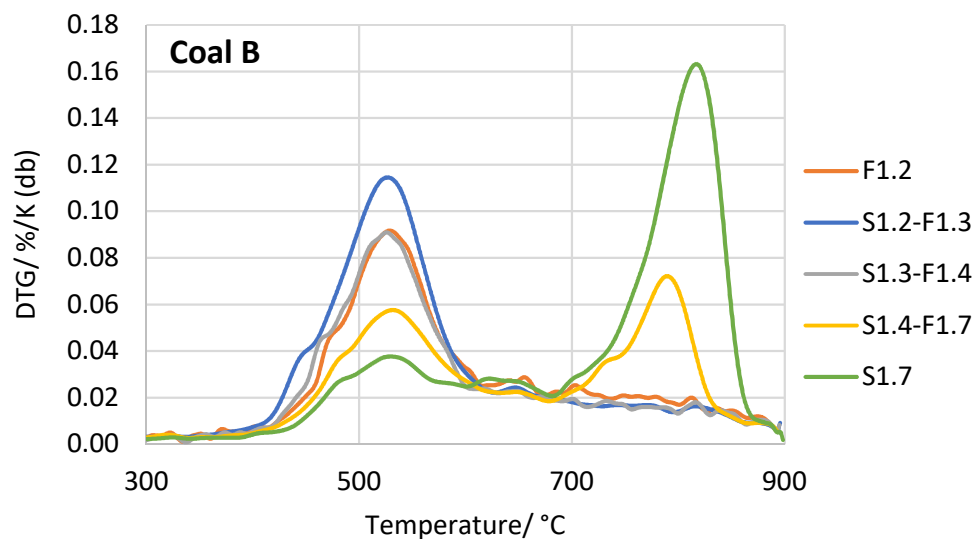
Figure 7.12: DTG analysis of non-density-separated coal B (a) and density fractions of coal B (b).

7.3.6   Gieseler fluidity of density fractions

Gieseler fluidity analysis of the density fractions was carried out, and the results are shown in Figure 7.13. For coal B the fractions S1.4-F1.7 and S1.7 did not produce any Gieseler fluidity. The remaining fractions exhibited maximum fluidity values in the descending order: S1.2-F1.3 > F1.2 > S1.3-F1.4. The temperature of maximum fluidity was relatively consistent, i.e. 469-475 °C. These results are consistent with the Gieseler fluidity results for coal B as a whole, which had a maximum fluidity of 7 ddpm at 477 °C (Table 4.1).

For coal A the highest swelling density fractions (F1.2 and S1.2-F1.3) did not yield sufficient material for separate Gieseler tests. Therefore, these fractions were combined and additional F1.3 material was obtained from the 90-125 µm and 75-90 µm sieve fractions to produce sufficient material for a Gieseler test. This test resulted in no fluidity as did tests on the denser fractions of coal A.
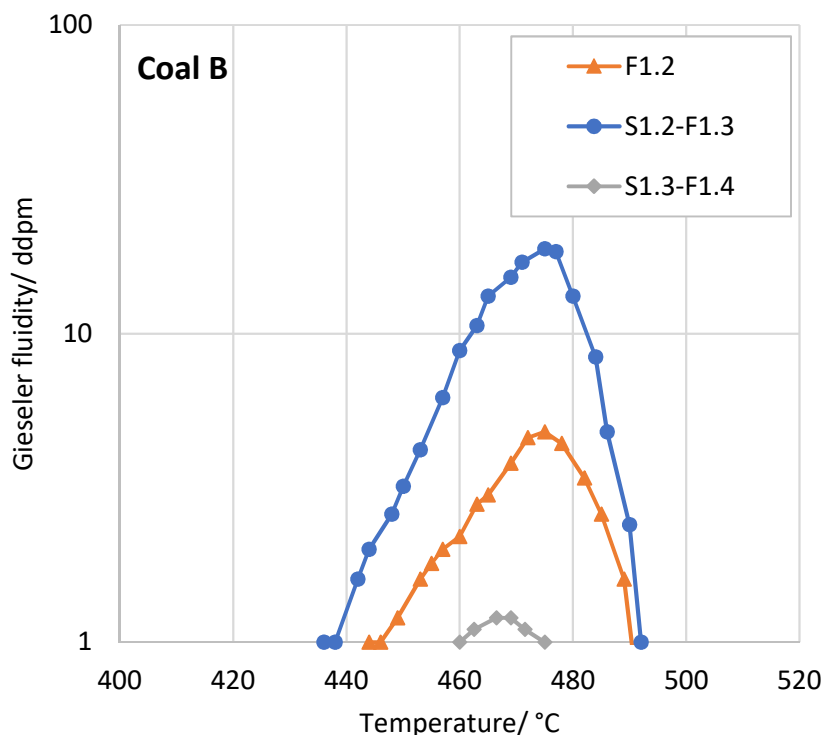
Figure 7.13: Gieseler fluidity data for density fractions of coal B. Density fractions not represented in this figure showed no Gieseler fluidity.

7.4 Discussion

7.4.1 HT-CSLM swelling in relation to density

Coals A and B have been separated into density fractions to examine the origin of the heterogeneous swelling behaviour observed in chapter 5. It is clear that different density fractions exhibit different average swelling behaviours; in general, the less dense the material the greater the maximum swelling ratio, the only exception being the F1.2 fraction of coal A (which has a maximum swelling ratio lower than the S1.2-F1.3 fraction of coal A) (Figure 7.6). Above a density of 1.4 differences in maximum swelling ratio become small for both coals. The trend of greater maximum swelling ratio with lower particle density is also observed for the two parent coal samples, i.e. coal B is less dense than coal A (Figure 7.1), whilst coal B also has the greater maximum swelling ratio (chapter 5, Figure 5.8). As discussed below it is the coal B particles less dense than 1.3 that contribute most to the greater swelling of coal B, and by contrast coal A contains very little material of density lower than 1.3 (Figure 7.1). However, it is also apparent that each density fraction of coal B reaches a greater maximum swelling ratio than the equivalent fraction of coal A.

Particle density is determined by mineral (inorganic) and maceral (organic) content (Tsai & Scaroni, 1987 and Yu *et al*., 2003), and dense mineral matter and inertinite macerals do not contribute to swelling therefore the higher levels of these in the higher density particles inhibits swelling. The vitrinite maceral is less dense and is responsible for producing swelling behaviour. In coal B the swelling can be related to the ratio of vitrinite to inertinite macerals. The fractions with density below 1.3 contain approximately 80 % vitrinite to 20 % inertinite, as density increases this gap narrows to the extent that the S1.7 fraction contains 44 % vitrinite and 52 % inertinite (Figure 7.5). For coal A, however, this is not the case; here the distribution of vitrinite and inertinite is relatively even in all density fractions for which data is available (50-54 % vitrinite to 47-50 % inertinite). This means that even the less-dense fractions of coal A have a significant percentage of inertinite, which hinders swelling. This evidence suggests that between density

fractions of coal A the differences in swelling must be due to influences other than the relative proportions of vitrinite and inertinite.

The petrographic histograms of density fractions of coal A (Figure 7.3) provide greater detail of the coal's petrography; although the overall proportions of vitrinite and inertinite are similar across the density fractions there is a difference in the reflectance distributions. The S1.2-F1.3 fraction of coal A has the highest maximum swelling ratio and is the only density fraction to show a clear vitrinite peak centred around reflectance groups 14 and 15. This is a feature that is similar to the reflectance distribution histograms of the highly-swelling coal B fractions (F1.2 and S1.2-F1.3), which have a vitrinite peak at reflectance groups 13 and 14, (Figure 7.4). Although a difference between the coals is that the vitrinite peak of the coal A S1.2-F1.3 fraction is lower (~9 vol. %) than those of the coal B F1.2 and S1.2-F1.3 fractions (>20 vol. % each) i.e. the material contributing to this peak is even more concentrated in coal B. It appears that a greater concentration of vitrinite material centred around reflectance groups 13-16 is associated with higher levels of swelling within coals A and B. This can be interpreted as a greater homogeneity of the organic material in these samples, which may facilitate the development of thermoplasticity since the homogenous organic material will become plastic within the same temperature range.

The temperature at which swelling occurs is largely unaffected by particle density within coals A and B, however an exception to this is the F1.2 density fraction of coal B, which reaches its maximum swelling ratio at a temperature 20 °C higher than the other density fractions (Figure 7.6). The reason for this is not clear as the maximum fluidity temperature of this sample and the temperatures at which devolatilisation occurs are consistent with other density fractions.

The phenomenon of greater swelling for lower density fractions within a coal can help explain the results of Sexton et al., (2018), who found that after heating in a drop tube furnace, agglomerated char particles had a higher reactivity than non-agglomerated char particles of the same coal, even when ground to a powder to minimise differences in structure. Sexton et al., suggested that the agglomerates were composed of a more intrinsically reactive organic material. The higher

swelling tendency of low-density particles would mean that these particles will be more prone to agglomeration than high-density particles due to higher fluidity and greater particle size when swollen, meaning that the likelihood of interparticle contact and the ability to fuse together upon contact are both increased. This can explain why agglomerates may be composed of more highly reactive material than non-agglomerated chars.

Although there are differences in the mean swelling ratios of the different density fractions this does not fully explain the heterogeneity of swelling behaviours observed within the parent coal samples (Figure 7.10). This is demonstrated by the greater degree of heterogeneity observed within the most highly swelling density fractions (Figure 7.9 and Table 7.5). This indicates that influences other than the density of particles contribute to the variations observed. One likely factor is the precise make-up of the particles in terms of maceral content. For example, the coal B S1.2-F1.3 fraction as a whole contains 1.2 % ash (db), 81.5 % vitrinite (daf), 17.4 % inertinite (daf) and 1.1 % liptinite (daf), however each particle will not contain each of those constituents in those proportions. Another factor may be the distribution of those constituents within the particle; the metaplast must be able to contain the evolving volatile gases for swelling to result, therefore if portions of metaplast are unable to connect to each other due to the positioning of mineral or inertinite material then this may facilitate the release of volatile gases without swelling the metaplast.

The observation that the less-dense, high-swelling fractions have a greater RSD (variability) than the denser, lesser-swelling fractions is contradictory to the work of Strezov *et al.*, (2005), who reported that the low-density fractions of a single coal in their work showed 'high uniformity in observed swelling behaviour' whilst some particles from the denser fraction showed 'diverse behaviour'. Strezov *et al.*, presented the data of six individual particles from one of the low-density fractions, however it was not clear what the total number of particles analysed was.

A feature of the coal particles, which would contribute to density, but which has not been discussed is the degree of enclosed porosity. The porosity of raw coal

particles is likely to be very low, however the presence of enclosed pores would reduce the density of a particle. The existence of enclosed porosity may explain why the F1.2 particles of coal B are the least dense despite having a higher ash content than the S1.2-F1.3 particles and a similar petrography. It is not known how the presence of porosity in a coal particle would influence the swelling of that particle.

7.4.2   DTG analysis

DTG data has been generated for the density fractions of coals A and B, showing changes in the rate of mass loss during devolatilization (Figures 7.10 and 7.11). Differences in the pattern of mass loss can be related to swelling; generally, the lighter fractions lose mass at a faster rate than the denser fractions in the early stages of devolatilisation (temperature range ~400-600 °C, within which the temperature of maximum swelling occurs). For coal A the order of the density fractions in terms of rate of mass loss within this temperature range is the same as the order in terms of maximum swelling ratio (except for the S1.7 fraction), i.e. S1.2-F1.3 > F1.2 > S1.3-F1.4 > S1.4-F1.7. The S1.7 fraction has the highest rate of mass loss but the lowest maximum swelling ratio, the mass loss may be due to a thermal reaction of the mineral matter given that this sample has a high ash content of ~58 % (db), although the possible nature of this reaction has not been identified.

A similar trend is observed for the density fractions of coal B; The order of the DTG peak heights at ~530 °C is similar to the order of maximum swelling ratios for the density fractions, with the exception that the F1.2 fraction has the highest maximum swelling ratio but the second highest rate of mass loss at ~530 °C.

Although the release of gaseous volatile matter is the driving force for swelling, the Proximate volatile matter content is a poor indicator of the likely level of swelling (Section 2.10.2). This is because a significant proportion of the mass loss measured during the determination of Proximate volatile matter can occur at temperatures above those at which swelling occurs, this higher temperature mass loss cannot contribute to driving the swelling process. Two aspects of this work illustrate this: Firstly, the total volatile matter (db) of all density fractions of coal B

is relatively similar (17-22 % (db) with the S1.7 fraction giving the highest value) (Table 7.3). However, the denser fractions (density >1.4) undergo a significant proportion of their mass loss at higher temperatures (~800 °C) when the swelling process is finished (Figure 7.12).

The second aspect relating to Proximate volatile matter content is the difference between the pattern of mass loss of coals A and B. The overall figure for total volatile matter is similar for coals A and B (14.4 % for A and 18.4 % for B (db)), however coal B releases volatile matter at a greater rate than coal A over the temperature range 400-600 °C, in which swelling occurs. Evolution of volatile matter is the driving force for swelling therefore this may be a factor in the different swelling properties of the two coals. Coal A loses mass at a lower rate than coal B initially but continues to lose mass at a steady rate when the rate of mass loss of coal B has become low. This is illustrated by Figure 7.14, which shows TGA data of >125 μm samples with no density separation. Note that the standard determination of total volatile matter is made after seven minutes residence time at 900 °C.
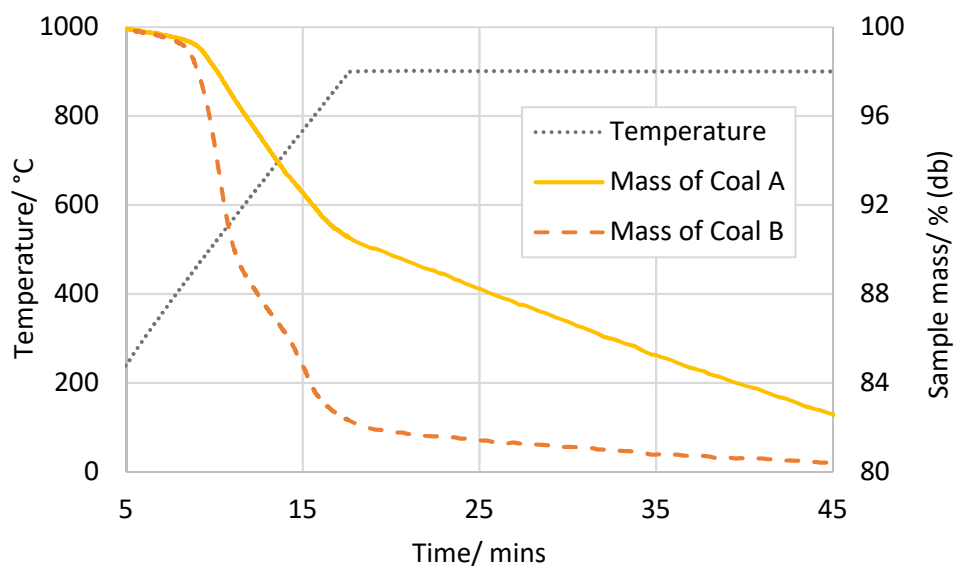
Figure 7.14: Thermo-gravimetric analysis of coals A and B under argon.

A peak in the rate of mass loss from coal B at ~800 °C was observed as mentioned above. A similar phenomenon has been reported previously (Tian *et al.*, 2016) and was attributed to the decomposition of the calcite mineral to release carbon

dioxide (Giroux et.al., 2006). This is the likely explanation for this feature in coal B and is supported by the differential scanning calorimetry (DSC) data (Figure 7.15) of the coal B density fractions, which indicates an endothermic process occurring in the S1.7 sample and, to a lesser extent, the S1.4-F1.7 sample; this endothermic event does not appear in the lighter samples. Further evidence is seen in the mass spectrometry of gaseous pyrolysis products of coal B (chapter 5, Figure 5.18), which indicate a peak in carbon dioxide levels close to 700 °C. This peak is not present in the results of coal A. A final piece of evidence is the high levels of calcium oxide, 15.5 %, in the XRF ash chemistry analysis of coal B (Appendix B), consistent with high levels of calcite.
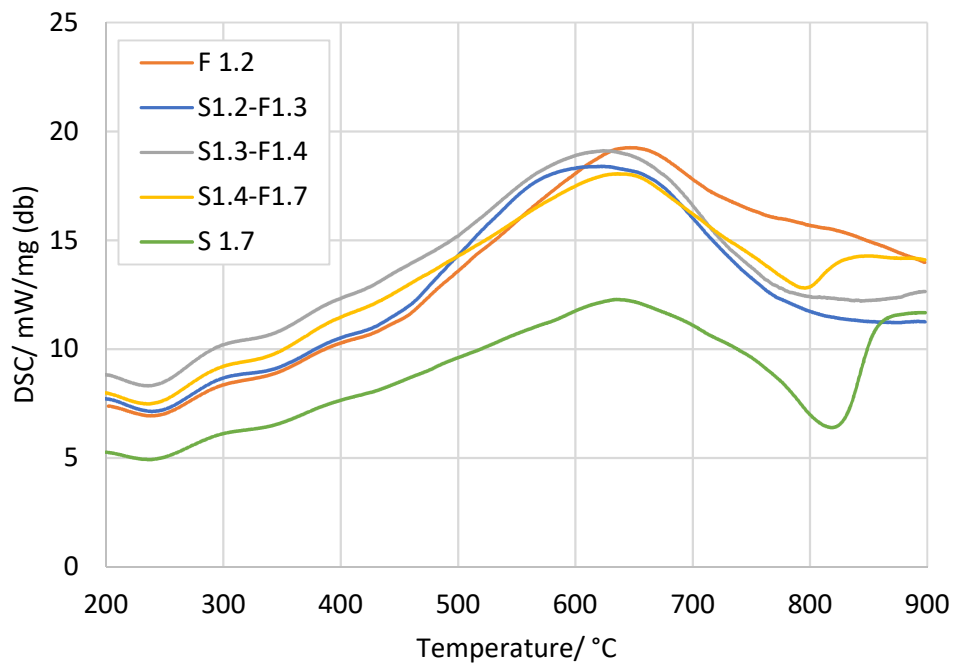
Figure 7.15: DSC measurements of coal B density fractions.

The decomposition of calcite is a different process to the breakdown and release of organic volatile matter; however, it still contributes to the Proximate volatile yield. The densest particles show this mass loss to the greatest extent as they contain the most mineral matter. In the blast furnace this process would be beneficial as it produces carbon dioxide, which can be converted to carbon monoxide, for the reduction of iron ore (section 2.4).

To summarise the relationship between DTG and swelling, it appears that there is some correlation between the rate of mass loss at the temperature at which

maximum swelling occurs and the maximum swelling ratio, although exceptions to this are observed in this work, but this does not equate to a relationship between maximum swelling ratio and Proximate volatile matter due to the influence of post-swelling mass loss on Proximate volatile matter content.

7.4.3   Gieseler fluidity

In previous work (Gao *et al.*, 1997) and chapter 5 of this thesis a correlation between maximum Gieseler fluidity and maximum swelling ratio has been suggested. Within the density fractions of coal B a strict correlation of this type is not observed (Figure 7.13). Although there is a tendency for the denser, lesser-swelling fractions to be less fluid (or exhibit no fluidity), the order of maximum fluidity does not follow the same order as that of maximum swelling ratio. The maximum swelling ratio does follow the same order as that of maximum rate of mass loss at ~530 °C (i.e. S1.2-F1.3 > F1.2 > S1.3-F1.4). The F1.2 fraction has the highest maximum swelling ratio but the second highest fluidity.

All density fractions of coal A show some degree of swelling in the HT-CSLM, however a composite sample of coal A fractions less dense than 1.3 showed no Gieseler fluidity. This is consistent with the results of coal B because the highest swelling fractions of coal A have a comparable maximum swelling ratio to the lowest swelling fractions of coal B, which also showed very low or no fluidity.

7.5 Conclusions

The novel contributions made in this chapter are the observation of correlation, within the density fractions of a particular coal, between maximum swelling ratio and the rate of mass loss at the temperature of maximum swelling, and the finding that separation of particles according to density does not fully explain the variation in swelling behaviours observed within a parent coal sample.

Separation of pulverised coal particles by centrifugation has been used, in conjunction with HT-CSLM, to investigate the effects of particle density on the transient swelling properties of particles of two coals, A and B, which have similar Proximate and Ultimate analyses.

Hypothesis 3 – Lighter coal particles attain a greater maximum swelling ratio than denser particles of the same coal – is accepted. The less dense coal swells more than the denser coal, and lighter density fractions of each coal swell more than denser fractions of that same coal. In the case of coal B this can be related to the decreasing ratio of vitrinite to inertinite as density increases. The presence of a strong vitrinite reflectance peak centred around the reflectance groups 13-16 is common to the most highly swelling density fractions of both coals. Above a density of 1.4 the differences in swelling behaviour become minimal. This result can be used to explain why agglomerated char particles are more reactive than non-agglomerated char particles of the same coal as has been reported by Sexton *et al.*, 2018.

A greater degree of variability (as measured by RSD) in maximum swelling ratio is observed for the lower-density, higher-swelling fractions of coals A and B.

The different rates of mass loss exhibited by different density fractions in the temperature range 400-600 °C shows some correlation with the relative degrees of swelling between density fractions. This is explained by the fact that volatile matter evolution is the driving force for swelling.

A clear correlation between the Gieseler fluidity of coal B density fractions and maximum HT-CSLM swelling ratio is not observed, however the three most highly swelling density fractions are those which exhibit Gieseler fluidity whereas the most dense, low swelling fractions exhibit no fluidity.

Hypothesis 4 – Coal swelling behaviour can be related to Gieseler fluidity and TGA mass loss, is accepted in the sense that relationships have been found between maximum swelling ratio and maximum Gieseler fluidity; maximum swelling temperature and maximum fluidity temperature; and maximum swelling ratio and rate of mass loss at the temperature of maximum swelling ratio (evidence from chapters 5 and 7). However, deviations from the trend have also been observed and it has not been possible to predict the level of swelling from Gieseler fluidity and DTG data.

8 Effect of particle size

8.1 Introduction

The effects of coal particle size on industrial operations is of interest to users of coal because particle size is controlled by crushing to produce optimum performance. However, the process of crushing material to smaller particle sizes requires resources. For example, time, energy, equipment and maintenance. Therefore, it is important to fully understand the effects of particle size, however this has not been comprehensively researched in relation to the thermal swelling of coal particles. The information from literature, reviewed in section 2.10.1, is inconclusive. When dealing with particle size it is often difficult to determine whether observed effects are due to physical particle size or because of different compositions. For example, size fractions obtained by sieving usually vary in terms of the coal characteristics; mineral matter is likely to concentrate in either the smaller or larger particles depending on the relative hardness of the mineral and coal material, and maceral composition is also likely to vary between sieve fractions. Yu *et al.*, (2005), reported vitrinite-rich material concentrating in the smaller size fractions in their work, leading to greater final swelling ratios. Tian *et al.*, (2016), discussed the phenomenon of segregation upon comminution, whilst Cloke *et al.*, (2002), studied this in some detail. The data in Appendix B also shows variation in the components of coals studied in this work according to particle size. As maceral and mineral composition is a significant factor in the swelling of coal particles (chapter 7) it is necessary to control these variables when investigating particle size. In this chapter the HT-CSLM is used to investigate the effect of particle size on swelling. Three size and density separated fractions of coals A and B are used to mitigate the effects of varying maceral and mineral content between sieve fractions.

Hypothesis to be investigated is Hypothesis 5 – The maximum swelling ratio of coal particles increases with increasing particle size within the size range 38-500 μm.

8.2 Experimental

Coals A and B are used in this chapter. Coal B has been shown to exhibit significant swelling properties during HT-CSLM tests while coal A, which has no Gieseler fluidity, Ruhr dilation and an FSI of zero, has shown limited swelling properties in the HT-CSLM. Three sieve fractions, 38-53 μm, 63-75 μm and >125 μm, were obtained by wet sieving, the particle size distribution within the sieve fractions was measured using a Malvern Mastersizer (Figure 8.1), Dv(0.5) values are shown in (Table 8.1), these are the diameter below which 50 vol. % of the sample exists. Figure 8.1 shows that 100 % of the particles in the >125 μm sample are below 500 μm. Of these sieve fractions narrow density fractions of S1.2-F1.3 were obtained by centrifugation to mitigate any effects of varying particle density between sieve fractions. This density fraction was chosen as it has been found to give high levels of swelling (chapter 7) and because the proportions (approximately 50 wt. % of coal B and 9 wt. % of coal A) of the coal sample falling within this range are greater than those of the F1.2 density fraction, which also showed high levels of swelling.

(a)

(b)
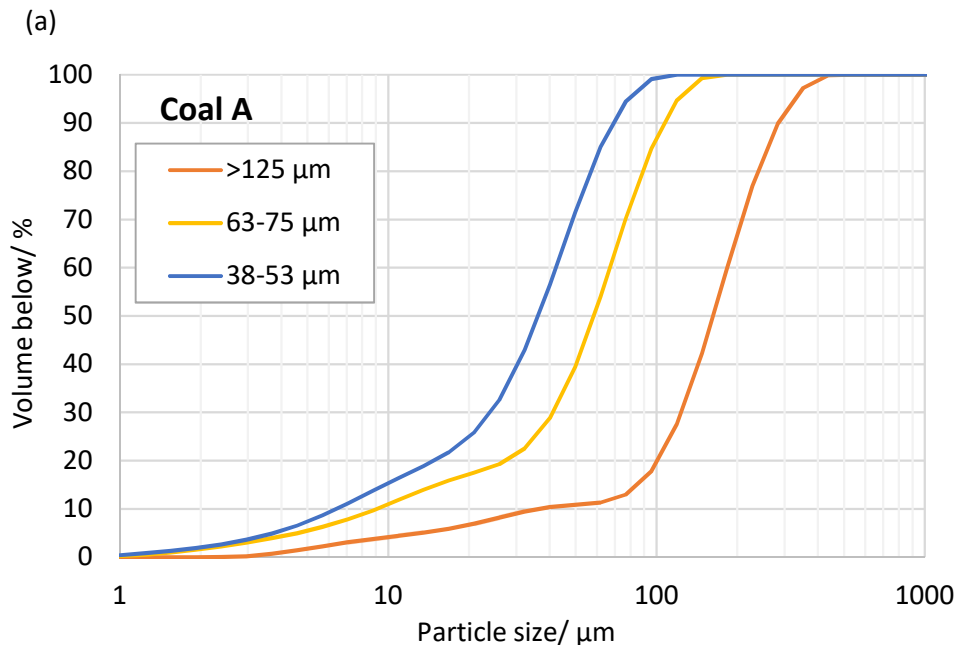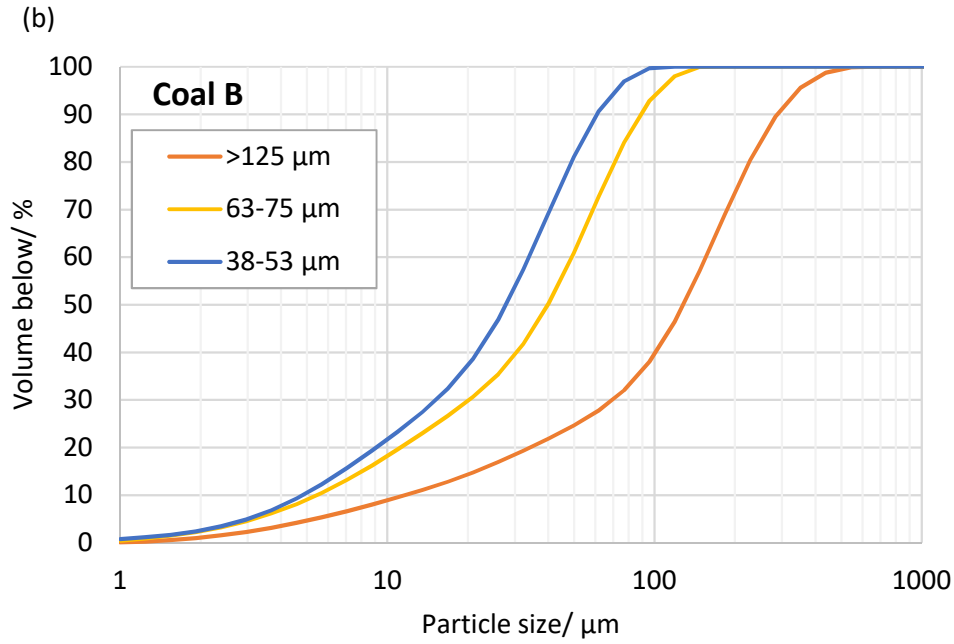
Figure 8.1: Particle size distribution of three sieved fractions of coals A and B (a and b) prior to centrifugation.

Sieve fraction/ µm	Dv(0.5) coal A/ µm	Dv(0.5) coal B/ µm
>125	162.7	128.1
63-75	58.6	39.9
38-53	36.3	27.8

Table 8.1: Values of Dv(0.5) for the three sieved fractions of coals A and B prior to centrifugation.

The method of coal preparation described aims to create samples of each coal that differ in particle size but are as similar as possible in all other respects. The Proximate, Ultimate and petrographic analyses of most of the experimental samples are shown in Table 8.2 and Figure 8.2, although there was insufficient quantity of the coal A material to complete all analyses. These results show that three samples have been created, which have similar properties but differ in terms of particle size. The swelling properties of these samples were measured using HT-CSLM with a heating rate of 700 K/min. The number of particles measured from each sample is given in Table 8.3.

	Coal A particle size/ μm			Coal B particle size/ μm		
	38-53	**63-75**	**>125**	**38-53**	**63-75**	**>125**
Proximate analysis						
Volatile matter/ % (db)	17.2	14.8	14.7	18.8	18.7	18.5
Ash/ % (db)	1.5	3.7	3.5	1.2	1.3	1.9
Fixed carbon/ % (db) (diff)	81.3	81.5	81.8	80.0	80.0	79.6
Ultimate analysis						
Carbon/ % (daf)	87.8	85.4	84.2	90.3	89.5	89.9
Hydrogen/ % (daf)	4.5	4.2	4.0	4.7	4.7	4.7
Nitrogen/ % (daf)	2.1	2.0	2.0	1.2	1.2	1.2
Sulphur/ % (daf)	Insufficient sample available for test			0.9	0.8	0.8
Oxygen/ % (daf) (diff)				2.9	3.9	3.4
Petrographic analysis						
Liptinite/ %	Insufficient sample available for test			0.6	0.8	1.1
Vitrinite/ %				87.8	85.3	81.5
Inertinite/ %				11.6	13.9	17.4
Vitrinite reflectance, Ro (max.)				1.5	1.5	1.5

Table 8.2: Proximate, Ultimate and petrographic data for the test samples, which represent three wet-sieved size fractions and only include particles within the density range S1.2-F1.3.

	38-53 μm	63-75 μm	>125 μm
Coal A	34	37	31
Coal B	39	21	20

Table 8.3: Number of particles of each sample analysed by HT-CSLM.

(a)

180

(b)

(c)
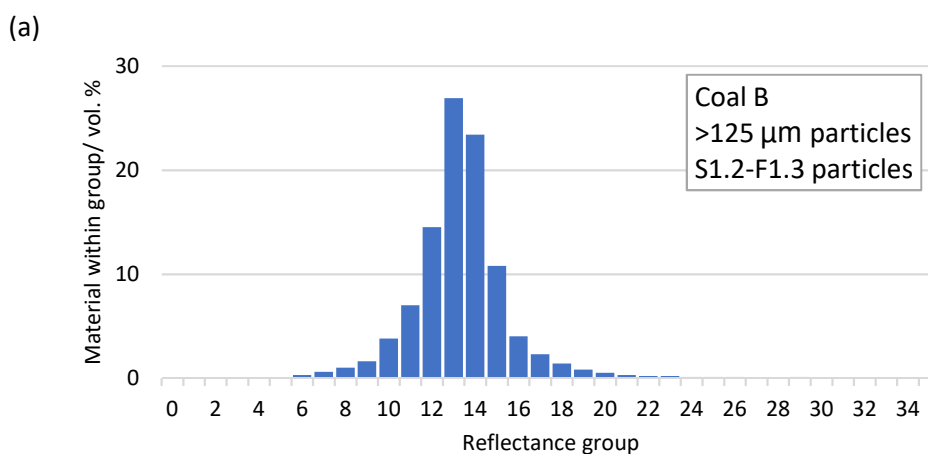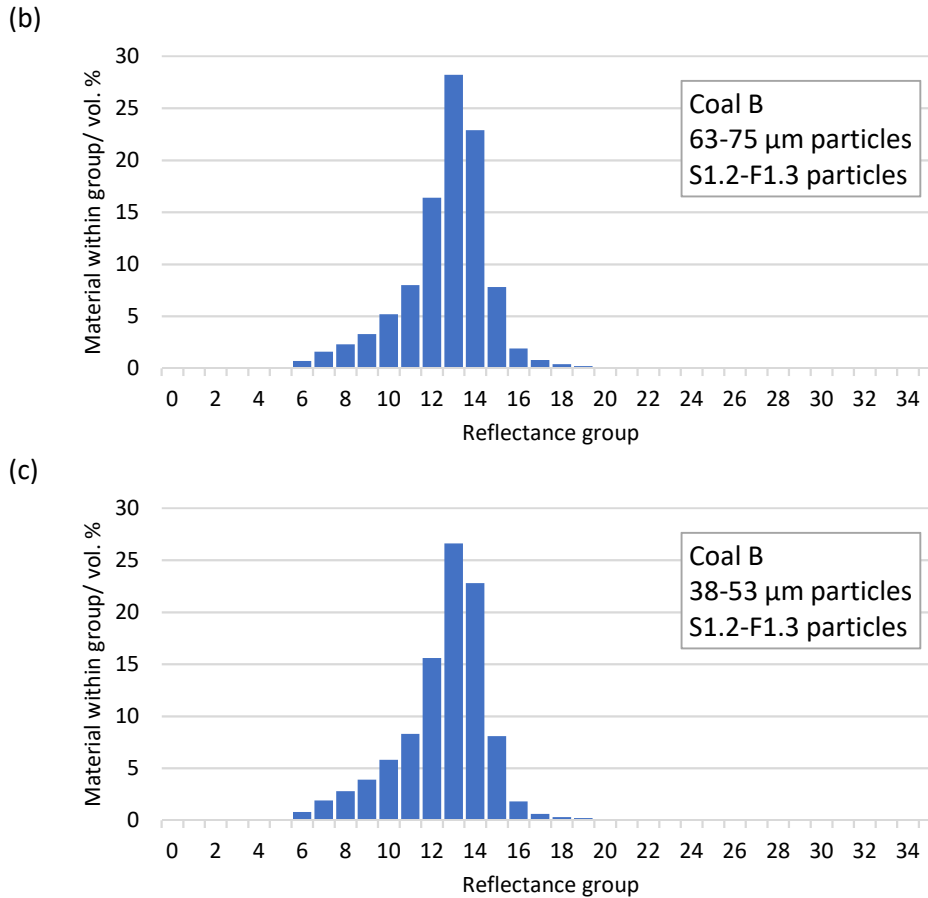
Figure 8.2: Coal reflectance histograms for the coal B test samples. In all cases X axis = reflectance group and Y axis = vol. % (daf) of sample within group. Note: there was insufficient material available to perform petrographic analysis on the coal A samples.

8.3 Results and analysis

8.3.1   HT-CSLM swelling

The swelling properties of the test samples were measured using HT-CSLM, and the results are shown in Figure 8.3. In the case of the coal B 38-53 µm and 63-75 µm samples, the results of 2 and 3 particles were omitted from the mean because they showed unusually high swelling ratios of around 5-6. It was considered that these particles are likely to have become so fluid that the material began to flow across the surface of the crucible, which has previously been observed for particles of the highly fluid coal D (chapter 5). It may be more likely to observe this phenomenon in smaller particles because the smaller the particles the greater the

probability that particles are of a single maceral type. The mean results of these omitted particles are shown in Figure 8.4. No particles of coal A exhibited this type of behaviour.

(a)
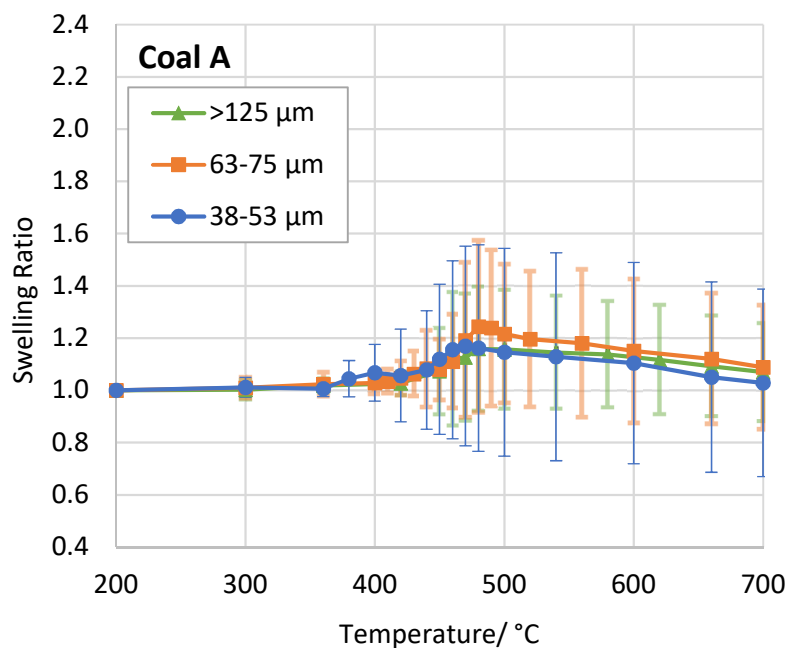
(b)
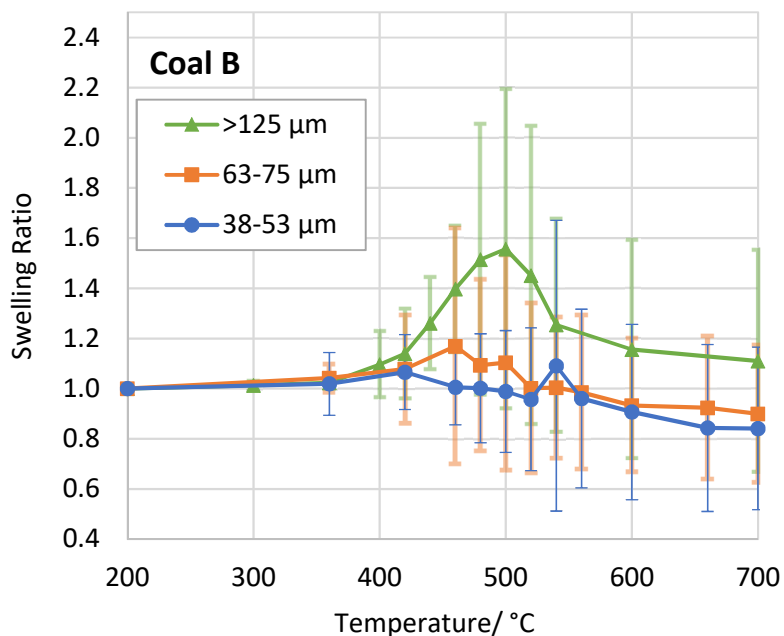
Figure 8.3: Mean swelling ratio of size fractions of coals A and B (a and b) within the density range S1.2-F1.3.

Figure 8.3a shows that the swelling behaviours of the coal A size fractions are quite similar, although the 63-75 μm sample has a slightly higher maximum swelling ratio than the other two. The temperature at which swelling begins is relatively consistent between the size fractions (360-410 °C), as is the temperature of maximum swelling ratio (480-490 °C). Overall the levels of swelling are low for coal A as has been observed in previous chapters.

(a)

(b)
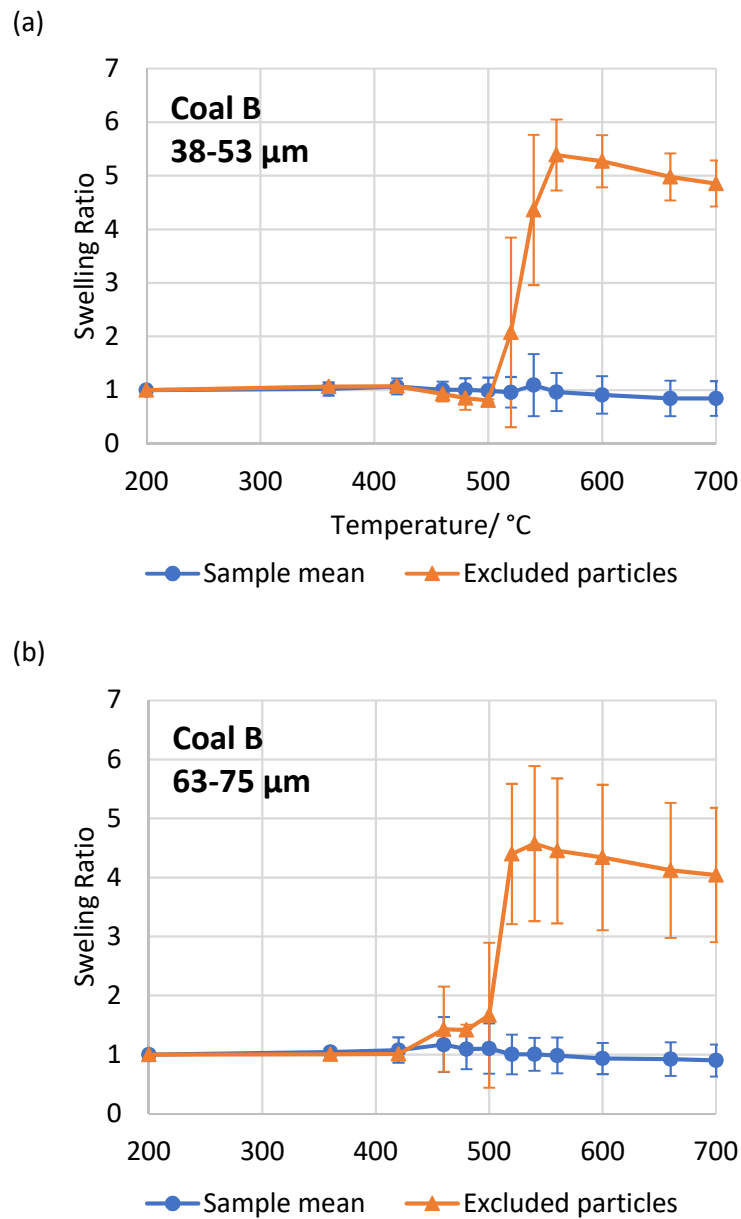
Figure 8.4: Mean swelling ratios of the particles excluded from the mean sample results in comparison with the mean sample results themselves for samples 38-53 μm and 63-75 μm.

Figure 8.3b shows a different pattern of results for the particle size fractions of coal B. The magnitude of the maximum swelling ratio follows the order of particle size i.e. the larger the particle size the greater the maximum swelling ratio. The temperature of maximum swelling ratio is not consistent between the samples, varying between 460 °C and 540 °C. The three fractions all begin swelling at around 360 °C, however the swelling ratio of the 38-53 µm particles decreases after 420 °C and the swelling ratio of the 63-75 µm particles decreases after 460 °C. Meanwhile the swelling ratio of the >125 µm particles continues to increase at a faster rate and reaches a peak of 1.56 at 500 °C. The 38-53 µm fraction exhibits an unusual peak in swelling ratio at 540 °C, which appears as a spike amidst a trend of otherwise decreasing swelling ratio. The final swelling ratio of the >125 µm particles (~1.1) is greater than that of the smaller particle size fractions, which both have final swelling ratios close to 0.9, i.e. mean particle size was smaller than at the beginning of the test for those samples.

The >125 µm particles of coal B have a significantly greater maximum swelling ratio (1.56) than those of coal A (1.16), however the 38-53 µm and 63-75 µm particles of coal A have a greater maximum swelling ratio than the equivalent coal B samples. The coal B samples in this study also shrink at a faster rate after maximum swelling ratio than those of coal A, so much so that at 700 °C the 38-53 µm and 63-75 µm samples of coal B had a swelling ratio <1 whereas those of coal A had a swelling ratio >1.

The coal A particles within the 38-53 µm and 63-75 µm samples can be divided into two sub-groups; high-swelling particles and low-swelling particles. The mean swelling ratio of the two sub-groups within each sample is shown in Figure 8.5. The percentage of particles within each sub-group is shown in Table 8.4. In the case of the >125 µm sample it was not possible to clearly distinguish sub-groups of high-swelling and low-swelling particles. Within this sample only 1 particle (out of 31 analysed) showed particularly high swelling behaviour – reaching a maximum swelling ratio of ~2.1 at 460 °C.

The 63-75 µm sample of coal A has a higher mean maximum swelling ratio than the 38-53 µm sample (Figure 8.3a), Figure 8.5 shows that this is due to the group

of low-swelling particles having a higher mean swelling ratio than the low-swelling particles of the 38-53 µm sample. This raises the overall mean swelling ratio of the 63-75 µm size fraction in spite of the high-swelling particles of this fraction actually having a lower mean swelling ratio than the high-swelling particles of the 38-53 µm sample.

(a)
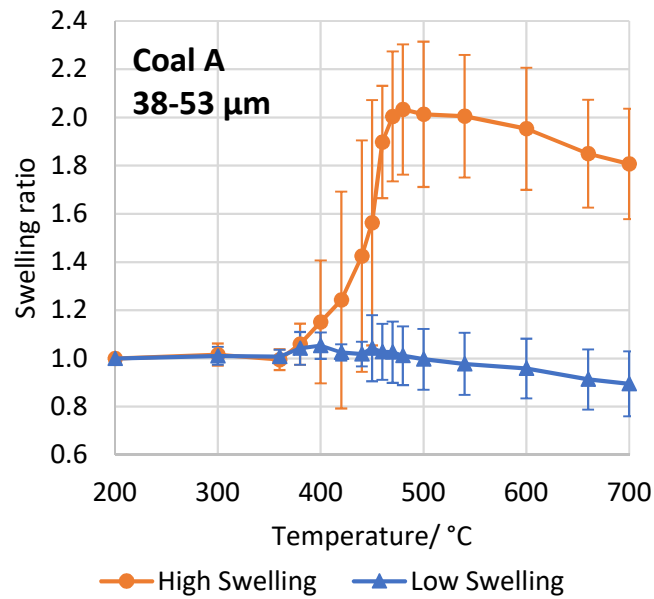
(b)

Figure 8.5: Mean swelling ratios of the two groups of particles (high-swelling particles and low-swelling particles) within the 38-53 µm (a) and 63-75 µm (b)

samples of coal A. Error bars represent 1 standard deviation either side of the mean.

Size fraction of coal A	High-swelling particles within sample/ %	Low-swelling particles within sample/ %
63-75 μm	14	86
38-53 μm	15	85

Table 8.4: Percentage of high-swelling and low-swelling particles within the 38-53 μm and 63-75 μm samples of coal A.

Table 8.4 shows that the ratio of high-swelling to low-swelling particles is consistent between the two size fractions. The low-swelling particles represent the vast majority of the sample (85-86 %). This explains why the behaviour of these particles is so influential in determining the overall mean swelling ratio of the sample.
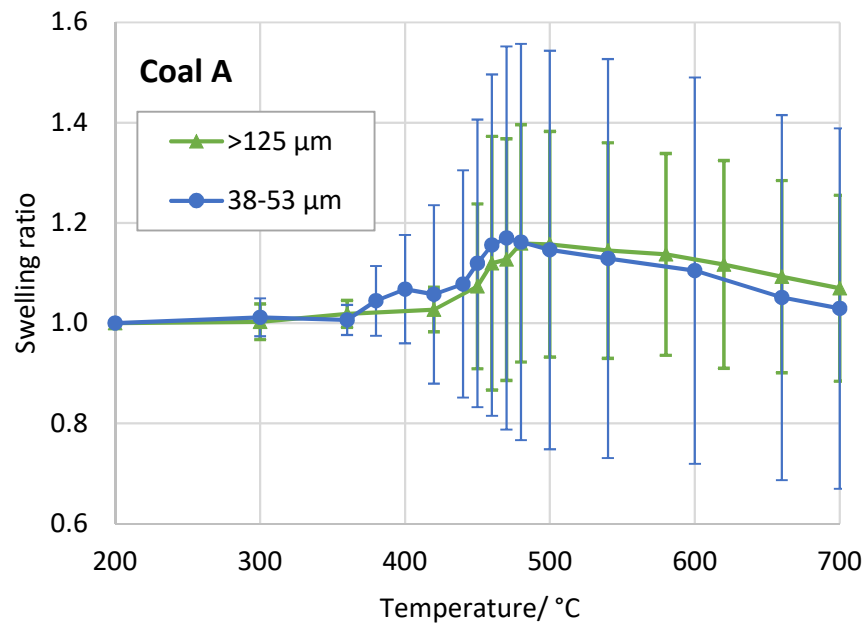
Figure 8.6: Mean swelling ratio of 38-53 μm and >125 μm size fractions of coals A. Error bars represent 1 standard deviation either side of the mean.

It is evident from Figure 8.5 that there is a greater degree of heterogeneity within the 38-53 μm particles than within the 63-75 μm particles. This trend extends to the >125 μm particles, for which two separate groups cannot be distinguished. This is illustrated by Figure 8.6, which shows mean swelling ratio values and

standard deviation error bars for the 38-53 μm and >125 μm samples. These samples have a very similar mean swelling ratio, however there is a greater degree of heterogeneity within the smaller particles. The trend of decreasing heterogeneity with increasing particle size is also shown in Table 8.5, which gives RSD values at maximum swelling ratio of the size fractions.

Size fraction of coal A	Max. swelling ratio	RSD at max. swelling ratio/ %
>125 μm	1.16	21.0
63-75 μm	1.24	24.0
38-53 μm	1.17	32.1

Table 8.5: Maximum swelling ratio and RSD at maximum swelling ratio of size fractions of coal A.

A similar analysis has been carried out on the results of coal B; in this case particles within the 38-53 μm and 63-75 μm samples can be divided into two sub-groups defined as particles exhibiting significant swelling and those exhibiting predominantly shrinkage. The mean swelling ratio of the two sub-groups within each sample is shown in Figure 8.7. As with coal A, the distinction between sub-groups was not apparent for the >125 μm particles as none of these particles showed a trend of predominantly shrinkage. Forty percent of the >125 μm particles did have a swelling ratio <1 at 700 °C, however even these particles exhibited significant swelling prior to shrinkage. Table 8.6 shows the proportions of particles falling within each sub-group.

The 63-75 μm sample of coal B has a greater maximum swelling ratio than the 38-53 μm sample (Figure 8.3). This is influenced by the shrinking sub-group of the 63-75 μm sample, which has a higher swelling ratio than the shrinking sub-group of the 38-53 μm sample (Figure 8.7). Meanwhile the maximum swelling ratio of the swelling sub-groups are very similar between these two size fractions. Another factor is that the 63-75 μm sample has a slightly greater percentage of swelling particles (62 %) than the 38-53 μm sample (60 %) (Table 8.6). A third factor is the fact that the maximum swelling ratio of the 38-53 μm sample occurs at a higher temperature (540 °C) than that of the 63-75 μm sample (460 °C), at which the shrinking particles have shrunk to a greater extent, thereby lowering the sample

mean. A difference between coal A and coal B is that there is a more even division of particles between the two sub-groups in coal B and the shrinking particles are in the minority (38-42 %) in coal B (Table 8.6). It is also apparent that there is a clearer distinction between the sub-groups within coal A.

(a)
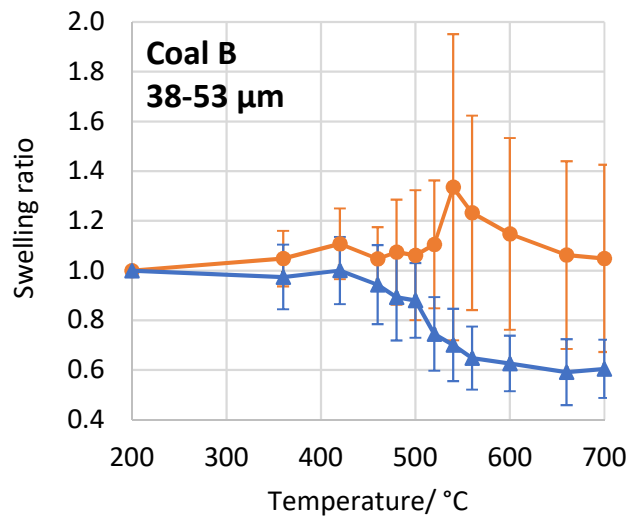
(b)

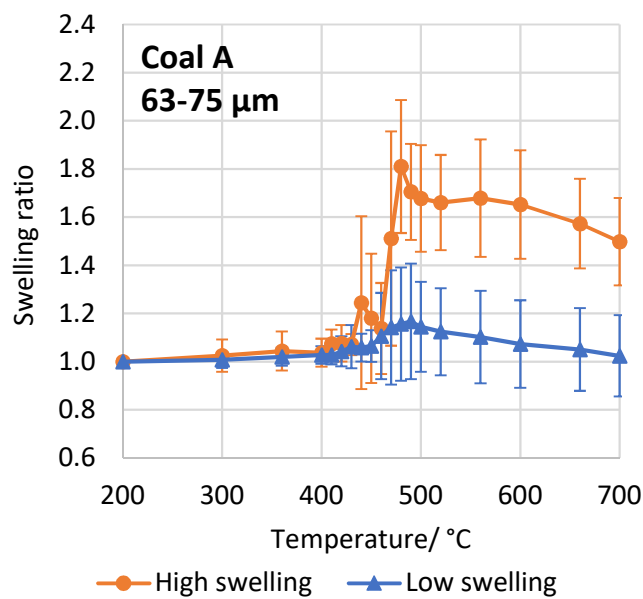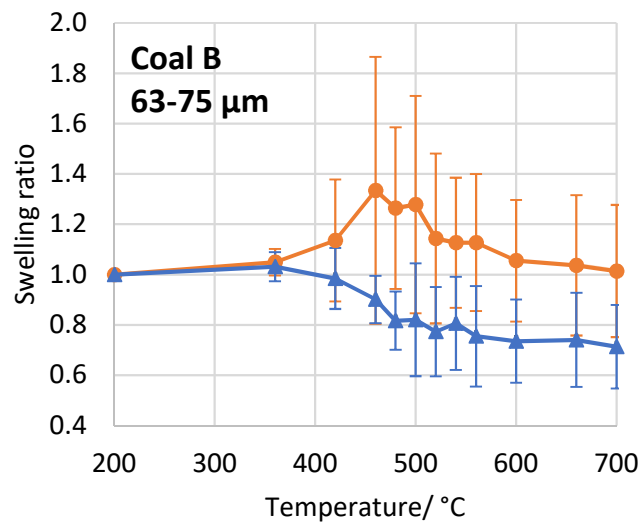Figure 8.7: Mean swelling ratios of the two groups of particles (swelling particles and shrinking particles) within the 38-53 μm (a) and 63-75 μm (b) samples of coal B. Error bars represent 1 standard deviation either side of the mean.

Size fraction of coal B	Swelling particles within sample/ %	Shrinking particles within sample/ %
38-53 µm	60	40
63-75 µm	62	38

Table 8.6: Percentage of swelling and shrinking particles within the 38-53 µm and 63-75 µm samples of coal B.

The RSD within the size fractions of coal B is shown in Table 8.7. The RSD is lower in the 63-75 µm sample than in the 38-53 µm sample, which is a similar trend to that observed for coal A, however, contrary to coal A, the >125 µm sample also has a high RSD, similar to that of the 38-53 µm sample.

Size fraction of coal B	Max. swelling ratio	RSD at Max. swelling ratio/ %
>125 µm	1.56	39.0
63-75 µm	1.17	30.3
38-53 µm	1.09	40.0

Table 8.7: Maximum swelling ratio and RSD at maximum swelling ratio of size fractions of coal A.

The results of the 38-53 µm particles are intriguing due to the two peaks at distinctly different temperatures; 420 °C and 540 °C (Figure 8.3). Both sub-groups contribute to the minor peak at 420 °C but above 420 °C the shrinking sub-group of particles continues to decrease in swelling ratio whereas the swelling sub-group produces the second peak in swelling ratio at 540 °C (Figure 8.4a). The two distinct peaks are not produced by two distinct groups of particles within the sample.

In the case of both the 38-53 µm and 63-75 µm samples of coal B the temperature at which the shrinking sub-group begins to shrink corresponds to the temperature at which the swelling sub-group begins to swell.

The >125 µm fraction of coal B does not readily divide into swelling and shrinking sub-groups. The fact that the most highly swelling particles within this sample reach a greater maximum swelling ratio than the swelling particles of the other

two samples, and the fact that there are very few shrinking particles, contribute to this sample having the greatest maximum swelling ratio of the three samples.

8.3.2   Differential thermo-gravimetry

DTG data of the size fractions of coals A and B is presented in Figure 8.8. For both coals A and B the DTG profiles of the 38-53 µm and 63-75 µm particle size samples are very similar to each other. The >125 µm samples differ slightly; they have a higher rate of mass loss initially (from around 450 °C) and reach their peak rate of mass loss at a slightly lower temperature than the smaller particle sizes (~10 °C lower). For coal A the >125 µm sample had a slightly lower peak rate of mass loss than the smaller particle sizes, whilst that of coal B had a slightly greater peak rate of mass loss than the smaller particle sizes.

For coal B a comparison can be made with previous results (chapter 7), which linked a greater rate of mass loss around the temperature of maximum swelling to a greater swelling ratio, i.e. the >125 µm faction of coal B has a greater swelling ratio than the two smaller size fractions. However, for coal A this is not the case, i.e. the 63-75 µm fraction of coal A has the greatest swelling ratio but not the greatest rate of mass loss around 490 °C. Overall this DTG data shows some differences between size fractions but not a clear correlation with swelling data. Tian *et al.*, (2016), proposed that, when heated in a crucible, smaller particles can coalesce during metaplast formation to reduce the interparticle space and impede volatile gas escape. Whereas larger particles have a greater interparticle space enabling more rapid diffusion of volatile gasses to the atmosphere. This may explain the initial higher rates of mass loss observed for the >125 µm fractions of coals A and B.

(a)
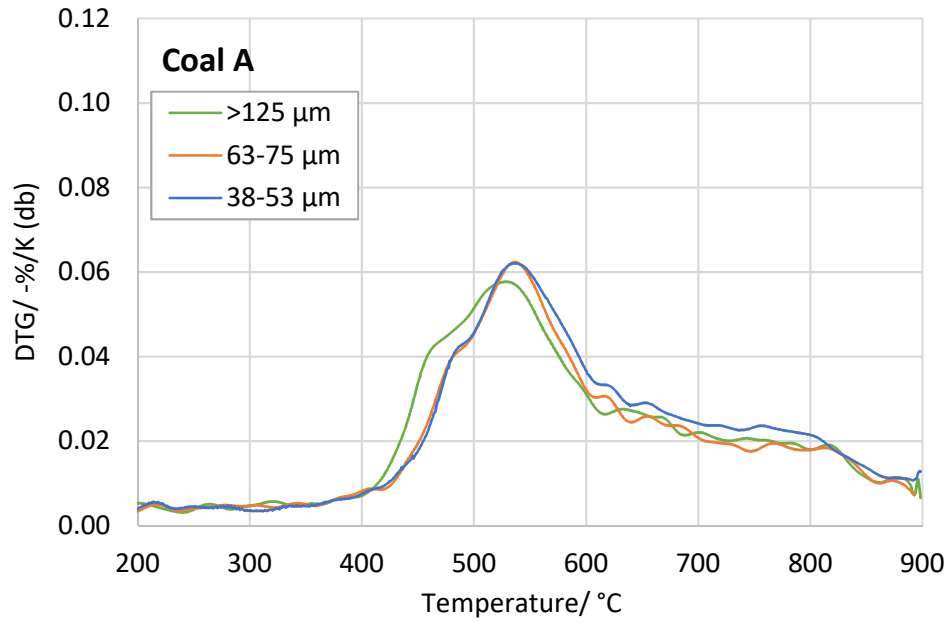
(b)
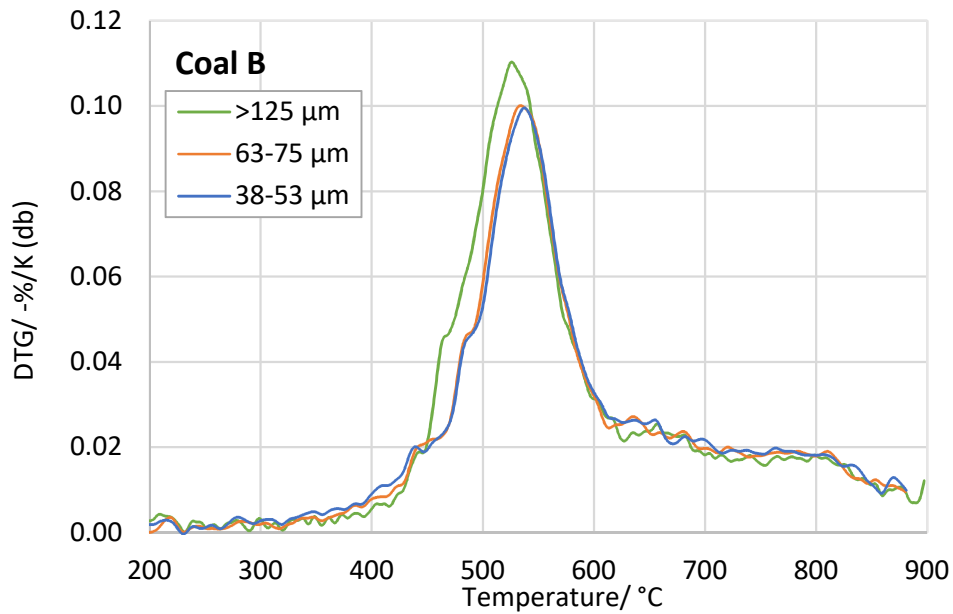
Figure 8.8: DTG analysis of the three size fractions of coals A and B (a and b).

8.3.3   Gieseler fluidity

The Gieseler fluidity results of the three size fractions of coal B are shown in Figure 8.9. The results of all three particle size fractions are very similar to each other; i.e. maximum fluidity 18-19 ddpm and maximum fluidity temperature 475-478 °C. Insufficient material was available to carry out Gieseler tests for the coal A size fractions, however evidence from chapter 7 indicates that no Gieseler fluidity

would be expected of the coal A samples. These results show that differences in swelling between the particle size fractions of coal B cannot be attributed to differences in Gieseler fluidity. In the Gieseler fluidity test particles are closely packed and able to fuse together to some extent rather than acting as individual particles, so particle size is less likely to influence results.
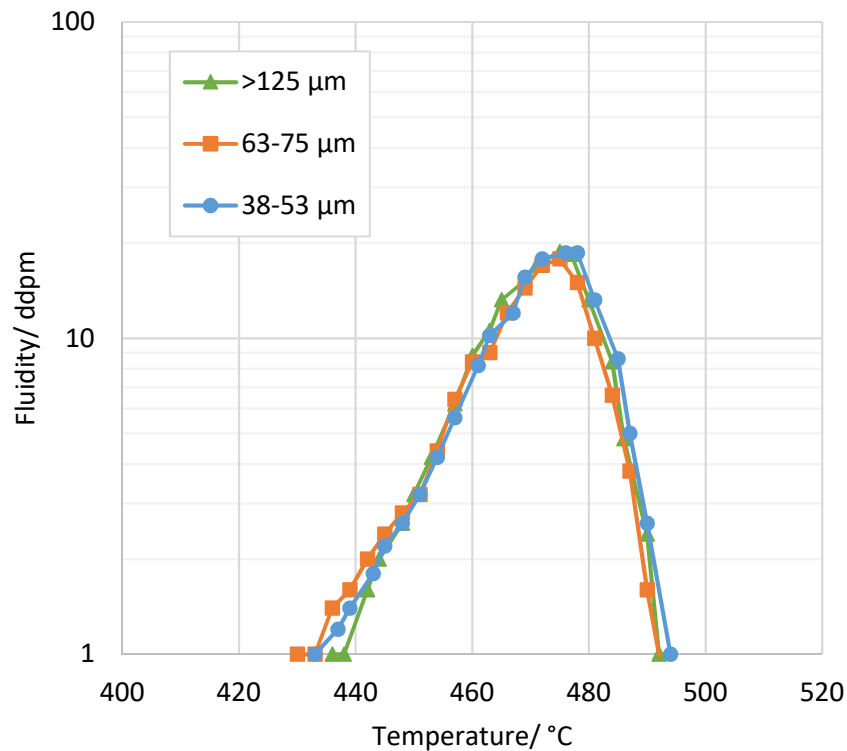
Figure 8.9: Gieseler fluidity measurements of the three size fractions of coal B.

8.4 Discussion

8.4.1   HT-CSLM swelling

The results of Proximate, Ultimate, petrographic (Table 8.1) and Gieseler fluidity analysis (Figure 8.9) show that the use of density and size separation is able to produce samples which vary in terms of particle size but are similar in other respects. This enables the study of particle size effects with minimal influence of segregation of constituents by particle size. The smallest particle size fraction analysed is 38-53 µm. Transient swelling behaviours of particles this small have not previously been published by researchers using techniques such as the Single

Particle Reactor (Yu *et al.*, 2003) (63-90 µm) and the laser heating system (Gao *et al.*, 1997) (100-355 µm).

Larger particles of coal B reach a greater maximum swelling ratio than smaller particles (within the range studied here) (Figure 8.3b). This can be explained in terms of the resistance to transport of volatile matter out of the particle during devolatilization. Larger particles have a smaller ratio of surface area to volume and a greater radius meaning that gaseous species must travel further to exit the particle. This greater resistance to volatile matter escape would allow a greater pressure to build up within the particle. The increased residence time of volatile matter within the particle may also allow the volatile matter to act as a plasticising agent as suggested by Lee *et al.*, (1991), in their study on the effects of ambient pressure. Increased temperature gradients may also have an effect. For example, in the larger particles volatile matter may evolve near the centre of the particle when the outer surface has become less fluid. This may reduce the frequency of bubble rupture and enable more swelling before re-solidification.

The trend of increasing swelling ratio with increasing particle size is not observed for coal A, in this case the mid-sized 63-75 µm particles reached the greatest maximum swelling ratio (Figure 8.3a). The substantial overlap of error bars suggests that this difference may not be significant. On the other hand, it may be that there is an optimum particle size for enabling greater swelling, which may be different for different coal types. The effect of particle size on swelling has been likened to the effect of heating rate (Saxena, 1990 and Yu *et al.*, 2007) due to similarities in the underlying factors, i.e. build-up of internal pressure and temperature gradients. There is an optimum heating rate for particle swelling therefore there may also be an optimum with regard to particle size. Above a certain particle size, the internal pressure may become so great that bubble rupture is more rapid than bubble growth, and at large particle sizes the outer shell may become completely solidified before all volatile matter is released, thereby locking the size of the particle.

8.5 Swelling behaviour of sub-samples

Analysis has been carried out to investigate the range of individual particle behaviours that contribute to the mean sample swelling ratios shown in Figure 8.3. This has revealed that for the smaller particle size fractions of coals A and B the particles can be divided into two sub-groups, which are high-swelling and low-swelling for coal A, and swelling and shrinking for coal B. The >125 μm particle size samples of each coal do not naturally divide into these sub-groups, which can be attributed to a decreasing likelihood of material being ground into separate constituents as particle size increases. This leads to greater heterogeneity of swelling behaviours within samples of smaller particle size.

Preceding chapters have shown that samples with a greater mean swelling ratio tend to have a greater RSD, i.e. heterogeneity, than those with a lower swelling ratio (this is true when comparing different coal types as in chapter 5 and different density fractions within the same coal type as in chapter 7). The different size fractions of coal A all have a relatively similar level of swelling ratio, as do the 38-53 μm and 63-75 μm fractions of coal B, therefore differences in RSD between these samples can be attributed to particle size effects. The >125 μm sample of coal B has a significantly greater swelling ratio than the other fractions of coal B, which is why this sample does not have the lowest RSD of the coal B size fractions.

A difference between the largest particle size fraction, >125 μm, of coal B and the two smaller fractions was that none of the largest particles showed a pattern of shrinkage without any significant prior swelling. The two smaller sieve fractions, 38-53 μm and 63-75 μm, both contained significant percentages of particles that showed overall shrinkage with minimal swelling (40 % and 38 % respectively). The reason that particles shrink with minimal prior swelling could be due to an insufficient build-up of pressure within the particle.

An unexpected observation is that the smaller particles of coal A (38-53 μm and 63-75 μm) swelled more than the corresponding size fractions of coal B (Figure 8.3). In all previous work coal B has swelled more than coal A. Contributing factors are that the swelling sub-groups of coal A within these size fractions reached high maximum swelling ratios of 1.8-2.0, compared to 1.1-1.2 for the swelling sub-

groups of coal B; and the low-swelling sub-groups of coal A did not shrink very much (only the 38-53 μm sub-group shrank to a small extent), whereas the shrinking sub-groups of coal B both shrank substantially. The greatest shrinkage was exhibited by the coal B >125 μm sample, although this sample showed a large degree of swelling prior to shrinkage. The greater thermoplasticity of coal B over coal A is likely to enable greater levels of shrinkage as well as swelling, When the particles are small, and swelling is not prominent, this shrinking behaviour of coal B may cause it to have a lower swelling ratio than coal A.

8.5.1   Temperature of maximum swelling

The temperature of maximum swelling varies amongst the coal B size fractions. The 63-75 μm and >125 μm fractions reach peak swelling ratio at 460 °C and 500 °C respectively, which is within the range seen previously for samples of coal B (Figures 6.1b and 7.6b), and broadly in line with maximum Gieseler fluidity (Figure 8.9). The 38-53 μm sample has a peak at a higher temperature of 540 °C, which is unusual in that it appears at a temperature at which the mean sample swelling ratio has already started decreasing. This is a result of the differing behaviours of the two sub-groups; the shrinking particles cause the overall decrease in mean swelling ratio, whilst the peak is caused by the swelling particles, which had not begun to shrink by that temperature. The reason for the higher maximum swelling temperature of this peak is not known. It may be that particles of this small size are unable to retain sufficient volatile matter for swelling until the material is more viscous i.e. further down the route to re-solidification (note that although 540 °C is above the Gieseler re-solidification temperature it has already been observed, for coal A samples, that swelling can take place when no Gieseler fluidity is registered).

8.5.2   Consequences for the blast furnace

Approximately 60 % of the coal injected during blast furnace pulverised coal injection (PCI) has a particle size smaller than 38 μm, results suggest that the swelling of these particles may be even lower than that of the 38-53 μm particles. In this case the implication for the blast furnace is that a low percentage of injected particles may undergo significant swelling; The denser particles have

limited swelling properties, and of the lighter particles only the largest particles, and a proportion of the smaller particles, swell. The larger particle size ranges used in granular coal injection (GCI) mean that swelling is likely to be more prominent in GCI operations than in PCI operations.

The two smaller particle size fractions of coal A swelled slightly more than those of coal B. This does not mean that the small particles of coal A will necessarily swell more than those of coal B under PCI conditions, because the S1.2-F1.3 density fraction isolated in this chapter represents a larger proportion of coal B than coal A (Figure 7.1), i.e. coal A has a greater proportion of denser particles.

8.5.3   Exclusion of highly fluid particles

Another factor contributing to the low swelling of the smaller coal B factions may be that some particles of these samples are excluded from the calculation of the sample mean due to their extremely high levels of apparent swelling. No particles are excluded from the >125 µm sample. It is suggested that these particles are of a very fluid material and have begun to flow over the surface of the crucible like coal D in chapter 5. If this is the case then presumably this fluid material also exists within the larger particles, but associated with other material within those particles, where it can contribute to the overall particle swelling. This is presumed because the petrography results are very similar for all 3 samples. If this is the case, then the results are potentially still being influenced by the distribution of material rather than simply the physical size of the particles despite the efforts made to avoid this.

8.5.4   Differential thermo-gravimetric analysis

DTG analysis of the samples (Figure 8.8) shows that the >125 µm particle fractions of coals A and B had a higher rate of mass loss at temperatures where swelling is occurring. This has been associated with greater swelling ratios in chapter 7 and is also the case here.

8.6 Conclusions

The novel contributions made in this chapter are the novel approach to studying the effect of particle size on maximum swelling ratio, and the observation of greater maximum swelling ratio for larger particle sizes.

Wet sieving and sink-float centrifugation separation have been used to create size and density separated fractions of coal particles, which have different particle sizes but similar properties in terms of Proximate and Ultimate analyses, Gieseler fluidity and petrography. The HT-CSLM has been used to measure the transient swelling behaviours of these particles. The smallest particle size fraction to be measured was the 38-53 µm sieve fraction, this is a smaller particle size than previously reported in the literature for this type of study (Yu *et al*., 2003) (63-90 µm) and (Gao *et al*., 1997) (100-355 µm)).

The larger particles of coal B reach a higher maximum swelling ratio than the smaller particles when heated at 700 K/min in the HT-CSLM. This is attributed to the increased resistance to volatile matter release, because of the lower surface area to volume ratio, resulting in an increased pressure build-up within the particles.

The mid-sized particles of coal A, 63-75 µm, reach a greater maximum swelling ratio than the other two size fractions. This is different to the trend for coal B. It is possible that an optimum particle size for swelling exists, which is dependent upon coal type. The optimum for coal B may be above the size range studied here.

The heterogeneity of swelling behaviours observed within the same sample (as measured by RSD) increases with decreasing particle size when differences in the mean swelling ratio are small. Samples with higher mean swelling ratio also tend to have higher heterogeneity. At smaller particle sizes it is possible to identify distinct sub-groups of swelling behaviour within a sample.

The two smaller particle size samples contained some particles, which reached a very high maximum swelling ratio and appeared to behave in a similar way to highly fluid particles, which began to flow over the crucible surface. These results

were excluded from the sample mean. The sample of >125 μm particles did not contain such particles.

Hypothesis 5 – The maximum swelling ratio of coal particles increases with increasing particle size within the size range 38-500 μm, appears to be true in the case of the coal B particles studied. However, an alternative hypothesis, that the lower swelling ratio of the smaller particle size fractions is due to the exclusion of highly fluid particles and not particle size, cannot be discounted. The results of the coal A particles indicate that it may be that an optimum particle size for swelling exists, which, for coal B, is above the range used in this study, or that particle size has no effect.

9 Drop tube furnace tests

9.1 Introduction

The HT-CSLM has been used to measure the transient swelling properties of particles of different coals and to study factors such as heating rate, particle density and particle size. Although the HT-CSLM technique has greater relevance to the blast furnace coal injection process than tests such as Gieseler fluidity, Ruhr dilatation and free swelling index, there are limitations associated with the technique: The maximum heating rate possible in the HT-CSLM is 700 K/min, much lower than that associated with blast furnace coal injection (10^6 K/s) (Carpenter, 2006). Also, the fact that particles are in contact with a crucible surface means that it is not possible to accurately measure the swelling of highly fluid particles (as in the case of coal D). Further to this, the question of what implications coal swelling has for the blast furnace arises. In this chapter a drop tube furnace (DTF) is used to provide a closer comparison to blast furnace coal injection. Heating rates are estimated to be 10^4 K/s and particles are fed into a moving stream of gas, which has a similarity to blast furnace coal injection. The 'final' swelling ratios (the swelling ratio at the point of quenching) of coal particles are measured using particle size analysis to see if the behaviours observed in the HT-CSLM are equivalent to those in the DTF. A limitation of the DTF is that transient swelling behaviours cannot be observed, however the quantity of char produced during DTF tests enables conversion and char reactivity to be measured, which is not practical with the quantities produced using the HT-CSLM technique. These characteristics are considered important for blast furnace coal injection therefore it will be possible to observe any correlations between coal swelling and levels of burnout and char reactivity.

Hypotheses to be investigated are:

Hypothesis 6 – The swelling ratio observed by HT-CSLM correlates with that observed after drop tube furnace treatment.

Hypothesis 7a – The rate of coal conversion is enhanced by particle swelling.

Hypothesis 7b – The rate of char reactivity is enhanced by particle swelling.

9.2 Experimental

The DTF method is described in section 4.7. However, to reiterate the important operating conditions used in this work: Furnace temperature was 1100 °C, gas composition was 99 % nitrogen and 1 % oxygen, flow rate was 20 L/min and particle residence time was 35 ms.

Coals A-D are included in this chapter. The change in particle size distribution was used as a measure of swelling ratio therefore it was important that all samples had the same starting size distribution, since particle size may affect the degree of swelling (chapter 8). This was achieved by first taking the samples crushed by Tema mill to a nominal specification of 80 % <5 µm and then wet-sieving, as described previously in section 4.2 (although with an extra sieve used of 212 µm aperture). As the size distributions were similar but not identical the sieve fractions were re-constituted using the 'recipe' given in Table 9.1. The <38 µm particles and the >212 µm particles were not included in the re-constituted samples.

Sieve fraction/ µm	Mass/ %
38-53	24
53-63	9
63-75	10
75-90	13
90-125	18
125-212	26

Table 9.1: The mass % of each sieve fraction used in the reconstituted test samples of coals A-D.

The <38 µm particles were not included as these particles have not been included in any HT-CSLM work. This particle size range represented approximately 60 wt. % of the crushed sample. The >212 µm particles were excluded to moderate the particle top size of the samples. A Retsch Camsizer was used for particle size analysis of re-constituted coal samples and DTF char samples. The results of the re-constituted samples were in good agreement with the expected values based

on the mass percentages given above. Proximate analysis results for the reconstituted test samples are given in Table 9.2.

	Coal A	Coal B	Coal C	Coal D
Volatile matter/ % (db)	12.8	17.4	36.5	34.9
Ash/ % (db)	9.8	7.9	3.7	5.9
Fixed carbon/ % (db)(diff)	77.4	74.7	59.8	59.2

Table 9.2: Proximate analysis of test samples of coals A-D.

Before any analysis of the char samples was carried out, the samples were screened using a 500 μm aperture sieve. This was to screen out the large agglomerates that can be present in the char. It has been observed by researchers working with the DTF that long, thin cylindrical agglomerates can build up during DTF tests and end up in the catch-pot. It is assumed that these structures are an artefact of the test method (for example, material becoming stuck and collecting in the feed tube) rather than a natural feature of the coal reaction within the furnace void itself (Sexton, 2016).

The Proximate analysis of the re-constituted coal samples and the char samples from DTF tests were carried out using Leco TGA. From this data coal conversion could be calculated by the ash-tracer method using equation 9.1. This method assumes that the mineral matter within the coal sample is unaffected by DTF treatment therefore the ash content of the char can be used as a tracer. Duplicate tests were carried out in the DTF so conversion measurements were made on both duplicates of each coal.

$$Conversion = 100\,\% \times \frac{(Ash_{Char} - Ash_{Coal})}{\left(Ash_{Char} \times \left(1 - \left(\frac{Ash_{Coal}}{100}\right)\right)\right)} \qquad \text{(Equation 9.1)}$$

Where Ash_{Char} is the ash content of the char and Ash_{Coal} is the ash content of the coal, both measured by Proximate analysis.

The Netzch STA was also used to carry out Proximate analysis of coal and char samples. This enabled the pattern of mass loss of coals and chars during devolatilization to be compared. The STA was used in a similar way to that

described in section 4.5, however the heating steps were adjusted to match the Leco TGA in some respects. The steps used were:

1. Dynamic heating from 20 °C to 900 °C at 41 °C/min under argon (30 mL/min)
2. Isothermal heating at 900 °C for 7 minutes under argon (30 mL/min)
3. Isothermal heating at 900 °C for 50 minutes under air (25 mL/min)

The heating rate of 41 K/min in step 1 matches the heating rate of the Leco TGA, as does the hold time of 7 minutes in step 2. The temperature of 900 °C was maintained in step 3 rather than decreasing to 815 °C, as in the Leco TGA, to maintain stability.

Char reactivity is measured using the Netzch STA as described in section 4.8.

9.3 Results

9.3.1 Particle swelling in the DTF

Figure 9.1 shows the particle size analysis of all coal feedstock samples and DTF chars.
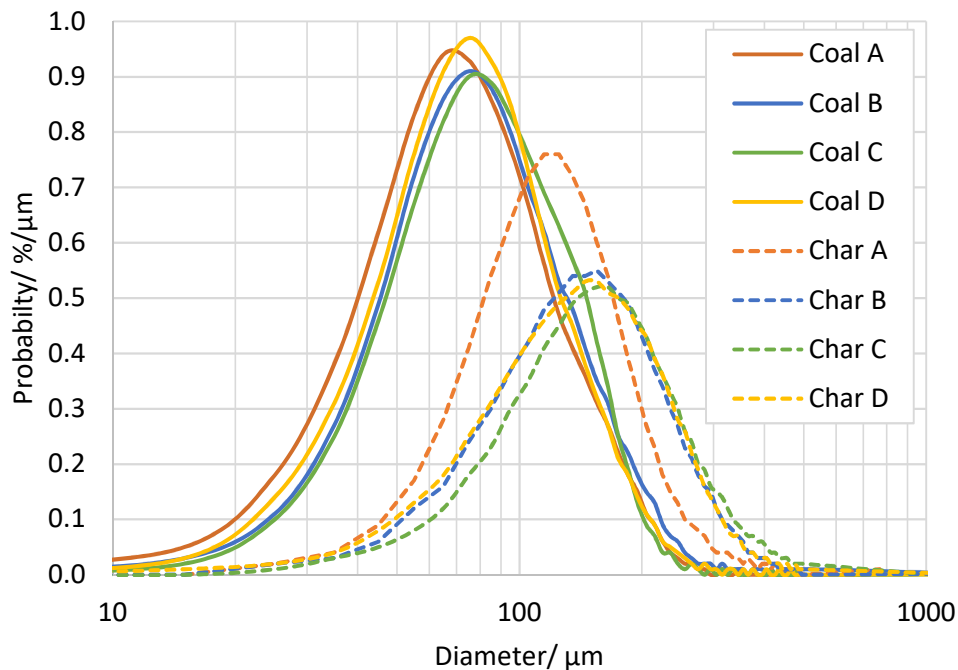
Figure 9.1: Particle size distribution of coals A-D before DTF tests and corresponding chars from DTF tests.

Figure 9.2 shows the same data separated according to coal type; this data is an average of two determinations. The method of sample preparation successfully created feedstock samples of very similar particle size distribution for each coal with Dv(0.5) values of 92-101 µm.
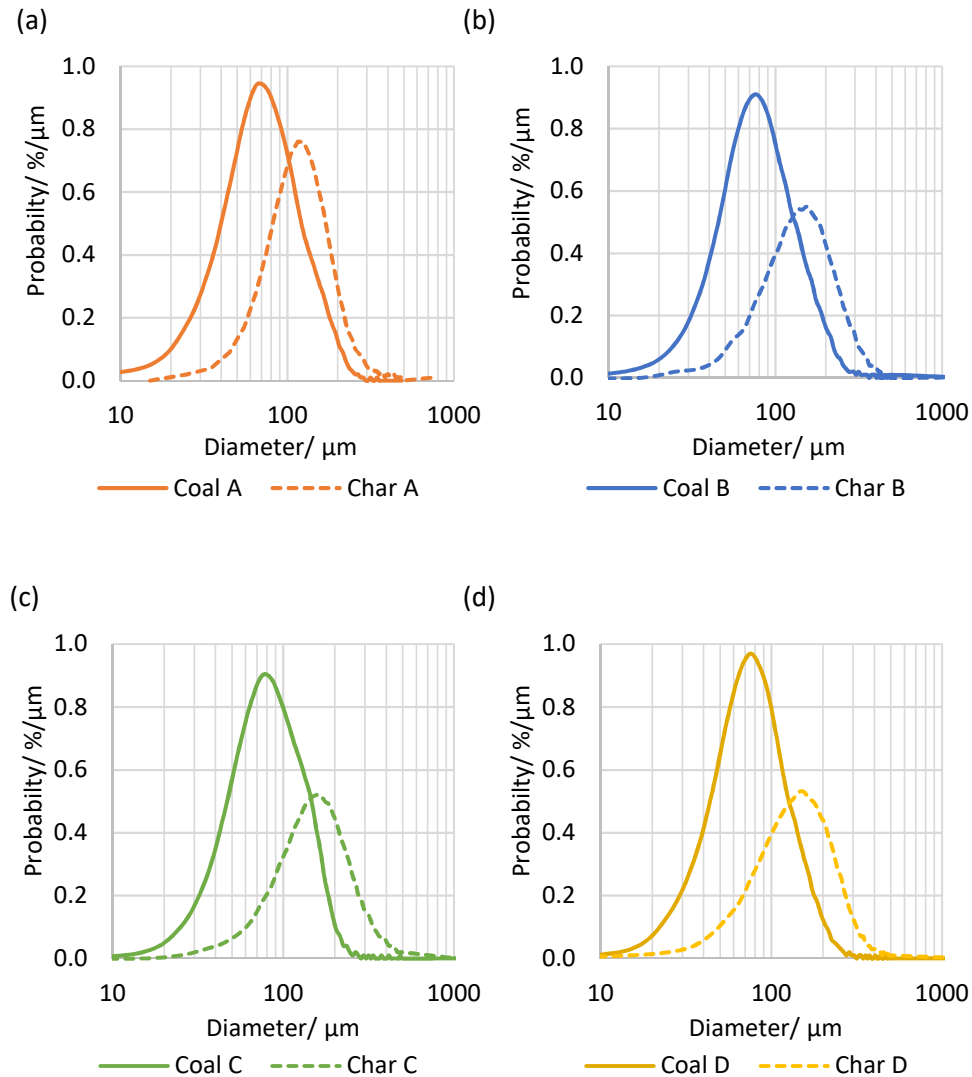
Figure 9.2: Particle size distribution of coals before DTF tests and chars after DTF tests; (a) coal A, (b) coal B, (c) coal C and (d) coal D.

Table 9.2 shows the Dv(0.5) values of coals and chars, along with swelling ratios calculated from these values. All coals showed swelling, coal A had the lowest swelling ratio of 1.4, coals B, C and D all had very similar swelling ratios of 1.7, 1.8 and 1.8 respectively. No fragmentation was indicated by the results, nor was any agglomeration at 2, 3, or 4 times the d(50) of the feedstock coal (>500 µm char

material was screened out prior to analysis). Particle size distribution becomes less consistent during DTF tests, i.e. the peaks become lower and broader, and the effect is greatest for the more highly swelling coals (B, C and D). This is expected due to the heterogeneous nature of particle swelling, i.e. particles within the sample swell to different extents.

Coal type	Dv(0.5)/ µm		Swelling ratio
	Coal	Char	
A	92	128	1.4
B	99	173	1.7
C	101	185	1.8
D	95	173	1.8

Table 9.3: The Dv(0.5) values of coals A-D before DTF tests and chars after DTF tests; and swelling ratios based on these values.

Figures 9.3-9.6 show SEM images of DTF char particles derived from coals A-D respectively. In the char A sample swollen particles are present, but many particles do not show evidence of swelling and remain angular. In the char B-D samples rounded swollen particles are common and shrunken particles are also observed. Swollen particles often have holes at the surface. Coal D chars often show evidence of many small bubbles and the fluid particles retain an overall structure when heated in the DTF, which is not the case when heated in the HT-CSLM.

(a)

250 μm

(b)

25 μm

(c)

50 μm
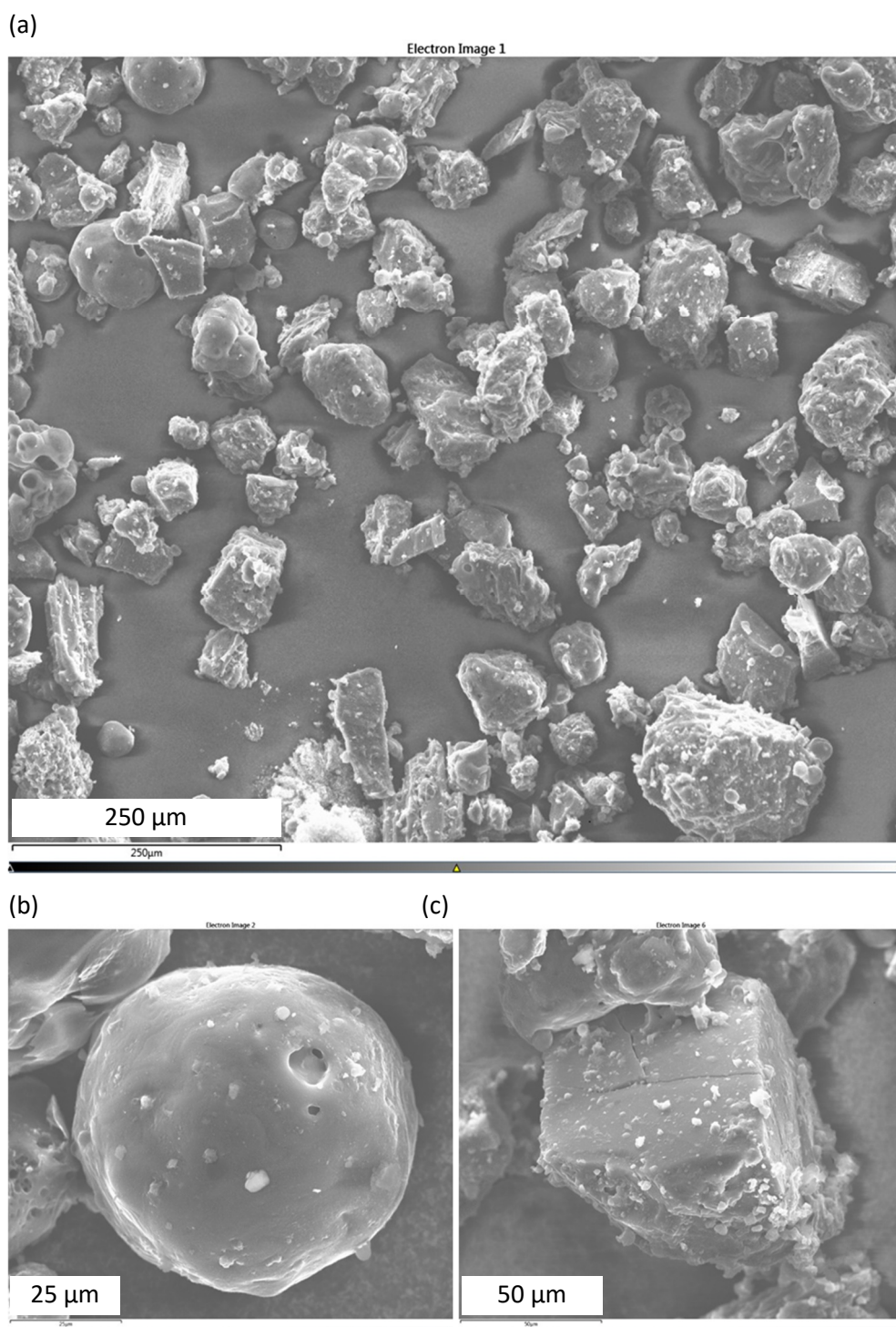
Figure 9.3: SEM images of DTF char particles derived from coal A, including a collection of particles (a), a swollen particle (b) and an un-swollen particle (c).

(a)

250 µm

(b)

50 µm

(c)

50 µm
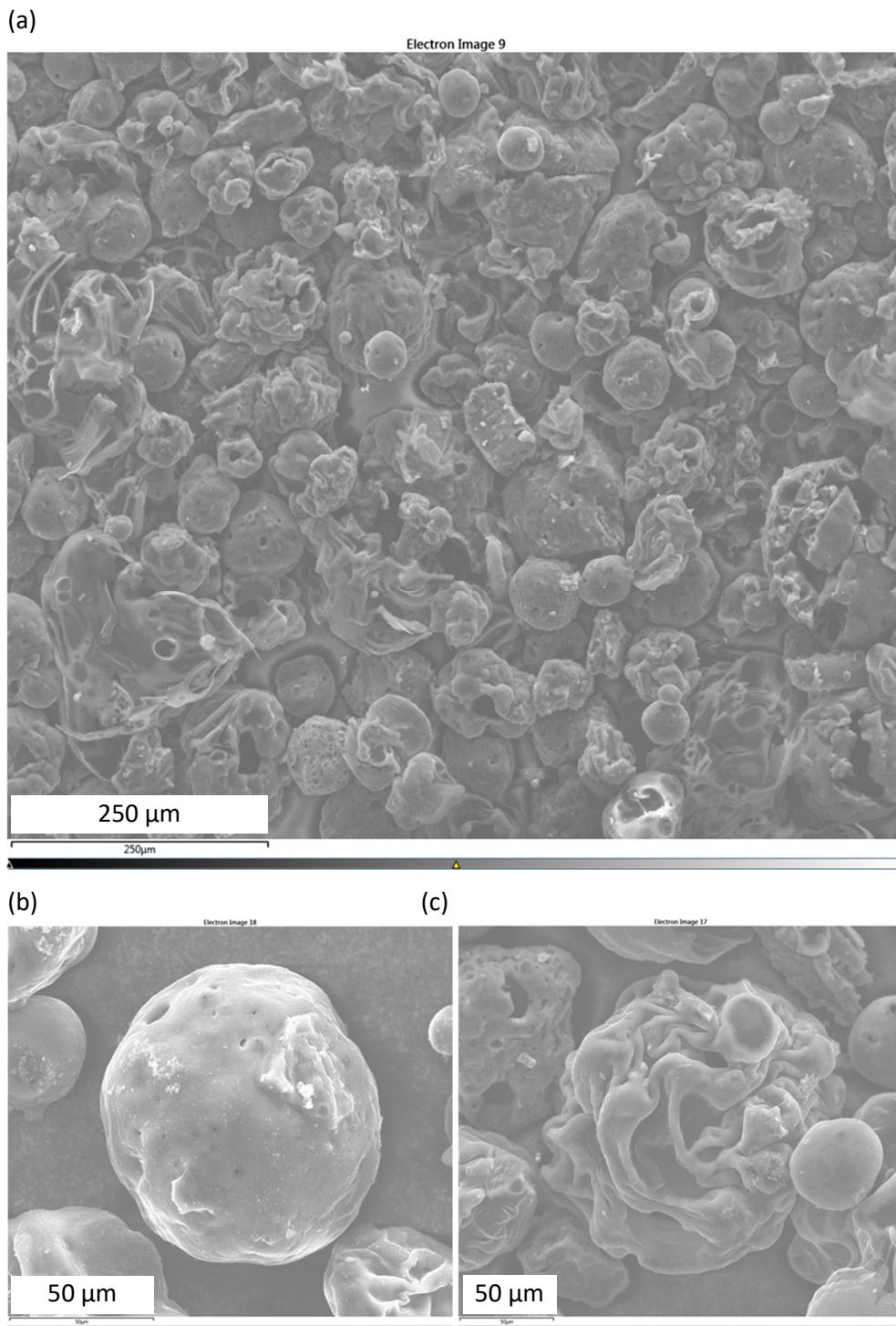
Figure 9.4: SEM images of DTF char particles derived from coal B, including a collection of particles (a), a swollen particle (b) and a shrunken particle (c).

(a)

250 µm

(b)

25 µm

(c)

50 µm
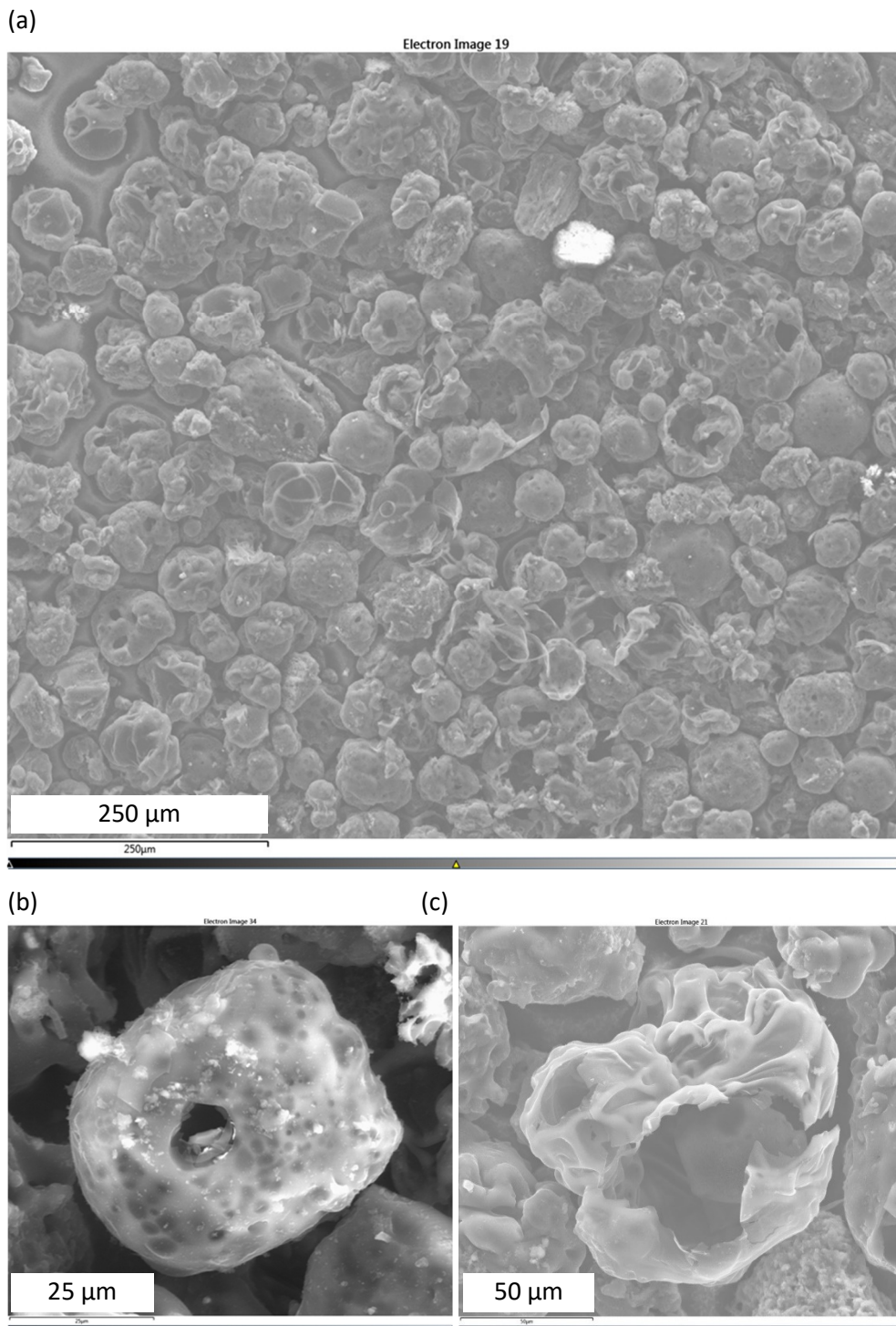
Figure 9.5: SEM images of DTF char particles derived from coal C, including a collection of particles (a), a swollen particle (b) and a shrunken hollow particle (c).
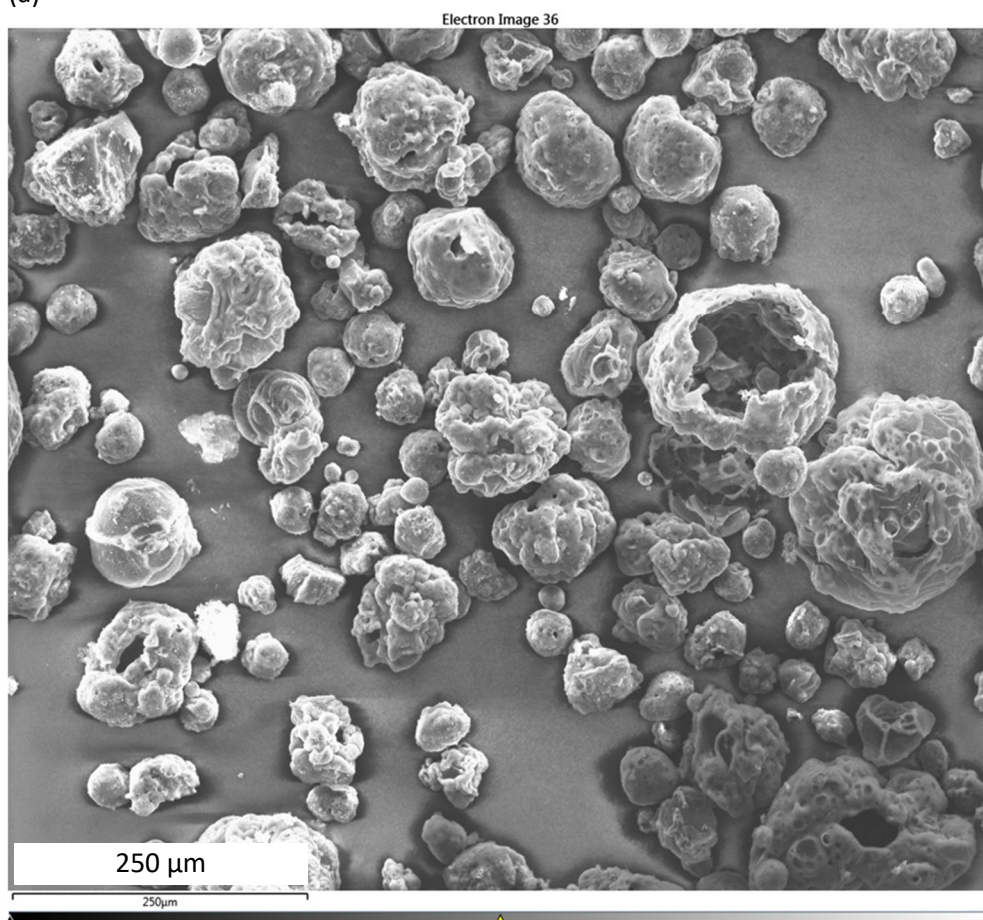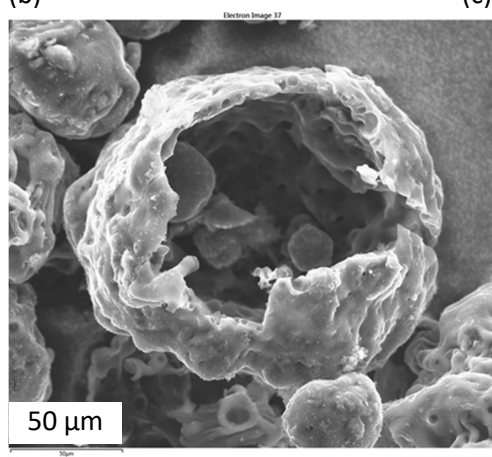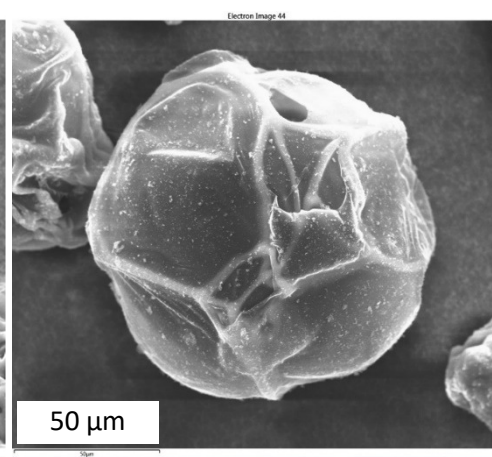
Figure 9.6: SEM images of DTF char particles derived from coal D, including a collection of particles (a), a cenosphere with a large opening (b) and a swollen particle (c).

9.3.2   Conversion

Table 9.4 shows the Proximate analysis of the DTF char samples derived from coals A-D, these figures are average results of duplicate DTF tests. Figure 9.7 shows the degree of conversion plotted against coal Proximate volatile matter, here the results of individual duplicate tests are shown. As the DTF atmosphere was essentially nitrogen the conversion is devolatilisation rather than combustion. However, in the very early stages of combustion, as is the case in these tests, the degree of combustion would be predominantly determined by the rate of devolatilisation rather than heterogeneous reaction between gaseous oxygen and solid fuel (Wu, 2005). Levels of conversion in these tests are relatively low, ranging from about 13-37 %, which is in-line with previously published results at the 35 ms residence time in which air was the carrier gas (Steer *et al.*, 2015a and 2015b). The results show the expected pattern of increasing conversion with increasing volatile matter. This general trend has been observed previously (Rogers & Wall, 2011) although the relationship is not exact, there is scatter around the trend-line as seen here with coals C and D.

	Char A	Char B	Char C	Char D
Volatile matter/ % (db)	8.3	7.0	9.1	7.4
Ash/ % (db)	10.6	9.6	6.6	11.3
Fixed carbon/ % (db)(diff)	81.1	83.4	84.3	81.3

Table 9.4: Proximate analysis of DTF chars derived from coals A-D.

The Proximate analysis of coal and char samples was also carried out using Netzch STA, which enabled the rate of mass loss during Proximate volatile matter analysis to be plotted (Figure 9.8). These graphs show mass loss during heating to 900 °C at 41 K/min, they do not show mass loss occurring during the 7-minute isothermal hold time, which is a feature of the Proximate volatile matter test. The greatest rates of mass loss for these samples occurs during the temperature range shown on these graphs (200-900 °C); during the 7-minute isothermal hold period rates of mass loss are low and tend to be similar for coal and char particles.
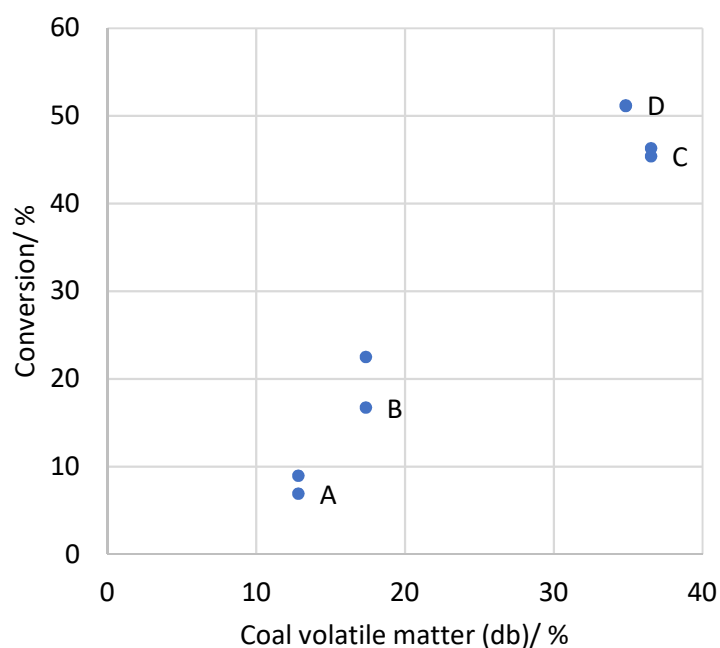
Figure 9.7: Degree of conversion (%) during DTF tests as a function of coal volatile matter (db).

The DTG profiles of all four char types are very similar; there is minimal mass loss before around 500 °C and the rate of mass loss peaks to around 0.02 %/K (db) between 700-800 °C. This shows that some mass loss from the chars is occurring during the volatile matter test i.e. the conversion of Proximate volatile matter was not complete in the DTF. The coal samples all show higher rates of mass loss than the chars between 400 °C and around 700 °C. The rates of mass loss of the coals and chars converge around 700-800 °C. The magnitude of the coal DTG peaks varies considerably between coals A-D. The DTF processing caused virtually all Proximate volatile matter up to 500 °C to be evolved from the coals and a proportion of that between 500 °C and 700 °C.

(a)

Coal & Char A

(b)

Coal & Char B

(c)

Coal & Char C

(d)
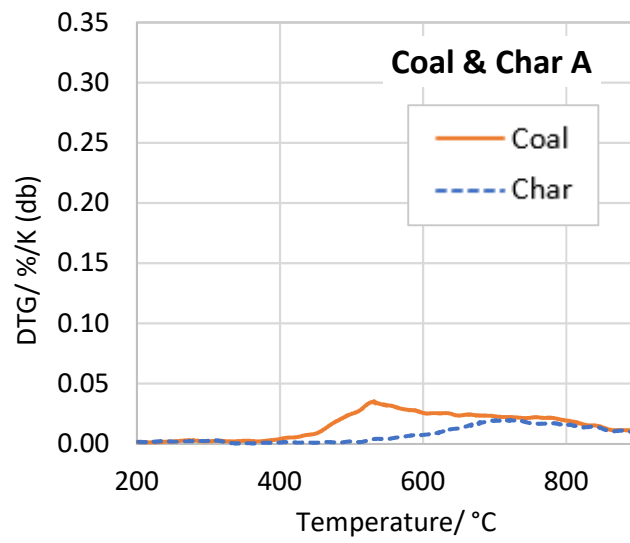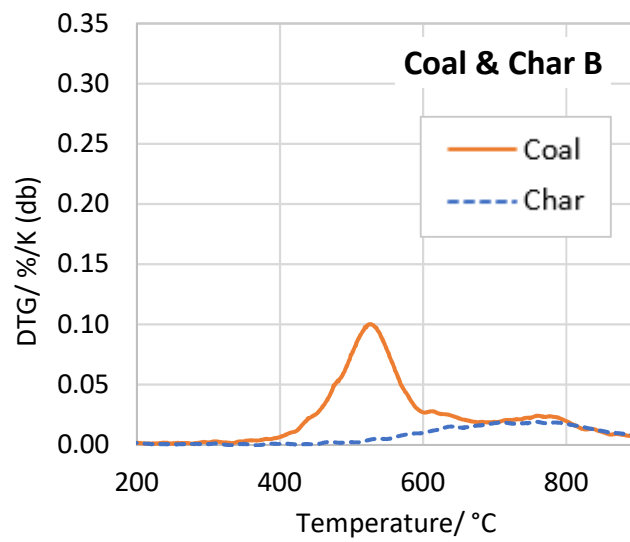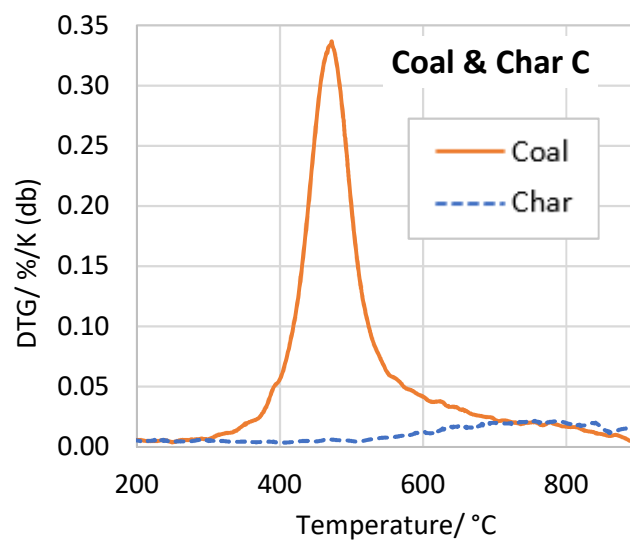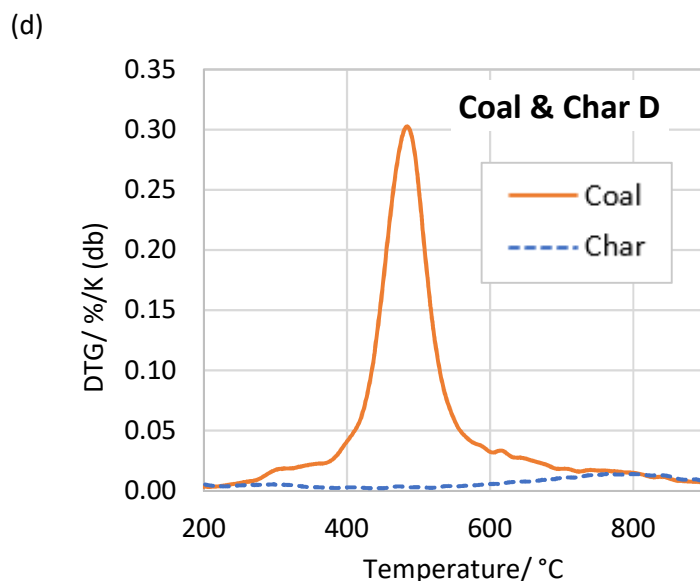
Figure 9.8: DTG graphs of coal and char samples A-D ((a)-(d) respectively) heated at 41 K/min.

9.3.3   Char reactivity

The reactivity of the DTF char samples towards carbon dioxide was measured using TGA, the results are shown in Figures 9.9 and 9.10. Figure 9.9 shows the progression of normalised mass loss against time for each char sample during reaction with carbon dioxide, each line is the average of four repetitions. Mass loss is normalised so that 100 % mass loss is set at the point of minimum sample mass. Figure 9.10 shows the char reactivity index for each char sample with error bars representing 1 standard deviation either side of the mean. Char A is the least reactive with a reactivity index of 0.21, chars B and C have similar reactivity index values to each other, 0.40 and 0.45 respectively, whilst char D is the most reactive, having a reactivity index of 1.20. The mass of char A begins to increase after reaching a minimum at around 1000 mins, this increase is assumed to be due to oxidation of mineral matter.
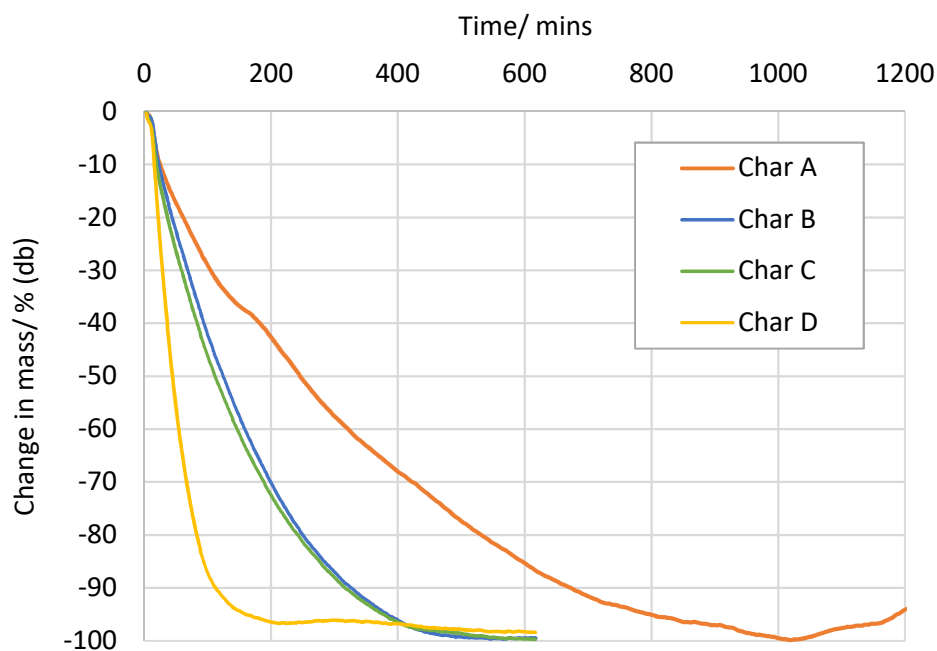
Figure 9.9: The normalised mass loss of char samples during char reactivity tests under carbon dioxide at 900 °C.
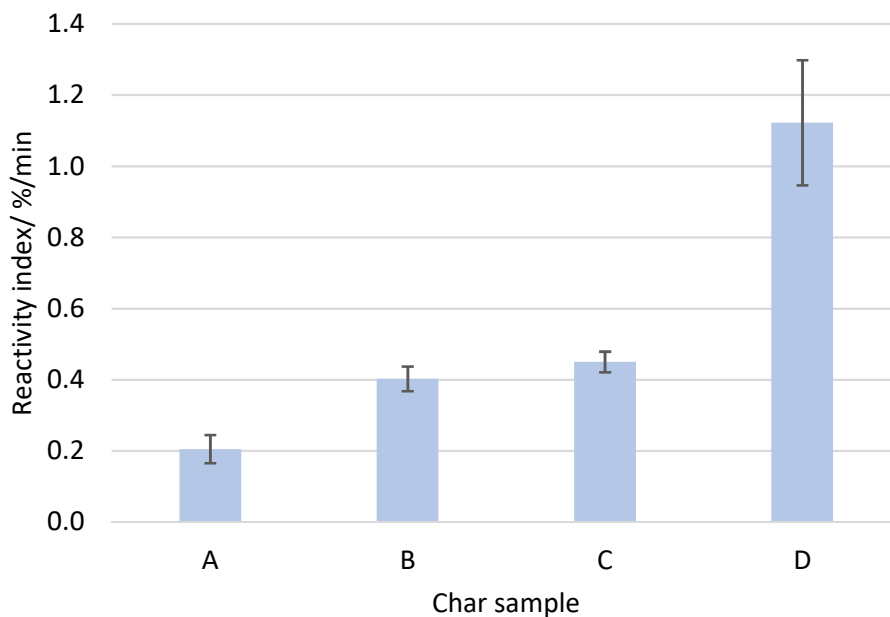
Figure 9.10: Char reactivity index of char samples with error bars showing 1 standard deviation either side of the mean.

It was necessary to ensure char samples were well mixed before reactivity testing. The char A sample, for example, was found to be susceptible to segregation, with swollen char particles segregating to the top of the sample container. When

segregation was deliberately induced, and these particles were preferentially sampled they produced more highly reactive char samples than the mixed sample, as illustrated by Figure 9.11. The reactivity indexes of the three samples of swollen particles were 0.43, 0.52 and 0.94. These values are within the range occupied by the B, C and D char samples.
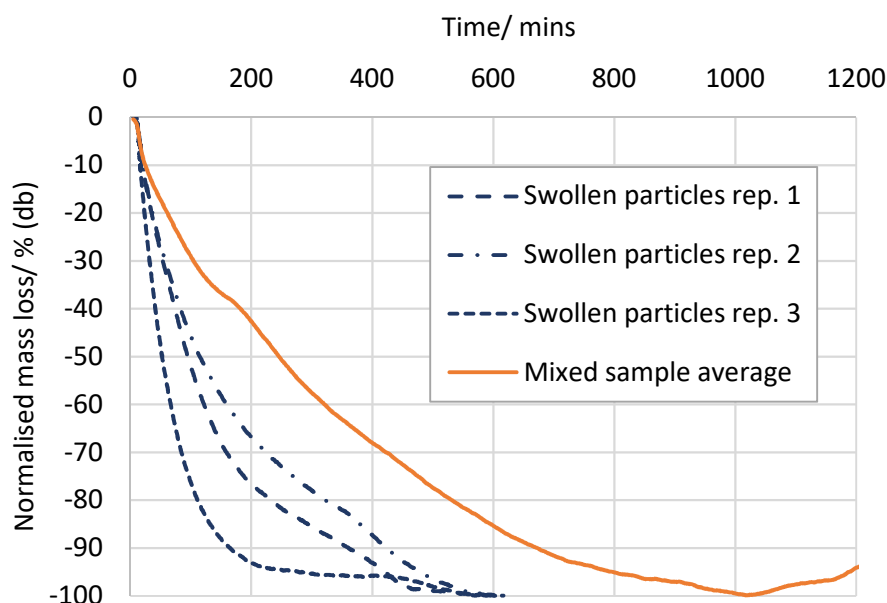
Figure 9.11: Normalised mass loss of char A samples; a well-mixed sample (average of 4 reps) and segregated swollen chars (3 reps shown separately) during char reactivity tests under carbon dioxide at 900 °C.

Chars C and D have the same swelling ratio yet distinctly different reactivity index values. To investigate this further samples of chars C and D were crushed to a powder using pestle and mortar. The resulting powders were able to pass a 75 µm aperture sieve and their reactivities were measured. The aim of this was to moderate the effects of char morphology (i.e. surface area) on reactivity. This technique has been applied in literature studies of char reactivity (Sexton *et al.*, 2018). The results are shown in Figure 9.12. The crushing has differing effects on chars C and D; char C becomes more reactive upon crushing, yet char D becomes less reactive. The crushed char D sample has a greater reactivity index than the crushed char C sample, but the difference is smaller than for the uncrushed samples, and the standard deviation associated with the crushed char C sample is comparatively large.
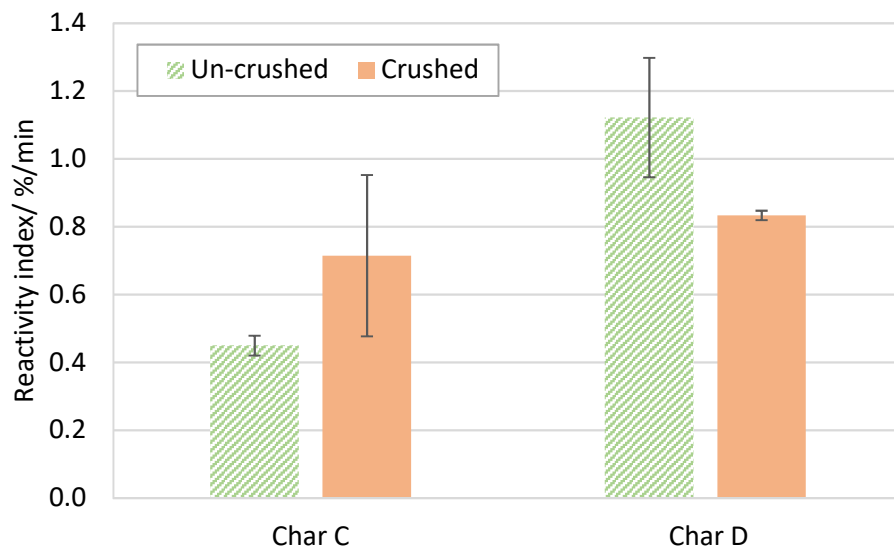
Figure 9.12: Char reactivity index of crushed and un-crushed samples of chars C and D with error bars showing 1 standard deviation either side of the mean.

9.4 Discussion

9.4.1 Comparison of HT-CSLM and DTF swelling patterns

The DTF tests were undertaken to discover whether the swelling trend observed in HT-CSLM tests is also observed in DTF tests, where the heating conditions are closer to the blast furnace raceway environment, and to investigate what effect swelling has on conversion and char reactivity. It is not possible to be certain exactly what temperature the particles reached in the DTF, therefore it is difficult to know whether samples had reached their maximum swelling ratio or not. However, a basic prediction of the peak particle temperature can be made as described below.

The distance between the feeder and receiver probes of the DTF was set to produce a residence time of 35 ms according to Equation 9.2 (Whitehouse, 1992).

$$d = 0.05 + (v\,s) \qquad\qquad \text{(Equation 9.2)}$$

Where d is the distance between the feeder and receiver probes (m), v is the axial velocity (m/s) of gas in the tube and s is the residence time (s). A correction factor

of 0.05 (m) is added to allow for the mixing of the carrier gas and secondary gas entering the tube; uniform mixing of gasses has been found to be complete at this distance (Whitehouse, 1992) i.e. the residence time at d = 0.05 m is considered to be zero. The axial velocity, v, can be assumed to be twice the plug flow (Whitehouse, 1992) and is calculated by Equation 9.3.

$$v = 2 \left(\frac{F}{1000 \times 60 \, \pi r^2} \right) \times \left(\frac{T_2}{T_1} \right) \qquad \text{(Equation 9.3)}$$

Where F is the total flow rate of gas into the furnace at ambient temperature (20.5 L/min in this work), r is the internal radius of the tube (0.026 m), T_1 is the ambient temperature in Kelvin, T_1 = 293 K is used here, and T_2 is the gas temperature. T_2 = 1293 K is used here as the gas temperature has been found to be approximately 100 °C lower than the measured heating element temperature (Whitehouse, 1992). This gives a velocity of approximately 1.54 m/s, therefore solving Equation 9.2 for s = 0.035 s results in d = 0.104 m.

In order to calculate the predicted peak temperature of the particles, not only the heating during the reported 35 ms residence time must be considered but also the heating during the 0.05 m gas-mixing drop. The residence time of this drop can be calculated by Equation 9.4 to be 33 ms.

$$s = \frac{d}{v} \qquad \text{(Equation 9.4)}$$

A heating rate of 10^4 K/s, based on previous estimates in literature (Du *et al.*, 2010), is assumed to occur during the 35 ms residence time. However, it seems that it would be inappropriate to assume this heating rate throughout the 33 ms gas-mixing drop because mixing of the carrier gas and secondary gas is not complete until the end of this time period. Instead it has been assumed that the heating rate at the point of exit from the feeder probe is 0 K/s, the heating rate at 0.05 m (i.e. reported residence time of zero) is 10^4 K/s and that a linear increase in heating rate exists between the two points. This is illustrated in Figure 9.13. A starting temperature of 20 °C is assumed, therefore the predicted peak temperature experienced by the particles is estimated by Equation 9.5.

$$T = 20 + (s \times 10^4) + \left(s \times \frac{10^4}{2} \right) \qquad \text{(Equation 9.5)}$$

Where T is the peak temperature of the particles (°C). Equation 9.5 gives 535 °C as the predicted peak temperature of coal particles at 35 ms residence time. This value is in some agreement with Figure 9.8, which shows very low rates of devolatilisation from the char particles below 500 °C, indicating that the char may have previously been heated to this temperature. The figure of 535 °C is an estimation and relatively small changes in the estimated heating rate and residence time could alter this final predicted temperature.
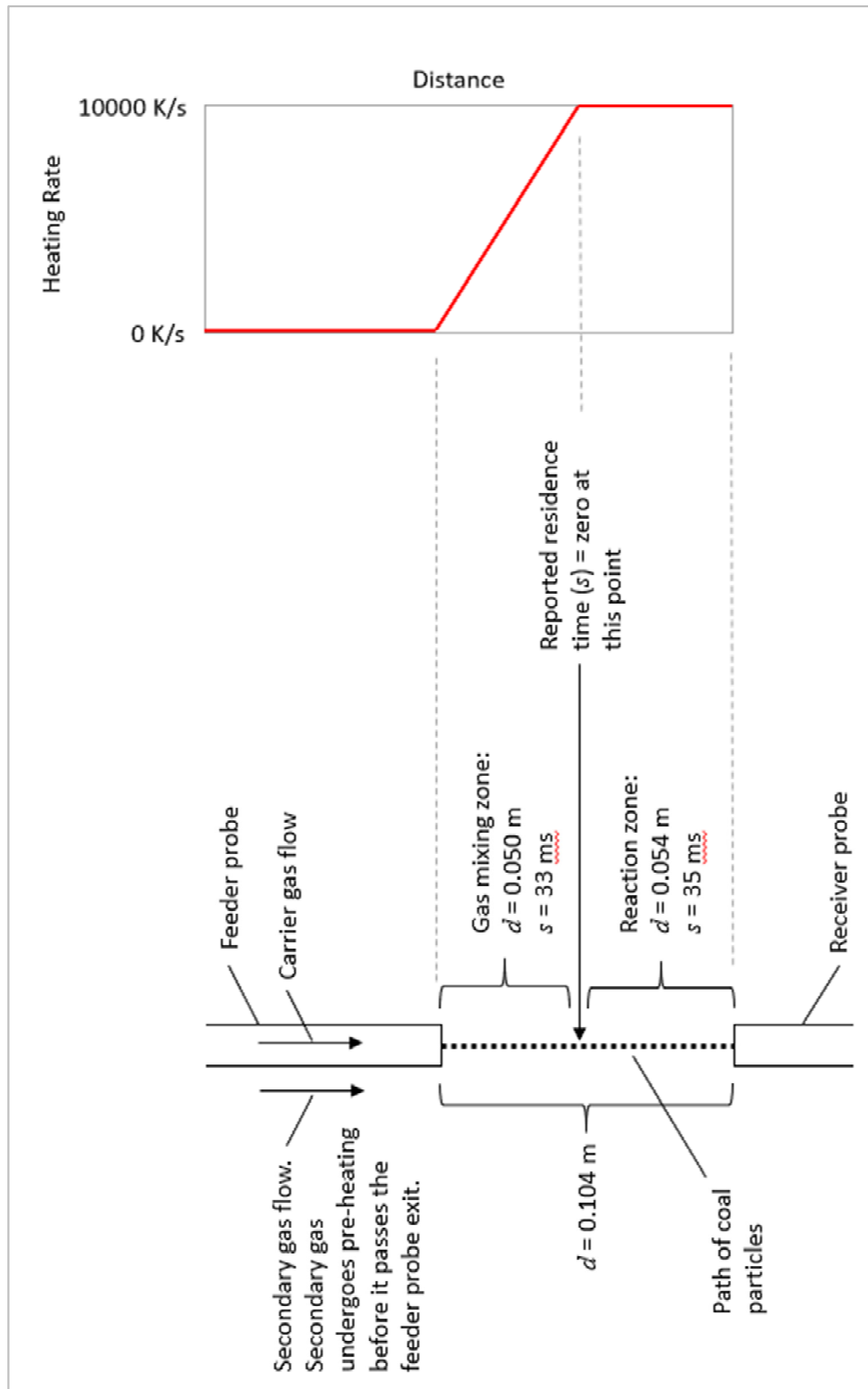
Figure 9.13: Schematic illustration of the path of coal particles within the DTF from feeder probe to receiver probe, showing residence times (s), distances (d) and assumed heating rates.

Figure 9.14 shows the swelling profiles of >125 µm particles of coals A-C heated at 700 K/min in the HT-CSLM (previously presented in chapter 5). The temperature of 535 °C is indicated by the dashed line. It can be seen that at this temperature in the HT-CSLM coal B had the greatest swelling ratio and coals A and C had lower swelling ratios, which were similar to each other. This contrasts with the DTF swelling results in which the swelling ratios of coals B and C are similar to each other and are greater than that of coal A. So there appears to be an inconsistency between the two techniques; however, a situation does exist within the HT-CSLM results, which correlates with DTF results; this is between the temperatures of 400 °C and 440 °C, which is indicated by red lines on Figure 9.14.
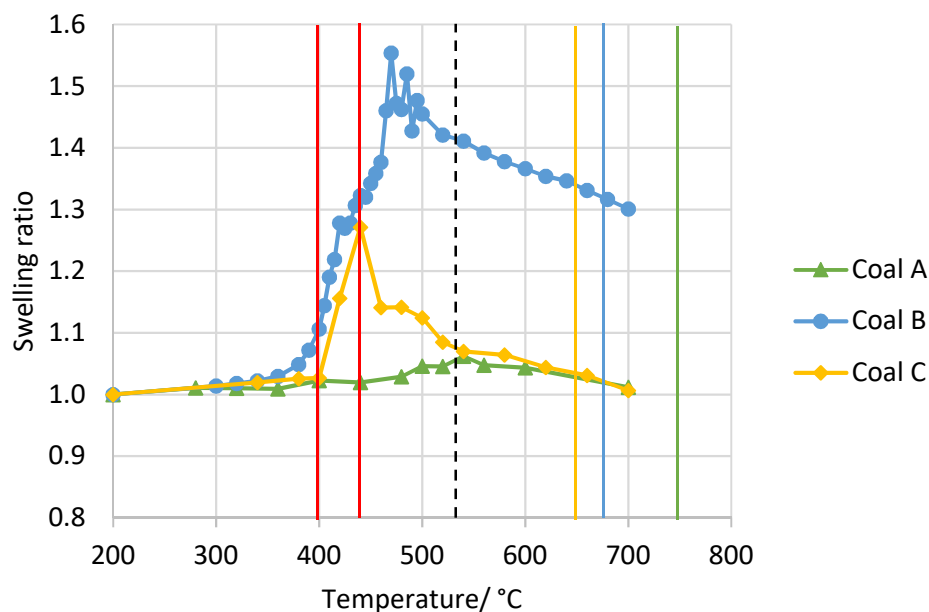
Figure 9.14: Mean swelling ratios of coal samples A-C (>125 µm particles) heated at 700 K/min in the HT-CSLM. See text for explanations of additional vertical lines.

It may be the case that the higher heating rates in the DTF have shifted the temperature of the respective maximum swelling ratios to higher temperatures. Evidence for this phenomenon has been reported by Gao *et al.*, (1997), and was discussed in chapter 6, in which Figure 6.5 showed how increasing the maximum heating rate increased the temperature of maximum swelling ratio in the laser experiments of Gao *et al*.

By using the relationship shown in Figure 6.5 the effect of increasing the heating rate from 11.67 K/s (700 K/min) to 10^4 K/s can be predicted to be an increase in the temperature of maximum swelling of approximately 208 °C. These increased temperatures of maximum swelling are illustrated in Figure 9.14 for coals A-C by the vertical green, blue and yellow lines respectively. The results of Gao *et al.*, (1997), also imply that the temperature of swelling onset is not shifted in the same way, i.e. swelling appeared to begin once the temperature increased sufficiently, at all heating rates used. This would effectively cause the area indicated by the red lines on Figure 9.14 to broaden significantly so that it may encompass the dashed line of predicted particle temperature at 35 ms in the DTF.

Although it is not straight forward to predict the precise temperature of coal particles after 35 ms in the DTF, the analysis above provides a possible explanation of the apparent differences in swelling behaviour in coals A-C between the HT-CSLM and the DTF.

If the assumptions above are correct, then the coal B particles had not reached their maximum swelling ratio when quenched in the DTF but those of coal C might have been close to theirs. Further DTF tests at slightly longer residence times would confirm whether this was the case and help to verify the assumptions made.

It was not feasible to measure the swelling ratio of coal D in the HT-CSLM due to the coal material flowing over the crucible surface as it became highly fluid. In the DTF the particles are not in contact with a crucible surface. SEM images (Figure 9.6) and particle size analysis (Figure 9.2d) show that particles of coal D swelled in the DTF, the high fluidity did not lead to fragmentation at the residence times used here. DTF tests at longer residence times would ascertain whether coal D is able to attain higher swelling ratios than observed in these tests, and whether fragmentation begins to become an influential factor later in the process.

The higher heating rates experienced in the DTF enable some further analysis of the effect of heating rate by comparing HT-CSLM results with DTF results. The swelling ratio figures from the HT-CSLM at 440 °C have been used, as the swelling results between the two techniques correlate reasonably well at this

temperature. In Figure 9.15 the swelling ratios of coals A-C obtained by the two methods are plotted against heating rate. A DTF heating rate of 10^4 K/s is assumed. The magnitude of swelling ratios increases with heating rate. SEM images (Figures 9.3-9.6) show that some particles of all chars had reached a highly swollen state in the DTF with a smooth, rounded appearance. The gradients associated with coals B and C are similar, whilst coal A produced a similar gradient above 11.67 K/s (700 K/min). The results of coal C are taken as an example and superimposed on the graph produced by Shurtz *et al*., (2011), (Figure 9.16), which illustrates the concept of the optimum heating rate for swelling; there is consistency between the previously published results and those of this present work. Note that the results of the previous works were based on values of final swelling ratio.
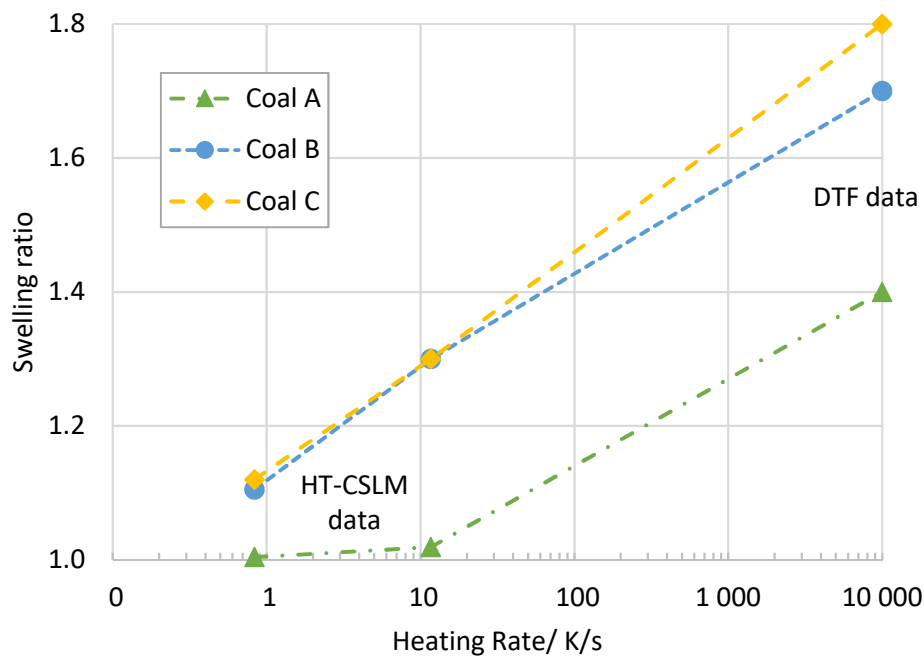
Figure 9.15: Effect of heating rate on swelling ratios of coals A-C.
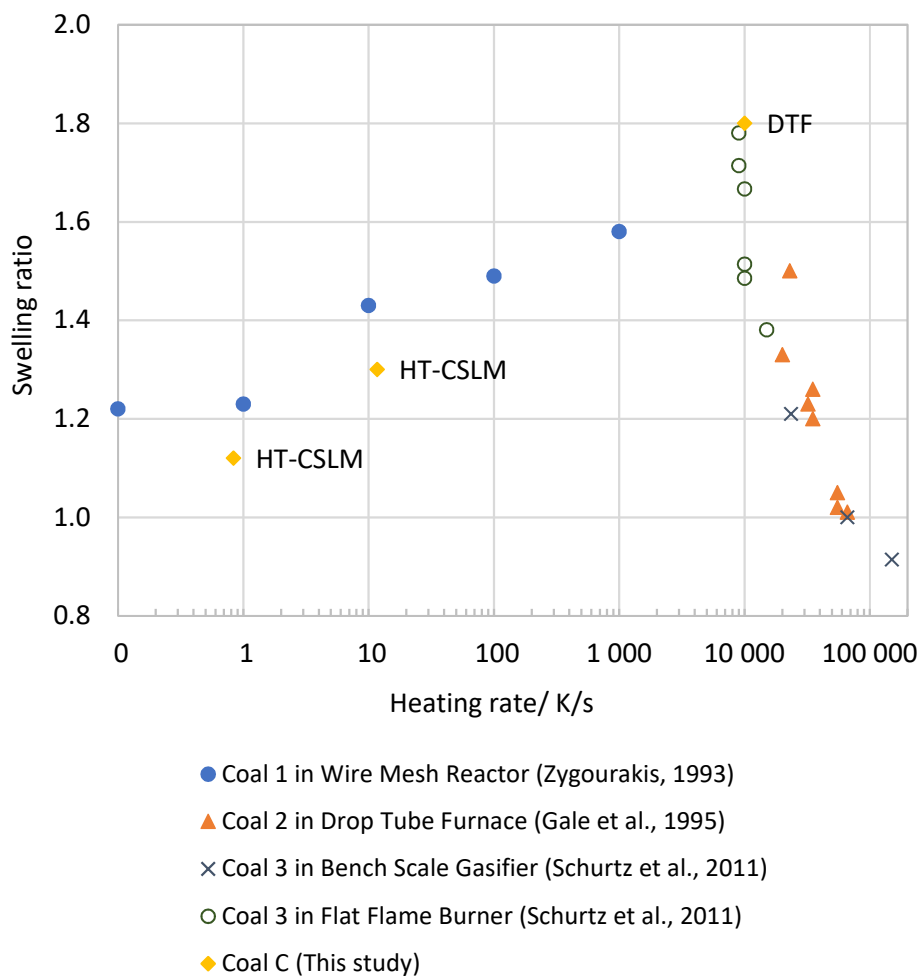
Figure 9.16: Swelling ratio of coal C in HT-CSLM and DTF overlaid on the graph produced by Shurtz *et al.*, (2011), showing the effect of heating rate on swelling ratio.

9.4.2 The influence of swelling on coal conversion and char reactivity

An aim of undertaking DTF tests was to investigate what effect swelling has on coal conversion and char reactivity. Although the higher levels of conversion are associated with the more highly swelling coals the conversion is essentially correlated with volatile matter. For example, coal B has a conversion in-line with what would be expected given its volatile matter content (in the context of the four coals studied here), yet it has a DTF swelling ratio close to coals C and D, which have higher levels of volatile matter and conversion, i.e. coal B's ability to

swell does not appear to have increased its conversion significantly. As mentioned above it is possible that char particles may not have reached their maximum swelling ratio at this residence time therefore it is possible that the swelling process may still influence conversion at higher residence times and temperatures.

Figure 9.8 shows that during DTF tests some Proximate volatile matter was not converted. On the other hand, Figure 9.7 shows that conversion levels for coals C and D, and one of the coal B duplicates, are greater than the Proximate volatile matter content. This is likely to be due to differences in heating conditions between the Proximate analysis test and the DTF. In the DTF particles experience much higher heating rates than in the Proximate test yet much shorter residence times and, it is suggested, a lower peak temperature than 900 °C. Higher heating rates supress secondary volatile matter reactions, therefore in the DTF the volatile matter may contain material which, under Proximate test conditions, would have remained within the coal and contributed to the fixed carbon value. Meanwhile some Proximate volatile matter may remain in the DTF char particles if the peak temperature was not high enough to cause this material to volatilise.

The order of char reactivity broadly follows the order of swelling ratio, i.e. higher swelling ratios are associated with higher reactivity index values, which would be expected due to the surface area increase. However, this is not a linear relationship because char D has a significantly greater reactivity index than char C, yet the swelling ratio of these samples is the same.

The results suggest that there are two reasons for this. Firstly, when chars C and D are crushed by pestle and mortar to moderate differences in morphology, char D has a slightly greater reactivity than char C. This implies that char D is composed of intrinsically more reactive material than char C.

Secondly char D appears to have a morphology, which allows great availability of reactive surface area to the gas. This is evidenced by an unexpected feature of char D, which is that it is more reactive in its uncrushed form than when crushed by pestle and mortar (Figure 9.12). Crushing creates a greater surface area to volume ratio, which would be expected to enhance reactivity, as in the case of

char C. However, the morphology of char D particles appears to be such that a greater surface area is available for reaction when uncrushed. It may be that the contact area between char particles, when placed in the crucible, is greater for crushed particles, thereby decreasing reactivity due to a reduction in surface area available for reaction. This may outweigh the benefits of increasing the total surface area in the case of char D.

The features of char D, which enhance its reactivity, are not necessarily revealed by the swelling ratio measurement, which is equivalent to that of char C. Bar-Ziv & Kantorovich, (2001), discussed the concept of 'reactive sites' within char particles, at which gas molecules will preferentially react. These were described as point defects such as crystal edges and joints between micro-crystals. The surface area of these sites does not develop in the same manner as total surface area, it was suggested. A greater availability of reactive sites within the coal D char particles may explain the greater reactivity of char D compared to char C.

It was observed that the more swollen particles of char A were more reactive than the average char A sample, this is likely to be due to surface area effects and also the fact that the swollen particles are derived from the more reactive components of the coal as discussed in chapter 7.

The results presented here indicate that coal D may perform well as a blast furnace injection coal as it has a high conversion at low residence times (higher than coal C, which has a higher volatile matter content) and the resulting char is highly reactive. It was also observed that coal D has a greater resistance to grinding than coals A-C (Table 4.3), indicating that greater resources would be required to crush coal D to the required size specification. On the other hand, this hardness may help to prevent the material handling problems that can arise from soft coals. However, the fluid properties of coal D are likely to make it a valuable coking coal, therefore its use as a PCI coal may be cost prohibitive.

9.5 Conclusions

The novel contribution made in this chapter is that the relative swelling behaviours of different coal types shows agreement (if certain assumptions are

made) when measured using the two different techniques; HT-CSLM technique and DTF.

The DTF has been used to provide a heating environment closer to the blast furnace raceway than the HT-CSLM to investigate how swelling patterns of coals A-D compare between the two techniques, and to investigate what effect swelling has on coal conversion and char reactivity.

The DTF swelling ratios were greater than the HT-CSLM swelling ratios, which is attributed to the higher heating rates in the DTF. Coal A has the lowest swelling ratio in both techniques. DTF peak temperatures may not have been sufficient, at 35 ms residence time, for coal B to achieve its maximum swelling ratio. **Hypothesis 6** – The swelling ratio observed by HT-CSLM correlates with that observed after DTF treatment, can only be accepted if assumptions are made regarding the effect of heating rate on the temperature of maximum swelling ratio, therefore further DTF tests at slightly longer residence times would be required to confirm the hypothesis. It was not possible to measure a meaningful swelling ratio for coal D using the HT-CSLM, however in the DTF coal D showed swelling and had the same swelling ratio as coal C at 35 ms.

The results provide no evidence that swelling is linked to greater levels of conversion than would be expected under the DTF conditions applied here. Fragmentation is also not observed for coals A-D at 35 ms. **Hypothesis 7a** – The rate of coal conversion is enhanced by particle swelling, is rejected.

The level of swelling can be linked to char reactivity to some extent. For example, char A has the lowest swelling ratio and the lowest reactivity. However, other factors must also influence char reactivity. For example, chars C and D have the same swelling ratio but different reactivities. **Hypothesis 7b** – The rate of char reactivity is enhanced by particle swelling, is accepted.

Differences in heating conditions between the DTF and the Proximate test means that material is not necessarily converted in the same way. For example, some Proximate volatile matter remains in the char samples after DTF tests, yet conversion is greater than the level of Proximate volatile matter in many cases.

10 Conclusions and further work

10.1 Conclusions

The novel contributions made in this work are summarised as follows:

- Novel application of the HT-CSLM to the field of coal particle swelling analysis.
- Observation of correlation between temperature of maximum swelling and the maximum Gieseler fluidity temperature.
- Observation of correlation between maximum swelling ratio and maximum Gieseler fluidity at low fluidity values.
- Experimental observation that the transient maximum swelling ratio increases with heating rate.
- Observation of correlation, within the density fractions of a particular coal, between maximum swelling ratio and the rate of mass loss at the temperature of maximum swelling.
- Finding that separation of particles according to density does not fully explain the variation in swelling behaviours observed within a parent coal sample.
- Novel approach to studying the effect of particle size on maximum swelling ratio, and the observation of greater maximum swelling ratio for larger particle sizes.
- Finding that the relative swelling behaviours of different coal types shows agreement (if certain assumptions are made) when measured using the two different techniques; HT-CSLM technique and DTF.

10.1.1 Application of HT-CSLM to the analysis of coal particle swelling

A novel technique, the HT-CSLM, has been applied to the measurement of the transient swelling properties of discrete coal particles by optical imaging in real time. This technique enables discrete, unconstrained particles to be observed, therefore the heating environment is more relevant to blast furnace coal injection

than traditional tests of coal thermoplasticity, which use packed volumes of particles, such as the Gieseler plastometer, Ruhr dilatometer and free swelling index tests.

The closely controlled heating rate associated with the HT-CSLM technique has enabled the effects of heating rate on the transient maximum swelling ratio of coal particles to be studied within the range of 50-700 K/min, with results obtained against precise temperature measurements. This is a differentiating feature of this technique compared to, for example, the Single Particle Reactor (Yu *et al*., 2003). Another differentiating feature is the ability to observe several particles simultaneously, which assists in obtaining representative results from samples in which a wide variety of swelling behaviours exist. In some instances, this has enabled sub-groups of different behaviours to be identified within a sample. The analysis of particles from the 38-53 μm sieve fraction has been achieved, which is a smaller particle size than previously reported for comparable techniques (Yu *et al*., 2003) (63-90 μm) and (Gao *et al*., 1997) (100-355 μm)). There is a limitation to the technique with regard to highly fluid coals, which deform so that a true particle size cannot be measured. When heated in a DTF environment the high fluidity coal showed true swelling behaviour and produced particles with swollen structures such as cenospheres.

Particles were heated up to 700 °C during HT-CSLM tests, during this temperature range a general pattern of behaviour was observed that is consistent with the observations of other researchers. This involves:

- Initial swelling of particles via a series of oscillations in particle size, which are attributed to bubble growth and rupture.
- Attainment of a transient maximum swelling ratio followed by shrinkage, which may initially be rapid and associated with oscillations in particle size.
- A reduction in the rate of shrinkage and cessation of oscillations. None of the samples showed a completely stable mean swelling ratio by 700 °C, i.e. on average some shrinkage was still occurring at this temperature.

The HT-CSLM technique was applied to four coal types revealing differences in their swelling properties. Results were compared with standard Gieseler plasometer and Ruhr dilatometer test results, which showed that a coal with no standard thermoplastic properties may exhibit swelling under HT-CSLM conditions, and that swelling can be observed at temperatures lower than the Gieseler and Ruhr dilatometer softening temperatures. The temperature of Gieseler maximum fluidity was found to be a good indicator as to the temperature of maximum swelling ratio, and a correlation between maximum HT-CSLM swelling ratio and maximum Gieseler fluidity was observed within the fluidity range of 0-7 ddpm. This extended the range of fluidity values over which the correlation with maximum swelling ratio has been observed.

10.1.2   The effect of heating rate

The effect of heating rate on maximum swelling ratio was investigated within the range 50-700 K/min. Increasing the heating rate from 50 K/min to 700 K/min has been shown to increase the transient maximum swelling ratio and the rate of swelling, the extent of this increase is coal dependent. The swelling onset temperature, the temperature of peak swelling ratio and the rate of shrinkage following peak swelling ratio are not significantly affected by heating rate within the range studied here. The effect of heating rate has previously been studied by other researchers, but most other work has looked at the effect on final swelling ratio rather than the transient maximum swelling ratio. In the current work the increase in heating rate was found to influence transient maximum swelling ratio and final swelling ratio (at 700 °C) by the same degree. It was also observed that increasing the heating rate had a greater effect on the coals with a higher Gieseler fluidity.

10.1.3   Effect of particle density

Separation of pulverised coal particles by sink-float centrifugation has been used, in conjunction with HT-CSLM, to investigate the effects of particle density on the transient swelling properties of particles of two coals which have similar Proximate and Ultimate analyses. Lighter particles within a coal, which contain higher levels of vitrinite and liptinite, have shown greater swelling properties than

the denser, lesser-swelling particles, which contain more inertinite and mineral matter. This agrees with previous research (Tsai & Scaroni, 1987 and Yu *et al.*, 2003). In addition, comparison between the coal types in this work shows that the less dense coal produces higher levels of swelling than the denser coal. In the case of the denser, lesser-swelling coal, differences between density fractions cannot be attributed to differences in the vitrinite to inertinite ratio (because this remains relatively constant), however the presence of a strong vitrinite reflectance peak centred around the reflectance groups 13-16 can be associated with greater levels of swelling in both coals.

As the swelling process is driven by the generation of gaseous volatile matter the rate of mass loss from coal samples heated at 50 K/min was measured using TGA and compared with HT-CSLM results obtained at the same heating rate. It was observed that swelling can begin to occur before a significant increase in the rate of mass loss, and that the maximum swelling ratio occurs during the initial rapid increase in the rate of mass loss associated with primary devolatilisation. The peak rate of mass loss occurs after the maximum swelling ratio has passed and there is some evidence for the peak swelling ratio coinciding with the temperature at which the rate of gas evolution decreases and the rate of tar evolution increases. The peak rate of mass loss then coincides with the temperature at which the rate of shrinkage decreases. The rate of mass loss of density fractions of two coals was measured and within each coal type the rate of mass loss at the temperature of maximum swelling ratio broadly reflected the extent of swelling within that coal (note that swelling was measured at 700 K/min in these latter tests and the rate of mass loss measured at 50 K/min).

10.1.4   Effect of particle size

The effect of particle size on swelling has been investigated. Wet sieving and sink-float centrifugation have been used to create three size and density separated fractions of coal particles, which have distinctly different particle sizes but similar properties in terms of Proximate and Ultimate analyses, Gieseler fluidity and petrography. HT-CSLM has been used to measure the transient swelling behaviours of these particles. Two coals were studied; one of these coals showed

an increasing maximum swelling ratio with increasing particle size, which is attributed to the increased resistance to volatile matter release, because of the lower surface area to volume ratio, resulting in an increased pressure build-up within the particles. However, for the other coal the middle size fraction showed the greatest swelling ratio, which suggests the possibility of an optimum particle size in relation to maximum swelling ratio. This would echo the effect of ambient pressure, for which there is also an optimum for coal particle swelling, and which the effect of particle size has been likened to.

Although the conclusions above have been drawn, the results provide the possibility of an alternative explanation. This is that the exclusion of a small number of particles from the mean results of the small and middle-sized particle fractions (due to loss of true particle form) resulted in the lower swelling ratios of these samples.

The relative standard deviation (RSD) of swelling ratio values at and around the temperature of maximum swelling ratio was used as a measure of the heterogeneity of swelling behaviours within samples. Samples with a higher mean swelling ratio were found to have a greater RSD, whilst smaller particle sizes were also associated with increased RSD values when samples of similar mean swelling ratio were compared. When studying the smaller particle sizes, it was possible to identify two sub-groups within the samples; these were essentially groups of greater-swelling and lesser-swelling particles. The relative abundance of particles within each group and the magnitude of swelling or shrinkage exhibited by each group determined the overall mean swelling behaviour of the sample.

10.1.5   Comparison with DTF tests

The drop tube furnace (DTF) has been used to provide a heating environment closer to the blast furnace raceway than that provided by the HT-CSLM. The aim was to investigate how swelling patterns of coals A-D compare between the two techniques, and to investigate what effect swelling has on coal conversion and char reactivity. The DTF swelling ratios were greater than the HT-CSLM swelling ratios, which is attributed to the higher heating rates in the DTF. The DTF results implied that the particles did not reach the DTF operating temperature of 1100 °C

during the 35 ms residence time and may have reached temperatures in the region of 535 °C. When assumptions are made about the effects of heating rate on the temperature of maximum swelling ratio there is good agreement between the HT-CSLM results and DTF results. Results of swelling ratio measurements from DTF tests were combined with HT-CSLM results at 440 °C to show a trend of increasing swelling ratio with increasing heating rate between 50 K/min and 10^4 K/s, which is consistent with previously published work.

The DTF results show that conversion essentially correlates with coal Proximate volatile matter, therefore these results do not indicate that higher levels of swelling produce increased rates of conversion at low residence times. There is evidence to suggest that char reactivity is enhanced by swelling, which can be attributed to an increased char surface area, however it is also evident that other factors are also influential in determining char reactivity.

10.1.6   Industrial Relevance

The specific impacts of the coal particle swelling process upon blast furnace performance are still not fully understood. Here, these potential impacts are discussed in more detail. Figure 10.1 illustrates the specific phenomena resulting from coal particle swelling, how each of these may impact upon blast furnace operations and the likely consequences of these impacts.
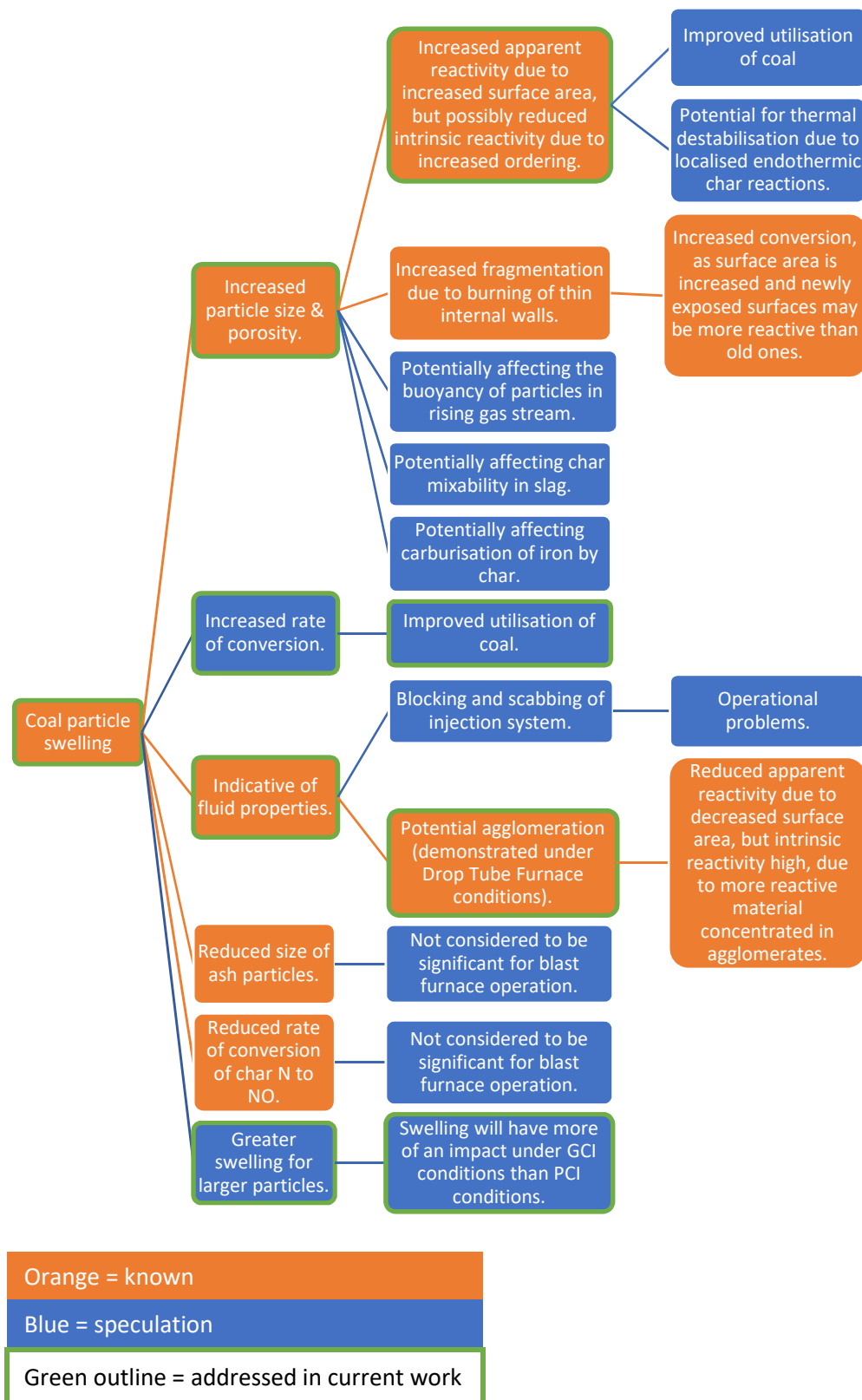
Figure 10.1: The implications of coal swelling, and potential consequences for the blast furnace.

The increase in particle size and porosity resulting from swelling will enhance apparent char reactivity due to increased surface area. Intrinsic reactivity may be decreased due to increased ordering; however, the apparent reactivity is of greater relevance to the blast furnace. This increased reactivity will improve coal utilisation although there is a potential for thermal destabilisation due to localised endothermic char reactions.

The increased char particle size resulting from swelling coals may increase the volume occupied per unit mass of unreacted char within the blast furnace. A larger volume occupied by this char may contribute to poor burden permeability. As a result of this work, a study on this topic will be carried out at the Materials Processing Institute.

The highly porous structure arising from swelling will facilitate increased char fragmentation due to burning of thin internal walls and reduced resistance to impact. This would increase conversion by increasing surface area and creating newly exposed surfaces, thereby improving coal utilisation. The high porosity and low density of swollen char particles may also affect the buoyancy of char particles in the upwardly moving gas streams within the furnace. Cenospheres may be more easily entrained in the gas and therefore carried out of the furnace top, or alternatively may be more easily filtered out by the burden materials and remain in the furnace. This would give them the opportunity to react and produce reducing gasses, yet excessive build-up of unburnt char is likely to negatively affect furnace permeability.

A piece of work, resulting from this project, is planned to be undertaken at Tata Steel IJmuiden. Historical data will be analysed to see if there is a correlation between the quantity of fine material recovered from blast furnace top gas and the maximum Gieseler fluidity of injection coals being used at the time. A correlation may indicate that the greater the swelling properties of the injection coal, the more likely its char is to become entrained in the top gas.

Char particles may potentially interact with liquid slag or liquid iron within the blast furnace. The morphology of char particles may influence the nature of these interactions, for example the diameter of char particles would affect the number

of particles able to adsorb to the surface of a slag droplet. Further work on the interactions between char particles and blast furnace slag is taking place at the Materials Processing Institute, including a study of the effects of char particle morphology.

The swelling of coal particles enables a particular mechanism of devolatilisation to occur in the early stages of combustion, i.e. bubble formation and rupture as opposed to pore diffusion. Whilst there is no evidence in this work to suggest that this alters the overall rate of conversion, this possibility should not be discounted, as a larger number of coals would need to be investigated to confirm this trend. It may be possible that coal swelling enhances the rate of conversion and therefore improves coal utilisation.

The phenomenon of swelling is indicative of coal thermoplastic properties, which may have other implications for the blast furnace. These include blocking or scabbing of the injection system during the injection process, and agglomeration of particles, both of which are negative issues for the blast furnace.

The increased tendency of larger particles to undergo swelling, as indicated by this work, would provide a reason why the same coal may behave differently under PCI conditions compared to GCI conditions. The larger particle sizes associated with GCI would lead to a greater degree of swelling. Any of the previously mentioned consequences of swelling would therefore be magnified by the use of coarser particles.

10.1.7   Summary

In summary, the HT-CSLM technique has been introduced as a suitable technique for the study of the transient swelling behaviour of discrete coal particles observed by optical imaging in real time. The technique is able to distinguish the behaviours of different coal types although there is a limitation with regard to high fluidity coals. This technique has illustrated the effect of heating rate on transient maximum swelling ratio up to 700 K/min and the measurement of small particles of 38-53 μm has been demonstrated. Some relationships between swelling behaviour and Gieseler fluidity and rate of mass loss (measured by TGA)

have been observed. A common petrographic feature associated with high-swelling samples is a strong vitrinite reflectance peak centred around the reflectance groups 14-16. The effect of particle size has been investigated, producing evidence for increasing maximum swelling ratio with increasing particle size and also for the possibility for an optimum particle size. DTF tests produced no evidence to suggest that swelling behaviour is associated with unexpectedly high conversion rates at low residence times, however increased char reactivity due to increased surface area does appear to be an impact of the swelling process.

10.2   Further work

1. The HT-CSLM technique has been shown to be suitable for measuring the transient swelling properties of coal particles. A means of further developing the technique would be to automate the image analysis process, which has so far been carried out manually. This would greatly increase the speed of analysis and enable larger numbers of particles to be studied. Some work may be required to develop a means of reliably creating a clear contrast between particle and crucible base, which can, at times, be indistinct.

2. In this work, the smallest particle size range studied was 38-53 µm. It should be possible to analyse even smaller particles as the magnification of the microscope will allow this. This would be relevant to the industrial process as ~60 wt. % of particles fall below 38 µm in size in a sample of pulverised injection coal.

3. The fluidity of coals has been shown to be a limiting factor when studying the swelling properties of coal particles using HT-CSLM, however it is not known where the limit is. This work has only shown that it is somewhere between 7 ddpm and 3433 ddpm.

4. A correlation between maximum swelling ratio and Gieseler fluidity has been observed amongst three coal types in this work, however these coals represent a narrow range of low fluidity coals (0-7 ddpm). The limits of this

correlation could be further investigated with the potential that it may be possible to predict maximum swelling ratio from the Gieseler fluidity test.

5. The effects of coal particle density on swelling have been investigated and results have been related to mineral and maceral content. Another factor, which will influence the density of a coal particle, is the presence of enclosed porosity. This may influence swelling behaviour as swelling is concerned with the development of pores. An influence of enclosed porosity may, for example, help to explain why the lightest particles of coal B do not have the lowest ash content or lowest inertinite content, and do not have the highest swelling ratio, which would be in line with the general trend.

6. The effect of particle size has been investigated, with measures taken to eliminate the effects of varying maceral composition between size fractions. The results indicate the possibility of an optimum particle size for particle swelling. This could be investigated further by using larger particle size fractions of coal B to discover the optimum (if it exists), and also by including another coal type in the investigation. The possibility that the lower swelling ratios of smaller particles is caused by the exclusion of highly fluid particles from the sample mean should also be investigated. This knowledge could improve our understanding of the different behaviours of coals under granular and pulverised blast furnace injection conditions.

7. The HT-CSLM swelling ratio results of three coals have been shown to scale-up to DTF conditions based on assumptions regarding the temperature that the particles reached in the DTF. Further DTF work at slightly longer residence times could validate this assumption. Longer residence times and therefore higher temperatures would reveal whether coal B particles achieve a higher maximum swelling ratio than coal C at the higher temperatures. The ability to vary the DTF residence times by small incremental changes in the position of the collector probe would enable the progression of particle swelling during DTF processing to be investigated in some detail.

8. This work has indicated that the process of coal particle swelling may not be associated with greater than expected levels of conversion at short residence times although there are benefits in terms of increased char surface area available for gasification reaction. Obtaining a full understanding of how coal particle swelling influences the success of that coal as an auxiliary blast furnace reductant is a potential subject area for further research. For example, the injection process itself may be affected if particles begin to swell before entering the raceway, and the lifecycle of particles within the blast furnace as a whole may be influenced by the size and density of char particles. Models of the blast furnace injection process may be improved by incorporating the specific swelling behaviours of coals. A potentially influential factor for blast furnace permeability and performance may be the total volume within the furnace occupied by non-combusted coal char. The swelling of coal particles would be a relevant factor to consider here, although many other factors such as coal burnout, char consumption, fragmentation and char carryover would also need to be quantified under blast furnace conditions to enable the volume of residual char to be calculated.

9. Finally, the precision and accuracy of predicting coal particle swelling behaviour from fundamental properties of the coals can be improved. The HT-CSLM technique presented in this work may provide experimental results for assisting validation of modelling work on this subject.

11 References

Alonso, M. J. G., Borrego, A. G., Alvarez, D. & Menéndez, R. (1999), "Pyrolysis Behaviour of Pulverised Coals at Different Temperatures", Fuel, Vol. 78, pp. 1501-1513.

Arenillas, A., Rubiera, F., Pisa, J.J., Jones, J.M. & Williams, A. (1999), **"**The Effect of the Textural Properties of Bituminous Coal Chars on NO Emissions", Fuel, Vol. 14, pp. 1779-1785.

Bar-Ziv & Kantorovich, (2001), "Mutual Effects of Porosity and Reactivity in Char Oxidation", Progress in Energy & Combustion Science, Vol. 27, pp. 667-697.

Barnes, N., Clark, S., Seetharaman, S., Mendeza, P.F. (2018), "Growth Mechanism of Primary Needles During the Solidification of Chromium Carbide Overlays", Acta Materialia, Vol. 151, pp. 356-365.

Barriocanal, C., Díez, M.A., Alvarez, R., Casal, M.D. & Canga, C.S. (2003), "On the Relationship Between Coal Plasticity and Thermogravimetric Analysis", Journal of Analytical and Applied Pyrolysis, Vol. 67, pp. 23-40.

Bharadwaj, A., Arunachalam, V. S., Sridhar, S. & Wang, Y. (2004), "Pyrolysis of Rice Husk", Current Science, Vol. 87, pp. 981-986.

Carpenter, A.M. (2006), "Use of PCI in Blast Furnaces", IEA Coal Research publications, Vol. 116, IEA Clean Coal Centre, ISBN 9290294329.

Chen, W-H., Du, S-W. & Yang, T-H. (2007), "Volatile Release and Particle Formation Characteristics of Injected Pulverized Coal in Blast Furnaces", Energy Conversion and Management, Vol. 48, pp. 2025-2033.

Cloke, M., Lester, E. & Belghazi A. (2002), "Characterisation of the Properties of Size Fractions from Ten World Coals and their Chars Produced in a Drop-Tube Furnace", Fuel, Vol. 81, pp. 699-708.

Coetzee, C., Neomagnus, H.W.J.P., Brunt, J.R., Strydom, C.A. & Schobert, H.H. (2014), "The Transient Swelling Behaviour of Large (-20 +16 mm) South African Coal Particles During Low-Temperature Devolatilisation", Fuel, Vol. 136, pp. 79-88.

Dakič, D., Honing, G vd. & Valk, M. (1998), "Fragmentation and Swelling of Various Coals During Devolatlization in a Fluidized Bed", Fuel, Vol. 68, pp. 911-916.

Du, S.W., Chen, W.H. & Lucas, J.A. (2010) "Pulverized Coal Burnout in Blast Furnace Simulated by a Drop Tube Furnace", Energy, Vol. 35, pp. 576-581.

Fletcher, T. H. (1993), "Swelling Properties of Coal Chars During Rapid Pyrolysis and Combustion", Fuel, Vol. 72, pp. 1485-1495.

Fong, W. S., Khalil, Y. F., Peters. W. A. & Howard, J. B. (1986), "Plastic Behaviour of Coal under Rapid-Heating High-Temperature Conditions", Vol. 65, pp. 195-201.

Fu, Z., Guo, Z., Yuan, Z. & Wang, Z. (2007), "Swelling and Shrinkage Behaviour of Raw and Processed Coals During Pyrolysis", Fuel, Vol. 86, pp. 418-425.

Gao, H., Murata, S. & Nomura, M. (1997), "Experimental Observation and Image Analysis for Evaluation of Swelling and Fluidity of Single Coal Particles Heated with CO_2 Laser", Energy & Fuels, Vol. 11, pp. 730-738.

Gale, T. K., Bartholomew, C. H. & Fletcher, T. H. (1995), "Decreases in the Swelling and Porosity of Bituminous Coals During Devolatilisation at High Heating Rates", Combustion and Flame, Vol. 100, pp. 94-100.

Geerdes, M., Toxopeus, H. & van der Vliet, C. (2009), "Modern Blast Furnace Ironmaking: An Introduction", 2nd edition, IOS Press, Amsterdam.

Giroux, L., Charland, J.-P. & MacPhee, J. A. (2006), "Application of Thermogravimetric Fourier Transform Infrared Spectroscopy (TG-FTIR) to the Analysis of Oxygen Functional Groups in Coal", Energy & Fuels, Vol. 20, pp. 1988-1996.

Greenslade, M. & Paskins, M. (2014), Tata Steel Europe, Personal communication.

Gu, J., Wu, S., Wu, Y., Li, Y. & Gao, J. (2008), "Differences in Gasification Behaviours and Related Properties Between Entrained Gasifier Fly Ash and Coal Char", Energy & Fuels, Vol. 22, pp. 4029-4033.

Hayhurst, A. N. & Lawrence, A. D. (1995), "The Devolatilization of Coal and a Comparison of Chars Produced in Oxidizing and Inert Atmospheres in Fluidized Beds", Combustion & Flame, Vol. 100, pp. 591-604.

Hechu, K., Slater, C., Santillana, B., Clark, S., Sridhar, S. (2017), "A Novel Approach for Interpreting the Solidification Behaviour of Peritectic Steels by Combining CSLM and DSC", Materials Characterization, Vol. 133, PP. 25-32.

Hippo, E. & Walker, P. L. (1975), "Reactivity of Heat-Treated Coals in Carbon Dioxide at 900 °C", Fuel, Vol. 54, pp. 246-248.

Kalkreuth, W., Borrego, A.G., Alvarez, D., Menendez, R., Osorio, E., Ribas, M., Vilela, A. & Cardozo Alves, T. (2005), "Exploring the Possibilities of Using Brazilian Subbituminous Coals for Blast Furnace Pulverized Fuel Injection", Fuel, Vol. 84, pp. 763-772.

Katjitani, S., Har, S. & Matsuda, H. (2002), "Gasification Rate Analysis of Coal Char with a Pressurized Drop Tube Furnace", Fuel, Vol. 81, pp. 539-546.

Khan, M. R. & Jenkins, R. G. (1986), "Swelling and Plastic Properties of Coal Devolatilized at Elevated Pressures: An Examination of the Influences of Coal Type", Fuel, Vol. 65, pp. 725-731.

Kidena, K., Murata, S. & Nomura, M. (1996), "Studies on the Chemical Structural Change during Carbonization Process", Energy & Fuels, Vol. 10, pp. 672–678.

Lee, C. W., Scaroni, A. W. & Jenkins, R. G. (1991), "Effect of Pressure on the Devolatilisation and Swelling Behaviour of a Softening Coal During Rapid Heating", Fuel, Vol. 70, pp. 957-965.

Li, H., Elliott, L., Rogers, H. & Wall, T. (2014), "Comparative Study on the Combustion Performance of Coals on a Pilot-Scale Test Rig Simulating Blast Furnace Pulverized Coal Injection and Lab-Scale Drop-Tube Furnace", Energy & Fuels, Vol. 28, pp. 363-368.

Loison, R., Foch, P. & Boyer, A. (1989), "Coke, Quality and Production", Butterworth-Heinemann, Great Britain, ISBN: 978-0-408-02870-7.

Lu, L., Sahajwalla, V. & Harris, D. (2000), "Characteristics of Chars Prepared from Various Pulverized Coals at Different Temperatures Using Drop-Tube Furnace", Energy & Fuels, Vol. 14, pp. 869–876.

Lungen, H.B. (2015), "Ironmaking in Western Europe – Status quo and future trends", METEC and 2nd European Steel Technology and Application Days (ESTAD) Conference, Dusseldorf, June 2015.

Mathieson, J.G., Truelove, J.S. & Rogers, H. (2005), "Toward an Understanding of Coal Combustion in Blast Furnace Tuyere Injection", Fuel, Vol. 84, pp. 1229-1237.

Menéndez, R., Vleeskens, J. M. & Marsh, H. (1993), "The use of Scanning Electron Microscopy for Classification of Coal Chars during Combustion", Fuel, Vol. 72, pp. 611-617.

Mochizuki, Y., Ono, Y., Uebo, K. & Tsubouchi, N. (2013), "The Fate of Sulfur in Coal During Carbonization and its Effect on Coal Fluidity", International Journal of Coal Geology, Vol. 120, pp. 50-56.

Murai, R., Asanuma, M., Sato, M., Inoguchi, T. & Terada, K. (2015), "Flow Behavior of Plastic Particles in the Lower Part of Blast Furnace", ISIJ International, Vol. 55, pp. 528-535.

Murata, S., Sako, T., Yokoyama, T., Gao, H., Kidena, K. & Nomura, M. (2008), "Kinetic Study on Solvent Swelling of Coal Particles", Fuel Processing Technology, Vol. 89, pp. 434-439.

Muto, M., Tanno, K. & Kurose, R. (2016), "A DNS Study on Effect of Coal Particle Swelling due to Devolatilization on Pulverized Coal Jet Flame", Fuel, Vol. 184, pp. 749-752.

Nomura, S., & Thomas, M. (1996), "Some Aspects of the Generation of Coking Pressure During Coal Carbonization", Fuel, Vol. 75, pp. 801-808.

Pauliuk, S., Milford, R.L., Müller, D.B. & Allwood, J.M. (2013), "The Steel Scrap Age", Environmental Science & Technology, Vol. 47, pp. 3448–3454.

Rogers, H. & Wall, T. (2011), "Review of Ironmaking Blast Furnace Pulverised Coal Injection Combustion Testing", Australian Coal Association Research Program (ACARP), Brisbane, Queensland, Australia, Project C19049.

Ross, D. P., Heidenreich C. A. & Zhang, D. K. (2000), "Devolatilisation Times of Coal Particles in a Fluidised-Bed", Fuel, Vol. 79, pp. 873-883.

Russell, N. V., Gibbins, J. R., Man, C. K. & Williamson, J. (2000), "Coal Char Thermal Deactivation under Pulverized Fuel Combustion Conditions", Energy & Fuels, Vol. 14, pp. 883-888.

Sahu, S.G., Mukherjee, A., Kumar, M., Adak, A.K., Sarkar, P., Biswas, S., Tiwari, H.P., Das, A. & Banerjee P.K. (2014), "Evaluation of Combustion Behaviour of Coal Blends for Use in Pulverized Coal Injection (PCI)", Applied Thermal Engineering, Vol. 73, pp. 1014-1021.

Saxena, S.C. (1990), "Devolatilization and Combustion Characteristics of Coal Particles", Progress in Energy and Combustion Science, Vol. 16, pp. 55-94.

Sexton, D. (2016), "Investigating the Effects of Char Physical Structure on Blast Furnace Coal Injection Performance", paper presented to the 11th European Conference on Coal Research and its Applications (ECCRIA), University of Sheffield, 5th-7th September 2016.

Sexton, D.C., Steer, J.M., Marsh, R. & Greenslade, M. (2018), "Investigating Char Agglomeration in Blast Furnace Coal Injection", Fuel Processing Technology, Vol. 178, pp. 24-34.

Shibata, H., Yin, H., Emi, T. & Earnshaw J.C. (1998), "The Capillary Effect Promoting Collision and Agglomeration of Inclusion Particles at the Inert Gas-Steel Interface" [and Discussion], Philosophical Transactions: Mathematical, Physical and Engineering Sciences, Vol. 356, pp. 957-966.

Shibata, H., Arai, Y., Suzuki, M., & Emi, T. (2000), "Kinetics of Peritectic Reaction and Transformation in Fe-C Alloys", Metallurgical and Materials Transactions B, Vol. 31, pp. 981-991.

Shurtz, R. C., Kolste, K. K. & Fletcher, T. H. (2011), "Coal Swelling Model for High Heating Rate Pyrolysis Applications", Energy & Fuels, Vol. 25, pp. 2163–2173.

Slater, C., Hechu, K., Sridhar, S. (2017), "Characterisation of Solidification using Combined Confocal Scanning Laser Microscopy with Infrared Thermography", Materials Characterization, Vol. 126, PP. 144-148

Smith, M. (2017), **"**Blast Furnace Ironmaking – A View on Future Developments", Procedia Engineering, Vol. 174, pp. 19-28.

Solomon, P. R., Hamblen, D. G., Carangelo, R. M., Serio, M. A. & Deshpande, G. V. (1988), "General Model of Coal Devolatilization", Energy & Fuels, Vol. 2, pp. 405-422.

Solomon, P. R., Serio, M. A. & Suuberg, E. M. (1992), "Coal Pyrolysis: Experiments, Kinetic Rates and Mechanisms", Progress in Energy and Combustion Science, Vol. 18, pp. 133-220.

Soskovets, O. N., Shevelev, L. N., Shatlov, V. A., Marsuverskii, B. A., Eremin, V. I., Roginko, S. A. (2014), "Improving the Energy Efficiency of Blast Furnaces by Means of Hot Reducing Gases", Steel in Translation, Vol. 44, pp. 394-398.

Spooner, S., Li, Z. & Sridhar, S. (2017a), "Spontaneous Emulsification as a Function of Material Exchange", Nature Scientific Reports.

Spooner, S., Rahnama, A., Warnett, J. M., Williams, M. A., Li, Z., Sridhar, S. (2017b), "Quantifying the Pathway and Predicting Spontaneous Emulsification

during Material Exchange in a Two Phase Liquid System", Nature Scientific Reports.

Steer, J. M., Marsh, R., Greenslade, M. & Robinson, A. (2015a) "Opportunities to Improve the Utilisation of Granulated Coals for Blast Furnace Injection", Fuel, Vol. 151, pp. 40-49.

Steer, J. M., Marsh, R., Morgan, D. & Greenslade, M. (2015b), "The Effects of Particle Grinding on the Burnout and Surface Chemistry of Coals in a Drop Tube Furnace", Fuel, Vol. 160, pp. 413-423.

Steer, J. M., Marsh, R., Sexton, D., & Greenslade, M. (2018), "A Comparison of Partially Burnt Coal Chars and the Implications of their Properties on the Blast Furnace Process", Fuel Processing Technology, Vol. 176, pp. 230-239.

Strezov, V., Lucas, J.A. & Wall, T.F. (2005), "Effect of Pressure on the Swelling of Density Separated Coal Particles", Fuel, Vol. 84, pp. 1238-1245.

Stubington J. F. & Linjewile, T. M. (1989), "The Effects of Fragmentation on Devolatilization of Large Coal Particles", Fuel, Vol. 68, pp. 155-160.

Suárez-Riaz, I. & Crelling, J. (2008), "Applied Coal Petrology", Elsevier Academic Press, United Kingdom, ISBN: 9780080450513.

Tian, B., Qiao, Y-y., Tian, Y-y. & Liu, Q. (2016), "Investigation on the Effect of Particle Size and Heating Rate on Pyrolysis Characteristics of a Bituminous Coal by TG-FTIR", Journal of Analytical Applied Pyrolysis, Vol. 121, pp. 376-386.

Toishi, A., Yamazaki, Y., Uchida, A., Saito, Y., Aoki, H., Nomura, S., Arima, T., Kubota, Y. & Hayashizaki, H. (2013), "Quantitative Evaluation for Relationship between Development of Pore Structure and Swelling of Coal in Carbonization of Single Coal Particle", ISIJ International, Vol. 53, pp. 1739-1748.

Tsai, C-Y. & Scaroni, A.W. (1987), "The Structural Changes of Bituminous Coal Particles During the Initial Stages of Pulverized-coal Combustion", Fuel, Vol. 66, pp. 200-206.

Wall, T. F., Liu, G., Wu, H., Roberts, D. G., Benfell, K. E., Gupta, S., Lucas, J. A. & Harris, D. J. (2002), "The Effects of Pressure on Coal Reactions During Pulverised Coal Combustion and Gasification", Progress in Energy and Combustion Science, Vol. 28, pp. 405-433.

Wang, C., Ryman, C. & Dahl, J. (2009), "Potential CO_2 Emission Reduction for BF–BOF Steelmaking Based on Optimised Use of Ferrous Burden Materials", Vol. 3, pp. 29-38.

Whitehouse, M. (1992), "Operating Manual for the Drop Tube Furnace", British Coal Corporation, Cheltenham, Power Generation Branch Report No. 181.

World Steel Association, (2014), [Online], (https://www.worldsteel.org/media-centre/press-releases/2014/New-video-campaign-highlights-the-positive-contribution-of-the-steel-industry-globally.html), (Accessed 11th July 2018).

World Steel Association, (2018), "Fact Sheet, Energy Use in the Steel Industry", [Online], (https://www.worldsteel.org/publications/fact-sheets), (Accessed 9th July 2018).

Wu, H., Wall, T., Liu, G. & Bryant, G. (1999), "Ash Liberation from Included Minerals during Combustion of Pulverized Coal: The Relationship with Char Structure and Burnout", Energy & Fuels, Vol. 13, pp. 1197-1202.

Wu, H., Bryant, G., Benfell, K. & Wall, T. (2000), "An Experimental Study on the Effect of System Pressure on Char Structure of an Australian Bituminous Coal", Energy & Fuels, Vol. 14, pp. 282-290.

Wu, Z. (2005), "Fundamentals of Pulverised Coal Combustion", IEA Clean Coal Centre, ISBN 92-9029-410-8.

Yang, H., Li, Sufen., Fletcher, T.H. & Dong, M., (2014), "Simulation of the Swelling of High-Volatile Bituminous Coal during Pyrolysis", Energy & Fuels, Vol. 28, pp. 7216-7226.

Yoshizawa, N., Maruyama, K., Yamashita, T. & Akimoto, A. (2006), "Dependence of Microscopic Structures and Swelling Property of DTF Chars Upon Heat-Treatment Temperature", Fuel, Vol. 85, pp. 2064-2070.

Yu, D., Xu, M., Yu, Y. & Liu, X. (2005), "Swelling Behavior of a Chinese Bituminous Coal at Different Pyrolysis Temperatures", Energy & Fuels, Vol. 19, pp. 2488-2494.

Yu, J., Strezov, V., Lucas, J., Liu, G.-S. & Wall, T. (2002), "A Mechanistic Study on Char Structure Evolution during Coal Devolatilisation – Experiments and Model Predictions", Proceedings of the Combustion Institute, Vol. 29, pp. 467-473.

Yu, J., Strezov, V., Lucas, J. & Wall, T. (2003), "Swelling Behaviour of Individual Coal Particles in the Single Particle Reactor", Fuel, Vol. 82, pp. 1977-1987.

Yu, J., Lucas, J.A. & Wall, T. (2007), "Formation of the Structure of Chars during Devolatilisation of Pulverized Coal and its Thermoproperties: A Review", Progress in Energy and Combustion Science, Vol. 33, pp. 135-170.

Zeng, D., Clark, M., Gunderson, T., Hecker, W. C. & Fletcher, T. H. (2005), "Swelling Properties and Intrinsic Reactivities of Coal Chars Produced at Elevated Pressures and High Heating Rates", Proceedings of the Combustion Institute, Vol. 30, pp. 2213-2221.

Zygourakis, K. (1993), "Effect of Pyrolysis Conditions on the Macropore Structure of Coal-Derived Chars", Energy & Fuels, Vol. 7, pp. 33-41.

Appendix A

Introduction to coal macerals

Coal was formed from plant material that died around 300 million years ago at a time when swamps covered much of the earth. As plants died their remains sank to the bottom of swamps and were prevented from decomposing in the oxygen-poor environment. Accumulation of plant material led to the formation of peat (peatification), which could slowly be transformed into coal (coalification) under the effects of heat and pressure when buried at great depths.

The manner in which coal has been formed leads to the existence of a wide variety of coal types, and results in heterogeneity within each specific coal. The classification of different components within the coal is used as a means of characterising coals types. Macerals are the microscopic organic components of coal, they are the coalified remains of different types of organic plant material, or plant-derived substances, existing at the time of peat formation (Suárez-Riaz & Crelling, 2008).

Macerals are classified into three groups: vitrinite, inertinite and liptinite. Further levels of sub-division exist within each group, which are not referred to in this work. Vitrinite is usually the most abundant maceral type within a coal, macerals of the vitrinite group are mainly derived from plant cell wall material i.e. from polymers such as cellulose and lignite. The chemical structure of vitrinites is typically, aromatic, hydroaromatic or polyaromatic. Inertinite macerals are derived from material that has been strongly altered, oxidised or degraded either prior to burial or during the peat stage. Chemically, inertinite macerals have a high degree of aromatisation and condensation, and high levels of cross-linking. They have the highest carbon content of the three groups and the lowest hydrogen and oxygen contents. Inertinite macerals are more inert than vitrinites or liptinites. Liptinite macerals are derived from waxy and resinous materials such as spores, cuticles and resins, and also from fats and oils of plant origin. Liptinites are composed of mainly aliphatic compounds and contain the highest proportion of hydrogen of the three maceral groups.

Macerals are differentiated by the percentage of light reflected from a polished surface of the coal sample during petrographic analysis. The relative order of maceral reflectance within a coal is inertinites > vitrinites > liptinites. To perform a petrographic analysis a representative sample of the coal is prepared in accordance with the standard (ISO:7404-2) by grinding to a suitable particle size and mounting in a resin block. One face of this block is polished to provide a flat, smooth surface for analysis. Analysis is carried out in accordance with the standard (ISO:7404-3). A reflected light microscope is used to examine the sample surface under oil immersion. Different maceral types are identified based on their relative reflectance values, and volumetric quantification of each group is made by a point-count procedure in which a minimum of 500 points are observed, excluding minerals. In addition to the relative proportions of vitrinite, liptinite and inertinite, the vitrinite reflectance value can also be measured in accordance with the standard (ISO:7404-4). This is the intensity of light reflected from the polished vitrinite surface, measured at 546 nm, and compared with a set of standard samples of known reflectance. The vitrinite reflectance can be used as a measure of the rank of a coal.

Appendix B
Characterisation of coals A-D

Figure B.1 shows petrographic reflectance distributions of coals A, B, C and D.

Table B.1 shows ash chemistry data for coals A-D produced by X-ray fluorescence (XRF), each result is the average of three measurements.
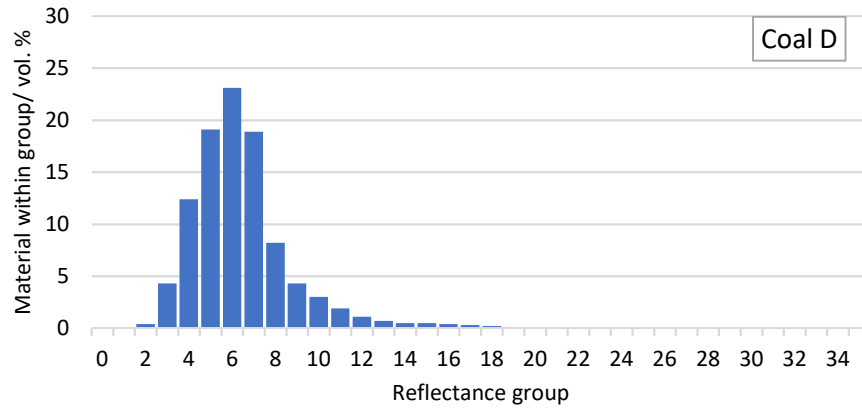
(a)

(b)

(c)
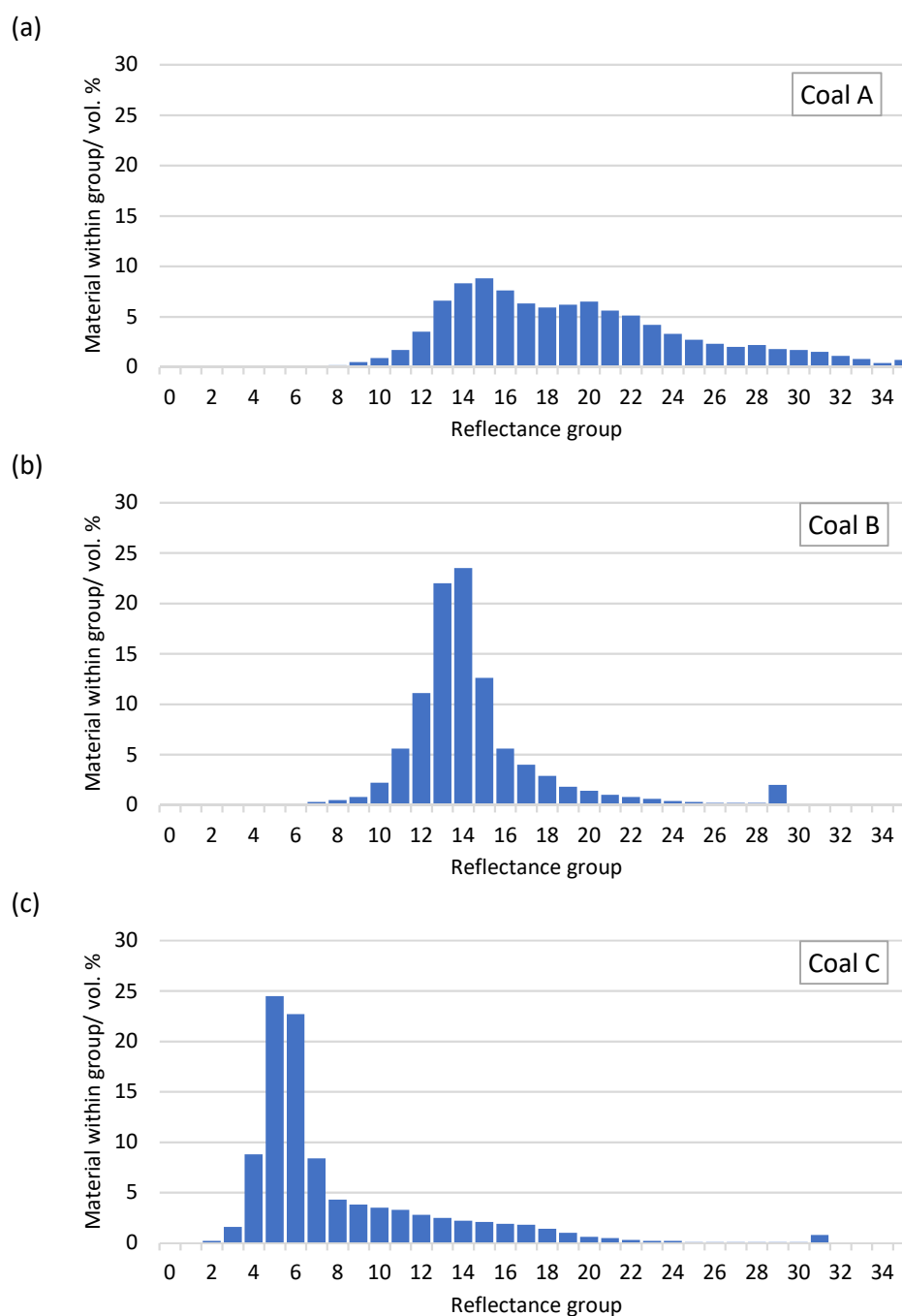
(d)

Figure B.1: Petrographic reflectance distribution of coals A-D (a-d respectively). X axis = reflectance group, Y axis = vol. % of sample within group.

Component	Coal A	Coal B	Coal C	Coal D
Fe	3.6	10.1	2.2	6.4
CaO	2.6	15.5	0.85	2
SiO_2	43.3	28.9	58.1	44.3
MnO	0.01	0	0	0
Al_2O_3	28.7	18.5	23.5	27.9
MgO	0.77	1.8	0.54	0.6
P_2O_5	0.5	0.03	0.04	0.11
K_2O	1.2	1.5	2.3	2.9
TiO_2	1	1	1.3	1.8
Na_2O	1.4	0.17	0.21	0.32
Cr_2O_3	0.07	0.07	0.08	0.08
V_2O_5	0.05	0.06	0.12	0.17
S	0.84	3.4	0.17	0.53

Table B.1: Ash chemistry results of coals A-D analysed by XRF. All results are in units of wt. %.

Figure B.2 shows Ruhr dilatometer results for coals B, C and D. Figure B.3 shows Gieseler plastometer results for coals B, C and D. Coal A produced no contraction or dilation in the dilatometer, nor plasticity in the plastometer.
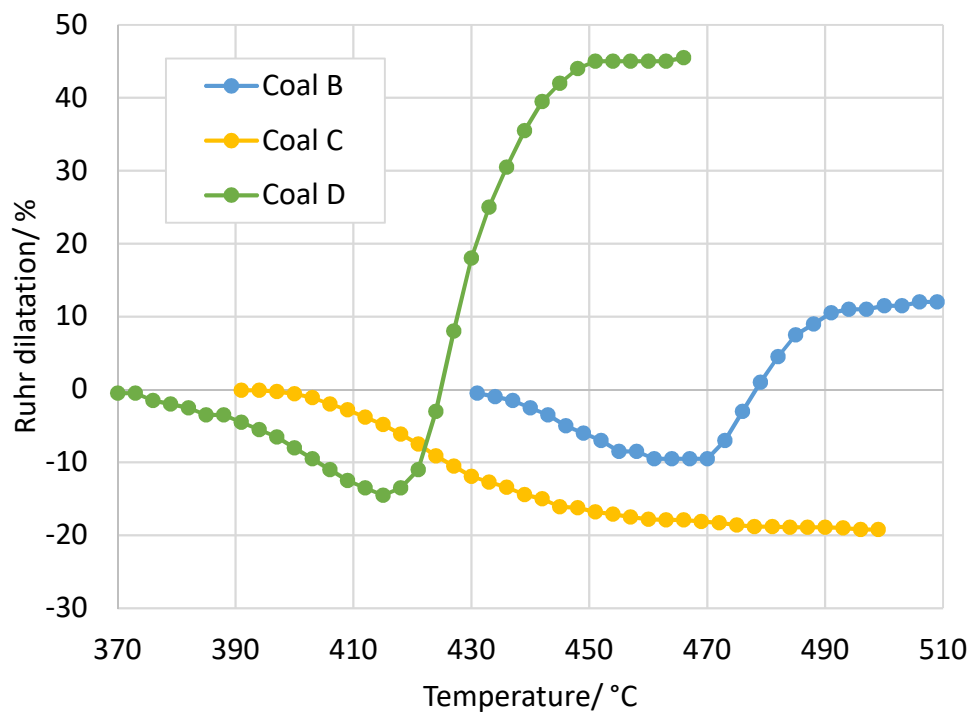
Figure B.2: Rhur dilatometer results for coals B, C and D.
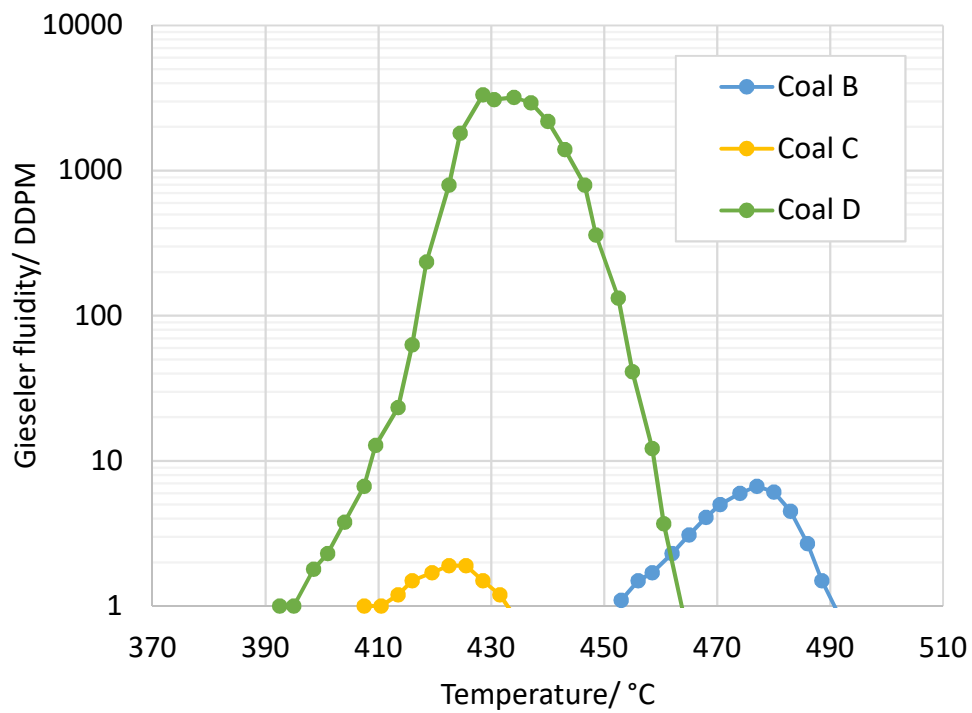
Figure B.3: Gieseler plastometer results for coals B, C and D.

Appendix C

Characterisation of sieve fractions of coals A-D

The particle size distribution within each separated sieve fraction of coals A-D (measured by Malvern Mastersizer) is shown in Figure C.1. The Dv(0.5) values (the diameter below which 50 vol. % of the sample exists) is shown in Table C.1. The Proximate, Ultimate and petrographic analysis data for each size fraction are presented in Table C.2. Figures C.2, C.3, C.4 and C.5 show the petrographic reflectance distribution graphs of the size fractions of coals A-D respectively.

(a)

(b)

(c)

(d)
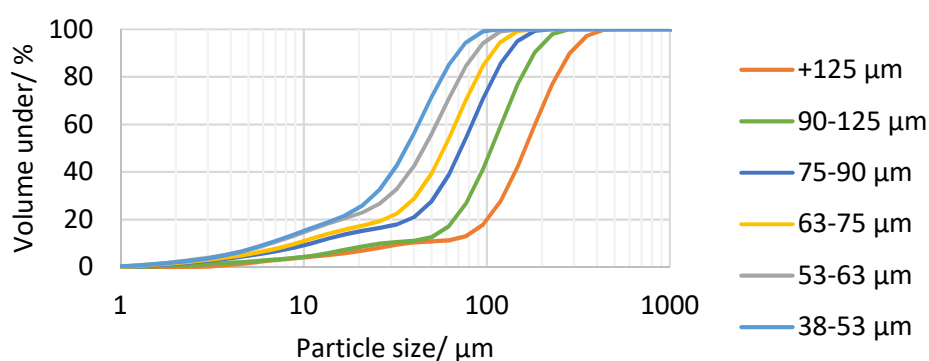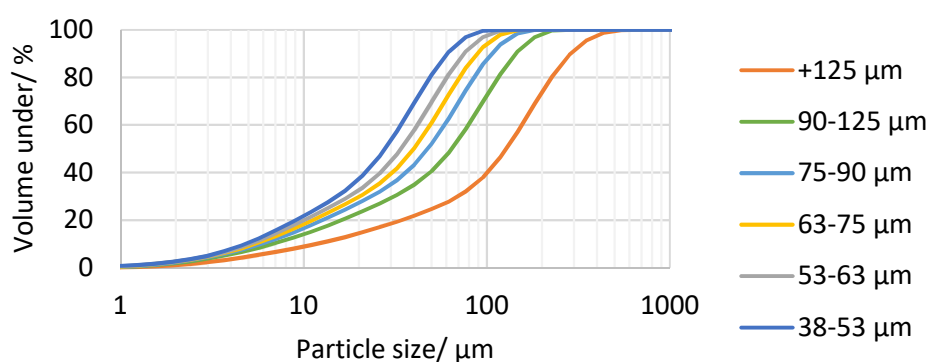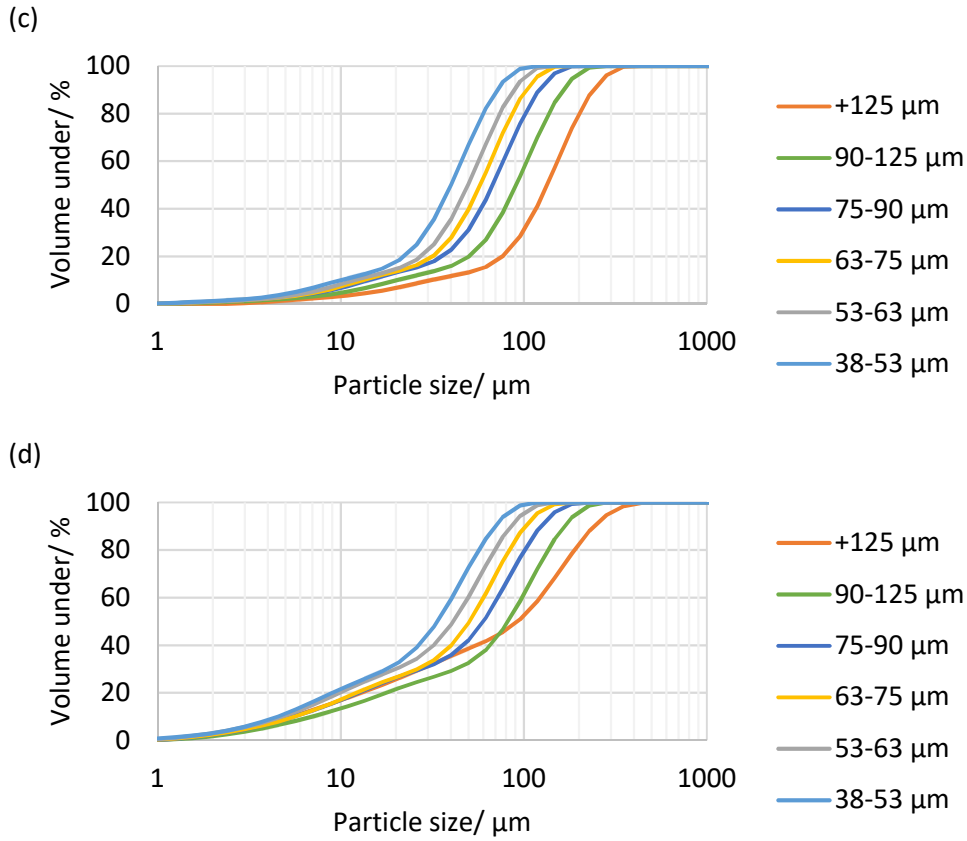
Figure C.1: Particle size distribution curves of separated size fractions of coal A, B, C and D (a-d respectively).

Particle size fraction/ μm	Dv(0.5) coal A/ μm	Dv(0.5) coal B/ μm	Dv(0.5) coal C/ μm	Dv(0.5) coal D/ μm
>125	162.7	128.1	134.3	92.7
90 – 125	105.1	64.4	91.2	82.3
75 – 90	72.8	47.7	67.7	60.1
63 – 75	58.6	39.9	57.8	50.4
53 – 63	45.5	34.1	49.5	41.2
38 – 53	36.3	27.8	40.0	33.8

Table B.1: Values of Dv(0.5) of the particle size fractions of coals A, B, C and D.

	Particle size fraction/ μm					
	>125	90-125	75-90	63-75	53-63	38-53
Coal A						
Proximate analysis						
Moisture/ % (ad)	2.4	2.1	2.0	2.1	2.1	1.9
Volatile matter/ % (db)	12.2	12.0	12.8	13.1	13.5	14.5
Ash/ % (db)	12.2	9.1	8.8	8.7	8.1	8.8

Fixed carbon/ % (db) (diff)	75.6	78.9	78.4	78.3	78.3	76.7
Ultimate analysis						
Carbon/ % (daf)	88.2	87.4	87.1	88.0	88.0	88.2
Hydrogen/ % (daf)	3.9	4.0	4.2	4.2	4.2	4.3
Nitrogen/ % (daf)	2.1	2.1	2.1	2.1	2.1	2.2
Sulphur/ % (daf)	0.4	0.4	0.4	0.4	0.4	0.4
Oxygen/ % (daf) (diff.)	5.8	6.5	6.6	5.7	5.7	5.3
Petrographic analysis						
Liptinite/ %	0.0	0.0	0.0	0.0	0.0	0.0
Vitrinite/ %	75.4	80.0	80.5	80.7	80.1	79.7
Inertinite/ %	24.6	20.0	19.5	19.3	19.9	20.3
Vitrinite reflectance, Ro (max.)	1.9	1.8	1.8	1.7	1.7	1.6
Coal B						
Proximate analysis						
Moisture/ % (ad)	0.8	0.8	1.0	1.5	0.8	0.8
Volatile matter/ % (db)	18.2	18.4	18.5	18.6	18.6	18.6
Ash/ % (db)	9.1	6.5	5.6	5.5	5.1	5.0
Fixed Carbon/ % (db) (diff)	72.7	75.1	76.0	75.9	76.4	76.5
Ultimate analysis						
Carbon/ % (daf)	88.1	89.5	88.0	88.9	88.7	88.8
Hydrogen/ % (daf)	4.7	4.8	4.7	4.7	4.8	4.8
Nitrogen/ % (daf)	1.2	1.3	1.3	1.3	1.3	1.2
Sulphur/ % (daf)	1.1	0.9	0.9	1.0	0.9	0.9
Oxygen/ % (daf) (diff.)	6.0	4.4	6.0	5.1	5.2	5.2
Petrographic analysis						
Liptinite/ %	1.6	1.2	1.0	0.9	0.9	0.8
Vitrinite/ %	68.1	73.7	75.1	77.5	76.5	77.7
Inertinite/ %	30.3	25.2	23.8	21.6	22.5	21.5
Vitrinite reflectance, Ro (max.)	1.7	1.6	1.6	1.7	1.7	1.7
Coal C						
Proximate analysis						
Moisture/ % (ad)	3.4	3.4	3.5	3.5	4.3	3.5
Volatile matter/ % (db)	39.4	38.9	38.7	38.7	38.8	38.7
Ash/ % (db)	4.8	4.1	3.7	3.5	3.2	3.2
Fixed carbon/ % (db) (diff)	55.8	57.0	57.6	57.9	58.1	58.2
Ultimate analysis						
Carbon/ % (daf)	81.2	80.4	80.0	80.1	79.9	80.0
Hydrogen/ % (daf)	5.5	5.4	5.3	5.3	5.3	5.3
Nitrogen/ % (daf)	1.8	1.7	1.8	1.8	1.8	1.8
Sulphur/ % (daf)	0.4	0.4	0.4	0.4	0.4	0.4
Oxygen/ % (daf) (diff)	11.2	12.1	12.5	12.4	12.5	12.5

Petrographic analysis						
Liptinite/ %	4.0	4.0	4.0	4.0	4.0	4.0
Vitrinite/ %	60.8	59.5	61.9	66.7	66.9	66.3
Inertinite/ %	35.2	36.5	34.2	29.3	29.1	29.7
Vitrinite reflectance, Ro (max.)	0.7	0.7	0.7	0.8	0.7	0.7
Coal D						
Proximate analysis						
Moisture/ % (ad)	1.5	1.4	1.4	1.4	1.5	2.3
Volatile matter/ % (db)	37.2	37.9	37.5	37.7	37.3	37.2
Ash/ % (db)	6.2	5.9	5.9	5.5	5.5	5.3
Fixed carbon/ % (db) (diff)	56.6	56.2	56.6	56.8	57.1	57.5
Ultimate analysis						
Carbon/ % (daf)	83.9	82.2	82.8	83.1	83.1	84.1
Hydrogen/ % (daf)	5.7	5.6	5.6	5.6	5.6	5.6
Nitrogen/ % (daf)	1.5	1.4	1.5	1.5	1.5	1.6
Sulphur/ % (daf)	1.1	1.1	1.1	1.1	1.1	1.1
Oxygen/ % (daf) (diff)	7.8	9.7	9.0	8.7	8.7	7.7
Petrographic analysis						
Liptinite/ %	4.0	4.0	4.0	4.0	4.0	4.0
Vitrinite/ %	65.1	72.5	75.3	75.9	76.9	65.1
Inertinite/ %	30.9	23.5	20.6	20.1	19.1	30.9
Vitrinite reflectance, Ro (max.)	0.8	0.8	0.9	0.9	0.9	0.8

Table C.2: Proximate, Ultimate and petrographic analysis results of the size fractions of coals A-D.

(a)

(b)

(c)

75-90 µm
particles
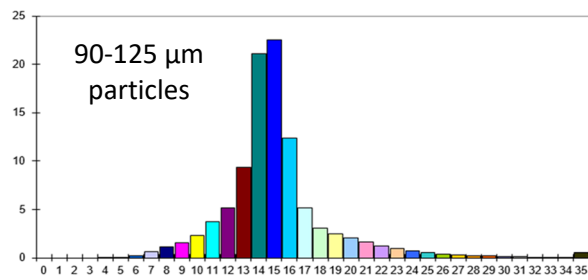
(d)

63-75 µm
particles

(e)

53-63 µm
particles

(f)

38-53 µm
particles
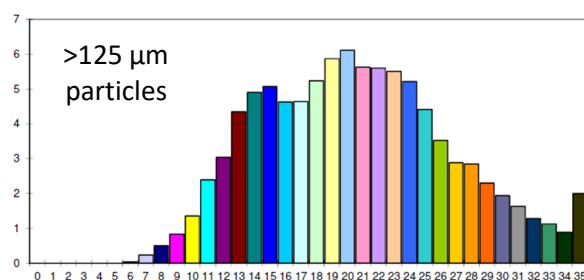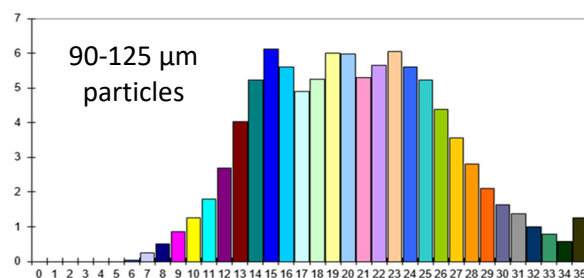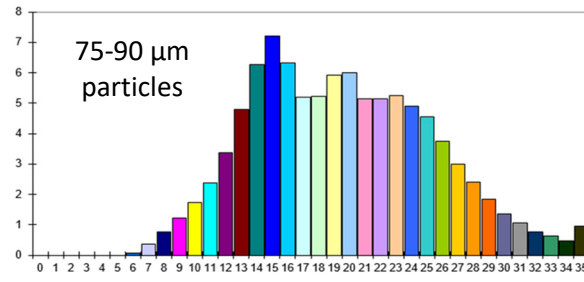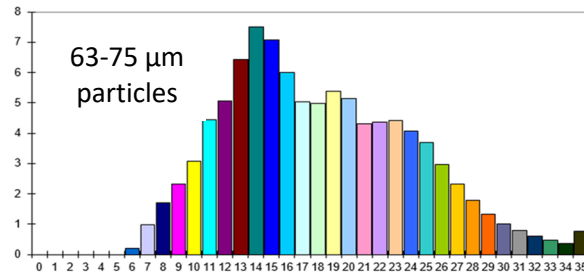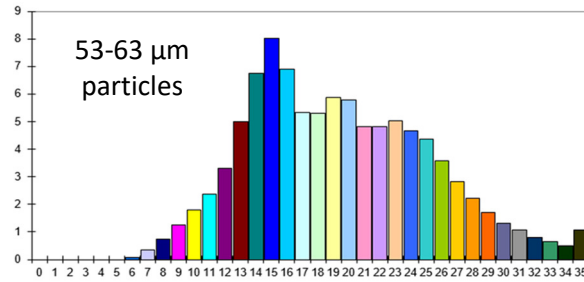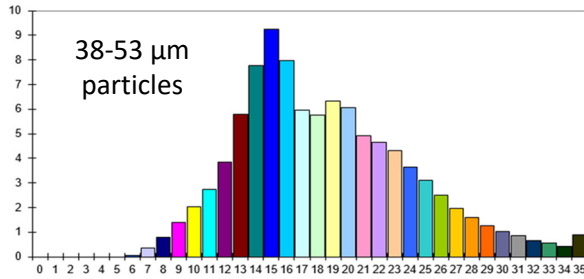
Figure C.2: Petrographic reflectance distribution graphs of the different size fractions of coal A. >125 µm (a), 90-125 µm (b), 75-90 µm (c), 63-75 µm (d), 53-63 µm (e) and 38-53 µm (f). In all cases X axis = reflectance group and Y axis = % of sample within group.
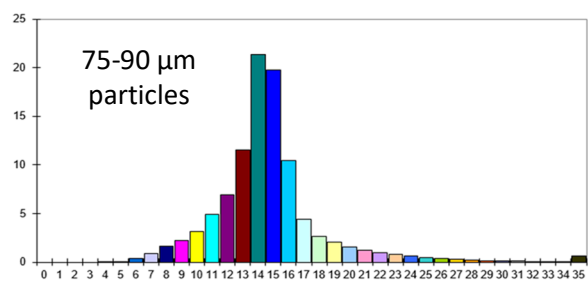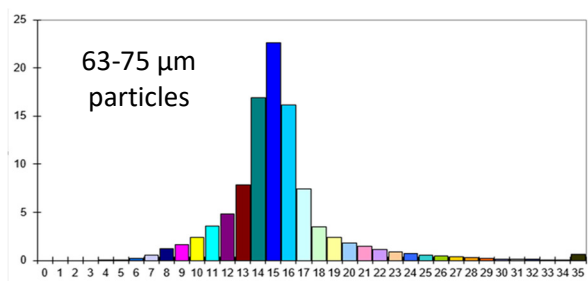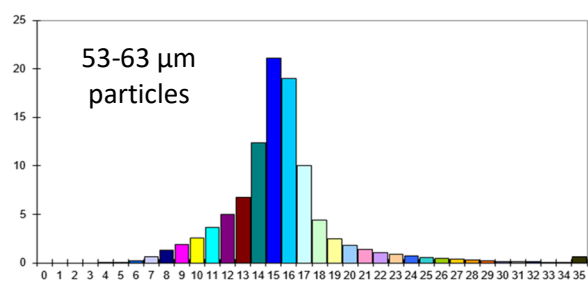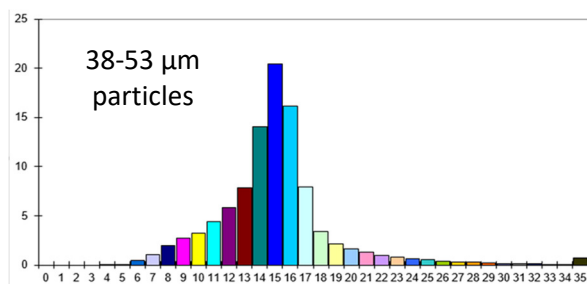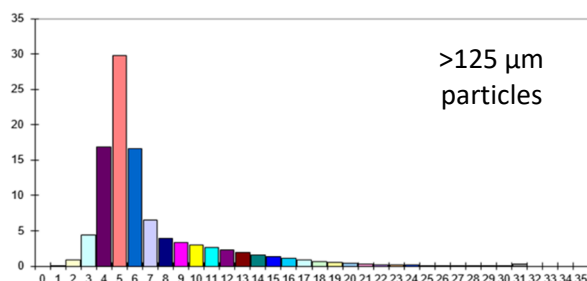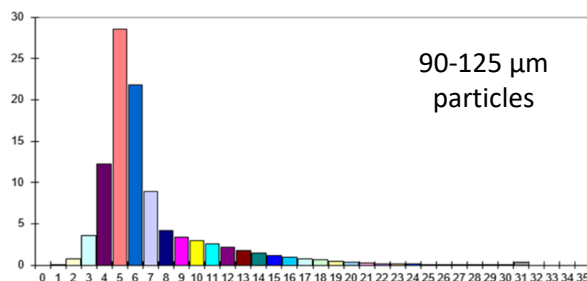
(a)

>125 μm
particles

(b)

90-125 μm
particles

(c)

75-90 μm
particles

(d)

63-75 μm
particles

(e)

53-63 μm
particles
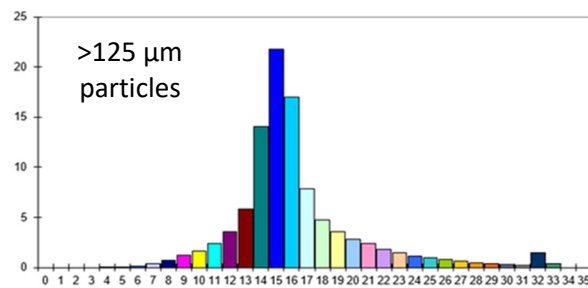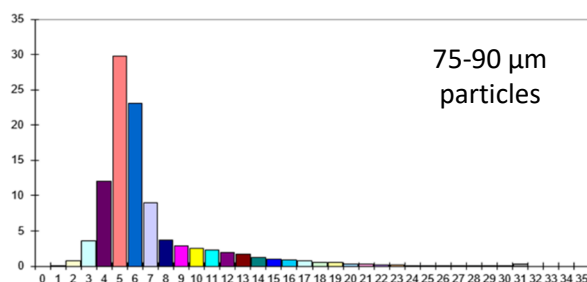
(f)

Figure C.3: Petrographic reflectance distribution graphs of the different size fractions of coal B. >125 μm (a), 90-125 μm (b), 75-90 μm (c), 63-75 μm (d), 53-63 μm (e) and 38-53 μm (f). In all cases X axis = reflectance group and Y axis = % of sample within group.

(a)

(b)

(c)

(d)

(e)

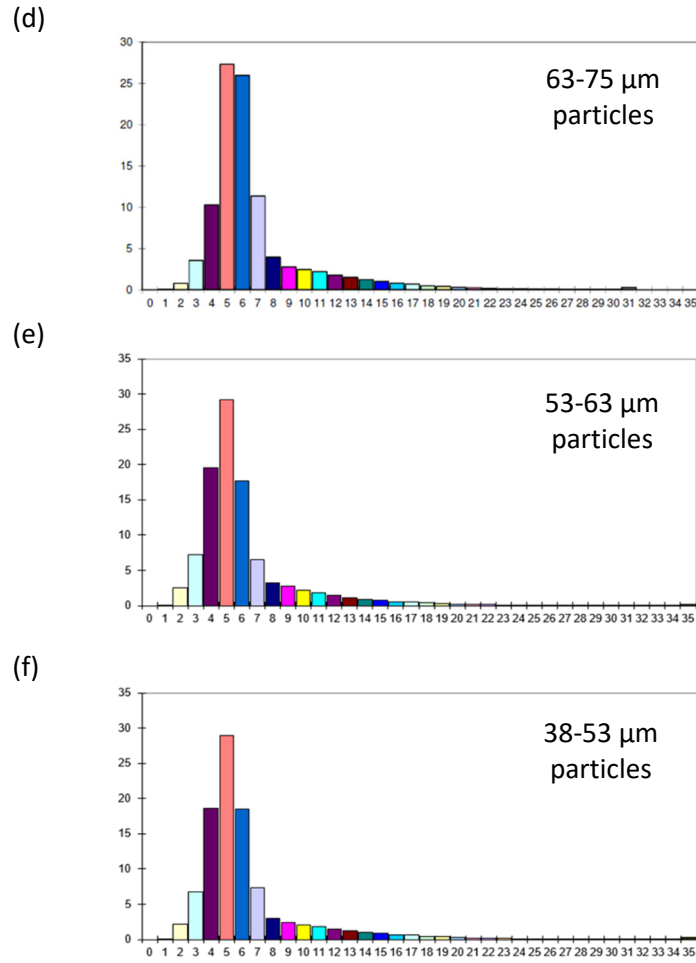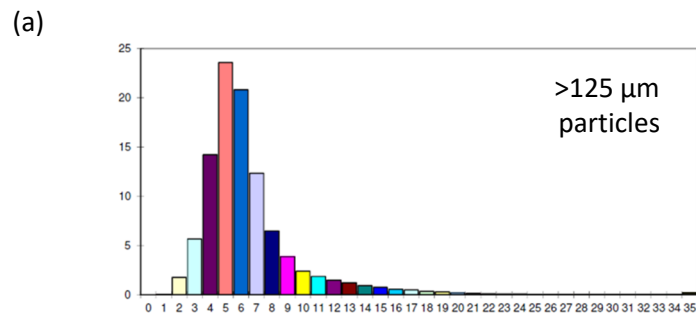(f)

Figure C.4: Petrographic reflectance distribution graphs of the different size fractions of coal C. >125 μm (a), 90-125 μm (b), 75-90 μm (c), 63-75 μm (d), 53-63 μm (e) and 38-53 μm (f). In all cases X axis = reflectance group and Y axis = % of sample within group.

(a)

(b)

90-125 µm
particles

(c)

75-90 µm
particles
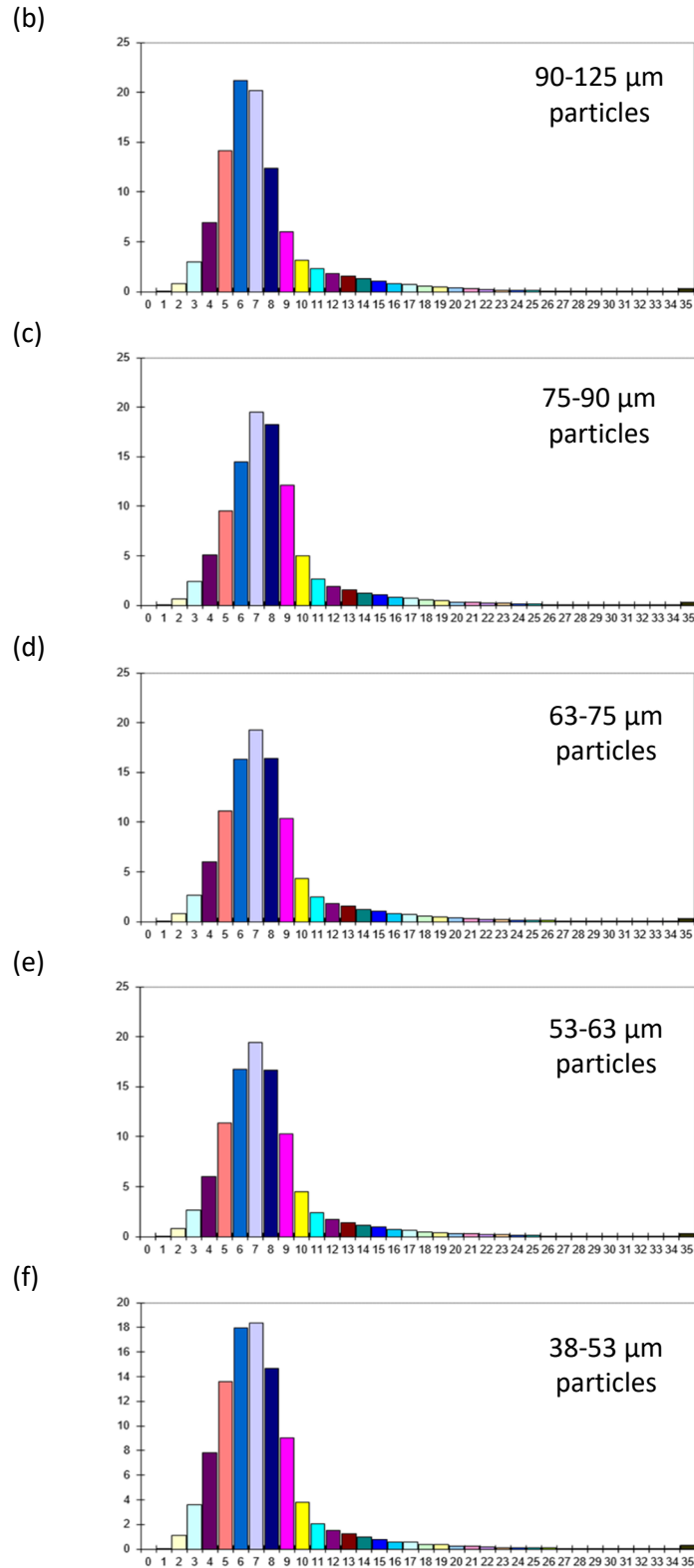
(d)

63-75 µm
particles

(e)

53-63 µm
particles

(f)

38-53 µm
particles

Figure C.5: Petrographic reflectance distribution graphs of size fractions of coal D.
>125 µm (a), 90-125 µm (b), 75-90 µm (c), 63-75 µm (d), 53-63 µm (e) and 38-53
µm (f). X axis = reflectance group and Y axis = % of sample within group.